Endothelin signalling in the retina

DISSERTATION

ZUR ERLANGUNG DES DOKTORGRADES

DER NATURWISSENSCHAFTEN (DR. RER. NAT.)

DER FAKULTÄT FÜR BIOLOGIE UND VORKLINISCHE MEDIZIN

DER UNIVERSITÄT REGENSBURG

Durchgeführt am Lehrstuhl für Humananatomie und Embryologie

der Universität Regensburg

vorgelegt von

Sabrina I. Schmitt

aus München

im Jahr 2019

Das Promotionsgesuch wurde eingereicht am:

25.04.2019

Die Arbeit wurde angeleitet von:

Prof. Dr. Dr. Barbara Braunger

_____

Sabrina I. Schmitt

Abstract

The three endothelin isoforms (Endothelin 1, 2, 3), signal through two G-protein coupled receptors: Endothelin receptor type a (Eta) and Endothelin receptor type a (Etb). In the eye, the role of Endothelin signalling is discussed controversially.

Thus, the main aim of the current thesis was to investigate the role of endothelin signalling in the eye and in particular whether Etb mediates neuroprotective effects for photoreceptor survival following experimentally induced photoreceptor degeneration. Moreover, the underlying molecular mechanisms mediating the potential neuroprotection were examined in detail.

First, the localization of Etb in the eye was analysed and its cell-type specific localization was identified using immunohistochemical co-staining. Furthermore, its quantitative expression in the retina was determined.

Next, we examined an activation of the entire Endothelin signalling in the retinae of wildtype mice in response to different ocular traumata (puncture of the eye, PBS-injections, light-induced damage).

Then, conditional knockout mice with a deletion of Etb in the entire eye ($Etb^{\Delta eye}$) and a second mouse line with a cell type specific deletion of Etb in retinal neurons and Müller cells ($Etb^{\Delta OC}$) were generated using the Cre-loxP-System. Additionally, photoreceptor cell lines ($661W^{\Delta Etb}$) with a stable deletion of Etb were created via CRISPR/Cas9.

The *in vivo* ablation of Etb in Müller cells and retinal neurons showed no obvious alterations of retinal morphology and vasculature. However, $Etb^{\Delta OC}$ mice showed a higher vulnerability of photoreceptors after light-induced photoreceptor degeneration concomitant with a significantly thinner outer nuclear layer (ONL). In accordance, our *in vitro* data obtained a significantly higher apoptosis rate in Etb-deficient photoreceptor cells after serum-deprivation compared to controls. Quite intriguingly, the expression levels of neuroprotective molecules *leukaemia inhibitory factor (Lif),* and *fibroblast growth factor 2 (Fgf2)* were significantly elevated in light-exposed $Etb^{\Delta OC}$ mice compared to light-exposed control littermates. Still we detected a significantly upregulated mRNA expression of *Caspase 8* indicating that the increased apoptosis of photoreceptors was mediated via extrinsic death-receptor mediated apoptosis in $Etb^{\Delta OC}$ mice. Furthermore, we identified an impaired activation (phosphorylation) of the neuroprotective Protein Kinase B (Akt) signalling pathway.

Taken together, our data identified Etb mediated signalling as the essential and even more potent neuroprotective event for photoreceptor survival compared to the neuroprotective factors fibroblast growth factor 2 (Fgf2) and leukaemia inhibitory factor (Lif). Downstream of Etb its neuroprotective signalling is mediated through activation of Akt signalling.

In summary, our data identified Etb mediated signalling for the first time as the essential pathway for photoreceptor survival. Thus, targeting Endothelin signalling might be a promising approach for the development of new therapeutic strategies in the context of retinal degenerations.

Zusammenfassung

Das vasoaktive Peptid Endothelin wird als drei Isoformen (Endothelin 1, 2, 3) exprimiert, die an zwei G-Protein gekoppelte Rezeptoren Endothelin Rezeptor Typ a (Eta) und Endothelin Rezeptor Typ b (Etb) binden können. Die Rolle von des Endothelin-Signalwegs im Auge ist noch weitgehendst unbekannt und wird kontrovers diskutiert.

Deshalb war es das Hauptziel dieser Arbeit die Rolle des Endothelin-Signalwegs im Auge zu untersuchen und besonders einem potenziellen neuroprotektiven Effekt von Etb für das Überleben von Photorezeptoren nach Licht-induzierter Schädigung nachzugehen. Außerdem sollten die zugrundeliegenden molekularen Mechanismen aufgeschlüsselt werden.

Zunächst wurde die Lokalisation des Etb im Auge untersucht und durch immunhistochemische Doppelfärbungen dessen zelltypspezifische Lokalisation bestimmt. Außerdem wurde die retinale Expressionstärke von Etb im Vergleich zu Eta ermittelt. Des Weiteren sollte die Expression des gesamten Endothelin-Signalwegs in wildtypischen Retinae im Falle von okulärem Trauma, hervorgerufen durch alleinige Perforation des Auges, PBS-Injektion oder Lichtschaden, untersucht werden. In allen drei Schadensmodellen kam es zu einer Aktivierung des gesamten Endothelin-Signalwegs.

Anschließend generierten wir mittels Cre-loxP-System eine Mauslinie mit einer Deletion von Etb im gesamten Auge (*Etb*$^{\Delta eye}$) und eine weitere Mauslinie mit einer Etb Deletion in Müllerzellen und retinalen Neuronen (*Etb*$^{\Delta OC}$). Darüber hinaus etablierten wir Photorezeptorzelllinien mit einer stabilen Deletion von Etb mittels des CRISPR/Cas9-System.

Die Deletion von Etb in retinalen Neuronen und Müllerzellen führte zu keinen offensichtlichen Veränderungen der retinalen Morphologie und Gefäßstruktur. Allerdings war die Vulnerabilität der Photorezeptoren bei *Etb*$^{\Delta OC}$ Mäusen nach Licht-induzierten Photorezeptor Degeneration signifikant höher, einhergehend mit einer signifikant dünner äußeren Körnerschicht 14 Tage nach Lichtschaden. Auch die Etb-defizienten Photorezeptor-Zelllinien wiesen eine signifikant höhere Apoptoserate nach Zellstress, verursacht durch Serum-Entzug, auf. Weiterführende molekulare Analysen zeigten, eine signifikante Erhöhung der neuroprotektiven Faktoren *leucaemia inhibitory factor (lif)* und *fibroblast growth factor (fgf2)* bei lichtgeschädigten *Etb*$^{\Delta OC}$ Mäusen im Vergleich zu lichtgeschädigten Kontrolltieren. Überraschenderweise detektierten wir dennoch eine signifikante Erhöhung von Caspase 8 bei lichtgeschädigten *Etb*$^{\Delta OC}$ Mäusen im Vergleich

zu lichtgeschädigten Kontrolltieren, was den Rückschluss nahelegt, dass die beobachtete verstärkte Degeneration der Photorezeptoren durch den extrinsischen, d.h. durch Todesrezeptoren vermittelten Signalweg ablief. Weiterführende Analysen identifizierten eine verminderte Aktivierung (Phosphorylierung) des neuroprotektiven Protein Kinase B (Akt) Signalwegs als den Signalweg worüber Etb sein neuroprotektives Signal vermittelt.

Zusammenfassend zeigen die erhobenen Daten erstmals, dass das durch den Etb vermittelte Signal essenziell und weitaus potenter für das Überleben von Photorezeptoren ist als die Wirkung der neuroprotektiven Faktoren fibroblast growth factor 2 (Fgf2) und leukaemia inhibitory factor. Downstream von Etb wird die Neuroprotektion über den Akt-Signalweg vermittelt.

Zukünftig kann dieser durch Etb vermittelte Signalweg einen vielversprechenden Ansatz für die Entwicklung von neuen Therapieansätzen zur Behandlung retinaler Degenerationen wie Retinopathia pigmentosa oder altersbedingte Makuladegeneration darstellen.

Table of content

1 Introduction

1.1 The retina

The retina, a light-sensitive layer, which lines the inner surface of the posterior part of the eye and can be described as visible part of the central nervous system (CNS) (Kaufman et al., 2003). The retina is organized in several different layers that can be clearly defined histologically (Figure 1).

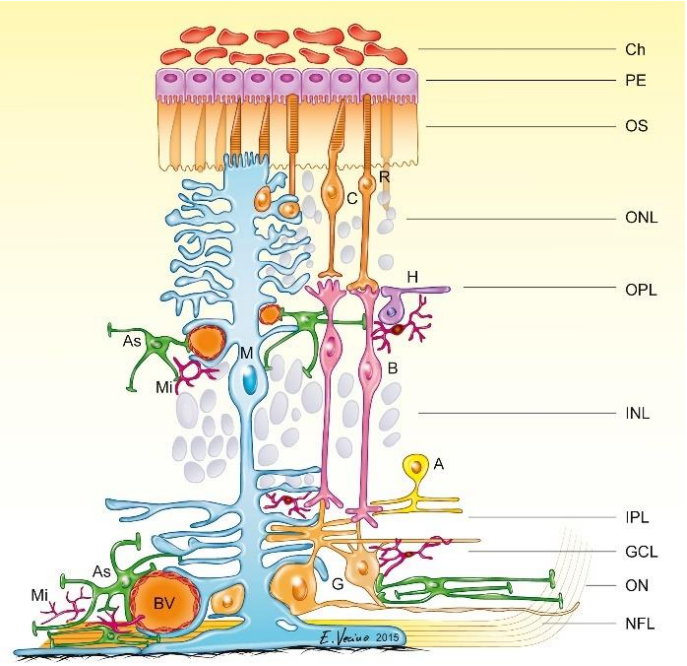

Figure 1 Schematic structure of the mammalian retina. Detailed schema is shown with the layers beginning from the outermost side (PE= pigment epithelium) to the innermost side (NFL= nerve fiber layer). Different cell types are situated in the retina. Ch=Choroid, PE=pigment epithelium, OS=outer segments of photoreceptors, ONL=outer nuclear layer, OPL=outer plexiform layer, INL=inner plexiform layer, IPL=inner plexiform layer, GCL=ganglion cell layer, ON=optic nerve, NFL=nerve fibre layer, R=rod, C=cone, H=horizontal cell, G=ganglion cell M=Müller cell, B=bipolar cell, A=amacrine cell, As=astrocyte, Mi=microglia, BV=blood vessel (Vecino et al., 2016)

The single layered retinal pigment epithelium (RPE or PE) is part of the blood retina barrier and provides nutrition and waste removal to photoreceptors, the light sensitive cells of the retina (Strauss, 2005). The outer limiting membrane is rather a narrow zone comprising a series of heterotypic adherens junctions between Müller cells themselves and between Müller cells and photoreceptors (Williams et al., 1990). The photoreceptors' cell bodies and processes constitute the outer nuclear layer (ONL), whereas their synapses form together with the synapses of bipolar and horizontal cells the outer plexiform layer (OPL). The cell bodies of horizontal, bipolar and amacrine cells and the nuclei of the Müller cells are located in the inner nuclear layer (INL), followed by the synapses between bipolar, amacrine and ganglion cells resulting in the inner plexiform layer (IPL) (Purves and Williams, 2001). The perikarya of the ganglion cells are located together with "displaced" amacrine cells in the ganglion cell layer (GCL), their axons build the nerve fiber layer (NFL) converging to form the optic nerve. At last, the Müller cell

endfeet form the inner limiting membrane, that separates the retina from the vitreous body (Purves and Williams, 2001; Kaufman et al., 2003)

1.1.1 Retinal neurons

The neural retina comprises an interacting network of five different specialized sensory neurons (Sachsenweger and Klauss, 2014): Ganglion cells, amacrine cells, bipolar cells, horizontal cells and photoreceptors. Photoreceptors are light-sensitive cells and capable of visual phototransduction (Kefalov, 2012), the initial step of vertebral vision. The visual phototransduction is the conversion of incident light energy into neural signals that can be transmitted to the brain by the optic nerve (Mannu, 2014).

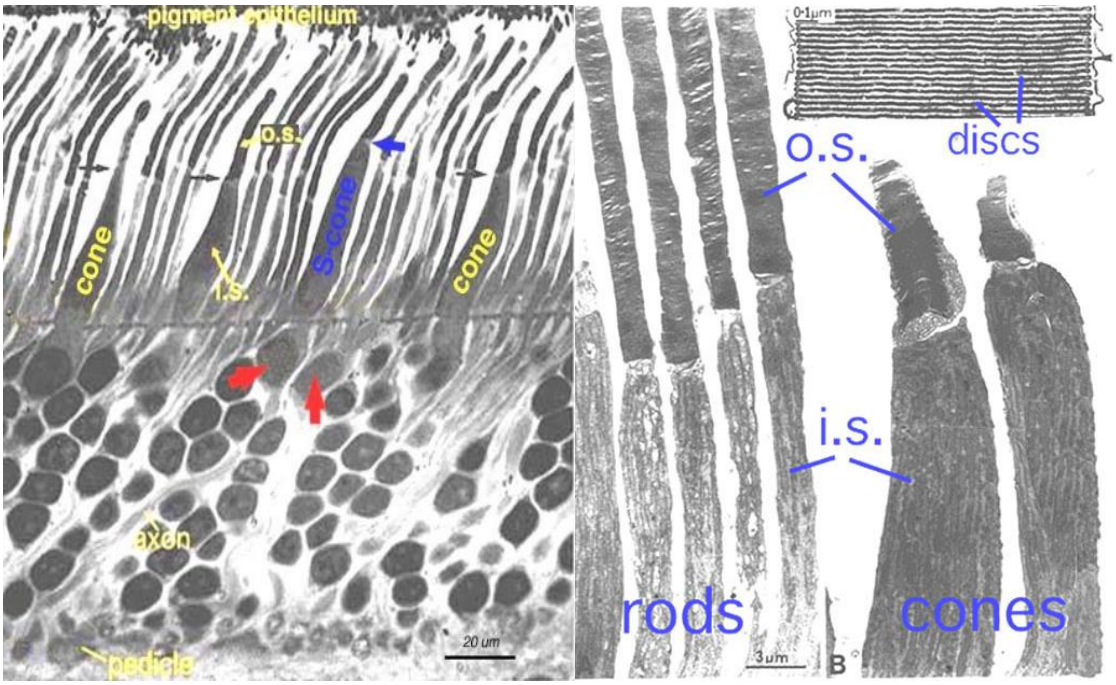

Figure 2 Left. Semithin section of a human retina illustrating rod and cones, differentiated in short wavelength cones (S-cone, blue) and long wavelength cones (red arrows) (Kolb et al., 1995). Right. Electronic microscopy of rod and cones of a monkey retina showing the inner and outer segments of rod and cones and a high magnification of the membrane discs (Anderson and Fisher, 1976). I.S.=inner segment, O.S.=outer segment

There are two different types of classic photoreceptors: the highly light-sensitive rods (100-125 million) for scotopic (night) vision, located mainly in the peripheral retina and the less sensitive cones (6-7 million) for achromatic (colour) vision located mainly at the fovea centralis in humans (Figure 2). Cones are divided in three types, each with different visual pigments, namely: S-cones, M-cones and L-cones. Each cone is therefore sensitive to visible wavelengths of light that correspond to short-wavelength (S-cones), medium-wavelength (M-cones) and long-wavelength (L-cones) (Mustafi et al., 2009).

Both photoreceptors show the same basic structure: An outer segment (O.S.) for light-absorption by containing photopigment-filled disks (rods) or membrane enfoldings (cones), an inner segment (I.S.) full of ATP-providing mitochondria and endoplasmatic reticulum, the cell body (located in the outer nuclear layer) with the nucleus and other cell's organelles and the synaptic terminal which is located in the outer plexiform layer (OPL). It releases neurotransmitter (e.g glutamate) to amacrine cells, interneurons which are responsible for lateral interaction in the retina, or to horizontal cells and bipolar cells which transmit the signal onwards to the ganglion cells, the neurons that transfer all visual information processed in the retina to the brain (Masland, 2012).

1.1.2 Retinal glia cells: Müller cells, astrocytes and microglia cells

The retinal glia cells consist of Müller cells, astrocytes and microglia cells (Vecino et al., 2016).

Müller cells radially span the retina with their processes from the outer to the inner limiting membrane and with their cells bodies residing in the inner nuclear layer (INL). They also infold all retinal neurons which enables a multifunctional interaction between Müller cells and neurons such as a homeostatic and metabolic support of retinal neurons (Bringmann et al., 2006; Reichenbach and Bringmann, 2013). A further important function of Müller cells is the release of neuroprotective (e.g. Fibroblast Growth Factor 2 (Fgf2), angiogenic factors (e.g. vascular endothelial growth factor (Vegf) and the recycling of neurotransmitters (Pierce et al., 1995; Bringmann et al., 2006). In case of retinal injury or disease, Müller cells become reactive and undergo a cytoskeleton remodelling called reactive gliosis which is characterized by a rounded shape and enlarged endfeet (García and Vecino, 2003) as well as an upregulation of the intermediate filament protein glial fibrillary acidic protein (Gfap) (Lupien et al., 2004).

In the healthy retina, Gfap is regularly expressed by astrocytes, a second type of glial cells in the central nervous system (Hol and Pekny, 2015). In the retina, their processes are almost confined to the nerve fiber layer (NFL) and ganglion cell layer (RGC) (Büssow, 1980; Hol and Pekny, 2015). As a main producer of the angiogenic factor Vegf (West et al., 2005), astrocytes are of significance in retinal vascularization (O'Sullivan et al., 2017).They migrate ahead of the vessels to promote the formation of superficial or deep vasculature (Stone et al., 1995; van der Wijk et al., 2018). Together with endothelial cells lining retinal microvessels and pericytes, they also support the integrity of the inner blood retinal barrier (BRB), which is constituted through the tight junctions of the endothelial cells (Klaassen et al., 2013).

The third glial subpopulation, the microglia cells, are the phagocytic immune cells of the CNS including the retina. Under physiological conditions, microglia cells remain in the

plexiform layers in a resting state and surveil their neuronal microenvironment to cleanse metabolic products and tissue debris (Langmann, 2007). In case of retinal injury, microglia react rapidly by transitioning to an activated status and undergoing gliosis. Therefore, they switch their appearance through dynamic remodeling of their cytoskeleton and they withdraw their filopodic processes to acquire an oval, amoeboid shape. (Wang and Wong, 2014).

1.1.3 Retinal vasculature

The eye obtains nutrients and oxygen from two different vascular systems: the retinal vessels within the inner parts of the retina and the uveal vessels within the iris, ciliary body and choroid (Luo et al., 2015). The choroid mostly persists of a fenestrated capillary network (*choriocapillaris*) and supplies the outer retinal layers and photoreceptors (Nickla and Wallman, 2009).

The inner ocular blood supply is predominantly provided by the ophthalmic artery, which is the first branch of the internal carotid artery. The branches of the ophthalmic artery extend form three intra-retinal vascular beds (plexus). In the murine retina, the plexus formation starts with the superficial plexus arising from the optic nerve head by a radial outgrowth to the periphery and lies on the RGC (Stahl et al., 2010). The superficial capillaries continue sprout vertically to first form the deep plexus in the outer plexiform layer and then the intermediate plexus located in the inner plexiform layer (Anand-Apte and Hollyfield, 2010; Stahl et al., 2010). Also in the human eye, the plexus formation also starts with the generation of the superficial plexus, but is then – in contrast to the murine retina- followed by the intermediate plexus and at least deep plexus (Figure 3).

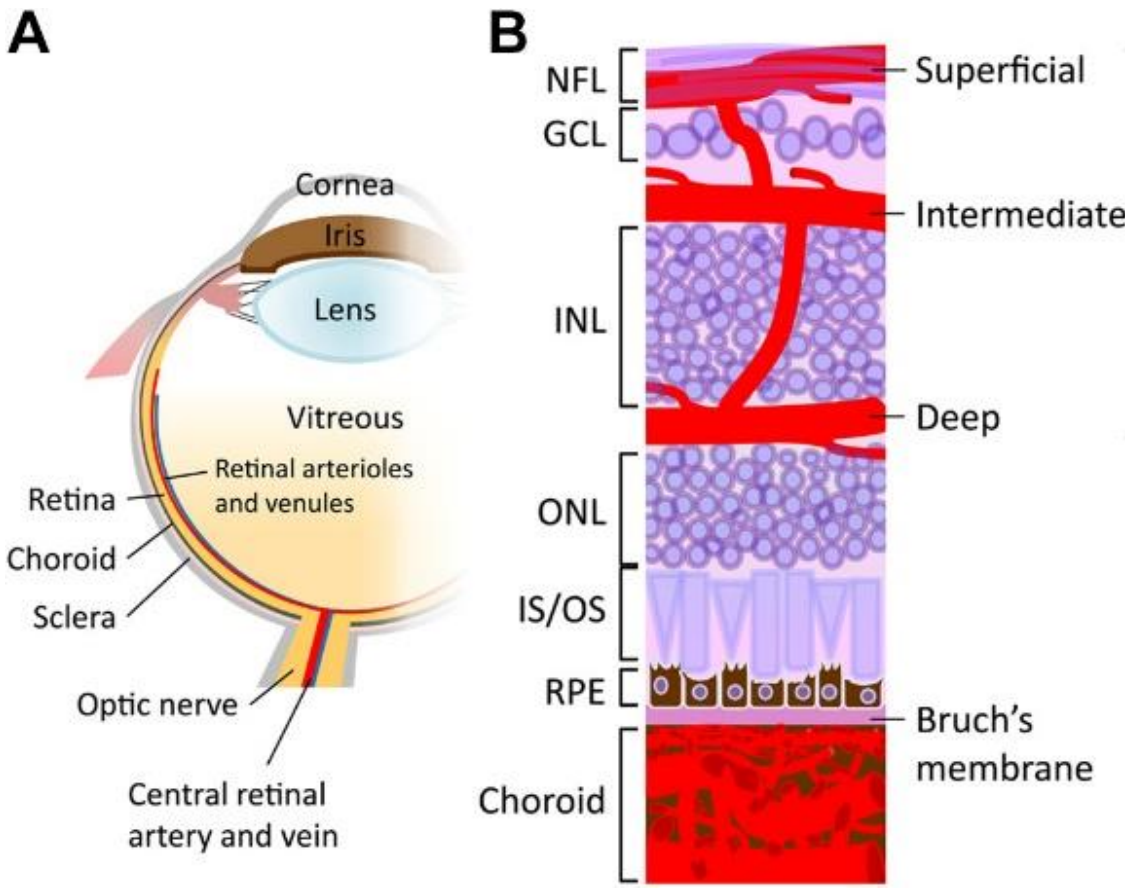

Figure 3 Schematic illustration of the ocular vasculature. A. Drawing showing a sagittal section of an entire eye B. Detailed illustration of a sagittal section of the retina including retinal and choroidal vasculature. Three capillary plexus of the retina are embedded among retinal neurons: the superficial plexus along the ganglion cell (GCL) and nerve fibre layer (NFL), the intermediate and deep plexus along each side of the inner nuclear layer (INL). The choroidal vessels are located beneath the RPE and Bruch's membrane and supply oxygen and nutrients to the outer portion of the retina. GCL=ganglion cell layer; INL=inner nuclear layer; IS/OS=inner segment/outer segment of photoreceptor; NFL=nerve fibre layer; ONL=outer nuclear layer; RPE=retinal pigment epithelium (Liu et al., 2017).

In human embryos, the development of vessels is dependent on oxygen-supply and bases on two different mechanisms: vasculogenesis and angiogenesis (Patan, 2004). Whereas vasculogenesis describes the *de novo* formation of primary vessels out of common progenitor cells (Anand-Apte and Hollyfield, 2010; Lutty and McLeod, 2018), angiogenesis characterises the maturation or rather sprouting of vessels from already existing vessels (Risau, 1997; Hughes et al., 2000). The retinal vessels differentiation out of the avascular, immature retina starts at 14-16 weeks of gestation and is nearly complete vascularized by term birth (Penn, 2008). In mice, the developmental process of the retinal vasculature is angiogenesis only and vessel growth begins at the optic nerve and sprouts peripherally. In contrast to humans, mice still possess immature vasculature with hyaloid vessels postnatal and (Gyllensten Lars J. and Hellström, 1954) the three vascular plexus will develop during the first three weeks postnatal (Stahl et al., 2010)).

1.2 Retinal degeneration in the context of photoreceptor cell death

The vision loss in hereditary retina degenerations is generated by a progressive dysfunction and apoptosis of photoreceptors (Wright et al., 2010). As in the healthy retina only a small number of photoreceptors undergo apoptosis, our workgroup uses the light-induced damage model to mimic photoreceptor degeneration that occur in retinal degenerations like Retinopathia Pigmentosa.

1.2.1 Retinopathia pigmentosa

Retinopathia pigmentosa (RP) is a clinically and genetically heterogeneous group of hereditary disorders, which are characterized by a progressive loss of photoreceptors and pigment epithelial function (Pagon, 1988). Its genetic heterogeneity is reflected in the different inheritance patterns (autosomal-dominant, autosomal-recessive or X-linked) and mapping of mutations in over 45 causative gene loci in the typical RP, with the majority of them expressed in either the photoreceptors or the retinal pigment epithelium (Dryja and Li, 1995; Hamel, 2006). With a prevalence of 1:4000 worldwide (Hamel, 2006), RP represents one of the most common causes of blindness or severe low-vision at the age from 20 to 60 years (Parmeggiani, 2011).

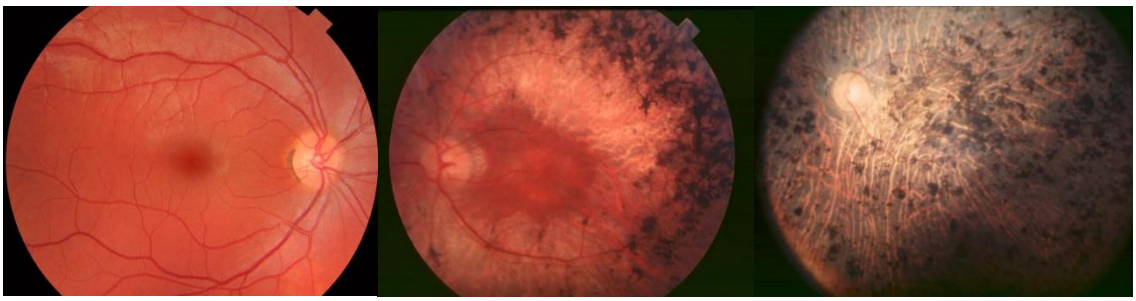

Figure 4 Fundus of patient with normal fundus (left) and patients with retinitis pigmentosa at mid stage (left) and end stage (right) show bone spicule-shaped pigment deposits and vascular atrophy (Hamel, 2006).

The typical RP is described as rod-cone dystrophy, which implies a primary degeneration of rod photoreceptors and a following degeneration of cones in later stages (Ferrari et al., 2011; Hamel, 2006). This order of photoreceptor degeneration correlates with the typically slow progress (over three to five decades) after its usual first manifestation from age 20 to 30 years (Dryja and Li, 1995), with initial symptoms of night blindness the loss of the mid-peripheral visual field, due to the fact that rod photoreceptors are almost entirely responsible for night vision and mainly located in the retinal periphery (Shintani et al., 2009). Further visual loss progresses to the central visual field resulting in tunnel vision and eventual blindness, which can also be accompanied by further clinical

hallmarks like photopsia and diminished or absent electroretinogram (Ferrari et al., 2011) and an abnormal fundus with bone-spicule deposits (Figure 4), formed by migration of pigment-containing cells to perivascular sites in the inner retina (Li et al., 1995).

At current status, there is no cure of RP available. The only treatment options aim to slow down the progression of disease. Besides a vitamin and nutritional supplementation therapy such as vitamin A and omega-3 fatty acid, several emerging technologies like retinal cell transplantation, retinal prosthesis devices and gene therapy may provide additional promising therapeutic options (Hamel, 2006).

1.1.1 Light-induced damage paradigm as mouse model for photoreceptor degeneration

In rodents, the exposure of eyes to bright, white light leads to the death of photoreceptors, which is typically confined to rod photoreceptors (Organisciak and Vaughan, 2010). This susceptibility to light was used for establishing an experimental animal model for the induction of photoreceptor degeneration, the light-induced damage paradigm (Grimm and Remé, 2013; Wenzel et al., 2005). Hereby, the exposure to excessive light leads to photoreceptor cell death via apoptosis, which is followed by morphological and functional retinal alterations, quite similar to photoreceptor cell death in retinal hereditary dystrophies and age-related macular degenerations (Marc et al., 2003). With the help of the light-induced damage model, a large number of photoreceptors undergo apoptosis at the same time, which simplifies the analysis of molecular mechanisms in photoreceptor apoptosis and neuroprotective signalling pathways in the retina. According to the length of light exposure, the light damage can be induced in an acute or chronic way. There are also different types of light qualities used such as energy-rich blue light or cool, white light with a similar emission spectrum like daylight (Grimm and Remé, 2013; Wenzel et al., 2005). In the current thesis, we used the acute protocol with cool white light to induce photoreceptor degeneration and to examine whether Endothelin receptor b has neuroprotective effects on photoreceptor cells and which underlying mechanisms might mediate this effect.

1.1.2 Neuroprotection in the retina following light-induced damage paradigm

Light-induced photoreceptor degeneration leads to the activation of Müller cells, which suggests the existence of a signalling system that informs Müller cells about the health status of photoreceptors and monitors the release of neuron-derived signalling molecules (Rattner and Nathans, 2005). Microarray analysis showed that transcripts

coding for *Endothelin 2* (*Et-2*) were highly upregulated following light induced damage (Rattner and Nathans, 2005). Its localization in the ONL was determined by using in situ hybridization, which indicates that photoreceptors react to excessive light exposure by the release of *Et-2* (Rattner and Nathans, 2005). A simultaneous upregulation of *Endothelin receptor b* (*Etb*) in Müller cells indicated that the release of *Et-2* leads to an activation of Müller cells via binding to Etb as response to light-induced damage (Rattner and Nathans, 2005).

Moreover, Müller cells react directly to photoreceptor cell stress by an upregulation of the neuroprotective factor leukemia inhibitory factor (Lif) (Joly et al., 2008; Gao and Hollyfield, 1996; Joly et al., 2007), which is essential for Müller cell activation and photoreceptors' survival (Joly et al., 2008; Gao and Hollyfield, 1996; Joly et al., 2007) Furthermore, Lif was also shown to interact with Et-2, as the expression of Et-2 reduced to 2% of wild-type levels in *Lif* deficient mouse retinae, as well with fibroblast growth factor 2 (Fgf2), as intravitreal injections of recombinant Lif lead to an induction of Et-2 and Fgf2 in wildtype and remarkably also in Lif-deficient mice, (Joly et al., 2008; Gao and Hollyfield, 1996; Joly et al., 2007). Fgf2 is considered to promote survival on photoreceptor cells in a paracrine manner in different models of photoreceptor degeneration (Faktorovich et al., 1990; Joly et al., 2007; Gao and Hollyfield, 1996). It is likely, that photoreceptor damage leads to the activation of Et-2 in photoreceptors, which mediates expression of Lif and Fgf-2 expression in Müller cells. As photoreceptor-derived Et-2 itself leads to an activation of Müller cells and in turn the expression of Lif, a positive feedback loop is very likely. Thus, the activation of Et-2 and its mediation of Lif and Fgf-2 expression is essential for retinal neuroprotection in response to photoreceptor degeneration.

1.2 The Endothelin system

In 1985, Hickey *et al.* first discovered a vasoconstricting factor obtained from the culture media of bovine aortic endothelial cells (Hickey et al., 1985). Three years later, Yanagisawa *et al.* identified the structure of this endothelin-derived vasoconstrictor and termed it endothelin (Yanagisawa et al., 1988). It is a 21-amino acid peptide linked with a free amino terminus and C-terminal carboxylic acid. This C-terminal helical tail seems to be crucial for receptor interaction, as well as two intramolecular disulfide bonds between Cys residues. Endothelin is expressed in three isoforms Endothelin 1, 2 and 3 (Et-1, Et-2, Et-3), which differ by the amount of amino acids (Davenport et al., 2016).

All three isoforms are first encoded as large precursor peptides (Prepro-Et-1/-2/-3) which are then abbreviated by 17 amino acids into proPeptides (proEt-1/2/3) by a signal peptidase. A second cleavage by furin enzymes removes 35 and 122 amino acids and

results in the immediate precursor of Endothelin (BigEt-1/2/3) (Xu et al., 1994). Its activation to mature Endothelin (Et-1/2/3) occurs via cleavage by membrane-bound metalloproteinases, the endothelin converting enzymes (ECE-1, ECE-2). Amongst the endothelin isoforms, Et-1 is the most extensively studied isoform and one of the most known potent vasoconstrictors (Yanagisawa et al., 1988).

Endothelins activate two main class I G-protein coupled receptor subtypes: endothelin receptor a (Eta) and b (Etb). ET-1 and ET-2 bind with equal affinity to the receptors, whereas Et-3 has a lower binding affinity for Eta (Sakurai et al., 1990; Arai et al., 1990; Barton and Yanagisawa, 2008; Kedzierski and Yanagisawa, 2001). Eta is predominantly expressed by vascular smooth muscle cells, whereas Etb is expressed by both vascular smooth muscle and endothelial cells (Guan et al., 2015). Given physiological conditions, the two receptors are considered to possess synergistic but also opposite actions with Eta and Etb promoting vasoconstriction by the release of calcium by the sarcoplasmic reticulum resulting in increased smooth muscle contraction and vasoconstriction (Schneider et al., 2007), whereas Etb on endothelial cells contributes additionally to vasodilation (Filep et al., 1991; Schneider et al., 2007; Hirata et al., 1993). In addition, Etb acts as clearing receptor of circulating Et-1 (Fukuroda et al., 1994a). Endothelin signaling is involved in a variety of physiological functions, above all the regulation of vasomotricity, blood pressure and vascular homeostasis (Rautureau et al., 2015).

1.2.1 Distribution of Endothelin signalling in the eye

In the eye, the expression of Et-1 is well described in tissues like lens epithelium, optic nerve , ciliary body, trabecular meshwork as well as vascular endothelial cells in the choroid and retina (Chakravarthy et al., 1994; Wollensak et al., 2002), whereas Et-2 is expressed by photoreceptors (Bramall et al., 2013; Alrashdi et al., 2018). The expression of Et-3 is barely known. It has been shown that Et-1 modulates pericyte contractility to regulate retinal blood flow (Kawamura et al., 2002, 2002) and is involved in the regulation of intraocular pressure and aqueous humor dynamics (Taniguchi et al., 1994) Eta and Etb are expressed on perivascular cells of retinal and choroidal blood vessels to promote vasoconstriction (Choritz et al., 2005; Torbidoni et al., 2005; MacCumber and D'Anna, 1994). Etb is additionally expressed on vascular endothelial cells to promote vasodilation (Clozel et al., 1992; Schneider et al., 2007). Furthermore, Etb is expressed on photoreceptors and Müller cells (Braunger et al., 2013a; Rattner and Nathans, 2005).

1.2.2 Diverse roles of Endothelin signalling in the ocular system

The role of the endothelin signalling in the eye is discussed controversially. Recently, our group and others could demonstrate its contribution to the protection of retinal neurons (Braunger et al., 2013a; Rattner and Nathans, 2005; Joly et al., 2007), with Et-2 being discussed to act as a general stress factor following photoreceptor damage and to mediate neuroprotection on photoreceptors in the light-induced damage model, presumably via Etb (Rattner and Nathans, 2005; Braunger et al., 2013a). However, there are conflicting reports concerning the protective properties of endothelin signalling, as it is dysregulated in several ocular diseases (Vingolo et al., 2010; Sorrentino et al., 2018; Good and Kahook, 2010). In particular, Et-1 has been suspected as contributing factor for the development of glaucoma as Et-1 levels were elevated in the aqueous humor (Noske et al., 1997; Tezel et al., 1997) and in the blood plasma of glaucoma patients (Li et al., 2016). The precise underlying mechanisms are still not fully understood, but it is discussed that Et-1 could promote ganglion cell death and contribute to optic nerve neuropathy through mechanisms of vascular dysregulation and (Krishnamoorthy et al., 2008; Lau et al., 2006). Furthermore, Et-2 is discussed to contribute to a breakdown of the blood retinal barrier with increased vascular leakage, vascular endothelial growth factor expression and infiltrating macrophages (Alrashdi et al., 2018). Thus, we aimed to examine the role of endothelin signaling in the retina in the current thesis.

2 Aim of study

This thesis focuses on Endothelin receptor b (Etb) mediated signalling and its potential neuroprotective function for the survival of photoreceptors. To this end, animals with an inducible, tamoxifen-dependent deletion of Etb in the entire retina (*Etb$^{\Delta eye}$*) and animals with a conditional deletion of Etb in retinal neurons and Müller cells (*Etb$^{\Delta OC}$*) will be generated using the Cre/*loxP* system. Additionally, an Etb-deficient murine photoreceptor cell line (*661W$^{\Delta Etb}$*) will be created via CRISPR/Cas9-System. A successful Etb-deletion in *Etb$^{\Delta eye}$* and *Etb$^{\Delta OC}$* mice and *661W$^{\Delta Etb}$* cells will be validated via molecular analysis (quantitative realtime RT-PCR and western blot analyses) and in situ hybridization (BaseScope®). To address this we will:

- We will characterize the localization of Etb in the eye

For a general characterization of the localization of Etb in the eye, we will first use wildtype albino (CD1) mice to examine the distribution of Etb in the murine eye by performing in situ hybridization (BaseScope®) and co-immunohistochemical staining for different retinal cell types (astrocytes: glial fibrillary acidic protein, Müller cells: glutamine synthetase, vasculature: Collagen IV).

- We will investigate the expression levels of the endothelin signalling family following ocular trauma

To this end, we will investigate the mRNA expression levels of the Endothelin signalling family following different damages of the retina or the eye, respectively (puncture of the eye, PBS-injection, light-induced photoreceptor degeneration).

- We will characterize the impact of an Etb deletion on the morphology of the eye and the molecular expression levels of the endothelin signalling family, the Tgf-β signalling family, pro-and anti-apoptotic factors and neuroprotective factors in the retina.

We will furthermore characterize the effect of the Etb-deficiency on the retinal architecture in *Etb$^{\Delta eye}$* and *Etb$^{\Delta OC}$* mice using semi-thin sections. To obtain statistically meaningful data, we will perform morphometric analyses and measure the thickness of the INL and ONL to generate Spider diagrams. We will analyse the morphology and a

potential leakiness of the retinal vessels in *Etb$^{\Delta eye}$* and *Etb$^{\Delta OC}$* mice by high molecular FITC-dextran perfusion, and immunohistochemical staining for their basal lamina (collagen IV) and for pericytes (neuron glia antigen 2 (Ng-2)). We will complete these analyses by studying the mRNA expression levels of the endothelial cell maker cluster of differentiation 31 (Cd31) and the perivascular cell markers alpha smooth muscle actin (α-Sma), neuron glia antigen 2 (Ng-2) and platelet-derived growth factor receptor beta (Pdgfrb). Moreover, we will analyse whether the Etb deletion might result in retinal hypoxia using hypoxia-inducible factor 1 alpha (Hif1α) western blot analyses. We will furthermore use specific antibodies (glial fibrillary acidic protein (Gfap) and ionized calcium-binding adapter molecule 1 (Iba1)) for immunohistochemical staining to analyse whether the deletion of Etb in *Etb$^{\Delta eye}$* and *Etb$^{\Delta OC}$* mice might influence the reactivity of Müller cells or microglia cells. To study whether the deletion of Etb will affect the mRNA expression levels of the other members of the Endothelin signalling pathway we will analyse their expression levels (*Endothelin receptor type a (Eta), Endothelin 1/2/3 (Et-1/-2-3*). In addition, we will analyse the mRNA expression levels of the transforming growth factor beta signalling pathway (*Tgf-β receptor 1 (Tgfbr1)*, *Tgf-β receptor* 2 (*Tgfbr2)*, *Tgf-β 1, Tgf-β 2, Tgf-β 3*), pro-apoptotic factors (*Caspase 8*, *Caspase 9*, *BH3-only BCL-2-interacting mediator of cell death (Bim)*, *Bcl2 associated X (Bax), Bcl2 associated death promotor (Bad))* and the anti-apoptotic factor *B-Cell Lymphoma 2 (Bcl2)* as well neuroprotective factors (*leukaemia inhibitory factor (Lif), fibroblast growth factor 2 (Fgf2))* .

Proteomic analyses of *661W$^{\Delta Etb}$* cells and controls will give unbiased and hypothesis-free information about the impact of an Etb deletion in photoreceptor cells.

- We will investigate a potential neuroprotective role of Etb mediated signalling for the survival of photoreceptors.

Therefore, we will use the light damage paradigm to induce photoreceptor apoptosis in *Etb$^{\Delta OC}$* mice and controls. We will additionally cause cell stress by serum-deprivation in *661W$^{\Delta Etb}$* cells and controls to induce their apoptosis. TUNEL labelling will be used to detect apoptotic cells and we will quantify the TUNEL labelled apoptotic cells to clarify, whether the apoptotic rate might be altered in Etb-deficient mice and *661W$^{\Delta Etb}$* cells compared to their respective controls. Furthermore, we will use semi-thin sections to investigate the retinal morphology and perform morphometric analyses to compare the thickness of the ONL between light-exposed *Etb$^{\Delta OC}$* mice and light-exposed controls. To learn more about the underlying molecular mechanisms, the transcript levels of the

members of the Endothelin signalling family (*Eta, Et-1/-2/-3*), transforming growth factor beta signalling pathway (*Tgf-βr1*, *Tgf-βr2*, Tgf-*β 1*, *Tgf-β 2*, *Tgf-β 3*), pro-apoptotic factors (*Caspase 8*, *Caspase 9*, *Bim, Bad, Bax)* and the anti-apoptotic factor *Bcl2* as well neuroprotective factors (*Lif, Fgf2)* will be examined by quantitative realtime RT-PCR. Western blot analyses for the cell survival factor Protein Kinase B (Akt) and its phosphorylated (p) form pAkt, a main component of the PI3K-Akt pathway, will be performed in light-exposed $Etb^{\Delta OC}$ mice and controls to clarify whether Etb might use this signalling pathway to mediate its neuroprotective effect.

3 Results

3.1 Expression of Endothelin receptor b in the eye

Initially, we used 6-week old albino (CD1) wildtype mice to study the expression and localization of *Etb* in the eye.

We first performed quantitative real-time RT-PCR of retinal lysates to detect the relative mRNA expression levels of *Endothelin receptor a* (*Eta*) and *Endothelin receptor b* (*Etb*) in the retina. Both receptors were detectable in the retina of wildtype mice (Figure 5). Quite intriguingly, *Etb* was identified as predominant receptor in the retina as the relative mRNA expression level of *Etb* (24.34 ± 3.34) was significantly (p=0.02) higher than *Eta* mRNA expression (9.72 ± 3.01).

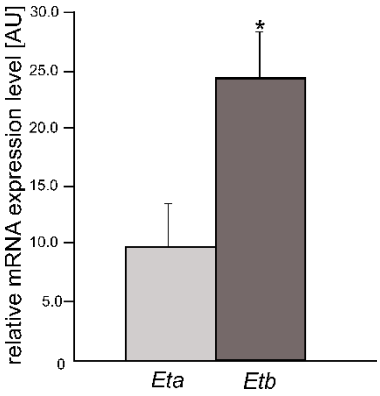

Figure 5 Relative mRNA expression of *Eta* and *Etb* in the retina.
Both receptors were detectable, but *Etb* was identified as predominant receptor with a significantly higher expression than *Eta*. The mean value of the housekeeping genes *Gapdh* and *Gnb2l* was used for normalization. Data are means ± SEM. Eta n = 6; Etb n = 4; p* = 0.02, student's t-test.

Next, we performed in situ hybridization BaseScope® (Chapter 6.5.7); which was friendly provided by Prof. Dr. Charlotte Wagner (University Regensburg, Germany) on sagittal sections of the entire eye to detect the mRNA signal of *Etb* and further localize *Etb* in the entire eye via conventional fluorescent microscopy (Figure 6 A-F). In the retina (A), the *Etb* signal was confined to the retinal ganglion cell layer (GCL), inner nuclear layer (INL), outer nuclear layer (ONL) and retinal pigment epithelium (RPE).There was also a distinct *Etb* mRNA signal detectable in the lens (B), strictly defined to the lens epithelium and lens fibres, whereas *Etb* signal was not visible in the lens capsule. In the iris (C), the *Etb* mRNA signal was only traceable in the stroma, whereas the iris epithelium had no signal for *Etb*. Furthermore, there were *Etb* mRNA signals in the entire cornea (D) detectable. The corneal epithelium as well endothelium showed intense *Etb* signals, whereas the stroma had less positive *Etb* mRNA signals. The entire ciliary body (E) showed an intense signal for *Etb*, in its pigmented as well as its non-pigmented epithelium. Furthermore, intense *Etb* mRNA signals were detected in the entire area of the optic nerve head and the optic nerve (F).

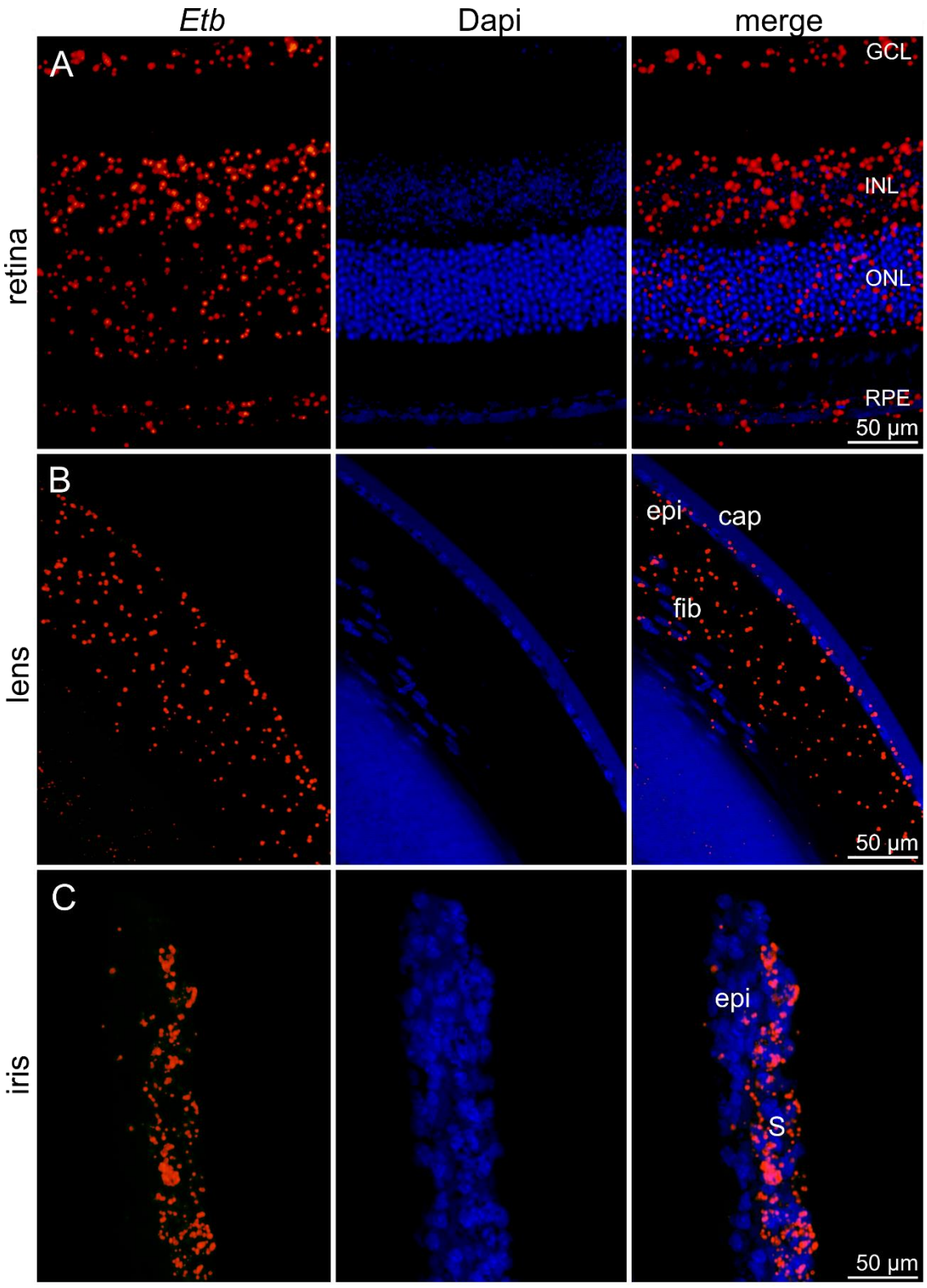
Etb
Dapi
merge
A
retina
GCL
INL
ONL
RPE
50 µm
B
lens
epi
cap
fib
50 µm
C
iris
epi
S
50 µm

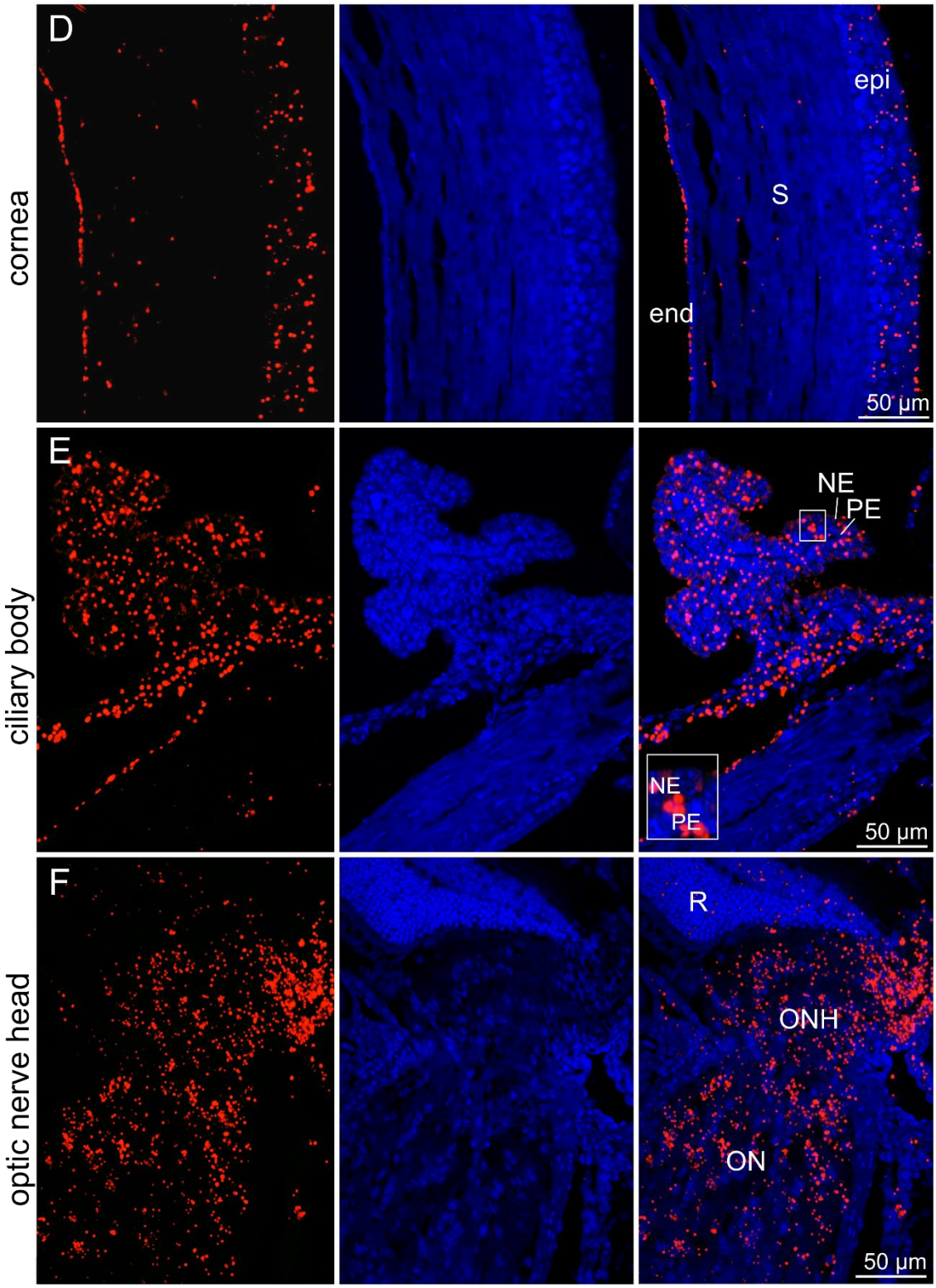

Figure 6 In situ hybridization BaseScope® of a 6-week old wildtype mouse.*Etb* mRNA signal (red); Nuclei were Dapi stained (blue). (A) Retina. There was an *Etb* mRNA signal in several layers of the retina detectable. GCL=ganglion cell layer, INL=inner nuclear layer, ONL=outer nuclear layer, RPE=retinal pigment epithelium (B) Lens. *Etb* was located in the lens epithelium as well as lens fibres, but not in the capsule. epi= epithelium, fib= lens fibres, cap=capsule (C) Iris. Only the iridal stroma depicted a positive *Etb* mRNA signal. epi= epithelium, S= stroma (D) Cornea. *Etb* was detectable in the entire cornea. epi= epithelium, S= stroma, end= endothelium (E) Ciliary body. *Etb* was detectable in the entire ciliary body. PE= pigmented epithelium, NE= non-pigmented epithelium (F) Optic nerve head. *Etb* was detectable in the entire area of the optic nerve head. R=retina, ONH=optic nerve head, ON=optic nerve

For a cell-specific *Etb* localization in the retina, the in situ hybridization BaseScope®-labelled sagittal sections were co-stained against Glial fibrillary acidic protein (Gfap) (Figure 7 A), a marker for astrocytes and reactive Müller cells and glutamine synthetase (Gs) (Figure 7 B), a Müller cell specific marker. Again, a positive *Etb* mRNA signal was detected in the GCL, INL and ONL, indicating a localization on neurons and photoreceptor cells. Immunohistochemical staining against Gfap (Figure 7 A) revealed a characteristic staining on top of the GCL, the typical localization of astrocytes. Here, no *Etb* mRNA signal was detectable, showing that astrocytes did not express *Etb* in the retina. The immunohistochemical staining against Gs (Figure 7 B) displayed the regular pattern of Gs Müller glia staining in the inner plexiform layer as well a distinct staining along the elongated glia processes stretching through the entire retina from the inner limiting membrane to the outer limiting membrane. Here, the *Etb* mRNA signal partly overlapped with GS within the inner plexiform layer and additionally in the region of the GCL, where the Müller cell endfeet are located, indicating an *Etb* expression in Müller cells, especially in their end feet.

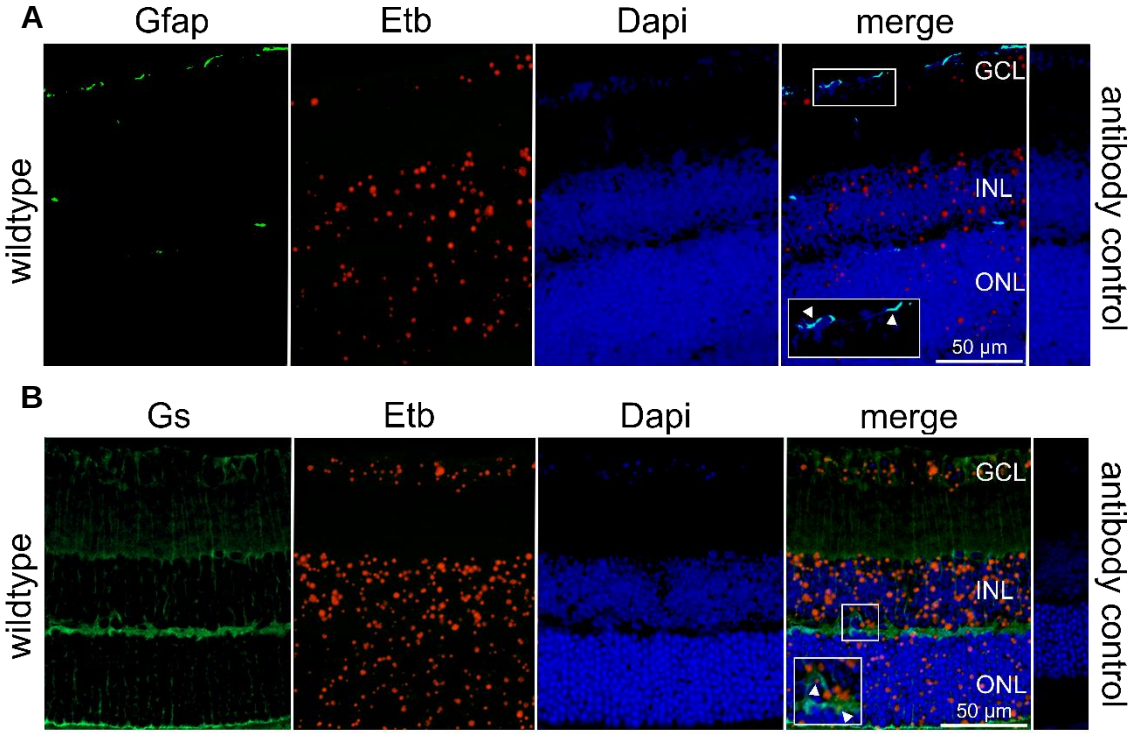

Figure 7 (A) In situ hybridization BaseScope® (red) and immunohistochemical staining against Gfap (green) of a 6 week-old wildtype mouse.Immunohistochemical staining against Gfap revealed a characteristic staining on top of the ganglion cell layer (GCL), the typical localization of astrocytes. Here, no *Etb* signal was detectable (detailed magnification, arrows) indicating that astrocytes do not express Etb. (B) In situ hybridization BaseScope® (red) and immunohistochemical staining against Gs (green) of a 6 week-old wildtype mouse. Gs staining displayed the regular pattern of Gs Müller glia staining with a distinct staining along the elongated glia processes stretching through the entire retina from the inner limiting membrane to the outer limiting membrane. *Etb* mRNA signal partly overlapped within the inner plexiform layer (detailed magnification, arrows) and additionally the GCL, indicating an Etb expression in Müller cells. GCL =ganglion cell layer, INL = inner nuclear layer, ONL = outer nuclear layer, RPE = retinal pigment epithelium. Nuclei were Dapi stained (blue). In situ hybridization BaseScope® was performed in cooperation with Dr. Thomas Neder (University Regensburg)

Next, we performed immunohistochemical staining against Collagen IV, an abundant protein of the basal lamina of blood vessels, that encloses endothelial cells located on the inner (luminal) side of the basal lamina, and perivascular cells still enclosed by the Collagen IV positive basal lamina but located at the outside of the vascular lumen. Thus, Collagen IV is a reliable marker to label the retinal vasculature and to distinguish between endothelial and perivascular cells, based on their inner (endothelial cells) or outer (perivascular cells) luminal position. E.g. positive Collagen IV staining was detected in retinal vessels located in the GCL showing a distinct *Etb* mRNA expression on the luminal side of the retinal vessels, indicating that *Etb* is expressed in retinal endothelial cells. Furthermore, we detected *Etb* positive signals at the outer luminal side of the vessels indicating the expression of *Etb* in perivascular cells.

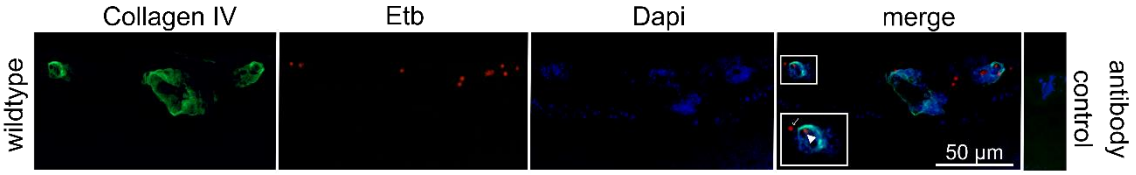

Figure 8 In situ hybridization BaseScope® (red) and immunohistochemical staining against Collagen IV (green) of a 6 week-old wildtype mouse.Collagen IV positive staining (green) was detected in retinal vessels located in the GCL showing a distinct *Etb* mRNA expression on the luminal side of the retinal vessels, indicating that *Etb* is expressed in retinal endothelial cells (arrowheads). Furthermore, we detected *Etb* positive signals at the outer luminal side of the vessels indicating the expression of *Etb* in perivascular cells (arrows). GCL =ganglion cell layer, INL = inner nuclear layer, ONL = outer nuclear layer, RPE = retinal pigment epithelium. Nuclei were Dapi stained (blue).

3.2 Role of Endothelin signalling in the damaged retina

Our workgroup and other already showed that *Et-2* is upregulated in experimentally induced photoreceptor degeneration (Braunger et al., 2013a; Rattner and Nathans, 2005; Joly et al., 2007). We aimed to characterize the role of the entire Endothelin signalling pathway in the damaged retina and therefore performed three different experimental setups leading to induce a retinal damage: Puncture of the eye (wildtype puncture, Figure 9 A) intravitreal injections of PBS (wildtype PBS,Figure 9 B) and light-induced damage (wildtype light, Figure 10)

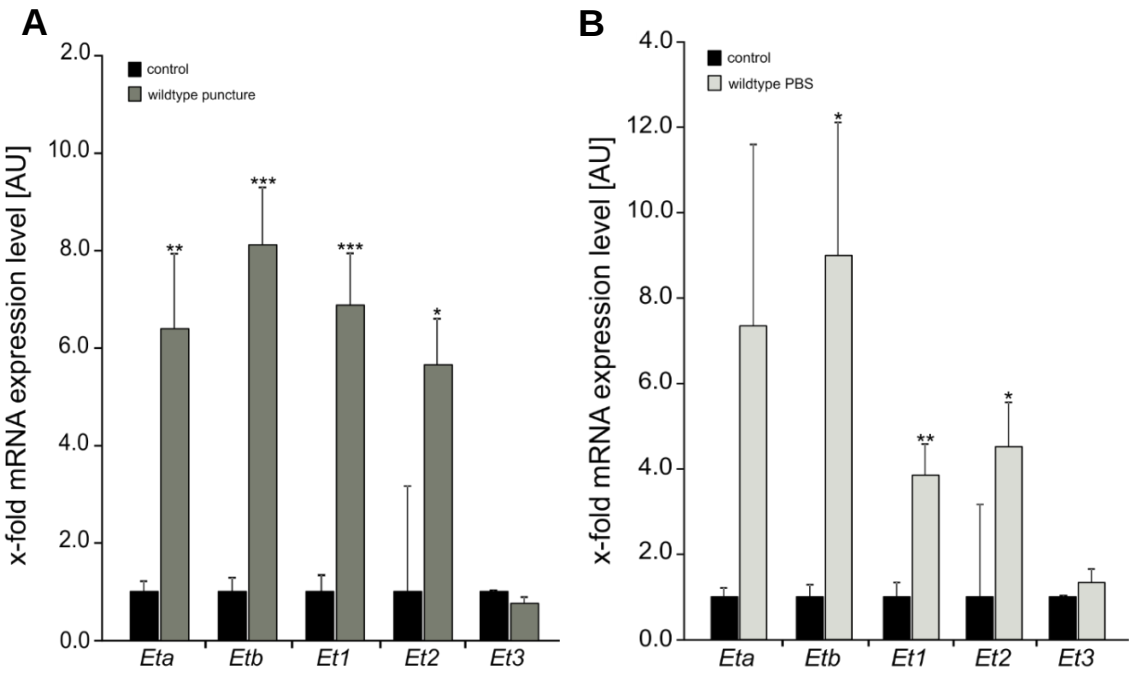

Figure 9 Quantitative real-time RT-PCR of retinal lysates of 6 to 8-week old wildtype mice (A) relative mRNA expression levels of *Eta*, *Etb*, *Et-1* and *Et2* were significantly elevated after the solely puncture of the eye into the vitreous (wildtype puncture) compared to controls. (B) The intravitreal injection with PBS (wildtype PBS) resulted in significantly elevated mRNA expression levels of *Eta*, *Etb*, *Et1* and *Et2* compared to controls. Expression was normalized to *Gnb2l*. Data are means ± SEM. Wildtype puncture: *Eta* (n≥ 3; *p***=0.005), *Etb* (n≥ 3; *p****=0.00005), *Et1* (n≥ 4; *p****=0.0001), *Et2* (n≥ 2; *p**=0.04), *Et3* (n≥ 3; *p*=0.7 (not significant); wildtype PBS: *Eta* (n≥ 3; *p*=0.09 (not significant)), *Etb* (n≥ 3; *p**=0.02), *Et1* (n≥ 4; *p***=0.003), *Et2* (n≥ 2; *p**=0.05), *Et3* (n≥ 3); *p*=0.6 (not significant). Student's t test. [AU]= arbitrary unit; Figures taken from Schmitt et al. New insights into endothelin signalling and its diverse roles in the retina, in press. Experiment performed by Sabrina Schmitt

Quite intriguingly, the sole puncture of the bulbus (wildtype puncture) led to significantly elevated mRNA expression levels of *Eta* (6.40 ± 1.53, *p***=0.005) and *Etb* (8.34 ± 1.01, *p****=0.00005) as well as *Et-1* (6.89 ± 1.05, *p****=0.0001) and *Et-2* (5.66 ± 0.93, *p* *=0.04) compared to untreated controls (*Eta*: 1.00 ± 0.21; *Etb*: 1.00 ± 0.28; *Et-1*: 1.00 ± 0.33; *Et-2*: 1.00 ± 3.57). The relative mRNA expression of *Et3* remained unaffected (control: 1.00 ± 0.02; wildtype PBS: 1.33 ± 0.32, *p*=0.7). Mice that received additionally an intravitreal injection of 3 µl PBS (wildtype PBS) showed a comparably increased relative mRNA

expression of *Eta* (7.34 ± 4.25, *p*=0.09) and a significant increase of *Etb* (8.99 ± 3.12, *p**=0.02), *Et-1* (3.85 ± 0.73, *p***=0.003) and *Et-2* (4.52 ± 0.95, *p**=0.05) compared to untreated controls (*Eta*: 1.00 ± 0.21; *Etb*: 1.00 ± 0.28; *Et1*: 1.00 ± 0.33; *Et2*: 1.00 ± 3.57). Again, the relative mRNA expression level of *Et-3* (control: 1.00 ± 0.02, wildtype PBS: 1.33 ± 0.32, *p*=0.6) remained unaffected.

Quite similarly, the light exposed mice (Figure 10) showed significantly elevated mRNA expression levels of *Eta* (10.15 ± 2.69, *p***=0.004)*, Etb* (7.10 ± 3.31, *p**=0.05)*, Et-1* (4.77 ± 0.56, *p****=0.0004) and predominantly, an up to 36-fold increase of *Et-2* (36.37 ± 2.32, *p***=0.002) compared to controls (*Eta*: 1.00 ± 0.22; *Etb*: 1.00 ± 0.30; *Et-1*: 1.00 ± 0.37; *Et-2*: 1.00 ± 3.60). However, *Et-3* (control: 1.00 ± 0.01, wildtype light: 1.2 ± 0.40, *p*=0.7) expression levels were not significantly altered following experimentally induced photoreceptor degeneration. Taken together, our results show, that endothelin signaling is upregulated following various retinal damages, indicating that the endothelin signaling pathway may act neuroprotective in the retina.

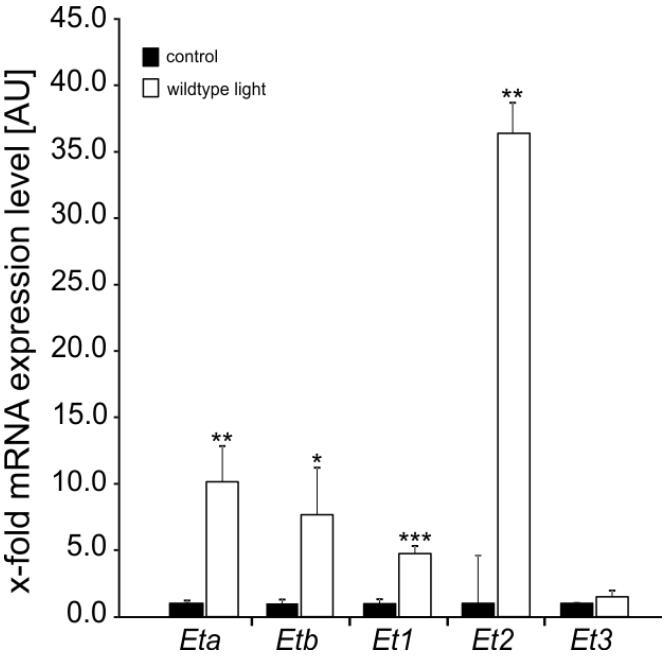

Figure 10 Quantitative real-time RT-PCR of 6 to 8-week old albino mice after light-induced damage.Relative mRNA expression levels of *Eta*, *Etb*, *Et1* and *Et2* are significantly upregulated after light-induced damage (wildtype light) compared to controls that were not exposed to light. Expression was normalized to Gnb2l. Data are means ± SEM. *Eta* (n≥ 3; *p***=0.004), *Etb* (n≥ 4; *p**=0.05), *Et1* (n≥ 4; *p****=0.0004), *Et2* (n≥ 3; *p***=0.002), *Et3* (n≥ 4; *p*=0.7. Student's t test. [AU]= arbitrary unit. Figures taken from Schmitt et al. New insights into endothelin signalling and its diverse roles in the retina, in press. Experiment performed by Sabrina Schmitt

3.3 Etb-deficiency *in vitro* and *in vivo*

To analyse the potential neuroprotective effect of Etb on photoreceptor cells in detail, we generated two mouse strains, one with a conditional deletion of Etb in the entire retina (*Etb*$^{\Delta eye}$ mice) and a second mouse strain with a cell type specific deletion in Müller cells and retinal neurons (*Etb*$^{\Delta OC}$ mice) via the CreloxP-System. Furthermore, we generated a stable Etb deletion in a photoreceptor cell line (*661W*$^{\Delta Etb}$) via the CRISPR/Cas9-System to further study its physiological and molecular function.

3.3.1 Characterization of *Etb*$^{\Delta eye}$ mice

For simplicity, *Etb*$^{flox/flox}$ mice lacking the Cre recombinase are referred to as controls and *Etb*$^{flox/flox}$ mice expressing Cre recombinase are referred to as *Etb*$^{\Delta eye}$ or conditional knockout mice.

3.3.1.1 Successful deletion of Endothelin receptor b in the entire retina

To activate the CAG-CreER^{TM}-Recombinase and thereby induce the conditional deletion of Etb in the entire retina via the CreloxP-System (Chapter 6.1.2), all mice were injected intraperitoneally with tamoxifen [20mg/ml] at the age of 4 weeks twice a day for five days. The mice were sacrificed at the age of 6 weeks for further analyses.

The relative mRNA expression levels of *Etb* in retinal tissue of *Etb*$^{\Delta eye}$ mice and controls were compared via quantitative real-time RT-PCR analysis. The mean value of the housekeeping genes *Gapdh* and *Gnb2l* was used for normalization. A significant (p = 0.001) decrease of 87% of the relative *Etb* mRNA expression level in the *Etb*$^{\Delta eye}$ mice (0.13 ± 0.30) compared to controls (1.00 ± 0.16) confirmed a successful deletion of Etb in the entire retina (Figure 11 A).

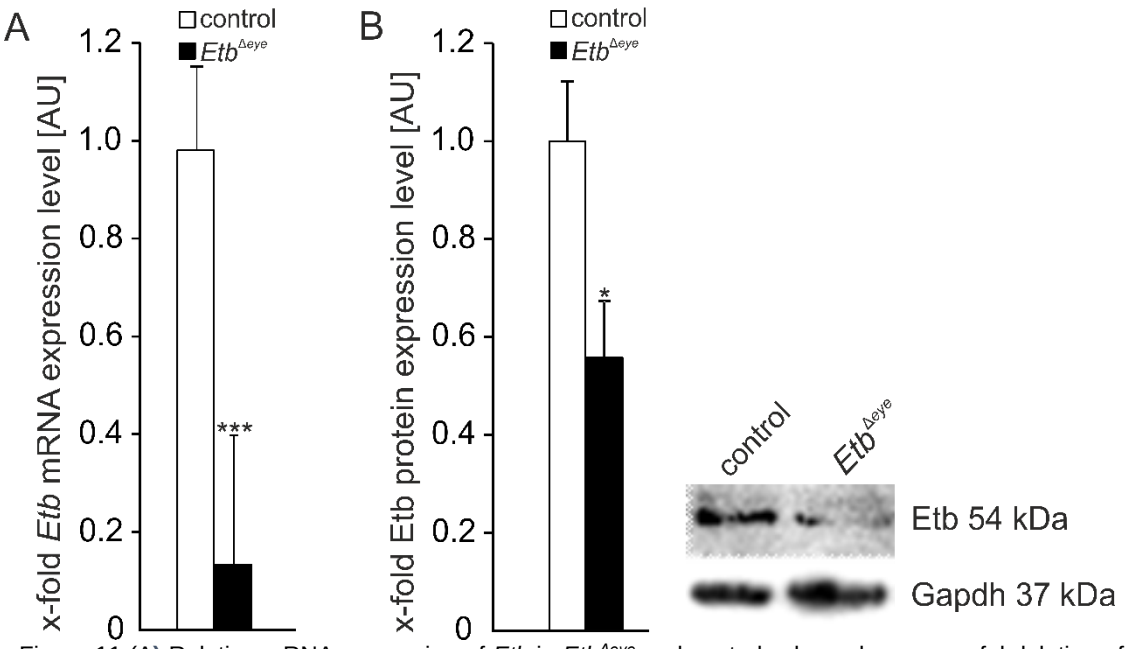

Figure 11 (A) Relative mRNA expression of *Etb* in *Etb*$^{\Delta eye}$ and controls showed a successful deletion of Etb in the entire retina following tamoxifen treatment. Mice with a conditional deletion of Etb expressed significantly lower amounts of *Etb* mRNA in the retina compared to controls. The mean value of the housekeeping genes *Gapdh* and *Gnb2l* were used for normalization. Data are means ± SEM. control n = 4; *Etb*$^{\Delta eye}$ n = 4; *p**** = 0.001, student's t-test. (B) Western blot analysis of retinal lysates and densitometry of Etb in *Etb*$^{\Delta eye}$ and controls following tamoxifen treatment. Significant decrease of Etb expression in the entire retina after tamoxifen treatment in *Etb*$^{\Delta eye}$ mice compared to controls. Gapdh was used as housekeeping protein. Data are means ± SEM. control n = 6, *Etb*$^{\Delta eye}$ n = 4; *p** = 0.03, student's t-test; Experiments were performed by Anna Huber and Sabrina Schmitt

The densitometric analysis of the relative protein expression level of Etb (54 kDa) showed a significantly (*p** = 0.03) decreased expression of Etb in *Etb*$^{\Delta eye}$ mice (0.55 ± 0.12) compared to controls (1.00 ± 0.12) again confirming the successful deletion of Etb in the entire retina (Figure 11). Gapdh (37 kDa) was used as housekeeping gene.

To further verify a successful deletion of *Etb* we performed in situ hybridization BaseScope® on sagittal sections, to detect mRNA signal of *Etb* and to precisely localize potentially remaining *Etb* in retina (Figure 12). In control mice, *Etb* was distributed throughout the entire retina (Figure 12 A). The detailed magnification (Figure 12 B) showed *Etb* mRNA signals as described before (Figure 6). In contrast, there was no *Etb* mRNA signal detectable in *Etb*$^{\Delta eye}$ mice validating a successful deletion of *Etb* in the retina of conditional knockout mice.

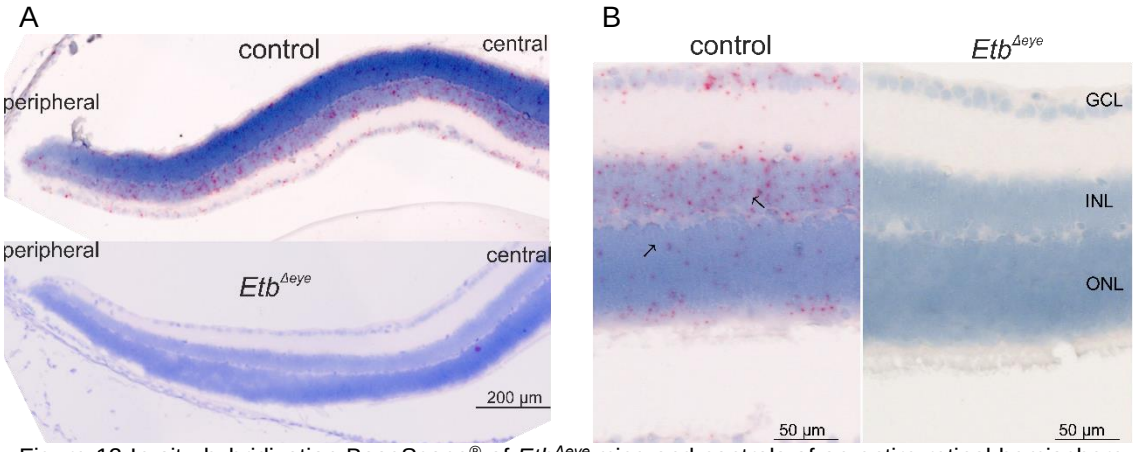

Figure 12 In situ hybridization BaseScope® of *Etb*$^{\Delta eye}$ mice and controls of an entire retinal hemisphere (A) and detailed magnification (B). Control mice showed an *Etb* mRNA signal (red spots, arrows) in the ganglion cell layer (GCL), inner nuclear layer (INL) and outer nuclear layer (ONL). Nuclei were stained with haematoxylin.

3.3.1.2 No obvious alterations on retinal morphology following Etb-deficiency

To examine whether the deletion of *Etb* in the entire retina influenced the retinal structure, we used conventional light microscopy to analyse the retinal morphology on Richardson stained horizontal semithin sections (1µm) of 6 week-old (Figure 13 A) *Etb*$^{\Delta eye}$ mice and controls.

The control mice as well as *Etb*$^{\Delta eye}$ mice both showed a normal architecture of the retina with all retinal layers present along the entire hemisphere (Figure 13 A).

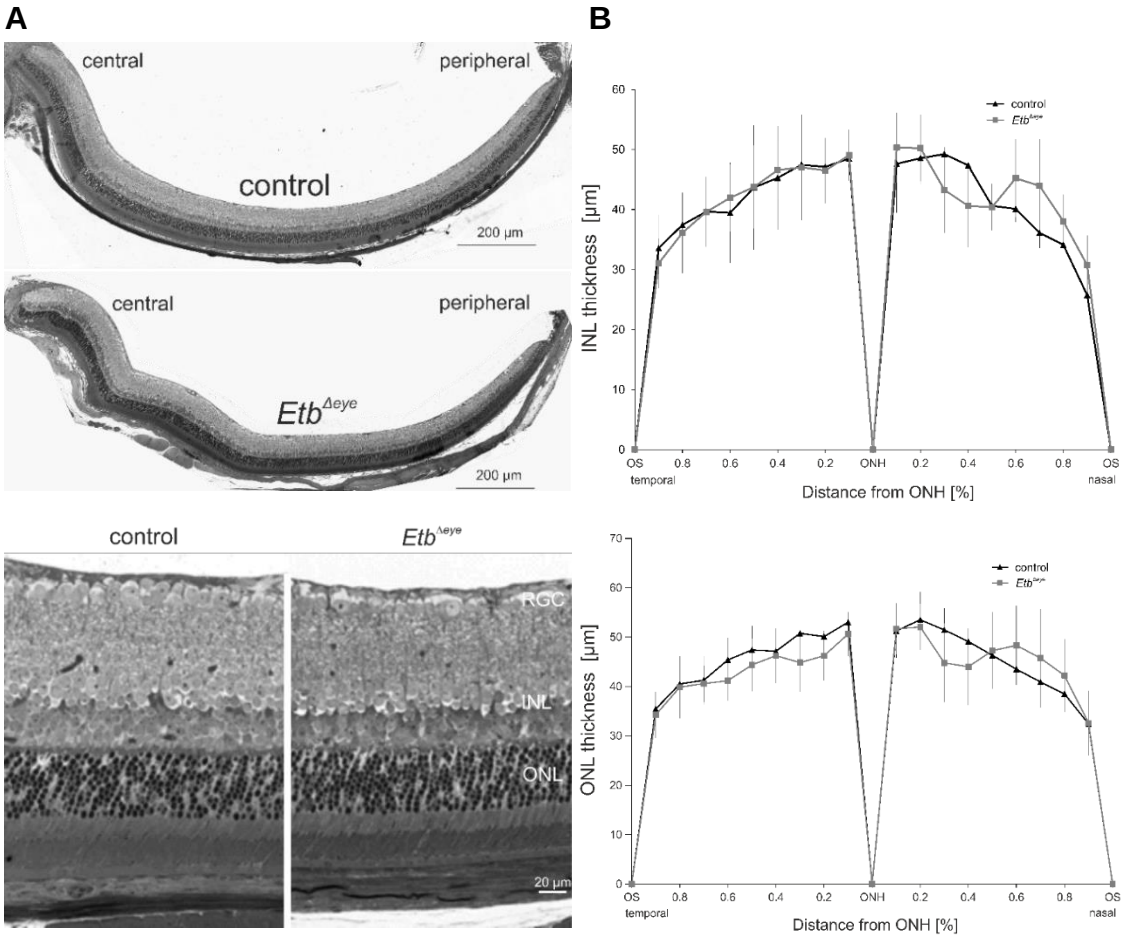

Figure 13 (A) Semithin-sections of a 6 week-old *Etb*$^{\Delta eye}$ mouse and controls. Horizontal (1µm) semithin-sections (Richardson stained) of retinal hemispheres showed no obvious alterations of retinal morphology. Lower panel shows a higher magnification of the central retina. RGC =retinal ganglion cell layer, INL = inner nuclear layer, ONL = outer nuclear layer, RPE = retinal pigment epithelium. (B) Spider diagram of the thickness of the INL and ONL in *Etb*$^{\Delta eye}$ mice and controls. The thickness of the ONL and INL was measured on semithin-sections at defined measure points from ora serrata to the optic nerve head. There were no differences in the thickness of ONL as well as INL detectable between *Etb*$^{\Delta eye}$ mice (n=6, $p > 0.05$ (not significant)) and controls (n=4, $p > 0.05$ (not significant)). OS = ora serrata; ONH = optic nerve head. Data are means ± SEM, student's t-test; Experiments were performed by Anna Huber and Sabrina Schmitt

For further quantification, the thickness of the ONL and INL was measured at defined, different measure points throughout the retinal hemispheres and their means were represented in a spider diagram (Figure 13 B). Following statistical analyses, the thickness of ONL and INL did not differ between conditional knockout mice and the controls.

3.3.1.3 Lens phenotype: Pathological morphology of the lens

Quite intriguingly, some of the *Etb*$^{\Delta eye}$ mice showed abnormalities of the lens, whereas all controls exhibited normal formed lenses. Semithin sections (Figure 13) of the entire eye showed a collapsed, vacuolated structure of the lens of *Etb*$^{\Delta eye}$ mice compared to controls. Presumably, a rupture of the lens capsule led to a release of lenticular material

in the vitreous. We furthermore observed scarring material in the raptured areas. This identifies a severe phenotype in the lens. Quantitative evaluation of the occurrence of this phenomenon demonstrated that lens abnormalities occurred in 30% of *Etb*$^{\Delta eye}$ mice, whereas the remaining 70% *Etb*$^{\Delta eye}$ mice manifested lenses with normal appearance.

Figure 14 Semithin-sections of the entire eye of 6 week-old control mouse.(A) *Etb*$^{\Delta eye}$ mouse without a lens-specific phenotype (*Etb*$^{\Delta eye}$) and a *Etb*$^{\Delta eye}$ mouse with a lens-specific phenotype (*Etb*$^{\Delta eye}$ phenotype). The *Etb*$^{\Delta eye}$ phenotype eye demonstrates a collapsed, vacuolated structure of the lens with a rupture of the lens capsule (arrows). Horizontal (1µm) semithin- sections were Richardson stained.

To further examine the constitution of the lens capsule, we labelled lenses of control mice, *Etb*$^{\Delta eye}$ mice without phenotype and *Etb*$^{\Delta eye}$ mice with phenotype against Collagen IV, a main constituent of the lens capsule. All sections were recorded at the identic exposure time via conventional fluorescence microscopy (Figure 15). Control mice showed a distinct Collagen IV expression on top of the lens capsule, whereas fluorescence intensity was attenuated in *Etb*$^{\Delta eye}$ mice without any phenotype. Remarkably, *Etb*$^{\Delta eye}$ mice with phenotype showed only a punctually Collagen IV expression with slight intensity on top of the lens capsule. For further investigations, only *Etb*$^{\Delta eye}$ mice without phenotype were used.

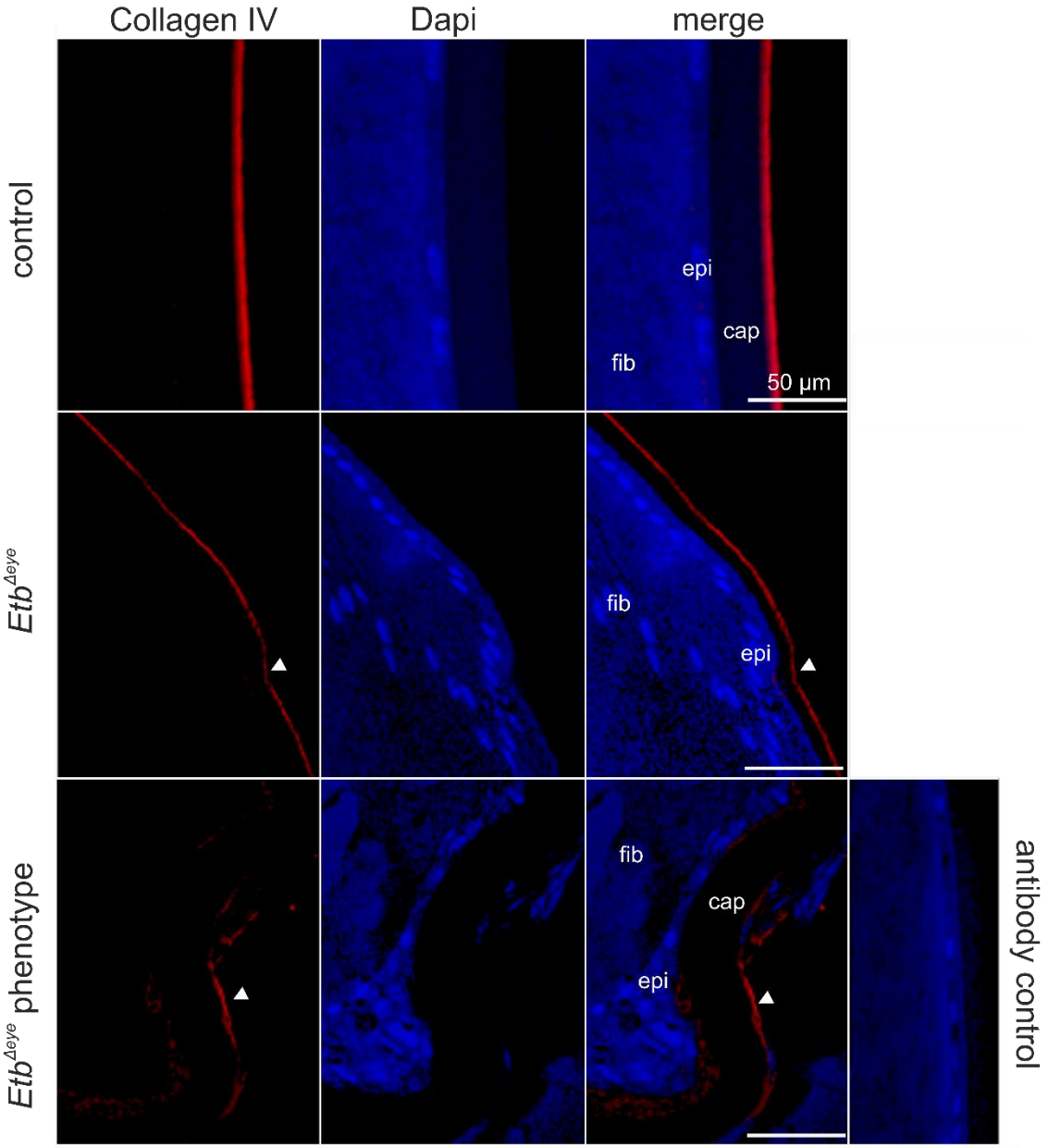

Figure 15 Immunohistochemical staining against Collagen IV (red) of the lens in a *Etb*$^{\Delta eye}$ mouse (with phenotype and without phenotype) and controls. Detailed magnification of the lens showed Collagen IV expression in the lens capsule (cap). Fluorescence intensity weakens in *Etb*$^{\Delta eye}$ mice without phenotype compared to controls (arrow). *Etb*$^{\Delta eye}$ mice with occurring phenotype only showed punctually Collagen IV expression (arrow). Nuclei were Dapi stained. fib = lens fibres; epi = lens epithelium, cap = capsule

3.3.1.4 No obvious alterations on retinal vasculature following Etb-deficiency

Endothelin signalling is involved in the regulation of vasomotricity, blood pressure and vascular homeostasis. As Endothelin usually acts in a vasoactive manner, the two receptors (Eta and Etb) are considered to possess opposite actions with Eta and Etb mainly promoting vasoconstriction, whereas Etb contributes additionally to vasodilation

under physiological conditions (Schneider et al., 2007). Consequently, we aimed to analyze the influence of the Etb-deficiency on the retinal vasculature.

We first stained sagittal sections of *Etb*$^{\Delta eye}$ mice and controls against Collagen IV (Figure 16), which is the most abundant protein of the basal lamina of blood vessels and thus a reliable target to label retinal vasculature.

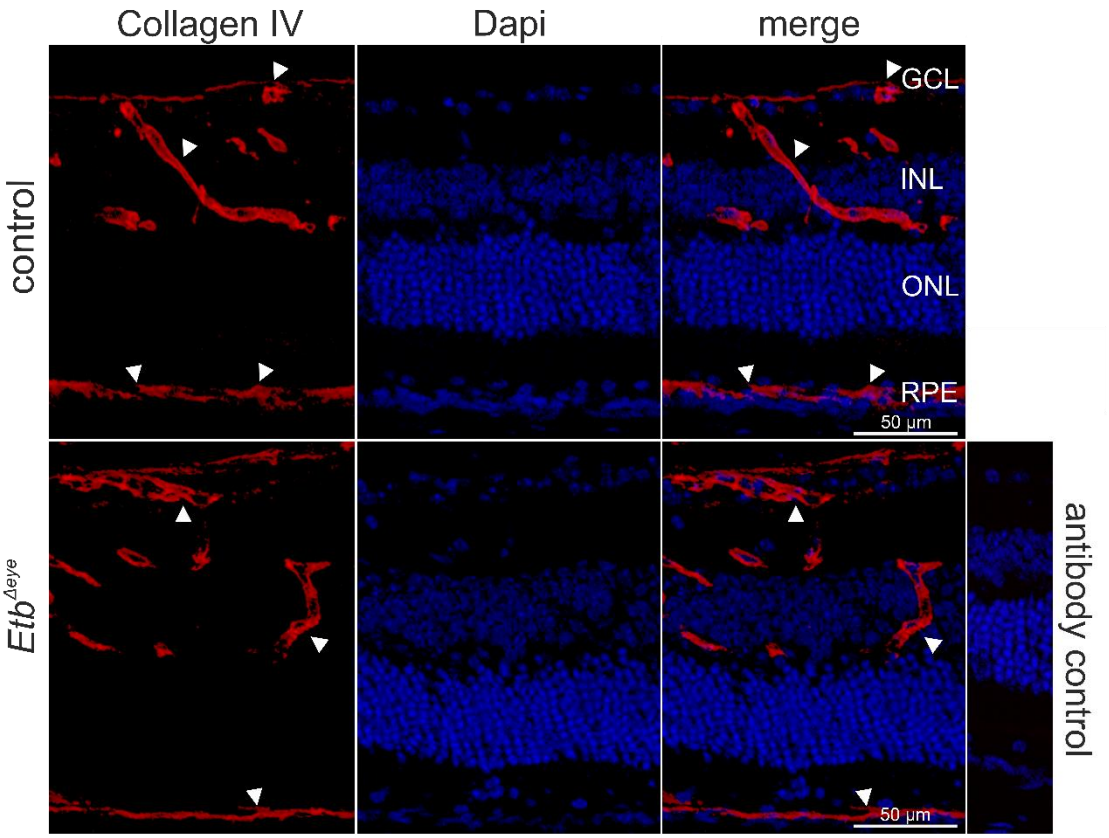

Figure 16 Immunohistochemichal staining against Collagen IV in an *Etb*$^{\Delta eye}$ mouse and control showed no alterations of the retinal vasculature with a regular deep, intermediate and superficial plexus (white arrows). GCL =ganglion cell layer, INL = inner nuclear layer, ONL = outer nuclear layer, RPE = retinal pigment epithelium. Nuclei were Dapi stained; Experiment performed by Anna Huber and Sabrina Schmitt.

There were no obvious alterations detectable in the three capillary plexus of the retinal vessels in *Etb*$^{\Delta eye}$ mice compared to controls. A regular deep and intermediate capillary plexus at the INL as well as a normal developed superficial plexus on top of the GCL were observed. Furthermore, an intact, continuous choriocapillaris was labelled next to the basal side of the RPE.

The choriocapillaris was additionally examined by labelling retinal sagittal sections against Plasmalemma Vesicle-Associated Protein (Pv-1). Pv-1 is involved in the formation of stomatal and fenestral diaphragms and may function in microvascular permeability. Diaphragmed fenestrae are characteristic structural elements of all fenestrated endothelia like the choriocapillaris in the eye. Pv-1 staining (white arrows, Figure 17) showed no obvious alterations in *Etb*$^{\Delta eye}$ mice and controls.

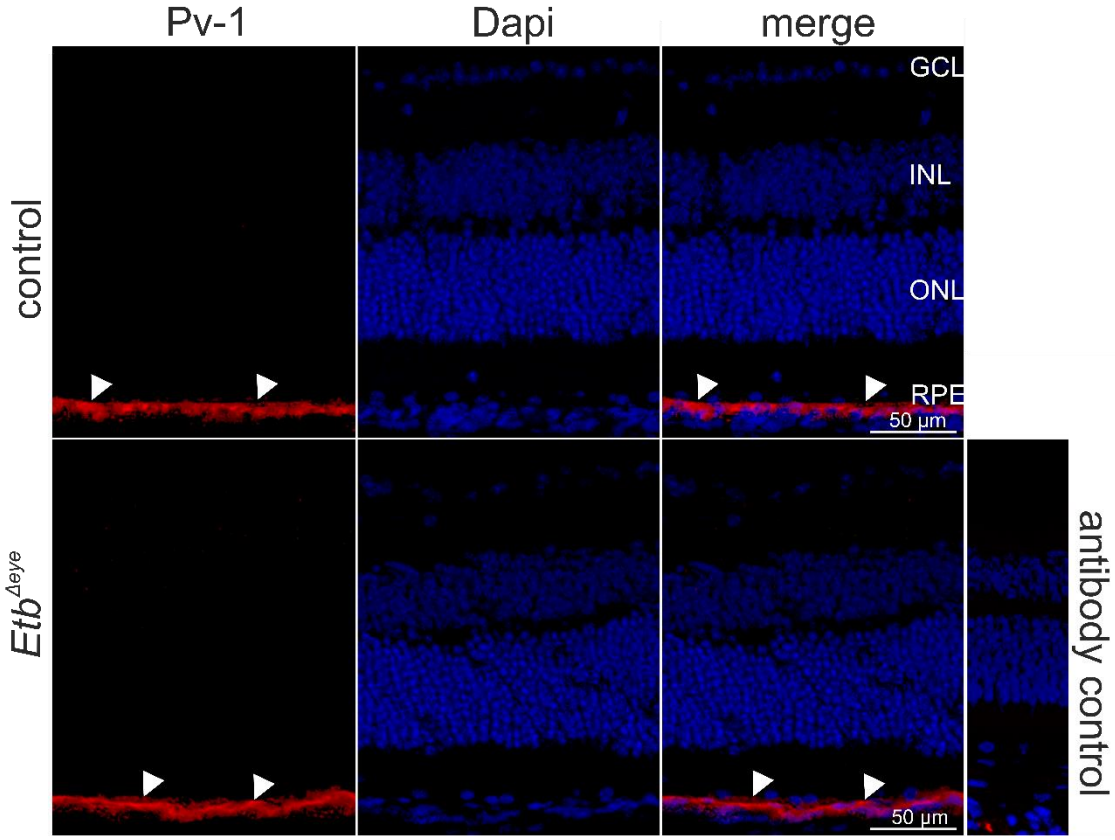

Figure 17 Immunohistochemical staining against Pv-1 of sagittal sections of an *Etb*$^{\Delta eye}$ mouse and control showed no obvious alterations of the choriocapillaris. GCL =ganglion cell layer, INL = inner nuclear layer, ONL = outer nuclear layer, RPE = retinal pigment epithelium. Nuclei were DAPI stained; supported by Anna Huber

To further confirm a regular formation of the capillary plexus, we perfused *Etb*$^{\Delta eye}$ mice and controls with high molecular weight FITC-dextran for vascular labelling. The detailed magnifications of retinal whole mounts of the FITC-dextran-labelled retinae showed a regular appearance of the superficial, intermediate and deep vascular plexus (Figure 18). Again, there were no obvious differences detectable, regarding the capillary networks in the retina of controls and conditional knockout mice.

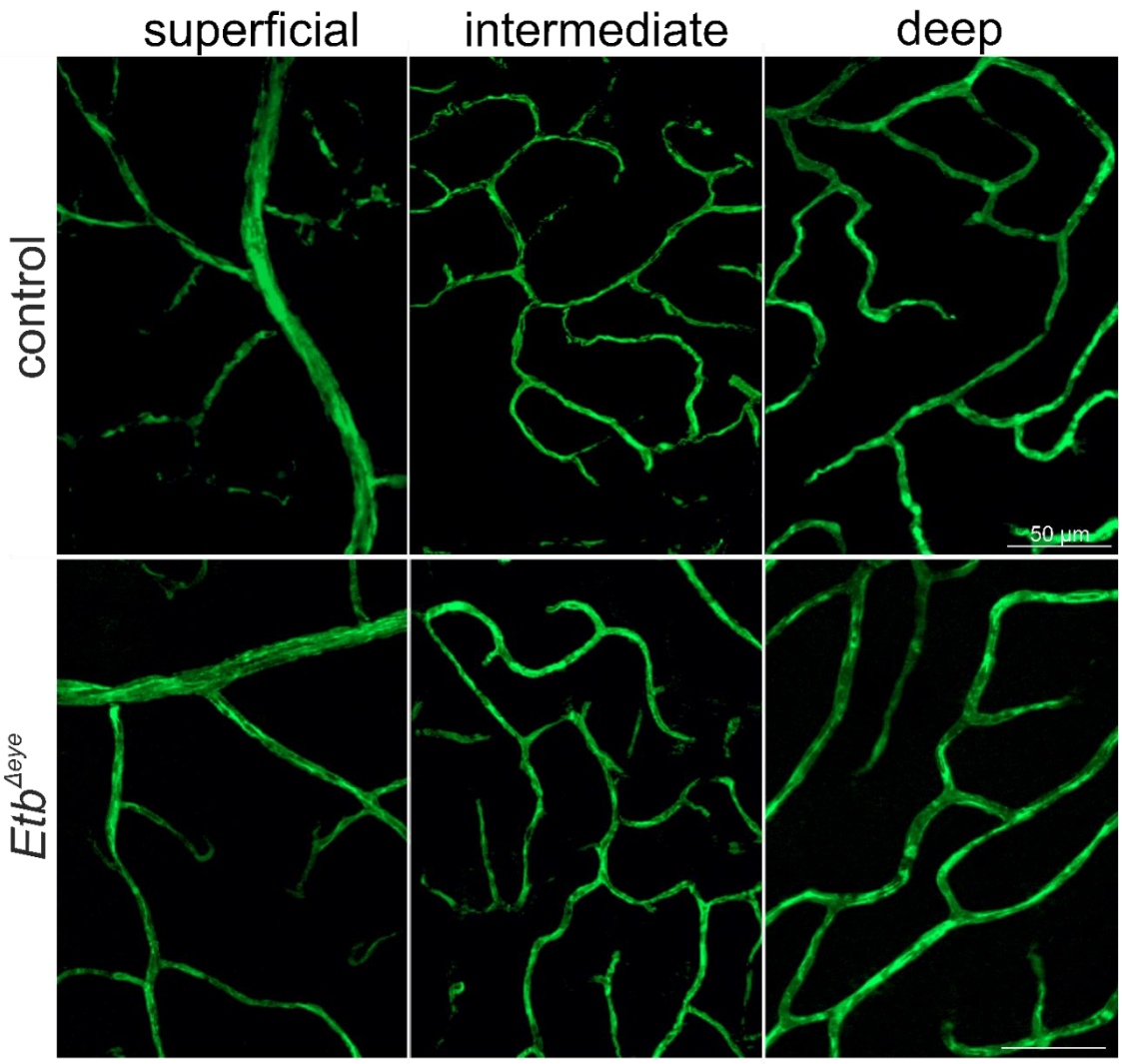

Figure 18 FITC-dextran perfused retinal wholemounts of *Etb*$^{\Delta eye}$ mouse and control at the age of 6 weeks. Control and *Etb*$^{\Delta eye}$ mice showed no alterations of the morphology of the superficial, intermediate and deep vascular plexus.

Furthermore, we analysed whether the deletion of Etb in the entire retina might influence the pericytes. We therefore labelled FITC-dextran perfused retinal whole mounts against the pericyte-marker Neuron-glial antigen 2 (Ng-2) and detected an increased number of pericytes wrapping around retinal vessels in *Etb*$^{\Delta eye}$ mice compared to controls (Figure 19 A). In accordance, the relative mRNA expression levels of *Ng-2* (Figure 19 B) were significantly ($p = 0.03$) increased in *Etb*$^{\Delta eye}$ mice (*Ng-2*: 2.97 ± 0.63) compared to controls (*Ng-2*: 1.00 ± 0.07). We further analysed the relative mRNA expression level of the further pericyte-marker *platelet-derived growth factor receptor (Pdgfrb)* (Figure 19 C), which showed a significant elevation ($p = 0.03$) in *Etb*$^{\Delta eye}$ mice; (*Pdgfrb*: 4.61 ± 1.46) compared to controls (*Pdgfrb*: 1.00 ± 0.27).

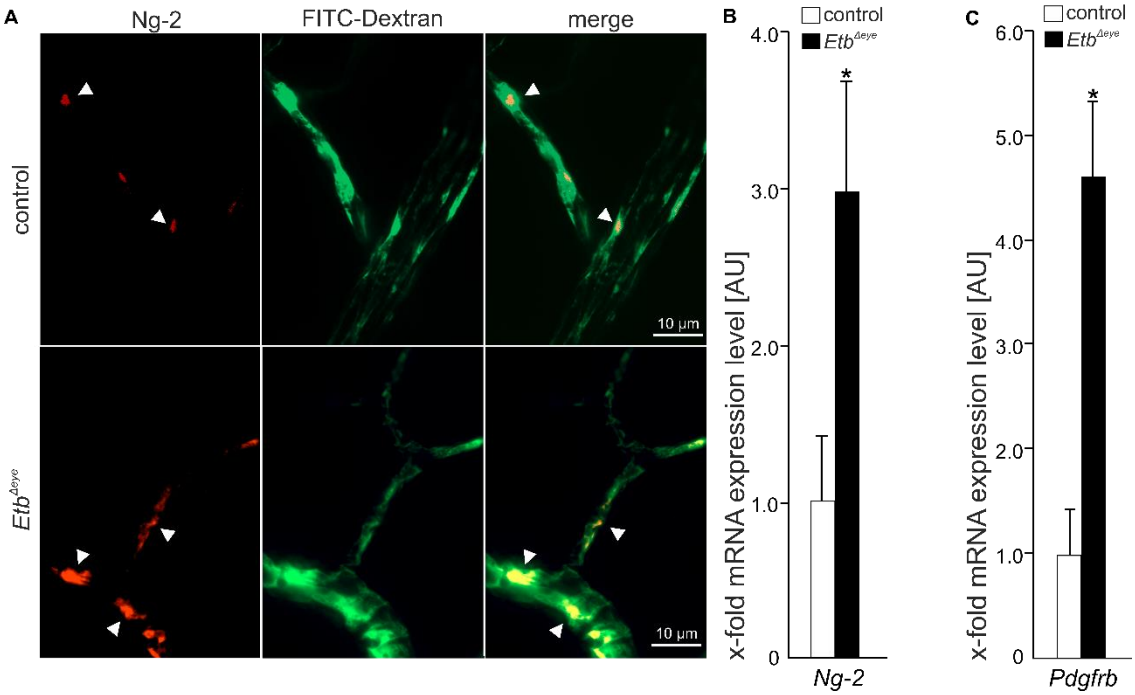

Figure 19 (A) Immunohistochemical staining against Ng-2 (red, arrows) of FITC-dextran perfused (green) retinal wholemounts of a *Etb*$^{\Delta eye}$ mouse and control showed an increased number of pericytes in the Etb$^{\Delta eye}$ mouse compared to the control. (B) Relative Ng-2 mRNA expression level was also significantly increased in Etb$^{\Delta eye}$ mice and controls. The mean values of the housekeeping genes *Gapdh* and *Gnb2l* were used for normalization. Data are means ± SEM; Ng-2: control n = 4; *Etb*$^{\Delta eye}$ n = 5; *p** = 0.03 (C) Relative *Pdgfrb* mRNA expression level was significantly increased in *Etb*$^{\Delta eye}$ mice compared to controls. The mean value of the housekeeping genes *Gapdh* and *Gnb2l* were used for normalization. Data are means ± SEM; student's t-test. control n = 6; *Etb*$^{\Delta eye}$ n = 5; *p** = 0.03; student's t-test.

In addition, we performed quantitative real-time RT-PCR to examine the relative mRNA expression levels of *alpha-smooth muscle actin* (*α-Sma*) and *cluster of differentiation 31* (*Cd31*) (Figure 20). Whereas α-Sma is expressed by smooth muscle cells of large vessels and pericytes of smaller capillaries, Cd31 is reliable marker for endothelial cells. The relative *α-Sma* mRNA expression level was not significantly altered in *Etb*$^{\Delta eye}$ mice (1.66 ± 0.36, *p* = 0.2) compared to controls (1.00 ± 0.18). Moreover, there were no significant alterations detectable concerning the relative *Cd31* mRNA expression levels in the retinae of *Etb*$^{\Delta eye}$ mice (1.34 ± 0.41, p = 0.5) and controls (1.00 ± 0.29).

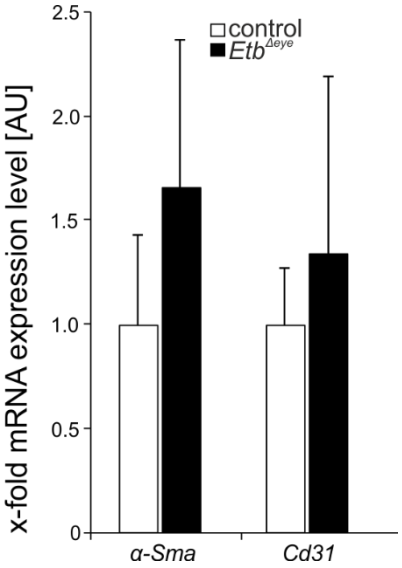

Figure 20 Relative mRNA expression levels of *α-Sma* and *Cd31* of retinal lysates of 6 week old mice showed no significant differences between *Etb*$^{\Delta eye}$ and controls. The mean value of the housekeeping genes *Gapdh* and *Gnb2l* were used for normalization. Data are means ± SEM; student's t-test. *α-Sma* control n = 4; *Etb*$^{\Delta eye}$ n = 4; *p* = 0.2; *Cd31* control n = 6; *Etb*$^{\Delta eye}$ n = 6; *p* = 0.5.

To analyse whether the deletion of Etb might result in hypoxia of the retina, the relative protein expression level of hypoxia-inducible factor 1-alpha (Hif1α), which is a very sensitive hypoxic marker, was compared in retinal lysates of *Etb*$^{\Delta eye}$ mice and controls. Western blot analysis and quantitative densitometry (Figure 21) showed comparable Hif1α expression levels in control (1.00 ± 0.17) and *Etb*$^{\Delta eye}$ mice (1.39 ± 0.16, p = 0.2). Gapdh was used as housekeeping protein.

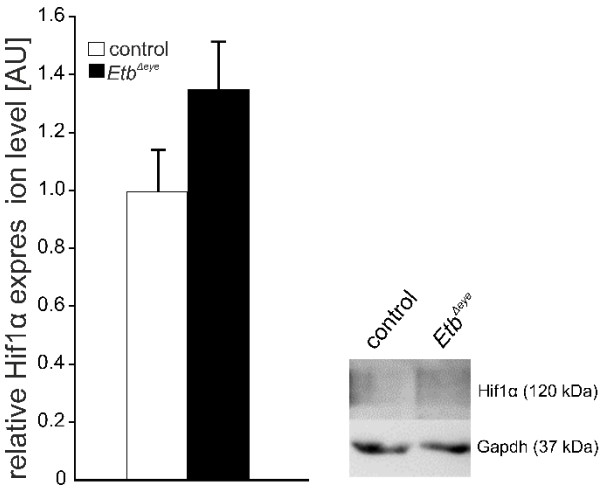

Figure 21 Western blot analysis of retinal proteins and relative densitometry of Hif1α in control and Etb$^{\Delta eye}$ mice. Western blot analysis of 6 week-old control and *Etb*$^{\Delta eye}$ mice for Hif1α (120 kDa). Gapdh (37 kDa) was used as housekeeping protein. The relative densitometry shows no differences of Hif1α expression levels between control and *Etb*$^{\Delta eye}$ mice. Data are means ± SEM. Control n = 3, *Etb*$^{\Delta eye}$ n = 3. *p* = 0.2

3.3.1.5 Influence of Etb-deficiency on macroglia and microglia cells

In the retina reside three main types of glial cells: astrocytes, microglia and Müller glia cells. All of them are involved in neurodegeneration (Seitz et al. 2013) and response prominently to retinal injury or disease by modifications of their function and morphological appearance, a process named as reactive gliosis (Nakazawa et al. 2007). We therefore labelled retinal sagittal sections of *Etb*$^{\Delta eye}$ mice and controls with markers

specific for macro- or microglia cells to examine whether the deletion of Etb affected the mentioned cell-populations.

First, we performed staining against Glial fibrillary acidic protein (Gfap) to detect astrocytes and reactive Müller cells, the prevalent macroglia cells in the retina. Gfap is an intermediate filament protein which is primarily detected in astrocytes. However, in case of retinal injury, Müller cells get reactive and express Gfap, too. As expected, sections of control and conditional knockout mice showed a staining against Gfap on top of the GCL, the characteristic location for astrocytes in the retina (Figure 22). Additionally, *Etb*$^{\Delta eye}$ mice showed an extended staining against Gfap in the inner parts of the retina showing the characteristic shape of reactive Müller cells. Their elongated glial processes spread through the entire retina from the inner limiting membrane to the outer limiting membrane, strongly indicating that the deletion of Etb resulted in the reactivity of Müller cells.

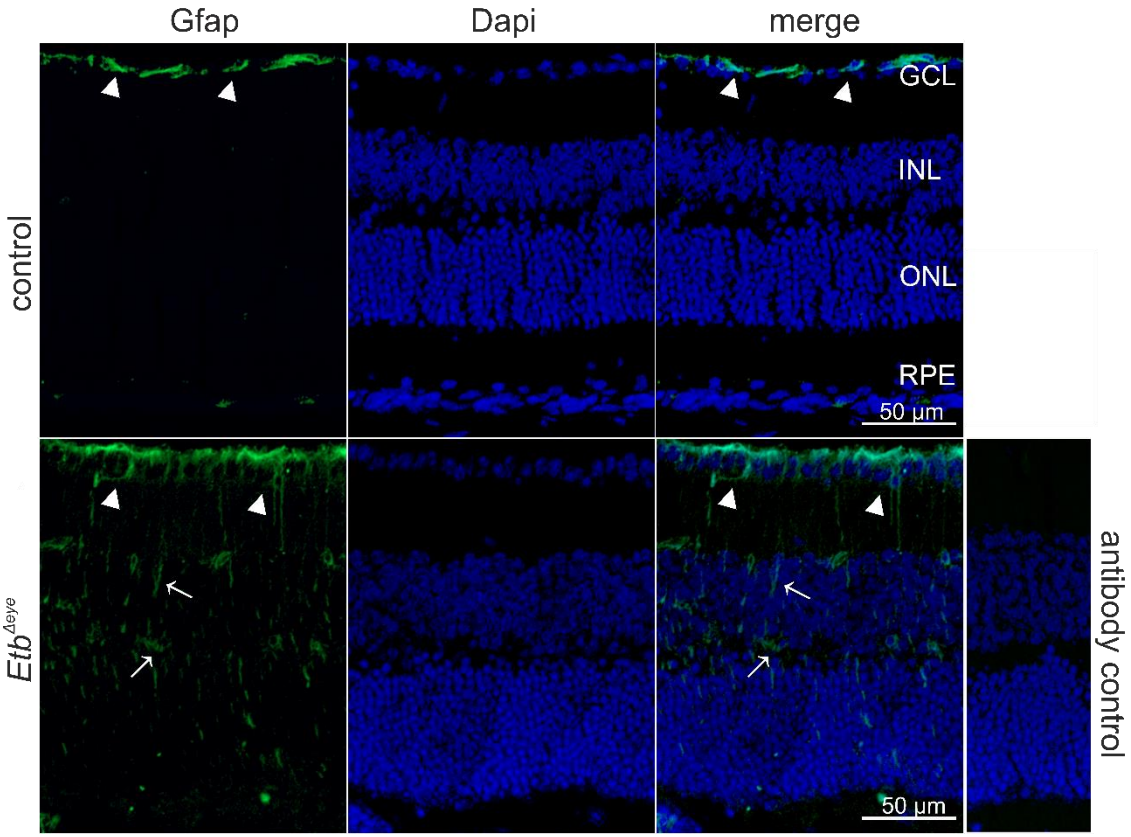

Figure 22 Immunohistochemical staining against Gfap of sagittal sections of a *Etb*$^{\Delta eye}$ mouse and control showed Gfap staining (green, arrowheads) in astrocytes on top of the GCL. *Etb*$^{\Delta eye}$ mice additionally showed a distinct staining along the elongated glia processes stretching through the entire retina from the inner limiting membrane to the outer limiting membrane (arrows). GCL =ganglion cell layer, INL = inner nuclear layer, ONL = outer nuclear layer, RPE = retinal pigment epithelium. Nuclei were Dapi stained.

Besides Müller cells, microglia cells are affected by degenerative processes in the retina, too. Microglia cells show a ramified shape in their mature resting stage. In response to injury they get reactive and switch their appearance through dynamic remodeling of their

cytoskeleton. Hence, they withdraw their filopodic processes to acquire an oval, amoeboid shape. Microglia cells express ionized calcium-binding adapter molecule 1 (Iba-1) which therefore served as marker for microglial cells in the retina. The staining against Iba-1 of sagittal sections of the control mice showed microglia cells in their resting stage with a branching appearance and their characteristic localization in the inner and outer plexiform layer (Figure 23, A). In contrast, the morphology of the Iba-1 positive microglia cells changed to an oval to roundish appearance indicating the reactivation of microglia cells in *Etb*$^{\Delta eye}$ mice. This finding was confirmed by Iba-1 staining of retinal whole mounts (Figure 23, B). The detailed magnification of single microglia cells confirmed the transformation of microglia cells from a resting (controls) to a reactive state (*Etb*$^{\Delta eye}$). The analysis of the relative *Iba-1* mRNA expression level showed no differences between *Etb*$^{\Delta eye}$ mice (1.01 ± 0.27, p = 0.9) and controls (1. ± 0.37) (Figure 23, C).

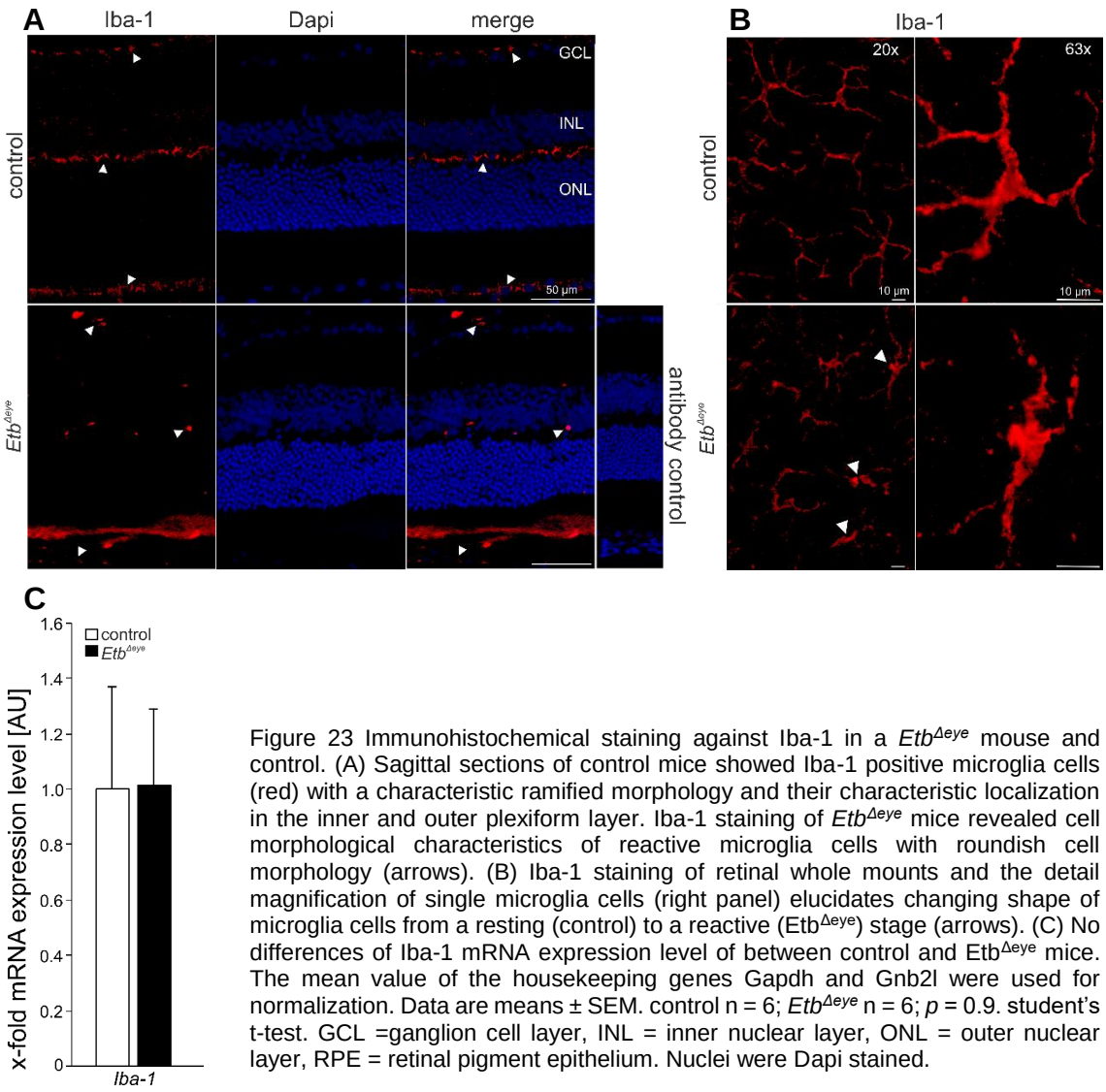

Figure 23 Immunohistochemical staining against Iba-1 in a *Etb*$^{\Delta eye}$ mouse and control. (A) Sagittal sections of control mice showed Iba-1 positive microglia cells (red) with a characteristic ramified morphology and their characteristic localization in the inner and outer plexiform layer. Iba-1 staining of *Etb*$^{\Delta eye}$ mice revealed cell morphological characteristics of reactive microglia cells with roundish cell morphology (arrows). (B) Iba-1 staining of retinal whole mounts and the detail magnification of single microglia cells (right panel) elucidates changing shape of microglia cells from a resting (control) to a reactive (Etb$^{\Delta eye}$) stage (arrows). (C) No differences of Iba-1 mRNA expression level of between control and Etb$^{\Delta eye}$ mice. The mean value of the housekeeping genes Gapdh and Gnb2l were used for normalization. Data are means ± SEM. control n = 6; *Etb*$^{\Delta eye}$ n = 6; *p* = 0.9. student's t-test. GCL =ganglion cell layer, INL = inner nuclear layer, ONL = outer nuclear layer, RPE = retinal pigment epithelium. Nuclei were Dapi stained.

3.3.2 Characterization of *Etb*$^{\Delta OC}$ mice

For simplicity, *Etb*$^{flox/flox}$ mice lacking the Cre recombinase are referred to as controls and *Etb*$^{flox/flox}$ mice expressing Cre recombinase are referred to as *Etb*$^{\Delta OC}$ or conditional knockout mice.

3.3.2.1 Successful deletion of Endothelin receptor b in Müller cells and retinal neurons

For the induction of the conditional deletion of Etb in Müller cells and retinal neurons via the CreloxP system, the self-inducible alpha Cre-Recombinase was used. This Cre recombinase starts its activity at embryonic day (E) 10.5 (Marquardt et al., 2001) and is not tamoxifen dependent. The experimental mice were sacrificed at the age of 6 weeks for further analysis, unless stated otherwise.

The relative mRNA expression levels of *Etb* in retinal tissue of *Etb*$^{\Delta OC}$ mice and controls were analysed via quantitative real-time RT-PCR. The mean value of the housekeeping genes *Gapdh* and *Gnb2l* were used for normalization. The relative *Etb* mRNA expression level was significantly (p = 0.02) decreased (-70%) *Etb*$^{\Delta OC}$ mice (0.29 ± 0.21) compared to controls (1.00 ± 0.29) confirming a successful deletion of *Etb* in Müller cells and retinal neurons (Figure 24 A).

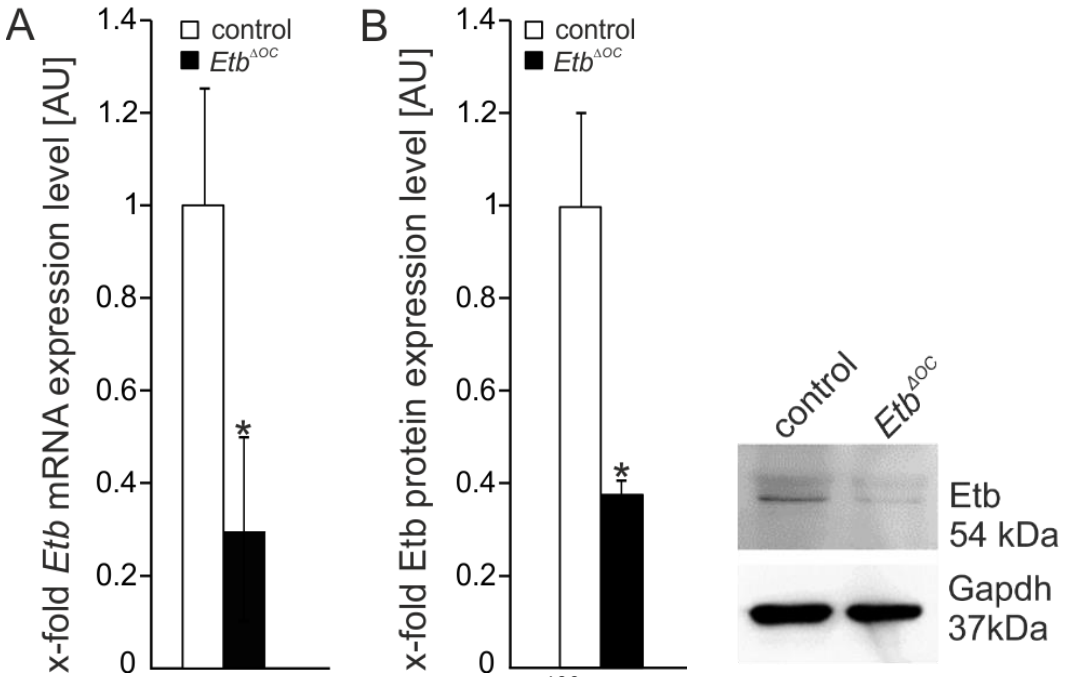

Figure 24 (*A)* Relative Etb mRNA expression in *Etb*$^{\Delta OC}$ mice and controls showed a successful deletion of Etb in Müller cells and retinal neurons. Mice with a conditional deletion of Etb express significantly lower amounts of *Etb* mRNA in the retina compared to controls. The mean value of the housekeeping genes *Gapdh* and *Gnb2l* were used for normalization. Data are means ± SEM. control n = 9; *Etb*$^{\Delta OC}$ n = 6; p* = 0.02, student's t-test. (B) Western blot analysis of retinal lysates and densitometry of Etb showed a significant decrease of Etb expression in the retinae in *Etb*$^{\Delta OC}$ mice compared to controls. Gapdh was used as housekeeping protein. Data are means ± SEM. control n = 6, Etb$^{\Delta OC}$ n = 7; p* = 0.05, student's t-test

Western blot analysis also confirmed a successful deletion of Etb in the retina as the relative protein expression levels of Etb (54 kDa) showed a significantly (p = 0.05) decreased expression (-60%) in *Etb*$^{\Delta OC}$ mice (0.38 ± 0.02) compared to controls (1.00 ± 0.19) (Figure 24 B). Gapdh (37 kDa) was used as housekeeping protein.

To further verify a successful deletion of *Etb*, In situ hybridization BaseScope® on retinal sagittal sections were performed to detect mRNA signals of *Etb* in the retina. In control mice, *Etb* was contributed throughout the entire retina (Figure 25 A). The detailed magnification (Figure 25 B) showed *Etb* mRNA signals (red spots, arrows) as described before (Figure 12). In contrast, there were only rare *Etb* mRNA signals detectable in *Etb*$^{\Delta OC}$ mice. A finding, that again validated a successful deletion of *Etb* in retinae of *Etb*$^{\Delta OC}$ mice compared to controls.

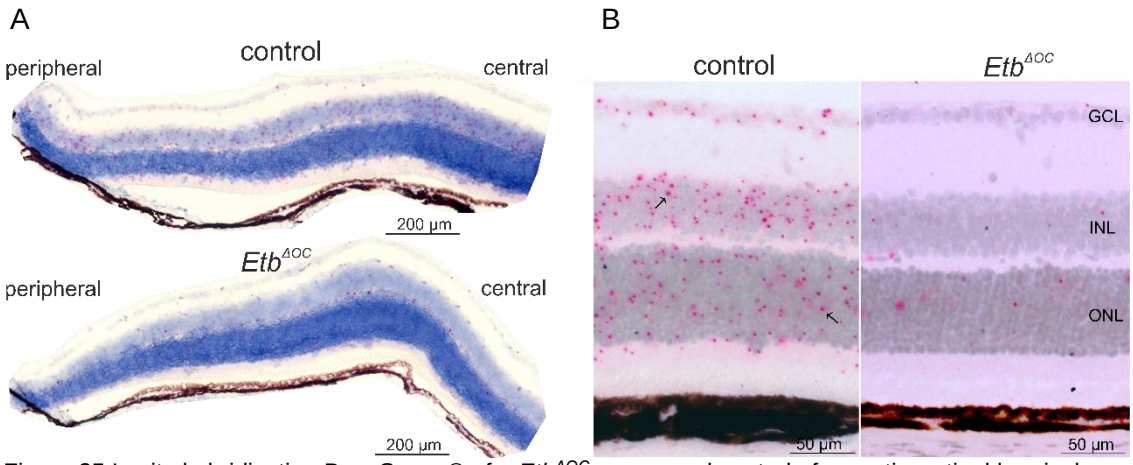

Figure 25 In situ hybridization BaseScope® of a *Etb*$^{\Delta OC}$ mouse and control of an entire retinal hemisphere (A) and detailed magnification (B). In comparison to *Etb*$^{\Delta OC}$ mice, control mice showed Etb mRNA signals (red, arrows) in the ganglion cell layer (GCL), inner nuclear layer (INL) and outer nuclear layer (ONL). Nuclei were stained with haematoxylin.

3.3.2.2 No obvious alterations on retinal morphology following ETB-deficiency

By using conventional light microscopy, retinal morphology was analysed on Richardson stained horizontal semithin sections (1µm) of 6 week-old (Figure 26 A) *Etb*$^{\Delta OC}$ mice and controls. We additionally analysed semithin sections of 6 month-old *Etb*$^{\Delta OC}$ mice (Figure 27 A) and controls to investigate whether an Etb-deletion leads to long-term effects on the retinal structures.

No alterations of the retinal morphology were detectable in the 6 week-old and in the 6 month-old control mice compared to *Etb*$^{\Delta OC}$ mice. Both, the control mice as well as *Etb*$^{\Delta OC}$ mice, showed a normal architecture of the retina with all retinal layers present along the entire hemisphere.

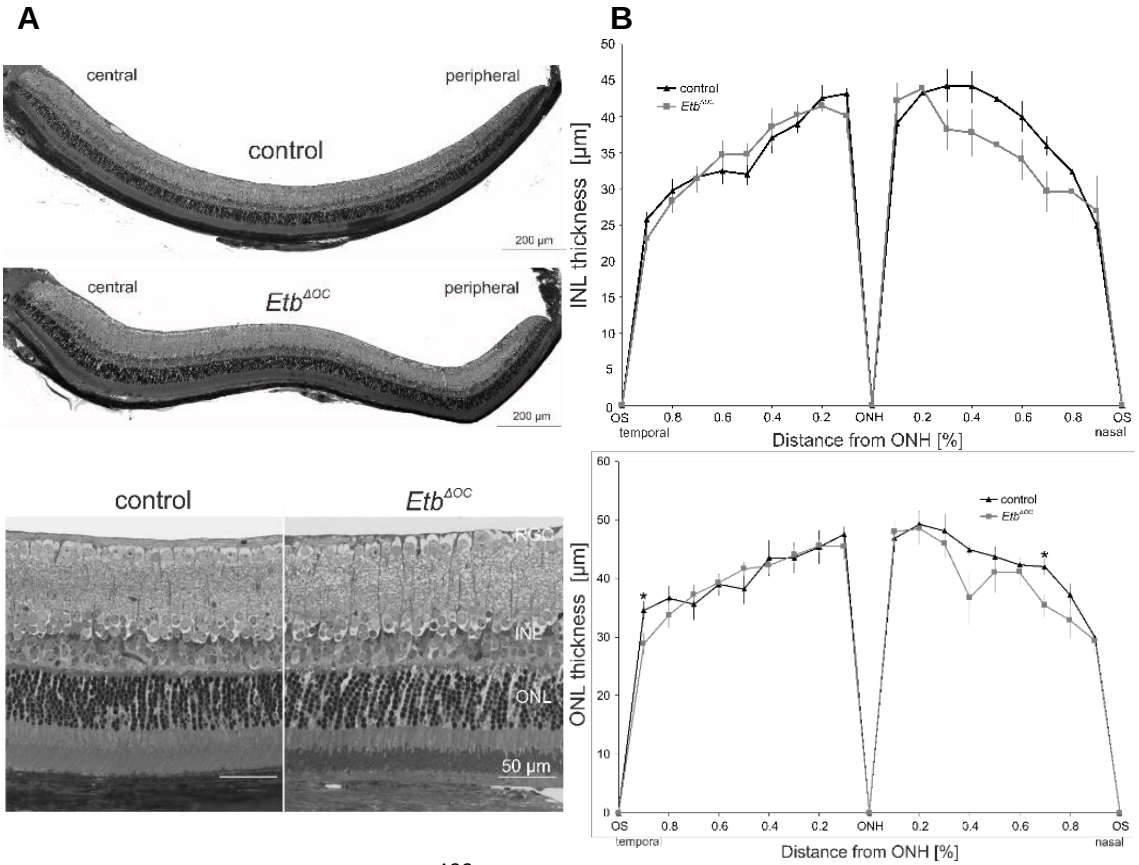

Figure 26 (A) Semithin-section of a *Etb*$^{\Delta OC}$ mouse and control (6 week-old). Horizontal (1µm) semithin-sections (Richardson stained) of retinal hemispheres showed no alterations of retinal morphology. Lower panel showed a higher magnification of the central retina. RGC =retinal ganglion cell layer, INL = inner nuclear layer, ONL = outer nuclear layer, RPE = retinal pigment epithelium. (B) Spider diagram of the thickness of the ONL and INL of *Etb*$^{\Delta OC}$ mice and controls (6 week-old). The thickness of the ONL and INL was measured on semithin-sections at defined measure points from ora serrata to the optic nerve head. There were no differences in the thickness of ONL as well as INL detectable between *Etb*$^{\Delta OC}$ mice and controls. OS = ora serrata; ONH = optic nerve head. Data are means ± SEM, student's t-test. Control: n=7, $p > 0.05$; *Etb*$^{\Delta OC}$: n=6, $p > 0.05$.

For further quantification, the thickness of the ONL and INL was measured along the entire retina and the mean values of 9 individual measure points were represented in spider diagrams. The thickness was measured on semithin-sections along the distance

from ora serrata to the optic nerve head. The thickness of ONL and INL does not differ between *Etb*$^{\Delta OC}$ mice and the controls at the age of 6 weeks (Figure 26 B) as well as at the age of 6 months (Figure 27 B).

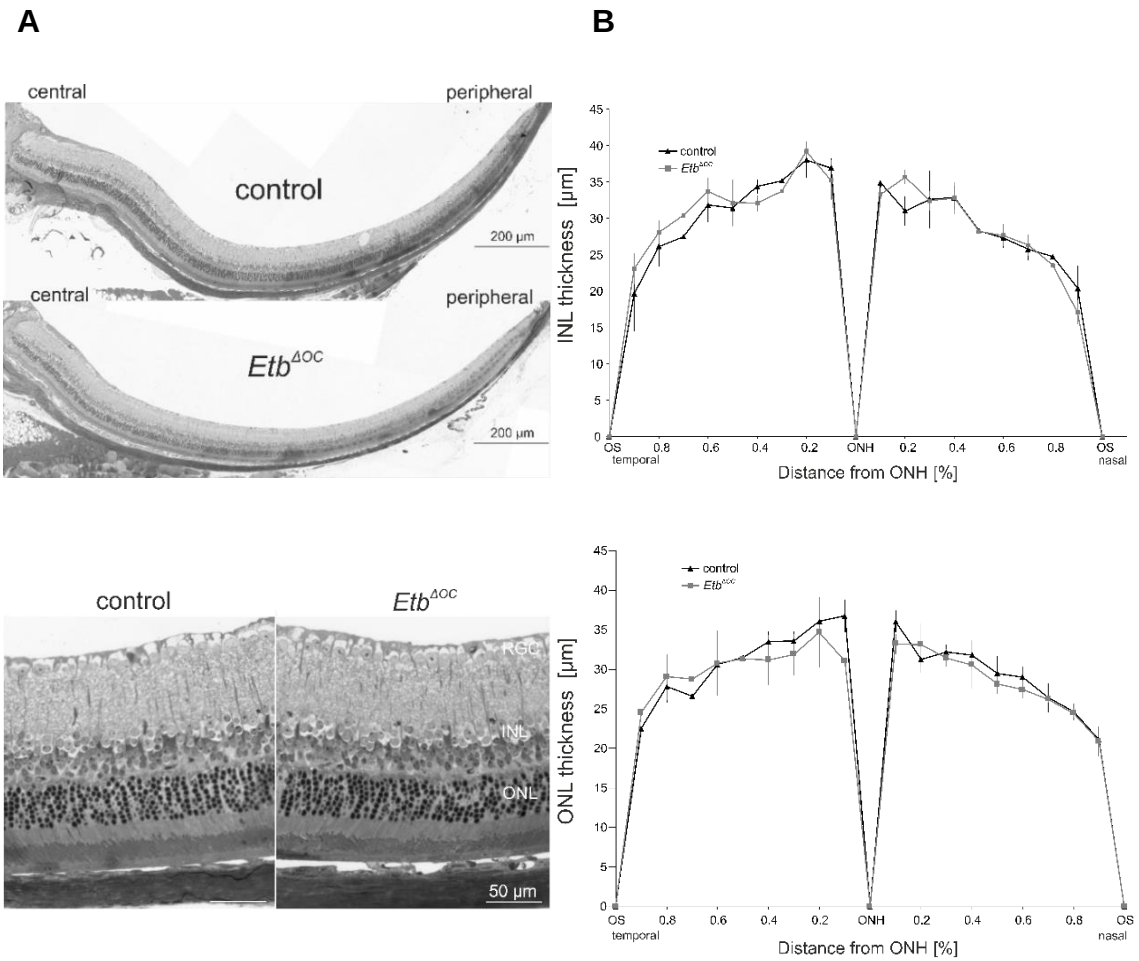

Figure 27 (A) Semithin-section of a *Etb*$^{\Delta OC}$ mice and control (6 month-old). Horizontal (1µm) semithin-sections (Richardson stained) of retinal hemispheres showed no alterations of the retinal morphology. Lower panel shows a higher magnification of the central retina. RGC =retinal ganglion cell layer, INL = inner nuclear layer, ONL = outer nuclear layer, RPE = retinal pigment epithelium. (B) Spider diagram of the thickness of the ONL and INL of *Etb*$^{\Delta OC}$ mice and controls (6 month-old). The thickness of the ONL and INL was measured on semithin-sections at defined measure points from ora serrata to the optic nerve head. There were no differences in the thickness of ONL as well as INL detectable between *Etb*$^{\Delta OC}$ mice (n=6, $p > 0.05$ (not significant)) and controls (n=7, $p > 0.05$ (not significant)). OS = ora serrata; ONH = optic nerve head. Data are means ± SEM, student's t-test. Controls: n=7, $p > 0.05$; *Etb*$^{\Delta OC}$ mice (n=6, $p > 0.05$.

3.3.2.3 No obvious alterations on retinal vasculature following Etb-deficiency

Next, we examined, whether Etb-deficiency in Müller cells and retinal neurons affected the retinal vasculature.

The immunohistochemical staining against Collagen IV of the basal lamina of retinal vessels on sagittal sections of *Etb*$^{\Delta OC}$ mice and controls (Figure 28) showed no obvious alterations of the morphological appearance of all three capillary plexus in the retina. A regular deep and intermediate capillary plexus of the inner and outer part of the INL as well as a normally developed superficial plexus on top of the GCL were clearly distinguishable. Moreover, the vessels of the choriocapillaris located characteristically next to the basal side of the retinal pigment epithelium (RPE) showed a regular morphology.

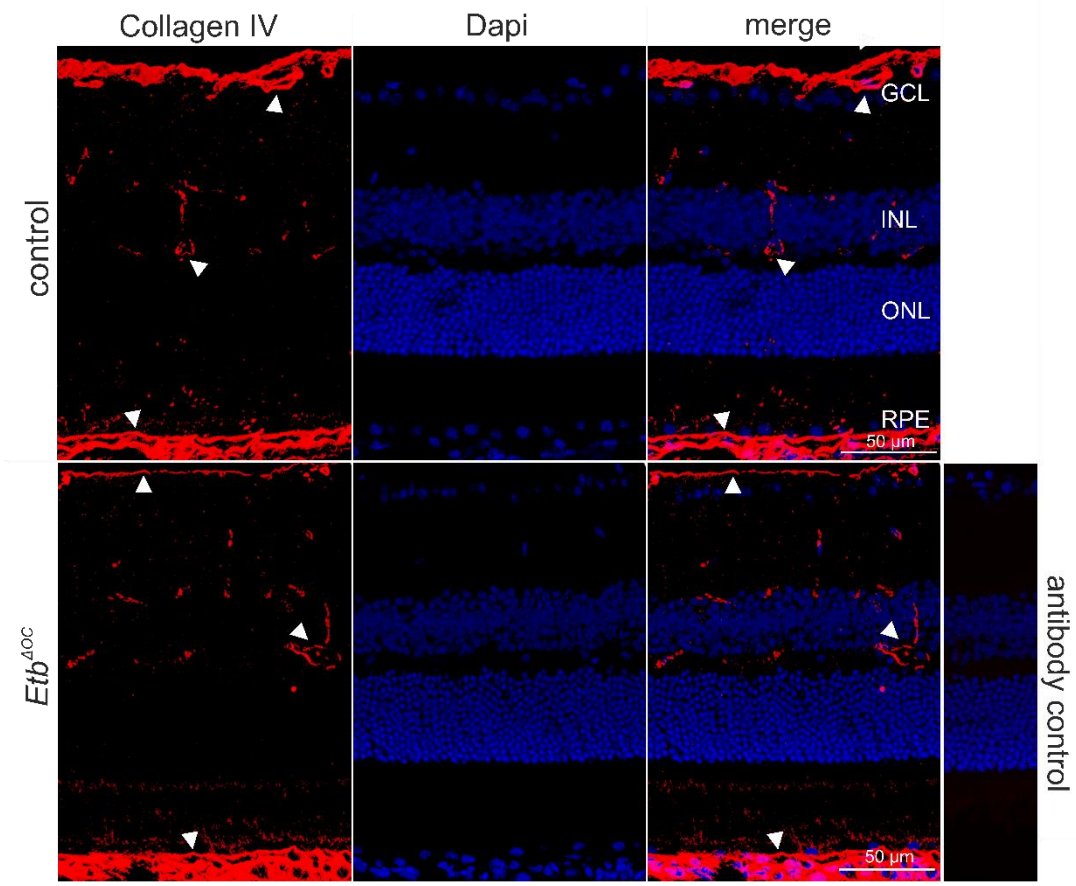

Figure 28 Immunohistochemichal staining against Collagen IV (red, arrows) in a *Etb*$^{\Delta OC}$ mouse and control showed no alterations of the retinal vasculature in the *Etb*$^{\Delta OC}$ mouse compared to control. GCL =ganglion cell layer, INL = inner nuclear layer, ONL = outer nuclear layer, RPE = retinal pigment epithelium. Nuclei were Dapi stained.

The choriocapillaris was investigated in more detail by staining sagittal sections against Plasmalemma Vesicle-Associated Protein (Pv-1), a marker for fenestrated epithelium

(Figure 29). There were no alterations of the fenestrations of the choriocapillaris between the *Etb*$^{\Delta OC}$ mice and their control littermates.

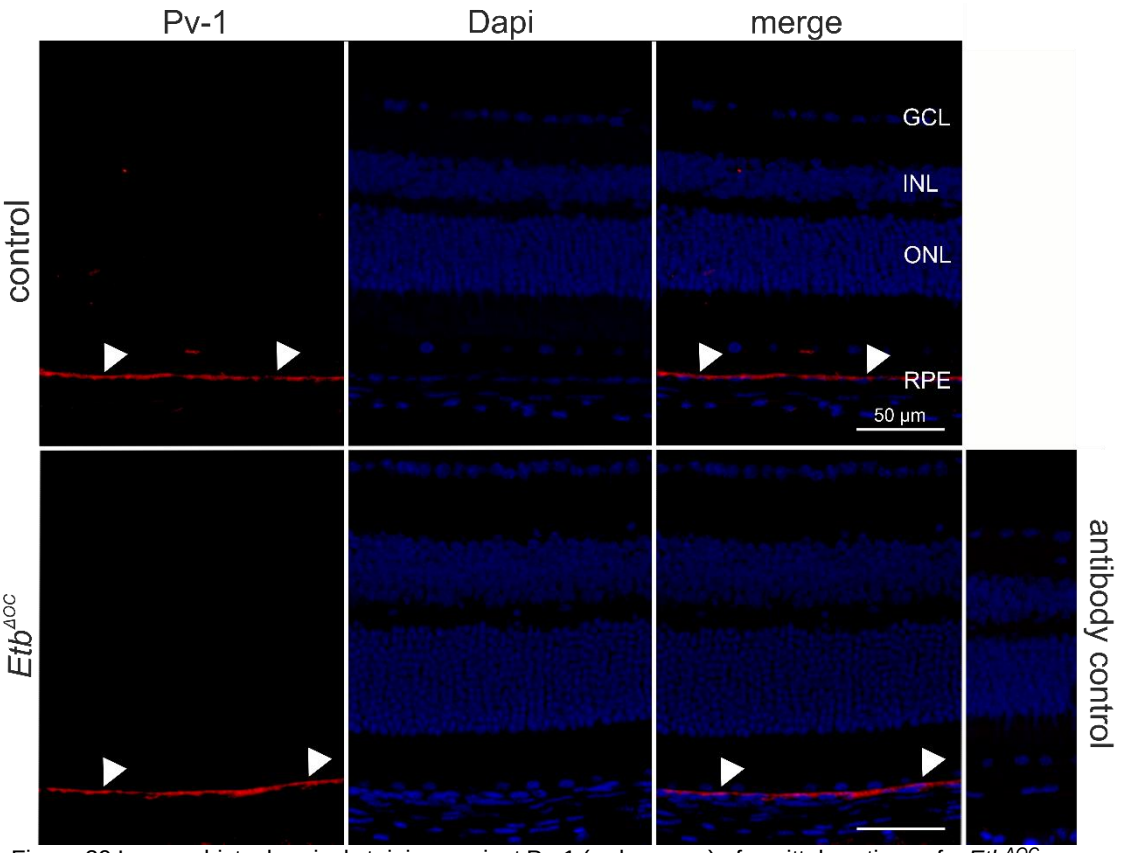

Figure 29 Immunohistochemical staining against Pv-1 (red, arrows) of sagittal sections of a *Etb*$^{\Delta OC}$ mouse and its control littermate showed no obvious alterations of the choriocapillaris. GCL =ganglion cell layer, INL = inner nuclear layer, ONL = outer nuclear layer, RPE = retinal pigment epithelium. Nuclei were Dapi stained.

To further confirm a regular formation of the capillary plexus, we perfused *Etb*$^{\Delta OC}$ mice and controls with high molecular weight FITC-dextran. Retinal whole mounts of the FITC-dextran-perfused retinae showed a regular appearance of the superficial, intermediate and deep vascular plexus. Again, there were no obvious differences regarding the architecture of the capillary networks in the retina of controls and *Etb*$^{\Delta OC}$ mice.

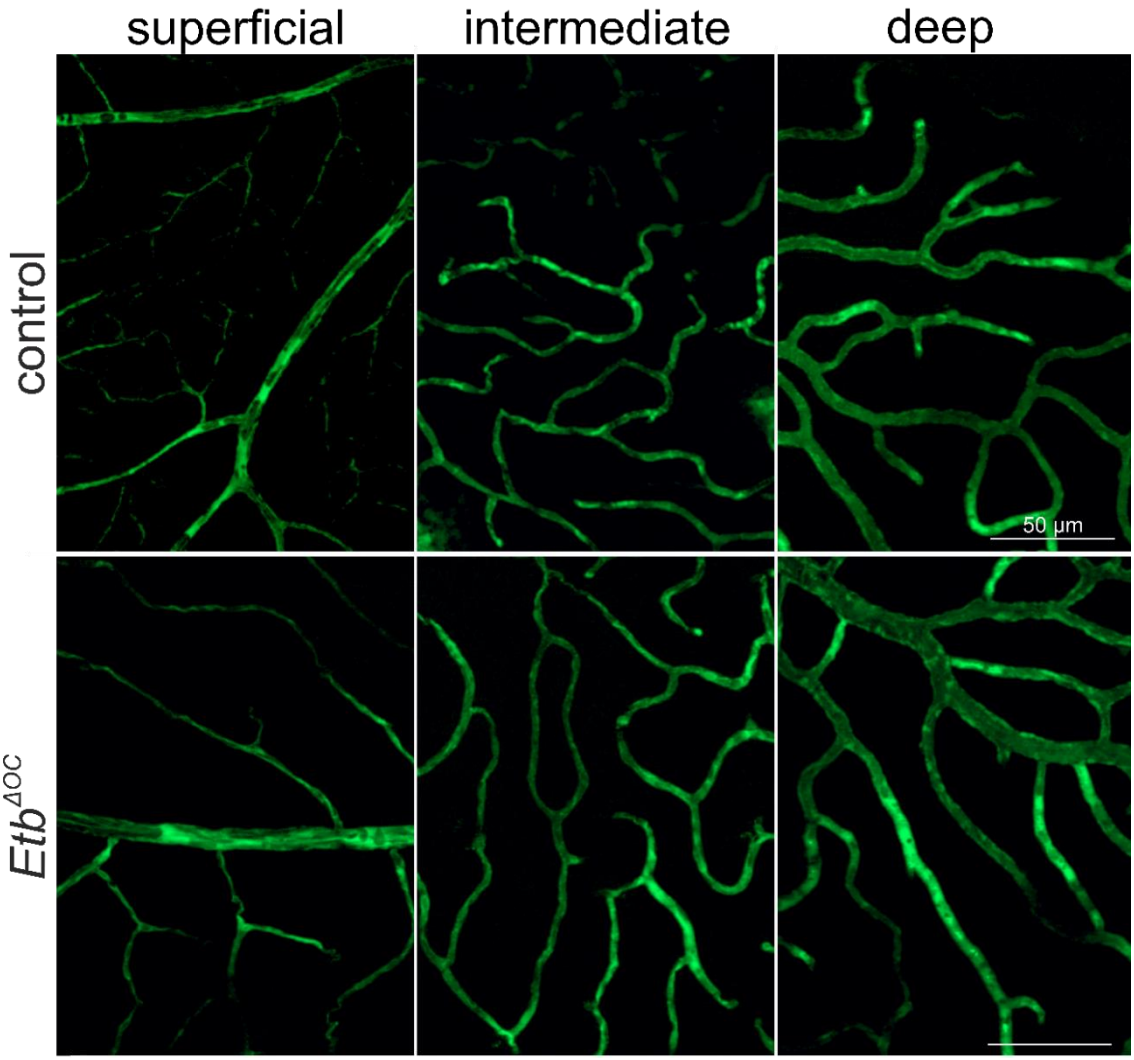

Figure 30 FITC-dextran (green) perfused wholemounts of a *Etb*$^{\Delta OC}$ mouse and its control littermate at the age of 6 weeks. Control and *Etb*$^{\Delta OC}$ mouse showed a comparable morphology of the superficial, intermediate and deep vascular plexus.

Furthermore, we analysed whether the deletion of Etb in retinal neurons and Müller cells might influence the pericytes. We therefore stained FITC-dextran perfused retinal whole mounts against the pericyte-marker Neuron-glial antigen 2 (Ng-2) and detected no influence on the location and appearance of pericytes (Figure 30 A). The retinal vessels were surrounded by pericytes in *Etb*$^{\Delta OC}$ mice and controls. We additionally analysed the relative mRNA expression levels of *Ng-2* (Figure 30 B) and *platelet-derived growth factor receptor (Pdgfrb)* (Figure 31 C), also a pericyte marker, in the retina, which did not significantly differ between *Etb*$^{\Delta OC}$ mice (*Ng-2*: 0.63 ± 0.14, $p = 0.2$; *Pdgfrb*: 1.09 ± 0.34, $p = 0.8$) and controls (*Ng-2*: 1.00 ± 0.19, *Pdgfrb*: 1.0 ± 0.43).

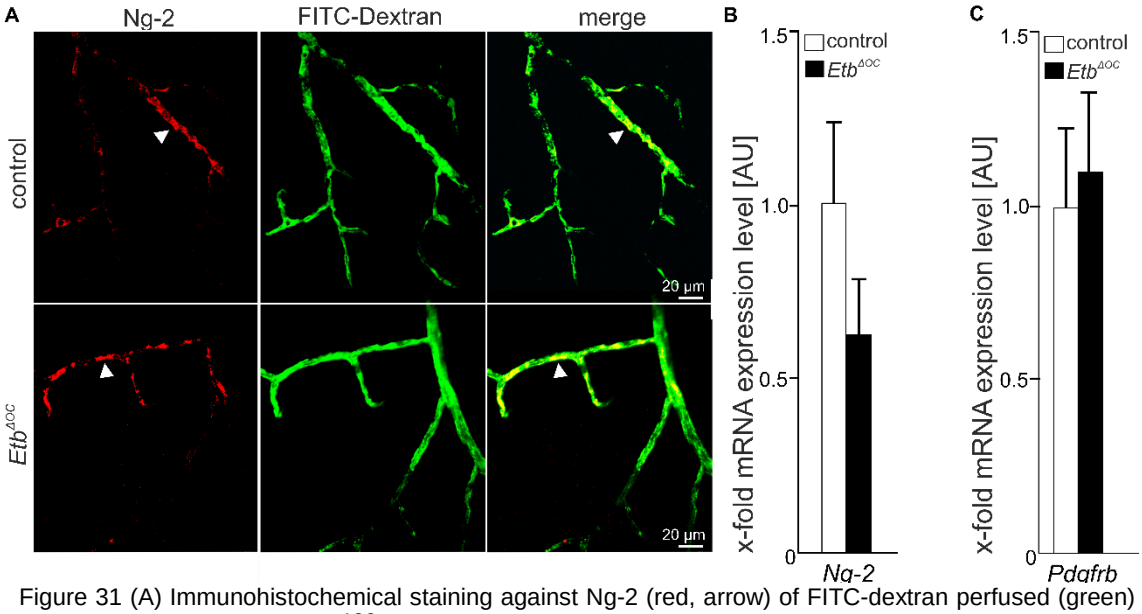

Figure 31 (A) Immunohistochemical staining against Ng-2 (red, arrow) of FITC-dextran perfused (green) retinal wholemounts of a *Etb*$^{\Delta OC}$ mouse and control showed no obvious alterations of pericytes. (B): Relative *Ng-2* mRNA expression levels also showed no differences between *Etb*$^{\Delta OC}$ mice and controls. The mean value of the housekeeping genes *Gapdh* and *Gnb2l* were used for normalization. Data are means ± SEM; control n = 5; *Etb*$^{\Delta OC}$ n = 6; p = 0.2; student's t-test. (C) Relative *Pdgfrb* mRNA expression levels showed no differences between *Etb*$^{\Delta OC}$ mice and controls. The mean value of the housekeeping genes *Gapdh* and *Gnb2l* were used for normalization. Data are means ± SEM; control n = 5; Etb$^{\Delta OC}$ n = 6; p = 0.8; student's t-test.

Furthermore, we performed quantitative real-time RT-PCR to measure the relative mRNA expression levels of *alpha-smooth muscle actin* (*α-Sma*) a specific marker for smooth muscle cells) and *cluster of differentiation 31* (*Cd31)*, a specific marker for endothelial cells) (Figure 32). Relative *α-Sma* mRNA expression level was not significantly affected in conditional knockout mice (1.36 ± 0.31, p = 0.5) compared to controls (1.00 ± 0.29) and there were no significant differences of the relative *Cd31* mRNA expression levels between *Etb*$^{\Delta OC}$ mice (1.16 ± 0.33, p = 0.5) and controls (1.00 ± 0.21) detectable.

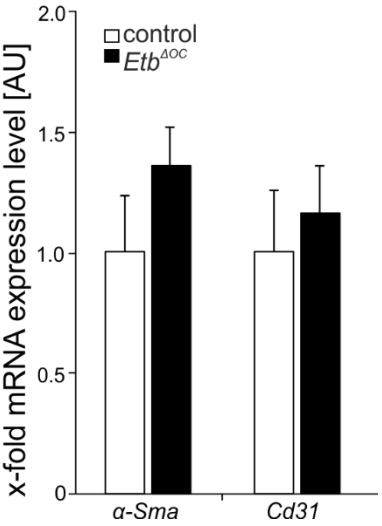

Figure 32 *Relative* mRNA expression levels of *α-Sma* and *Cd31* of retinal lysates *Etb*$^{\Delta OC}$ mice and controls. The mean value of the housekeeping genes *Gapdh* and *Gnb2l* were used for normalization. Data are means ± SEM; *α-Sma*: control n = 5; *Etb*$^{\Delta OC}$ n = 5; $p = 0.5$; Cd31: control n = 6; *Etb*$^{\Delta OC}$ n = 6; $p = 0.5$; student's t-test.

Additionally, the protein expression level of the very sensitive hypoxic marker hypoxia-inducible factor 1-alpha (Hif1α) was compared in retinal lysates of conditional knockout mice and controls. Western blot analysis and relative densitometry (Figure 33) showed comparable expression levels of Hif1α between control (1.00 ± 0.41) and *Etb*$^{\Delta OC}$ mice (1.12 ± 0.19, $p = 0.8$). Gapdh was used as housekeeping protein. Taken together our findings strongly indicate that the deletion of Etb in retinal neurons and Müller cells did not affect the retinal vasculature.

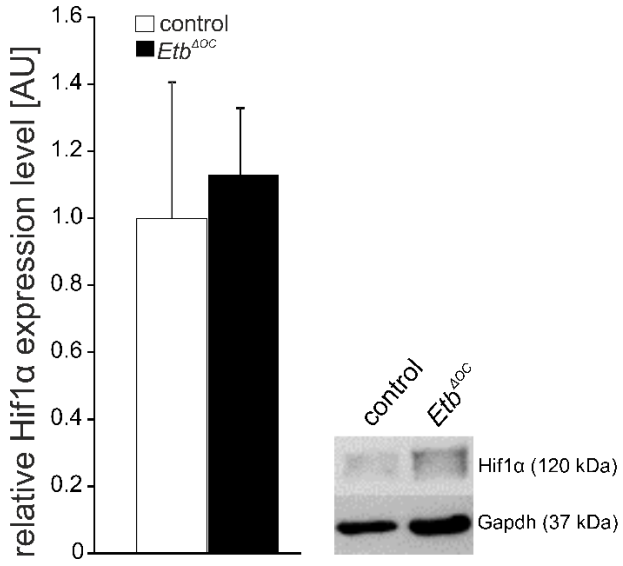

Figure 33 Western blot analysis and relative densitometry of retinal lysates of *Etb*$^{\Delta OC}$ mice controls . (6 week-old) for Hif1α (120 kDa). Gapdh (37 kDa) was used as housekeeping protein. The relative densitometry showed no significant differences of Hif1α expression levels between control and *Etb*$^{\Delta OC}$ mice. Data are means ± SEM. Control n = 8, *Etb*$^{\Delta OC}$ n = 6. $p = 0.8$; student's t-test.

3.3.2.4 Influence of Etb-deficiency on retinal macro- and microglia cells

To examine whether Etb-deficiency leads to a reactivity (gliosis) of Müller cells (macroglia cells) and microglia cells, retinal sagittal sections of *Etb*$^{\Delta OC}$ mice and controls were stained against markers specific markers for macro- or microglia cells.

Glial fibrillary acidic protein (Gfap) is an intermediate filament protein which is primarily detected in astrocytes and also expressed by reactive Müller cells. A Gfap-positive staining was detected on top of the GCL, the characteristic location for astrocytes in the retina in control as well as in *Etb*$^{\Delta OC}$ mice (Figure 34). We did not observe the characteristic stripe-like appearance of Gfap positive signals that would indicate a reactivity of Müller cells, indicating that the deletion of Etb in retinal neurons and Müller cells did not induce a gliotic reaction in Müller cells.

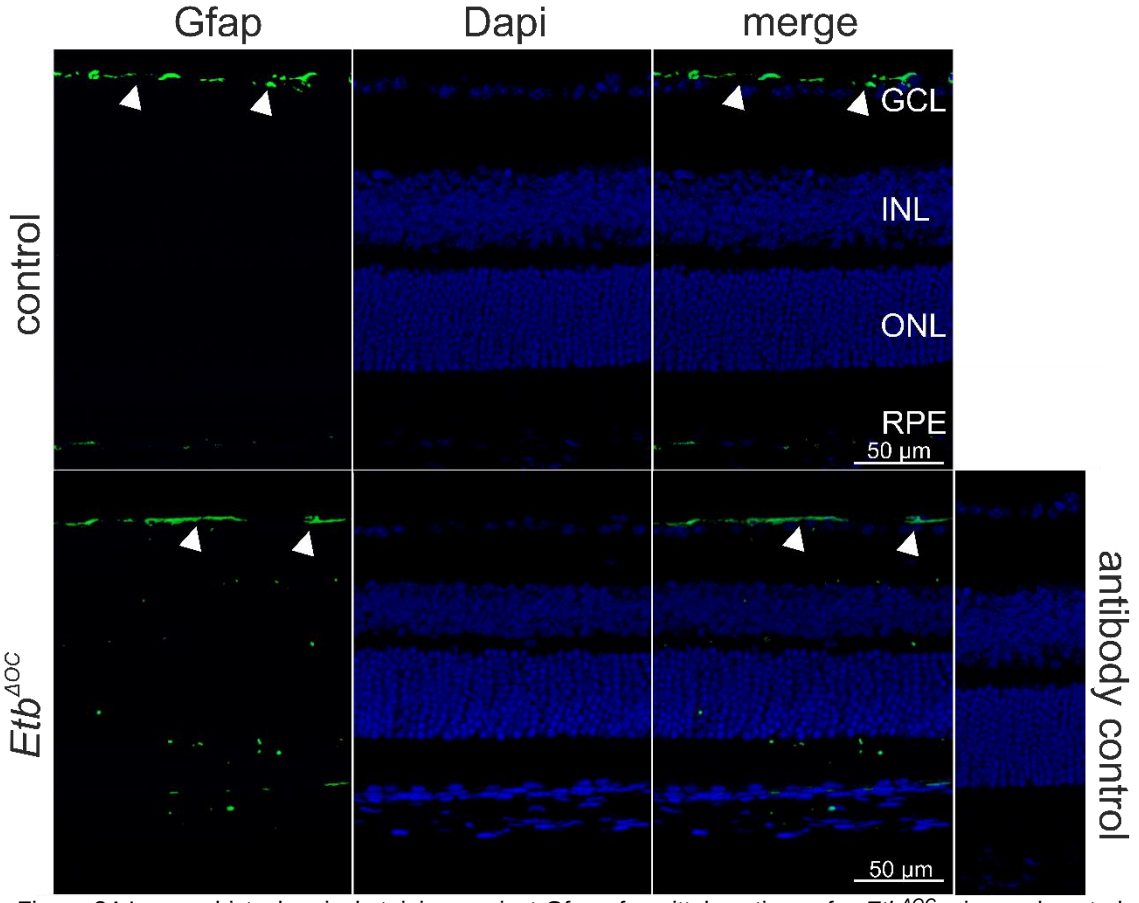

Figure 34 Immunohistochemical staining against Gfap of sagittal sections of a *Etb*$^{\Delta OC}$ mice and control showed Gfap staining (green, arrowheads) in astrocytes on top of the GCL. GCL =ganglion cell layer, INL = inner nuclear layer, ONL = outer nuclear layer, RPE = retinal pigment epithelium. Nuclei were Dapi stained

To analyse whether the deletion of Etb in retinal neurons and Müller cells might influence the activation state of microglia cells, sagittal sections were stained against express ionized calcium-binding adapter molecule 1 (Iba-1), a marker for microglial cells and macrophages. Both, controls and *Etb*$^{\Delta OC}$ mice showed microglia cells in their resting stage with a branching appearance and their characteristic localization in the inner and outer plexiform layers in sagittal sections (Figure 35 A). The detailed magnification of single microglia cells in retinal whole mounts also illustrated resting microglia cells in controls and *Etb*$^{\Delta OC}$ (Figure 35 B). In addition, we analysed the *Iba-1* mRNA expression

levels and detected no differences between *Etb*$^{\Delta OC}$ mice (0.85 ± 0.23, p = 0.4) and controls (1.00 ± 0.29) (Figure 35 C).

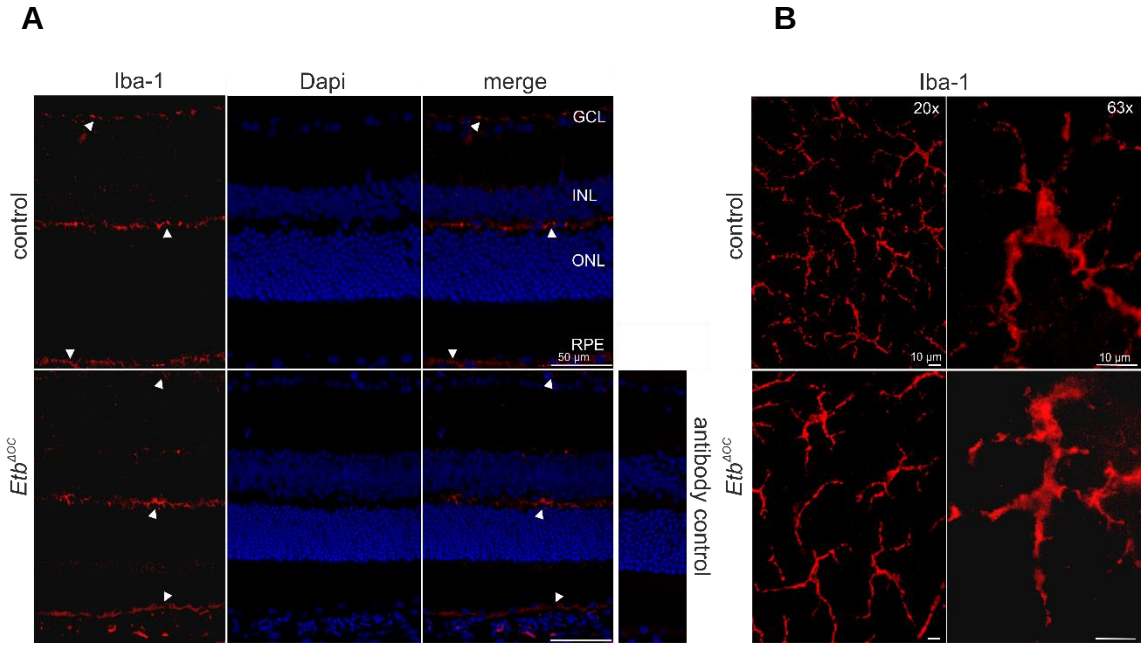

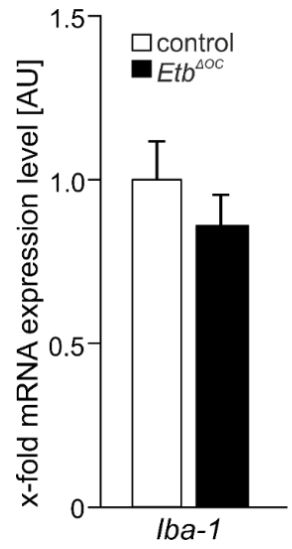

Figure 35 (A)Immunohistochemical staining against Iba-1 on sagittal sections of a *Etb*$^{\Delta OC}$ mouse and its control littermateshowed Iba-1 positive microglia cells (red, arrows) with a characteristic ramified morphology and their characteristic localization in the ganglion cell layer, outer plexiform layer and retinal pigment epithelium. GCL =ganglion cell layer, INL = inner nuclear layer, ONL = outer nuclear layer, RPE = retinal pigment epithelium. Nuclei were DAPI stained. (B) Iba-1 staining of retinal whole mounts and the detail magnification of single microglia cells (right panel) confirmed the resting microglia cells in control and *Etb*$^{\Delta OC}$ mice. (C) No differences of mRNA expression analysis of *Iba-1* in control and *Etb*$^{\Delta OC}$ mice. The mean value of the housekeeping genes *Gapdh* and *Gnb2l* were used for normalization. Data are means ± SEM. control n = 6; *Etb*$^{\Delta OC}$ n = 6; p = 0.4. student's t-test.

3.3.3 Characterisation of *661W$^{\Delta Etb}$*

To generate an *in vitro* model system that would allow more mechanistic analyses about the function of Etb in photoreceptors, we additionally created a murine, immortalized photoreceptor cell line (661W) with a stable deletion of Etb via the CRISPR/Cas9-System. In the following, these cells are referred to as *661W$^{\Delta Etb}$*. As controls, we used 661W cells which were only transfected with the Cas9 enzyme and consequently still express Etb. These cells are referred to as 661W control cells. In summary, we generated four individual colonies of 661W controls as well as four individual colonies of *661W$^{\Delta Etb}$* with a stable deletion of Etb. Those individual colonies were created out of the expansion of single cells isolated after transfection. The cells were harvested during the period of passage (P) 10 to P 15.

To verify a successful deletion of Etb in the individual colonies of photoreceptor cells, we performed western blot analysis and used Gapdh (37 kDa) as housekeeping gene for normalization. The densitometric analysis of cell lysate illustrated a significant (p= 0.02) decrease of the relative Etb protein expression (-94%) in *661W$^{\Delta Etb}$* (0.06 ± 0.2) compared to controls (1.00 ± 0.8) confirming the successful deletion of Etb (Figure 36 A).

We furthermore performed in situ hybridization BaseScope® of each individual colony of 4%PFA-fixed *661W$^{\Delta Etb}$* cells and 661W control cells, to detect and identify mRNA signals of *Etb* in photoreceptors cells. In control cells, we observed a robust *Etb* mRNA signal in 661W control cells (Figure 36 B). In contrast, there was no *Etb* mRNA signal detectable in *661W$^{\Delta Etb}$* cells, again validating a successful deletion of *Etb* in the *661W$^{\Delta Etb}$*.

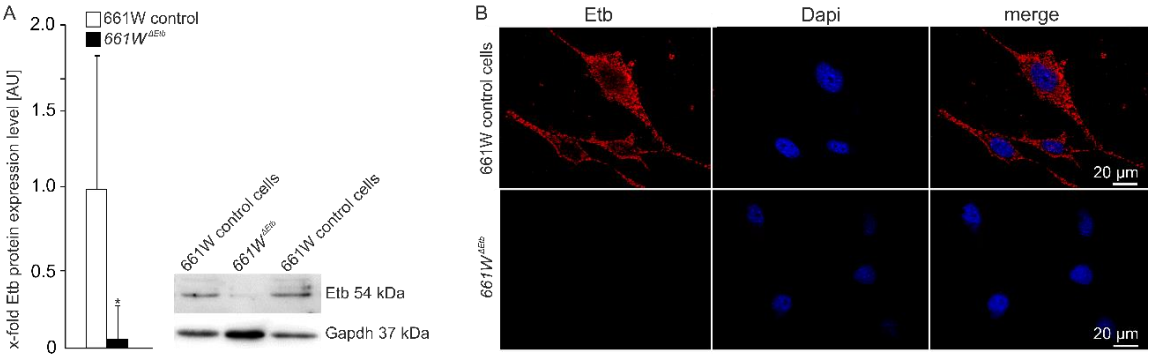

Figure 36 (A) Western blot analysis of cell lysates and densitometry of Etb in *661W$^{\Delta Etb}$* and 661W control cells. Gapdh was used as housekeeping protein. The statistical analysis confirmed the significant decrease of Etb expression in *661W$^{\Delta Etb}$* cells compared to 661W control cells. Data are means ± SEM. 661W control cells n = 4, *661W$^{\Delta Etb}$* n = 4; p*= 0.02, student's t-test (B) In situ hybridization BaseScope® of *661W$^{\Delta Etb}$* cells and 661W control cells. An intense *Etb* mRNA signal could be detected in the 661W control cells, that was no longer detectable in *661W$^{\Delta Etb}$* cells. Nuclei were stained with Dapi (blue).

3.4 Impact of an Etb-deficiency *in vivo* and *in vitro* under physiological conditions

Next, we aimed to study the impact of a deletion of Etb under physiological conditions on the expression levels of 1.) members of the endothelin signalling family, 2.) the TGF-ß signalling pathway, 3.) neuroprotective factors and 4.) pro- and antiapoptotic factors. We therefore analysed the expression levels of the mentioned pathways in the two different experimental mice strains with a conditional deletion of Etb in the entire retina (*Etb*$^{\Delta eye}$) or in Müller cells and retinal neurons (*Etb*$^{\Delta OC}$) at the age of 6 weeks. For the *in vitro* studies, four individual photoreceptor cell lines with a stable deletion of Etb (*661W*$^{\Delta Etb}$) were used and four individual 661W control cell lines expressing Etb were used and are referred to as controls. The experimental cells (*661W*$^{\Delta Etb}$ and 661W control cells) were analysed in three independent experiments and harvested at P13, P14 and P15.

3.4.1 Relative mRNA expression levels of Endothelin signalling

First we analysed whether the deletion of Etb in the entire retina (*Etb*$^{\Delta eye}$), retinal neurons and Müller cells (*Etb*$^{\Delta OC}$) or photoreceptor cells (*661W*$^{\Delta Etb}$) would have an impact on the expression levels of members of the endothelin signalling pathway *in vivo* and *in vitro* (Figure 37).

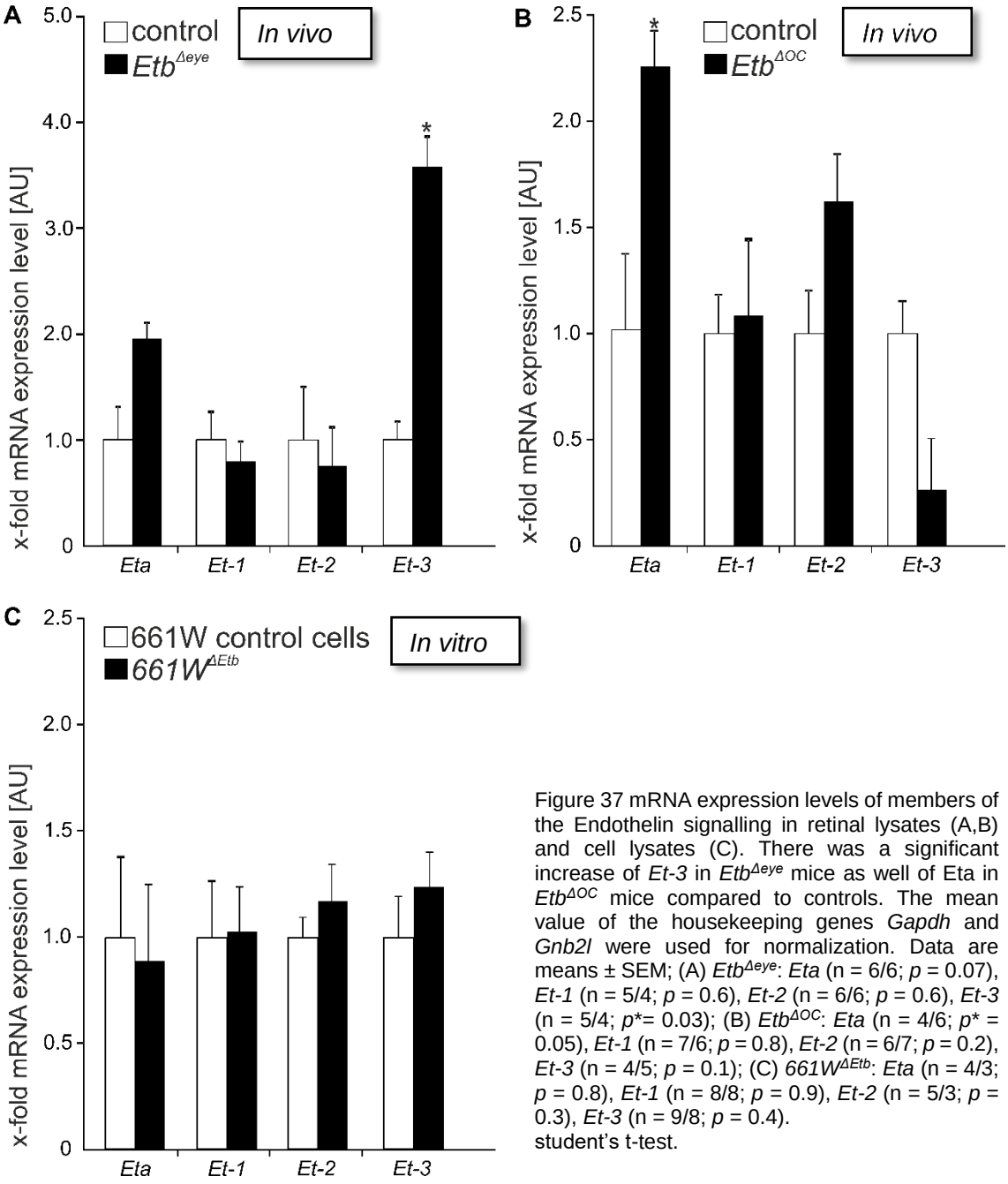

Figure 37 mRNA expression levels of members of the Endothelin signalling in retinal lysates (A,B) and cell lysates (C). There was a significant increase of *Et-3* in *Etb*$^{\Delta eye}$ mice as well of Eta in *Etb*$^{\Delta OC}$ mice compared to controls. The mean value of the housekeeping genes *Gapdh* and *Gnb2l* were used for normalization. Data are means ± SEM; (A) *Etb*$^{\Delta eye}$: *Eta* (n = 6/6; $p = 0.07$), *Et-1* (n = 5/4; $p = 0.6$), *Et-2* (n = 6/6; $p = 0.6$), *Et-3* (n = 5/4; $p^* = 0.03$); (B) *Etb*$^{\Delta OC}$: *Eta* (n = 4/6; $p^* = 0.05$), *Et-1* (n = 7/6; $p = 0.8$), *Et-2* (n = 6/7; $p = 0.2$), *Et-3* (n = 4/5; $p = 0.1$); (C) *661W*$^{\Delta Etb}$: *Eta* (n = 4/3; $p = 0.8$), *Et-1* (n = 8/8; $p = 0.9$), *Et-2* (n = 5/3; $p = 0.3$), *Et-3* (n = 9/8; $p = 0.4$).
student's t-test.

The relative mRNA expression levels of the members of the endothelin signalling pathway *in vitro* the showed comparable levels of all evaluated factors in *661W$^{\Delta Etb}$* (*Eta*: 0.89 ± 0.32, *p* = 0.8; *Et-1*: 1.01 ± 0.22, *p* = 0.9; *Et-2*: 1.16 ± 0.15; *p* = 0.3; *Et-3*: 1.21 ± 0.19, *p* = 0.4) compared to 661W control cells (*Eta*: 1.00 ± 0.3; *Et-1*: 1.00 ± 0.2; *Et-2*: 1.00 ± 0.1; *Et-3*: 1.00 ± 0.2).

Et-1 and *Et-2* were expressed at comparable mRNA levels in *Etb$^{\Delta eye}$* (*Et-1*: 0.79 ± 0.19, *p* = 0.6; *Et-2*: 0.76 ± 0.37, *p* = 0.7) and control mice (*Et-1*: 1.00 ± 0.26; *Et-2*: 1.00 ± 0.51). The relative mRNA expression of *Eta* was not significantly altered in *Etb$^{\Delta eye}$* mice (1.96 ± 0.15, *p* = 0.07) compared to controls (1.00 ± 0.31).Strikingly*, Etb$^{\Delta eye}$* mice depicted a significant (*p* *= 0.03) 3.6-fold increase of relative *Et-3* mRNA expression levels (3.57 ± 0.29) compared to controls (1.00 ± 0.17)

In *Etb$^{\Delta OC}$* mice, the relative mRNA expression levels of *Et-1*, *Et-2* and *Et-3* showed no significant alterations (*Et-1*:1.07 ± 0.34, *p* = 0.8*; Et-2*: 1.59 ± 0.19, *p* = 0.2; *Et-3*: 0.31 ± 0.20, *p* = 0.1) compared to controls (*Et-1*: 1.00 ± 0.36; *Et-2*: 1.00 ± 0.31; *Et-3*: 1.00 ± 0.44). The relative mRNA expression level of *Eta* was significantly increased (2.22 ± 0.18, *p** = 0.05) in *Etb$^{\Delta OC}$* mice compared to controls (1.00 ± 0.21).

Taken together, our results showed that the ablation of Etb *in vivo* resulted in an upregulation of members of the Endothelin signalling.

3.4.2 Relative mRNA expression levels of transforming growth factor β (Tgf-β) signalling

Tgf-β signalling is discussed to be associated with Endothelin signalling. Unpublished data from our group showed, that mice with a deletion of *Tgf-β* signalling in retinal neurons and Müller cells had significantly reduced *Et-2* mRNA expression levels in the retina. Moreover, Castañares and coworkers (2007) depicted an induction of *Et-1* by *Tgf-β* as there was a time-dependent increase in the steady-state *Et-1* mRNA levels of cultured vascular endothelial cells after incubation with Tgf-β compared with cells incubated under basal conditions (Castañares et al., 2006). Thus, we aimed to analyse whether the deletion of Etb in the entire retina (*Etb$^{\Delta eye}$*), retinal neurons and Müller cells (*Etb$^{\Delta OC}$*) or photoreceptor cells (*661W$^{\Delta Etb}$*) would have an impact on the expression levels of members of the *Tgf-β* signalling pathway. Consequently, we analysed the mRNA expression levels of *Tgf-β receptor 1* (*Tgfbr1*) and *Tgf-β receptor 2* (*Tgfbr2*) as well their ligands *Tgf-β1, Tgf-β2* and *Tgf-β3* in retinal lysates of 6 week-old *Etb$^{\Delta eye}$* (Figure 38 A left), *Etb$^{\Delta OC}$* (Figure 38 A right) mice and cell lysates of *661W$^{\Delta Etb}$* photoreceptor cells

(Figure 38 B) and 661W control cells.

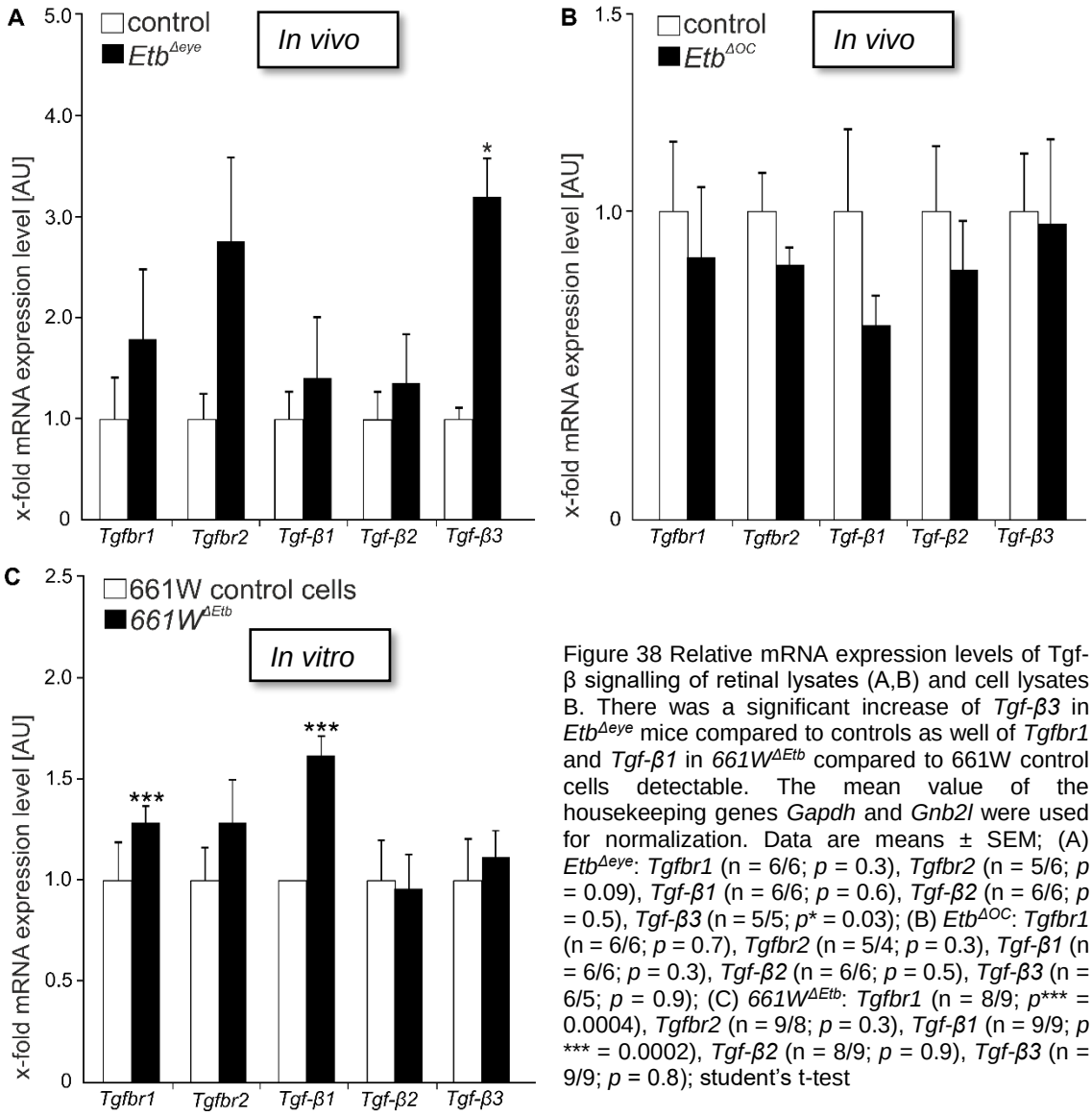

Figure 38 Relative mRNA expression levels of Tgf-β signalling of retinal lysates (A,B) and cell lysates B. There was a significant increase of *Tgf-β3* in $Etb^{\Delta eye}$ mice compared to controls as well of *Tgfbr1* and *Tgf-β1* in $661W^{\Delta Etb}$ compared to 661W control cells detectable. The mean value of the housekeeping genes *Gapdh* and *Gnb2l* were used for normalization. Data are means ± SEM; (A) $Etb^{\Delta eye}$: *Tgfbr1* (n = 6/6; p = 0.3), *Tgfbr2* (n = 5/6; p = 0.09), *Tgf-β1* (n = 6/6; p = 0.6), *Tgf-β2* (n = 6/6; p = 0.5), *Tgf-β3* (n = 5/5; p^* = 0.03); (B) $Etb^{\Delta OC}$: *Tgfbr1* (n = 6/6; p = 0.7), *Tgfbr2* (n = 5/4; p = 0.3), *Tgf-β1* (n = 6/6; p = 0.3), *Tgf-β2* (n = 6/6; p = 0.5), *Tgf-β3* (n = 6/5; p = 0.9); (C) $661W^{\Delta Etb}$: *Tgfbr1* (n = 8/9; p^{***} = 0.0004), *Tgfbr2* (n = 9/8; p = 0.3), *Tgf-β1* (n = 9/9; p *** = 0.0002), *Tgf-β2* (n = 8/9; p = 0.9), *Tgf-β3* (n = 9/9; p = 0.8); student's t-test

In $Etb^{\Delta OC}$ mice (Figure 38 B), the relative mRNA expression levels of all members of the *Tgf-β* signalling pathway remained unaffected in retinae of $Etb^{\Delta OC}$ mice (*Tgfbr1*: 0.85 ± 0.23, p = 0.7; *Tgfbr2*: 0.83 ± 0.06, p = 0.3; *Tgf-β1*: 0.63 ± 0.10, p = 0.3; *Tgf-β2*: 0.81 ± 0.16; p = 0.5; *Tgf-β3*: 0.95 ± 0.27, p = 0.9) compared to controls (*Tgfbr1*: 1.00 ± 0.23, p = 0.7; *Tgfbr2*: 1.00 ± 0.06, p = 0.3; *Tgf-β1*: 1.00 ± 0.27, p = 0.3; *Tgf-β2*: 1.00 ± 0.21; p = 0.5; *Tgf-β3*: 1.00 ± 0.19, p = 0.9).

In $Etb^{\Delta eye}$ mice (Figure 38 A), the relative mRNA expression levels of both receptors (*Tgfbr1*: 1.83 ± 0.38, p = 0.3; *Tgfβr2*: 2.81 ± 0.31, p = 0.09) and controls (*Tgfbr1*: 1.00 ± 0.43; *Tgfbr2*: 1.00 ± 0.27) as well as of the ligands *Tgf-β1* (1.42 ± 0.44, p = 0.6) and *Tgfβ2* (1.42 ± 0.45, p = 0.5) compared to controls (*Tgf-β1*: 1.00 ± 0.31; *Tgf-β2*: 1 ± 0.28) remained unaffected. $Etb^{\Delta eye}$ mice with a deletion of *Etb* in the entire retina showed a

significant increase (p = 0.03) of the relative mRNA expression level of *Tgf-β3* (3.25 ± 0.24) compared to controls (1.00 ± 0.29).

In Etb-deficient *661W*$^{\Delta Etb}$ photoreceptor cells (Figure 38 C), the relative mRNA expression levels of *Tgfbr2* (1.27 ± 0.23, p = 0.3), *Tgf-β2* (0.99 ± 0.15, p = 0.9) and *Tgf-β3* (1.13 ± 0.14, p = 0.8) were not altered significantly compared to 661W control cells (*Tgfbr2:* 1.00 ± 0.17, *Tgfβ2*: 1.00 ± 0.19; *Tgfβ3*: 1.00 ± 0.18). In contrast, there were significant elevations of *Tgfbr1*(1.27 ± 0.15, p= 0.0004) as well as *Tgfβ1* (1.64 ± 0.11, p = 0.0002) in cell lysates of *661W*$^{\Delta Etb}$ cells compared to 661W control cells (Tgfbr1: 1.00 ± 0.15; Tgfβ1: 1.00 ± 0.08) ascertainable.

Taken together, our results showed that, depending on the affected cellular population(s), the deficiency of Etb results in an upregulation of the Tgf-β signalling pathway.

3.4.3 Relative mRNA expression levels of pro-apoptotic and anti-apoptotic factors

As the overall aim of this thesis was to investigate whether the deletion of Etb might result in retinal neurodegeneration, we consequently analysed whether the Etb deletion itself might influence the expression levels of pro- and anti-apoptotic factors *in vivo* (*Etb*$^{\Delta eye}$; *Etb*$^{\Delta OC}$) and *in vitro* (*661W*$^{\Delta Etb}$) and their corresponding controls. We analysed the expression levels of pro-apoptotic factors *Caspase 8*, *Caspase 9*, *BH3-only BCL-2-interacting mediator of cell death (Bim)*, *Bcl2 associated X (Bax), Bcl2 associated death promotor (Bad)* and the anti-apoptotic *factor B-Cell Lymphoma 2 (Bcl2)* (Figure 39). Whereas *Caspase 8* is a key player in the extrinsic apoptotic signalling pathway via death receptors (Kominami et al., 2012), C*aspase 9* plays a decisive role in the intrinsic or mitochondrial pathway of apoptosis. This intrinsic pathway is regulated by proteins, which are pro- or anti-apoptotic, depending on their ability to promote (*Bim, Bax, Bad*) or suppress (*Blc2*) apoptotic mechanisms (Elmore, 2007).

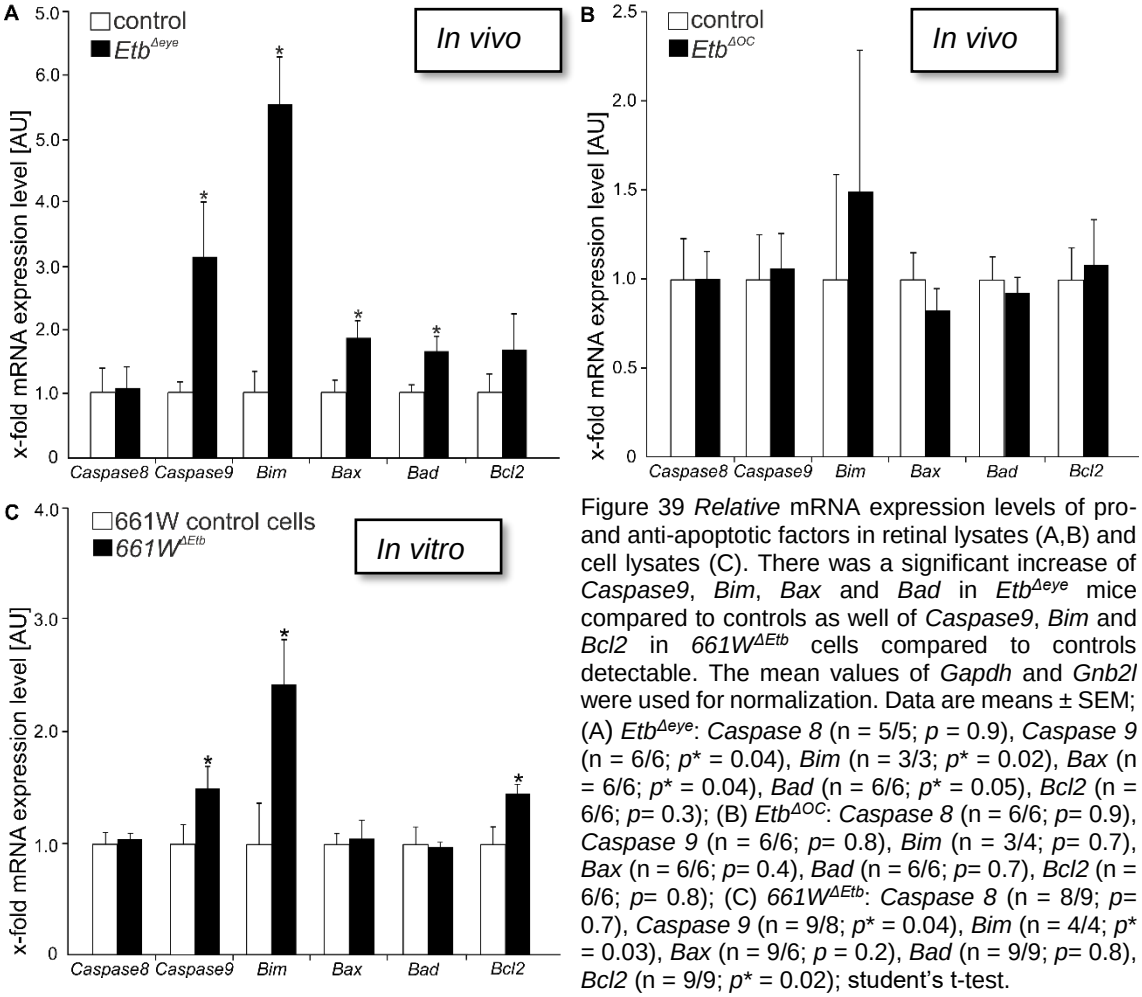

Figure 39 *Relative* mRNA expression levels of pro- and anti-apoptotic factors in retinal lysates (A,B) and cell lysates (C). There was a significant increase of *Caspase9*, *Bim*, *Bax* and *Bad* in $Etb^{\Delta eye}$ mice compared to controls as well of *Caspase9*, *Bim* and *Bcl2* in $661W^{\Delta Etb}$ cells compared to controls detectable. The mean values of *Gapdh* and *Gnb2l* were used for normalization. Data are means ± SEM; (A) $Etb^{\Delta eye}$: *Caspase 8* (n = 5/5; *p* = 0.9), *Caspase 9* (n = 6/6; *p** = 0.04), *Bim* (n = 3/3; *p** = 0.02), *Bax* (n = 6/6; *p** = 0.04), *Bad* (n = 6/6; *p** = 0.05), *Bcl2* (n = 6/6; *p*= 0.3); (B) $Etb^{\Delta OC}$: *Caspase 8* (n = 6/6; *p*= 0.9), *Caspase 9* (n = 6/6; *p*= 0.8), *Bim* (n = 3/4; *p*= 0.7), *Bax* (n = 6/6; *p*= 0.4), *Bad* (n = 6/6; *p*= 0.7), *Bcl2* (n = 6/6; *p*= 0.8); (C) $661W^{\Delta Etb}$: *Caspase 8* (n = 8/9; *p*= 0.7), *Caspase 9* (n = 9/8; *p** = 0.04), *Bim* (n = 4/4; *p** = 0.03), *Bax* (n = 9/6; *p* = 0.2), *Bad* (n = 9/9; *p*= 0.8), *Bcl2* (n = 9/9; *p** = 0.02); student's t-test.

$Etb^{\Delta OC}$ mice (Figure 39 B) showed no alterations of the relative mRNA expression levels of pro- as well as anti-apoptotic factors (*Caspase 8*: 1.01 ± 0.16, *p* = 0.9; *Caspase 9*: 1.07 ± 0.19, *p* = 0.8; *Bim*: 1.51 ± 0.81, *p* = 0.7; *Bax*: 0.83 ± 0.13, *p* = 0.4; *Bad*: 0.93 ± 0.10, *p* = 0.7; *Bcl2*: 1.09 ± 0.19 *p* = 0.8) compared to controls (*Caspase 8*: 1.00 ± 0.24; *Caspase 9*: 1.00 ± 0.20; *Bim*: 1.00 ± 0.60; *Bax*: 1.00 ± 0.16; *Bad*: 1.00 ± 0.16; *Bcl2*: 1.00 ± 0.26).

In $Etb^{\Delta eye}$ mice (Figure 39 A) the mRNA expression levels of the anti-apoptotic factor *Bcl2* (1.68 ± 0.35, *p* = 0.3) and *Caspase 8* (1.09 ± 0.32, *p* = 0.9) as part of an extrinsic pathway of apoptosis were not significantly altered compared to controls (*Bcl2:* 1.00 ± 0.35; *Caspase 8*: 1.00 ± 0.31). There were significant elevations of pro-apoptotic factors of the intrinsic pathway of apoptosis $Etb^{\Delta eye}$ mice detectable, as the relative mRNA expression levels of *Caspase 9* (3.12 ± 0.29, *p*= 0.04), *Bim* (5.51 ± 0.14, *p*= 0.02), *Bax* (1.86 ± 0.15; *p* = 0.04) and *Bad* (1.65 ± 0.15, *p* = 0.05) compared to controls (*Caspase 9*: 1.00 ± 0.21; *Bim*: 1.00 ± 0.37; *Bax*: 1.00 ± 0.22; *Bad*: 1.00 ± 0.14).

The *in vitro* studies (Figure 39 C) constituted no significant alterations of *Caspase 8* (1.03 ± 0.06, $p = 0.7$), *Bax* (1.07 ± 0.15, $p = 0.2$) and *Bad* (0.95 ± 0.05, $p = 0.8$) in cell lysates of photoreceptor cells lacking *Etb* (*661W*$^{\Delta Etb}$) compared to 661W control cells (*Caspase* 8: 1.00 ± 0.10; *Bax*: 1.00 ± 0.12; *Bad*: 0.95 ± 0.15) detectable. Noticeably, there was a 2.5-fold significant increase ($p = 0.03$) of the relative *Bim* mRNA expression level traceable in *661W*$^{\Delta Etb}$ cells (2.45 ± 0.38) compared to controls (1.00 ± 0.38). The relative mRNA expression level of *Caspase 9* (1.49 ± 0.15, $p = 0.04$) and *Bcl2* (1.45 ± 0.08, $p = 0.02$) were also significantly increased in *661W*$^{\Delta Etb}$ cells compared to controls (*Caspase* 9: 1.00 ± 0.10, *Bcl2*: 1.00 ± 0.13).

Taken together, our results showed that the deficiency *in vivo* in the entire retina (*Etb*$^{\Delta eye}$) and *in vitro* in photoreceptor cells (*661W*$^{\Delta Etb}$) resulted in an activation of an intrinsic pathway of apoptosis.

3.4.4 Relative mRNA expression levels of neuroprotective factors

Next, we aimed to investigate whether the mRNA expression levels of, *leukaemia inhibitory factor (Lif), fibroblast growth factor 2 (Fgf2)* and again of *Endothelin 2* (*Et-2*) (Chapter 3.4.1), all crucial factors of the neuroprotective loop in the retina, as well as brain-derived neurotrophic factor (*Bdnf*), debated as survival factor for photoreceptors, were affected by an *Etb*-deficiency *in vivo* (Figure 40 A, B) and *in vitro* (Figure 40 C).

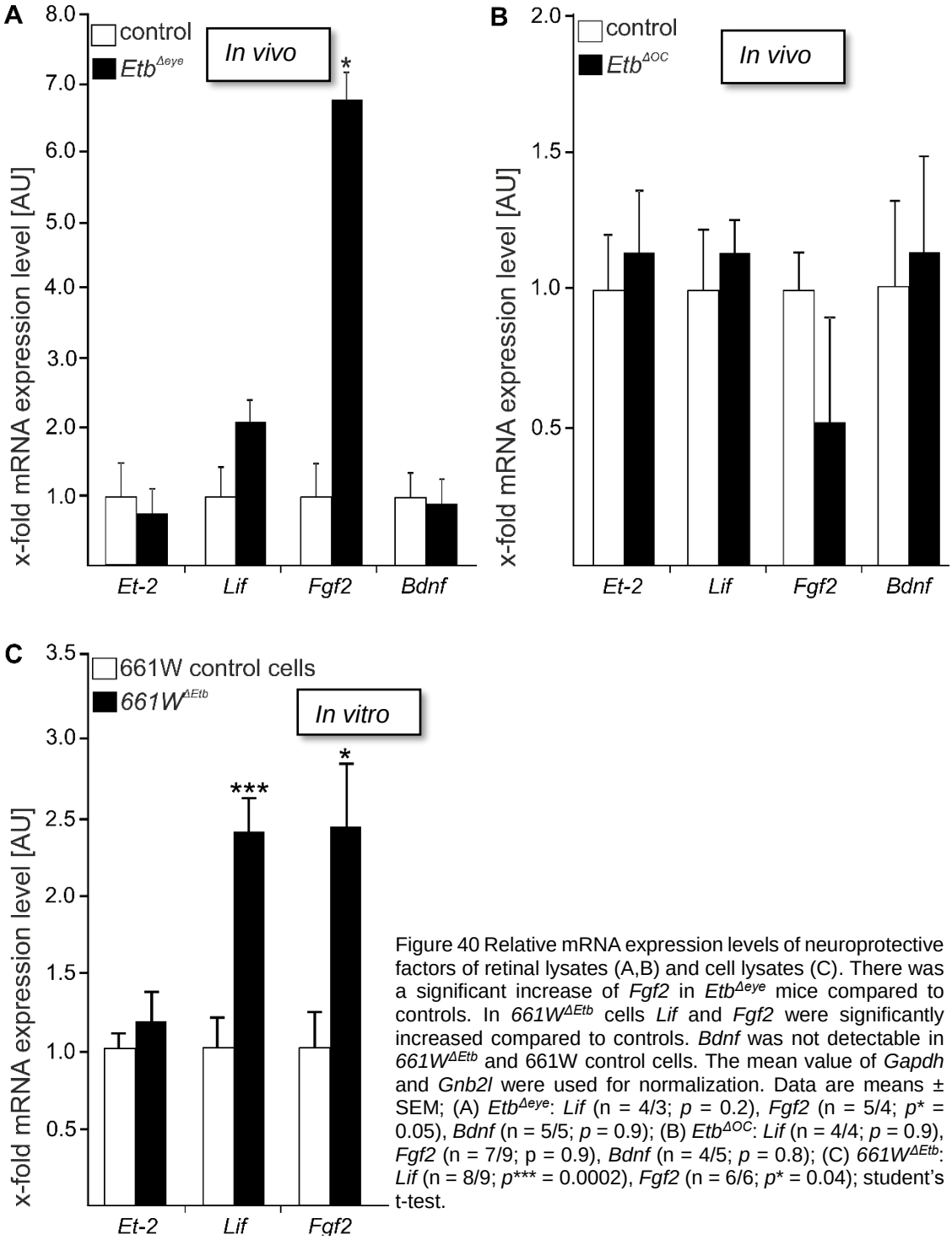

Figure 40 Relative mRNA expression levels of neuroprotective factors of retinal lysates (A,B) and cell lysates (C). There was a significant increase of *Fgf2* in $Etb^{\Delta eye}$ mice compared to controls. In $661W^{\Delta Etb}$ cells *Lif* and *Fgf2* were significantly increased compared to controls. *Bdnf* was not detectable in $661W^{\Delta Etb}$ and 661W control cells. The mean value of *Gapdh* and *Gnb2l* were used for normalization. Data are means ± SEM; (A) $Etb^{\Delta eye}$: *Lif* (n = 4/3; p = 0.2), *Fgf2* (n = 5/4; p^* = 0.05), *Bdnf* (n = 5/5; p = 0.9); (B) $Etb^{\Delta OC}$: *Lif* (n = 4/4; p = 0.9), *Fgf2* (n = 7/9; p = 0.9), *Bdnf* (n = 4/5; p = 0.8); (C) $661W^{\Delta Etb}$: *Lif* (n = 8/9; p^{***} = 0.0002), *Fgf2* (n = 6/6; p^* = 0.04); student's t-test.

In *Etb*$^{\Delta eye}$ mice (Figure 40 A) the relative mRNA expression levels of *Lif* (2.08 ± 0.32, p = 0.2) and *Bdnf* (0.91 ± 0.37, p = 0.9) were not altered significantly compared to controls (*Lif*: 1.00 ± 0.42; *Bdnf*: 1.00 ± 0.39) Predominantly, the relative mRNA expression level of *Fgf2* (6.76 ± 0.39) were significantly p = 0.05 increased compared to controls (1.00 ± 0.49).

In *Etb*$^{\Delta OC}$ mice, the relative mRNA expression levels of *Lif, Fgf2* and *Bdnf* did not differ between *Etb*$^{\Delta OC}$ mice (*Lif*: 1.06 ± 0.37; *Fgf2*: 1.04 ± 0.35; *Bdnf*: 1.12 ± 0.34) and controls (*Lif*: 1.00 ± 0.15; *Fgf2*: 1.00 ± 0.36, *Bdnf*: 1.00 ± 0.31).

As photoreceptors do not express receptors for *Bdnf*, the were no relative *Bdnf* mRNA expression levels detectable of *661W*$^{\Delta Etb}$ cells and 661W control cells. Tough, the relative mRNA expression of both *Lif* and *Fgf2* were significantly increased at comparable levels in *661W*$^{\Delta Etb}$ cells (*Lif*: 2.43 ± 0.18; *Fgf2*: 2.43 ± 0.39) compared to controls (*Lif*: 1.00 ± 0.18; *Fgf2*: 1.00 ± 0.23).

Taken together, our results showed that the deficiency of Etb led to elevated levels of neuroprotective factors of the retina *in vivo* (*Etb*$^{\Delta eye}$) and *in vitro* (*661W*$^{\Delta Etb}$).

3.5 Neuroprotective role of Etb *in vivo* and *in vitro* under pathological conditions

Next, we wanted to investigate potential neuroprotective aspects of Endothelin signalling for the survival of photoreceptor cells under pathological conditions *in vitro* (serum-deprivation) as well as *in vivo* (light-induced damage).

3.5.1 *In vivo*: Neuroprotective role of Etb on photoreceptors in the light-damaged retina

To examine whether Etb mediates a neuroprotective effect on photoreceptor survival, light-induced damages were performed to experimentally induce photoreceptor degeneration. As the rupture of the lens and the subsequent scar formation that we have observed in $Etb^{\Delta eye}$ mice, would tremendously affect the efficiency of the experimentally induced light damages, we decided to perform the following light-induced damages exclusively in $Etb^{\Delta OC}$ mice and controls. For light-induced damage, the experimental mice were dark adapted for a period of five days and then kept in transparent plastic cages and illuminated with cool white light (5000 lux) from the top for 1 h. The light-exposed $Etb^{\Delta OC}$ mice and the dark-adapted controls are referred to as $Etb^{\Delta OC}$ light or control light, respectively. In addition, light-unexposed $Etb^{\Delta OC}$ and control mice that were kept in the dark period of five days without any light exposure served as light-damage reference groups and referred to as $Etb^{\Delta OC}$ and controls.

3.5.1.1 TdT-mediated dUTP-biotin nick end labeling (TUNEL): Validation of light-induced damage and analysis of Etb-mediated neuroprotection

The examine whether *Etb* mediates a neuroprotective effect on photoreceptor survival, the rate of apoptotic photoreceptor cells was assessed in 6 week-old $Etb^{\Delta OC}$ light and control light animals after light exposure (light-induced damage). The eyes were enucleated 30 h after light-induced damage. To validate a successful induction of light induced apoptosis in photoreceptors and to investigate whether the deletion of Etb in retinal neurons and Müller cells might influence the rate of apoptosis, TdT-mediated dUTP-biotin nick end labeling (TUNEL) was performed on horizontal retinal sections to label apoptotic cells. To allow for statistical meaningful data, the number of apoptotic cells in light-exposed $Etb^{\Delta OC}$ mice and controls was determined and normalized to the area of the ONL (Figure 41).

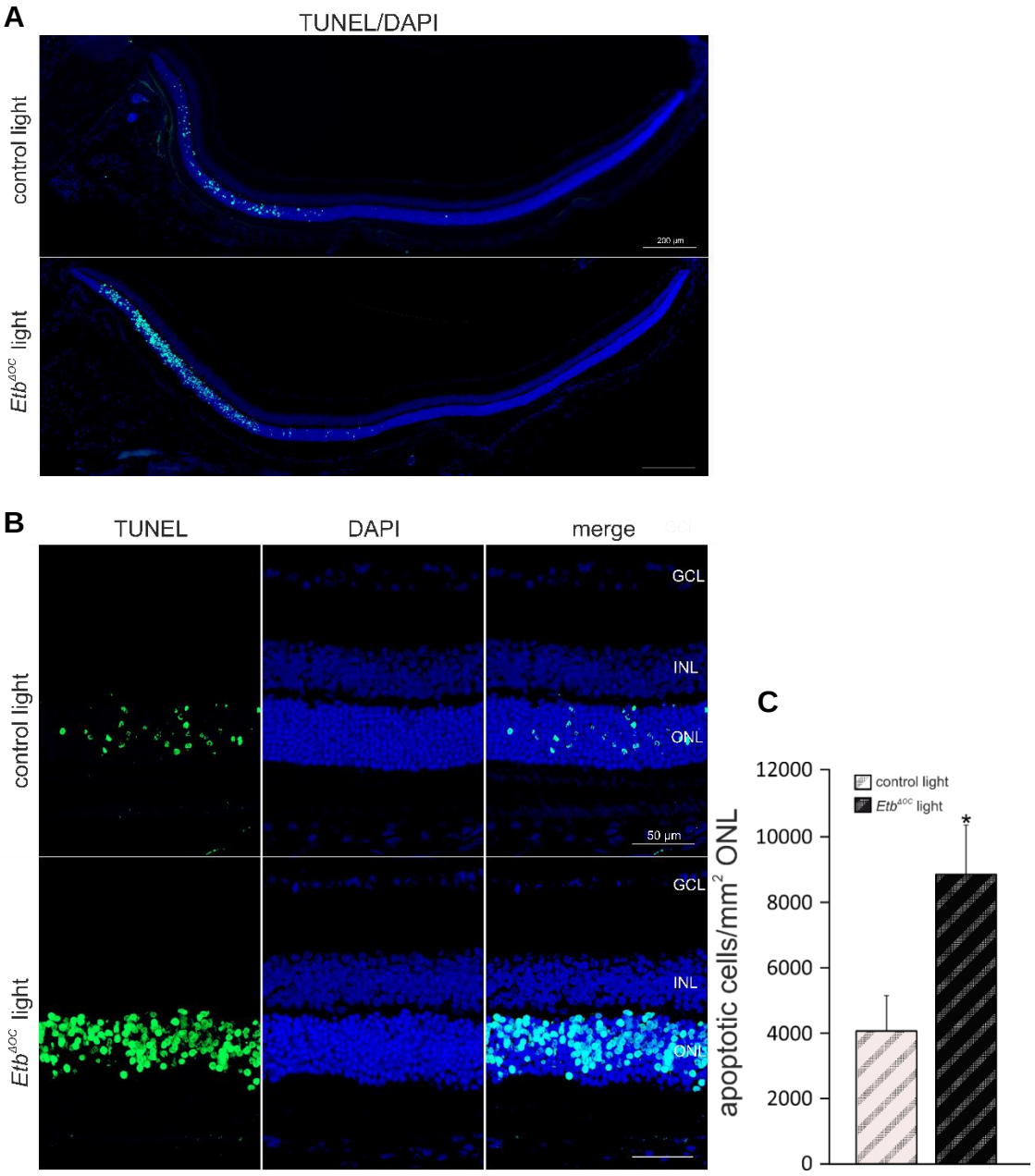

Figure 41 TUNEL staining of horizontal sections of the entire eye (A) and detailed magnification of the central retina (B) of a 6 week-old light exposed *Etb*$^{\Delta OC}$ and control mouse. TUNEL staining (green) showed a higher amount of apoptotic cells in the central part of the retina and in the outer nuclear layer (ONL) 30 h after light exposure in *Etb*$^{\Delta OC}$ mice compared to controls. The nuclei were stained with Dapi (blue). GCL= ganglion cell layer, INL= inner nuclear layer, RGC= retinal ganglion cell layer. (C) The number of apoptotic cells was counted and calculated as TUNEL-positive cells (= apoptotic cells)/mm^2 ONL in controls and *Etb*$^{\Delta OC}$ mice. Statistical analysis showed a significantly higher apoptosis rate in *Etb*$^{\Delta OC}$ mice than in controls. Data are means ± SEM. Control light n = 6; Etb$^{\Delta OC}$ light n = 8. *p** = 0.04; student's t-test.

On horizontal retinal sections, we observed the characteristic distribution of apoptotic cells following light exposure with only a small number of TUNEL-positive cells in the periphery, and numerous apoptotic cells in the central part of the illuminated retinae of *Etb*$^{\Delta OC}$ mice and controls (Figure 41 A). Remarkably, the number of TUNEL-positive cells (Figure 41 B) was significantly (p = 0.04) higher in light-exposed *Etb*$^{\Delta OC}$mice (4004.23 ± 1143.41) compared to controls (8769.04 ± 15776.61).

3.5.1.2 Morphometric analysis after light-induced damage

To verify, whether the observed higher rate of apoptotic cells in the ONL would affect the number of surviving photoreceptor cells, we used morphometric analysis of horizontal semithin-sections from nasal to temporal orientation of *Etb*$^{\Delta OC}$ mice and controls 14 days after light-induced damage (Figure 42). As expected, the light-induced damage was restricted to the central part of the retina resulting in a thinning of the ONL (Figure 42 A). A detailed magnification of the central retina (Figure 42 B) exemplified a remarkable thinning of the ONL following light exposure, which was considerably more pronounced in the *Etb*$^{\Delta OC}$mice compared to controls.

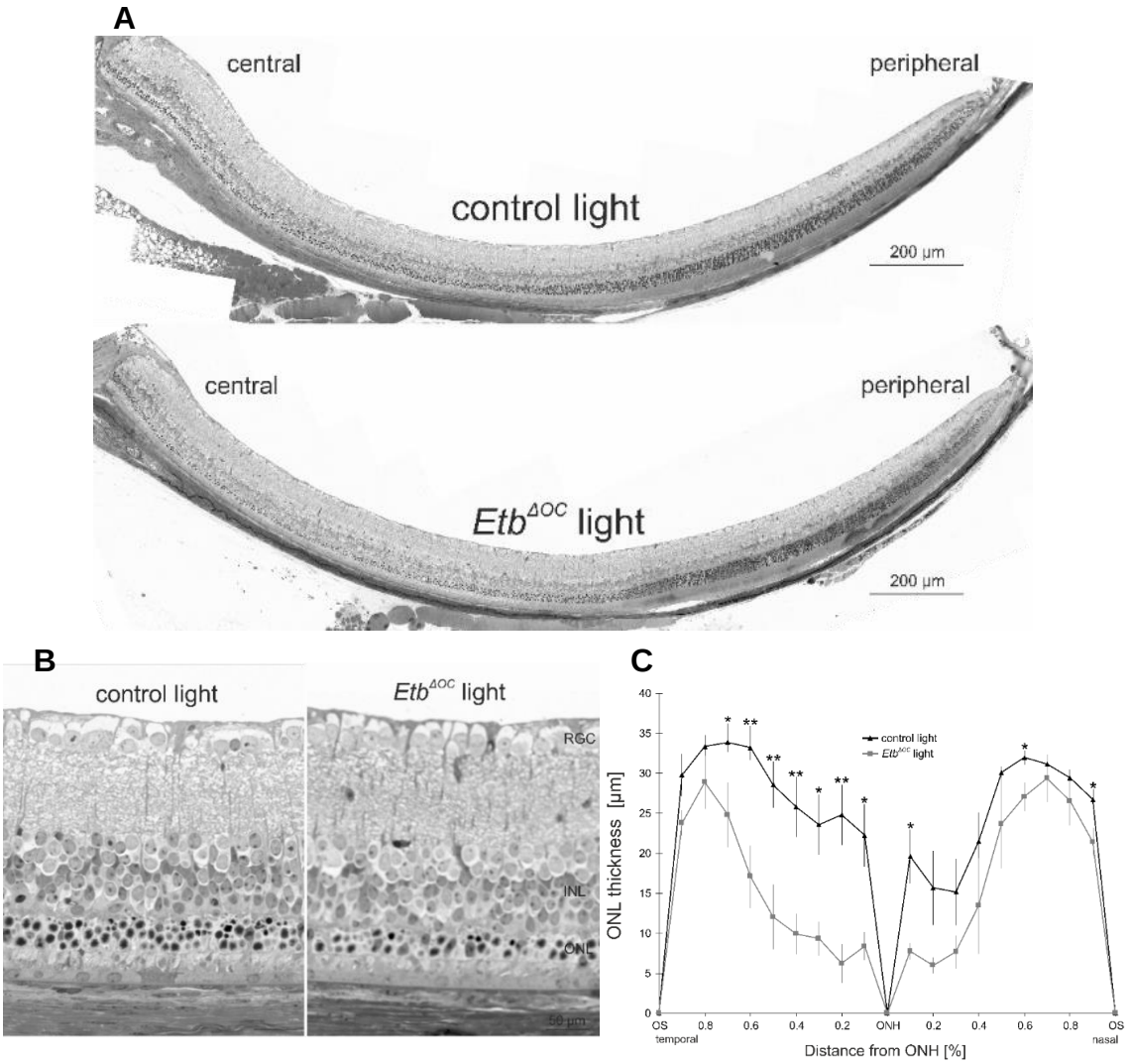

Figure 42 Semithin-sections of the eyes of a *Etb*$^{\Delta OC}$ mouse and its control littermate (8 week-old) 14 days after light-induced damage. Horizontal (1µm) semithin- sections (Richardson stained) of retinal hemispheres (A) and the central part of the retinae (B) showed an obvious thinning of the ONL in the central part which is more pronounced in *Etb*$^{\Delta OC}$ mice compared to controls, RGC =retinal ganglion cell layer, INL = inner nuclear layer, ONL = outer nuclear layer, RPE = retinal pigment epithelium. (C) Spider diagram of the thickness of the ONL in *Etb*$^{\Delta OC}$ mice and controls after light exposure. The thickness was measured on semithin-sections at 21 measure points from temporal to nasal side and the mean values of the ONL measurements were blotted in spider diagrams. There was a significant thinning of the INL and especially ONL detectable in the *Etb*$^{\Delta OC}$ mice (INL n=5, $p > 0.05$ (not significant); ONL n=5, $p^* \leq 0.05$, $p^{**} \leq 0.01$) and controls (n=4, $p^{**} \leq 0.01$). OS = ora serrata; ONH = optic nerve head. Data are means ± SEM, student's t-test.

For further quantification, the remaining thickness of the ONL was measured at 21 measure points from temporal to nasal side and the mean values of the ONL measurements were blotted in spider diagrams (Figure 42 C). The ONL *Etb*$^{\Delta OC}$ mice showed a significant thinning at 10 measure points compared to controls strongly indicating that the evaluated higher rate of apoptotic cells following light exposure indeed resulted in a pronounced degeneration of photoreceptors. In summary, these findings identify Etb mediated signalling as neuroprotective for the survival of photoreceptors.

3.5.1.3 Relative mRNA expression of Endothelin signalling after light-induced damage

An increased expression of Endothelin2 is well described in the context of photoreceptor degeneration and we furthermore recently showed that other members of the endothelin signaling pathway are upregulated following different ocular trauma (Chapter 0) (Rattner and Nathans, 2005; Joly et al., 2008; Braunger et al., 2013a). Hence, we analysed the mRNA expression levels of *endothelin receptor a* (*Eta)*, *endothelin 1* (*Et-1)*, *endothelin 2* (*Et-2)* and *endothelin 3* (*Et-3)* (Figure 43). 6 h after light damage, the eyes of *Etb*$^{\Delta OC}$ light and control light were enucleated and analysed via quantitative real-time RT-PCR. Two further experimental groups, light un-exposed *Etb*$^{\Delta OC}$ and control mice, served as reference groups for the light damage experiments. For that purpose, these mice were kept in the dark period for five days without any light exposure. These dark-adapted mice are referred to as *Etb*$^{\Delta OC}$ and control.

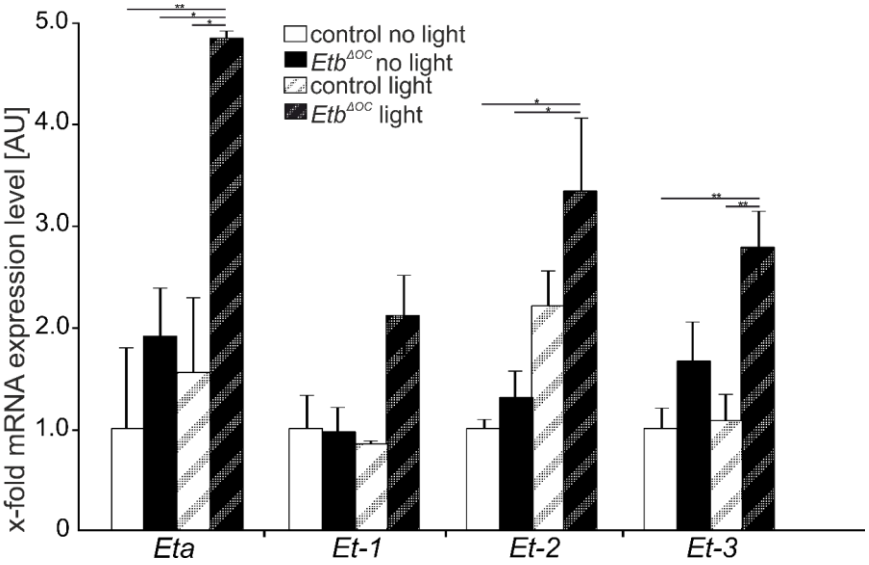

Figure 43 Relative mRNA expression levels of Endothelin signalling in 6 week-old controls and $Etb^{\Delta OC}$ retinae 6 h after light exposure and without light exposure. Relative *Et-1* mRNA levels were not significantly altered in control and $Etb^{\Delta OC}$ mice without and with light exposure. However, the relative Eta mRNA expression levels were significantly increased in $Etb^{\Delta OC}$ light retinae compared to un-exposed and light-exposed controls and $Etb^{\Delta OC}$ retinae without light exposure. The *Et-2* mRNA expression levels of $Etb^{\Delta OC}$ were significantly increased after light exposure compared to un-exposed $Etb^{\Delta OC}$ and controls. The *Et-3* mRNA expression was significantly elevated in light exposed $Etb^{\Delta OC}$ retinae compared to un-exposed and light-exposed controls. The mean value of *Gapdh* and *Ubiquitin c* were used for normalization. Data are means ± SEM. *Eta*: control no light n =3, control light n = 2, $Etb^{\Delta OC}$ no light n = 3, $Etb^{\Delta OC}$ light n = 2; *Et-1*: control no light n =4, control light n = 5, $Etb^{\Delta OC}$ no light n = 3, $Etb^{\Delta OC}$ light n = 6; *Et-2*: control no light n =3, control light n = 6, $Etb^{\Delta OC}$ no light n = 6, $Etb^{\Delta OC}$ light n = 6; *Et-3*: control no light n =4, control light n = 5, $Etb^{\Delta OC}$ no light n = 5, $Etb^{\Delta OC}$ light n = 5. $p^* \leq 0.05$, $p^{**} \leq 0.01$, one-way ANOVA.

After light exposure, the relative *Et-1* mRNA expression levels were not significantly altered in $Etb^{\Delta OC}$ mice (2.11 ± 0.39) compared to controls (control no light: 1.00 ± 0.33, p=0.47; $Etb^{\Delta OC}$ light: 2.11 ± 0.34, p=0.21, control light: 0.96 ± 0.03, p=0.96). In light-exposed $Etb^{\Delta OC}$ mice, there was a significant increase of the relative mRNA expression levels of *Eta* (4.84 ± 0.47) compared to un-exposed controls (1.00 ± 0.79, p=0.007), un-exposed $Etb^{\Delta OC}$ mice (1.91 ± 0.47, p=0.04). and light-exposed controls (1.55 ± 0.74, p=0.03), *Et-2* (3.33 ± 0.72) compared to un-exposed controls (1.00 ± 0.09, p=0.05) and un-exposed $Etb^{\Delta OC}$ mice (2.21 ± 0.47, p=0.34) and *Et-3* (3.33 ± 0.72) compared to un-exposed controls (1.00 ± 0.21, p=0.01) and light-exposed controls (1.07 ± 0.26, p=0.01).

Taken together, our results show that there was an activation of endothelin signalling (*Eta*, *Et-2*, *Et-3*) in $Etb^{\Delta OC}$ mice after light exposure.

3.5.1.4 Relative mRNA expression of Tgf-β Signalling after light-induced damage

Furthermore, we examined the effect of the deletion of Etb in retinal neurons and Müller cells following light damage on the relative mRNA expression levels of members of the Tgf-β signalling pathway (Figure 44).

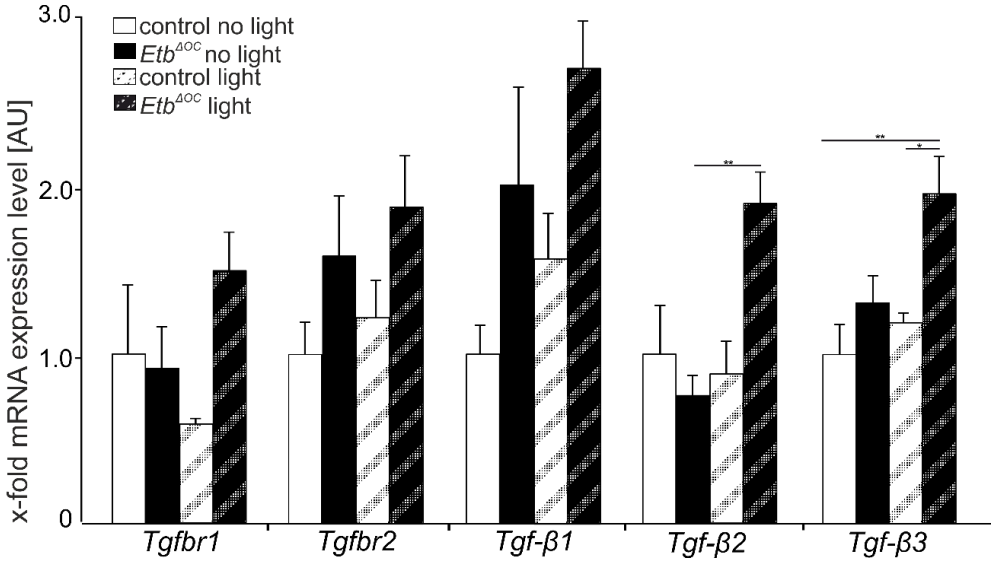

Figure 44 Relative mRNA expression levels of Tgf-β signalling in 6 week-old controls and $Etb^{\Delta OC}$ retinae without and 6 h after light exposure. Relative *Tgfbr1*, *Tgfbr2* and *Tgf-β1* mRNA expression levels were not significantly altered in all experimental mice. However, there was a significantly increased *Tgf-β2* mRNA expression level in light-exposed $Etb^{\Delta OC}$ mice compared to un-exposed $Etb^{\Delta OC}$ mice. Relative *Tgf-β3* mRNA levels were significantly increased $Etb^{\Delta OC}$ mice after light damage compared to un-exposed and light-exposed controls. The mean value of *Gapdh* and *Ubiquitin c* were used for normalization. Data are means ± SEM. *Tgfβr1*: control no light n =4, control light n = 6, $Etb^{\Delta OC}$ no light n = 5, $Etb^{\Delta OC}$ light n = 5; *Tgfβr2*: control no light n =4, control light n = 6, $Etb^{\Delta OC}$ no light n = 6, $Etb^{\Delta OC}$ light n = 5; *Tgfβ1*: control no light n =4, control light n = 6, $Etb^{\Delta OC}$ no light n = 6, $Etb^{\Delta OC}$ light n = 6; *Tgfβ2*: control no light n =4, control light n = 6, $Etb^{\Delta OC}$ no light n = 6, $Etb^{\Delta OC}$ light n = 5; *Tgfβ3*: control no light n =4, control light n = 6, $Etb^{\Delta OC}$ no light n = 6, $Etb^{\Delta OC}$ light n = 6. $p^* \leq 0.05$, $p^{**} \leq 0.01$, one-way ANOVA

In light exposed $Etb^{\Delta OC}$ mice, the relative mRNA expression levels of *Tgfbr1* (1.49 ± 0.23), *Tgfbr2* (1.87 ± 0.31) and *Tgfβ1* (2.71 ± 0.28) were not significantly altered (compared to *Tgfbr1*: control no light: 1.00 ± 0.42, p= 1.05; $Etb^{\Delta OC}$ no light: 0.91 ± 0.25, p= 0.95; control light: 0.58 ± 0.04, p= 0.12 ; *Tgfbr2*: control no light: 1.00 ± 0.20, p= 0.43; $Etb^{\Delta OC}$ no light: 1.58 ± 0.36, p= 0.83; control light: 1.22± 0.23, p= 0.77;*Tgf-β1*: control no light: 1.00 ± 0.17, p= 0.45; $Etb^{\Delta OC}$ no light: 2.00 ± 0.59, p= 0.063; control light: 1.56 ± 0.28, p= 0.39). Following light exposure the relative mRNA expression level of *Tgfβ-2* was significantly increased in $Etb^{\Delta OC}$ light mice (1.89 ± 0.18) compared to un-exposed $Etb^{\Delta OC}$ mice (0.75 ± 0.12, p= 0.004). Also the relative mRNA expression level of *Tgfβ-3* was significantly increased in $Etb^{\Delta OC}$ light mice (1.95 ± 0.22) compared to light-exposed control mice (1.19 ± 0.06, p= 0.02) and un-exposed control mice (1.00 ± 0.19, p= 0.008).

Taken together, our results show that there was an activation of Tgf-β signalling (*Tgfβ-2*, *Tgfβ*) in $Etb^{\Delta OC}$ mice after light exposure.

3.5.1.5 Relative mRNA expression of pro- and anti-apoptotic factors after light-induced damage

Furthermore, the impact of excessive light exposure on the relative mRNA expression levels of extrinsic (*Caspase 8*) and intrinsic (*Caspase 9, Bim, Bax, Bad)* apoptotic

signalling as well as the anti-apoptotic factor *Bcl2* was determined in *Etb*$^{\Delta OC}$ animals and controls (Figure 45).

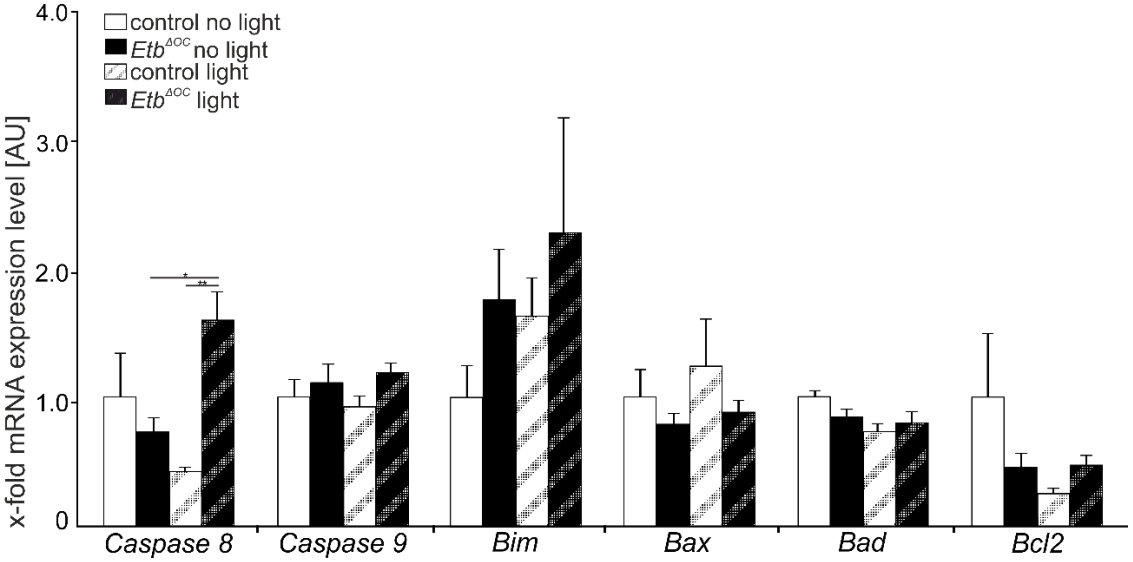

Figure 45 Relative mRNA expression levels of pro- and anti-apoptotic factors in 6 week-old controls and *Etb*$^{\Delta OC}$ retinae without and 6 h after light exposure. Relative Caspase 8 mRNA expression levels were significantly increased in light-exposed *Etb*$^{\Delta OC}$ mice compared to un-exposed *Etb*$^{\Delta OC}$ mice and light-exposed controls. There were no significant alterations of the relative mRNA expression levels of the other investigated pro- and anti-apoptotic factors. The mean values of *Gapdh* and *Ubiquitin c* were used for normalization. Data are means ± SEM. *Caspase 8*: control no light n =4, control light n = 6, *Etb*$^{\Delta OC}$ no light n = 5, *Etb*$^{\Delta OC}$ light n = 5; Caspase 9: control n =4, control light n = 5, *Etb*$^{\Delta OC}$ n = 6, *Etb*$^{\Delta OC}$ light n = 5; Bim: control n =2, control light n = 6, *Etb*$^{\Delta OC}$ no light n = 4, *Etb*$^{\Delta OC}$ light n = 2; *Bax*: control no light n =2, control light n = 4, *Etb*$^{\Delta OC}$ no light n = 5, *Etb*$^{\Delta OC}$ light n = 3; Bad: control no light n =4, control light n = 6, *Etb*$^{\Delta OC}$ no light n = 6, *Etb*$^{\Delta OC}$ light n = 6; Bcl2: control no light n =3, control light n = 5, *Etb*$^{\Delta OC}$ no light n = 6, *Etb*$^{\Delta OC}$ light n = 5. $p^* \leq 0.05$, $p^{**} \leq 0.01$; one-way ANOVA

Following light-induced damage, the relative mRNA expression levels of *Caspase 9* (1.19 ± 0.62)*, Bim* (2.23 ± 0.89)*, Bax* (0.88 ± 0.09)*, Bad* (0.80 ± 0.09) *and Bcl2* (0.47 ± 0.09) were not significantly altered in *Etb*$^{\Delta OC}$ mice (compared to *Caspase* 9: control no light: 1.00 ± 0.14, p=0.25; *Etb*$^{\Delta OC}$ no light: 1.11 ± 0.15, p=0.29; control light: 0.93 ± 0.08, p=0.11; *Bim*: control no light: 1.00 ± 0.25, p=0.31; *Etb*$^{\Delta OC}$ no light: 1.75 ± 0.39, p=0.56; control light: 1.63 ± 0.31, p=0.42; *Bax*: control no light: 1.00 ± 0.22, p=0.61; *Etb*$^{\Delta OC}$ no light: 0.79 ± 0.08, p=0.49; control light: 1.24 ± 0.38, p=0.11; *Bad*: control no light: 1.00 ± 0.07, p=0.17; *Etb*$^{\Delta OC}$ no light: 0.85 ± 0.07, p=0.69; control light: 0.73 ± 0.07, p=0.57; *Bcl2*: control no light: 1.00 ± 0.50, p=0.22; *Etb*$^{\Delta OC}$ no light: 0.46 ± 0.11, p=0.41; control light: 0.25 ± 0.05, p=0.11). Intriguingly, there was a significant elevation of the relative *Caspase 8* mRNA expression in light-exposed *Etb*$^{\Delta OC}$ mice (1.59 ± 0.22) compared to un-exposed *Etb*$^{\Delta OC}$ mice (0.73 ± 0.11, p=0.02) and light-exposed control mice (0.43 ± 0.004)

Taken together, our results show that light exposure promotes the extrinsic pathway of apoptosis (*Caspase 8*) in *Etb*$^{\Delta OC}$ mice.

3.5.1.6 Relative mRNA expression of neuroprotective factors after light-induced damage

Next, we examined the influence of the light-induced photoreceptor degeneration in *Etb*$^{\Delta OC}$ animals and controls on the expression levels of neuroprotective factors *Lif*, *Fgf2* and *Bdnf*, all involved in a molecular neuroprotective loop in the retina (Figure 46). As *Et-2* (already mentioned in Chapter 3.5.1.3) also distributes to retinal neuroprotection, it is again shown in this chapter.

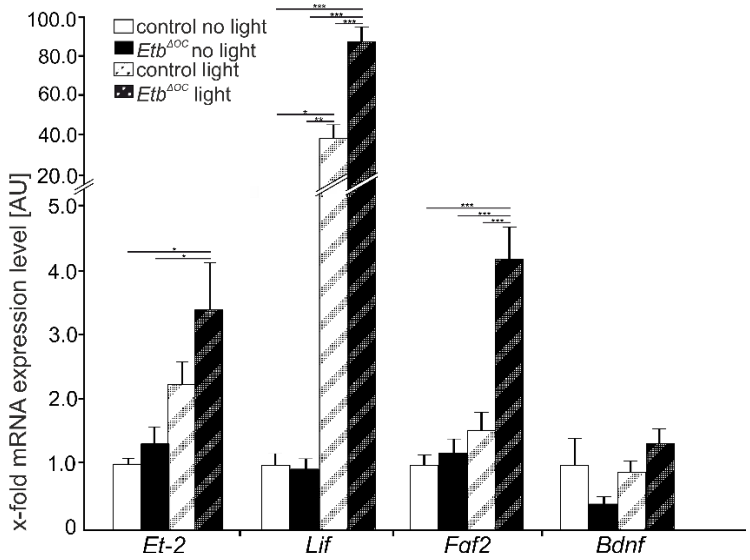

Figure 46 Relative mRNA expression levels of neuroprotective factors in 6 week-old controls and *Etb*$^{\Delta OC}$ retinae without and 6 h after light exposure. There were no significant alterations of the relative mRNA expression of *Bdnf* detectable Relative *Lif* and *Fgf2* mRNA expression levels were significantly increased in light-exposed *Etb*$^{\Delta OC}$ mice compared to un-exposed controls, un-exposed *Etb*$^{\Delta OC}$ mice and light-exposed controls. The mean value of *Gapdh* and *Ubiquitin c* were used for normalization. Data are means ± SEM. *Lif*: control no light n =4, control light n = 6, *Etb*$^{\Delta OC}$ no light n = 5, *Etb*$^{\Delta OC}$ light n = 5; Fgf2: control no light n =4, control light n = 5, *Etb*$^{\Delta OC}$ no light n = 6, *Etb*$^{\Delta OC}$ light n = 5; *Bdnf*: control no light n =2, control light n = 6, *Etb*$^{\Delta OC}$ no light n = 4, *Etb*$^{\Delta OC}$ light n = 2, $p^{*} \leq 0.05$, $p^{**} \leq 0.01$, $p^{***} \leq 0.001$ one-way ANOVA

The relative *Bdnf* mRNA expression levels were not significantly altered in light-exposed *Etb*$^{\Delta OC}$ mice (1.33 ± 0.22) (compared to control no light: 1.00 ± 0.39, *p*=; *Etb*$^{\Delta OC}$ no light: 0.39 ± 0.12, *p*=0.18; control light: 0.89 ± 0.18, *p*=0.47). There was a significant increase of the relative mRNA expression levels of *Lif* in light-exposed *Etb*$^{\Delta OC}$ mice (89.12 ± 7.54) compared to un-exposed controls (1.00 ± 0.19, *p*=0.0003), un-exposed *Etb*$^{\Delta OC}$ mice (0.95 ± 0.16, *p*=0.0001) and light-exposed controls (39.63 ± 7.02, *p*=0.0002) The excessive light exposure led also to a significant elevation of the relative *Fgf2* mRNA expression in *Etb*$^{\Delta OC}$ mice (4 ± 0.5) compared to un-exposed mice (control: 1.00 ± 0.16,

p=0.0002), un-exposed *Etb*$^{\Delta OC}$ mice (1.18 ± 0.23, *p*= *p*=0.0001) as well as light-exposed controls (1.54 ± 0.28, *p*= *p*=0.0002).

Taken together, our results show that light exposure induces the neuroprotective signalling, which is mediated by *Et-2*, *Lif*, *Fgf2*.

3.5.1.7 Relative protein expression level of pAKT/AKT signalling

Finally, we examined whether the observed increase in *Lif* and *Fgf2* after light-induced damage might have an impact on the activation of the Akt signaling pathway, a signal transduction pathway that promotes directly survival on the cell by its phosphorylated and activated form p(phospho)Akt. Western blot analysis and relative densitometry of retinal protein lysates of controls and *Etb*$^{\Delta OC}$ mice following light exposure (Figure 47 A) showed comparable relative protein levels of Akt in control (1.00 ± 0.29) and *Etb*$^{\Delta OC}$ mice (1.12 ± 0.23, *p* = 0.8).

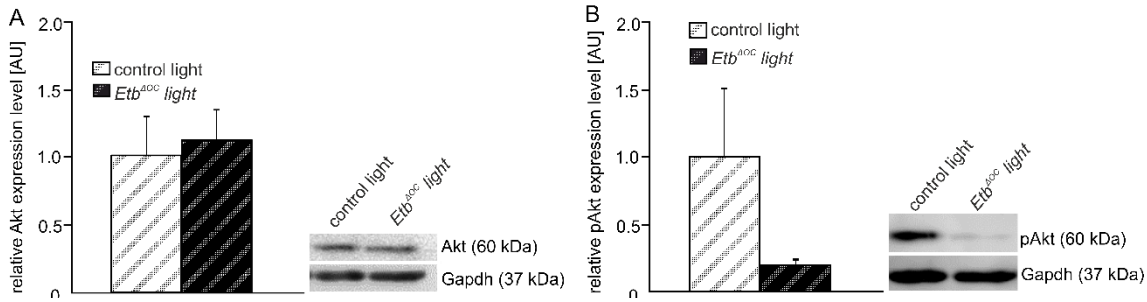

Figure 47 Relative densitometry of Akt and phospho-Akt in 6 week-old control and *Etb*$^{\Delta OC}$ retinae 6 h after light exposure. (A) Relative densitometry of Akt showed comparable protein expression levels in *Etb*$^{\Delta OC}$ mice compared to controls. (B) Relative densitometry of pAkt showed decreased expression in *Etb*$^{\Delta OC}$ mice compared to controls. Gapdh was used as for normalization. Data are means ± SEM, Akt: Control light n = 6; *Etb*$^{\Delta OC}$ light n = 6; *p* = 0.8; pAkt: Control light n = 5; *Etb*$^{\Delta OC}$ light n = 5; *p* = 0.2. student's t-test.

Quite intriguingly, the relative protein level of the activated form pAkt was remarkably decreased in the *Etb*$^{\Delta OC}$ mice (0.19 ± 0.05, *p* = 0.2) compared to controls (1.00 ± 0.51), a finding that might well explain the observed higher rate of apoptotic photoreceptors in *Etb*$^{\Delta OC}$ mice following light exposure.

3.5.2 *In vitro*: Neuroprotective role of Etb on cultured photoreceptor cells following serum-deprivation

To allow for a more detailed analysis of the impact of a deletion of etb on photoreceptor cells (*in vitro*) under pathological conditions, we caused a starvation stress in *661W*$^{\Delta Etb}$ and controls (P13) by serum-deprivation for 24 h. These cells are referred to as *661W*$^{\Delta Etb}$ serum-free and controls serum-free. *661W*$^{\Delta Etb}$ and 661W control cells were maintained

in normal amounts of serum and served as reference groups for the serum-free conditions.

3.5.2.1 TdT-mediated dUTP-biotin nick end labeling (TUNEL): Validation of serum-deprivation

To examine whether *Etb* mediates a direct neuroprotective effect on photoreceptor survival in an autocrine manner, we analysed the number of apoptotic cells in *661W$^{\Delta Etb}$* cells and 661W control cells after serum-deprivation for 24 h as well as in serum-treated *661W$^{\Delta Etb}$* cells and 661W control cells. To validate a successful cell stress via serum-deprivation, TdT-mediated dUTP-biotin nick end labeling (TUNEL, Chapter 6.5.6) was performed on 4%-PFA-fixed cells and the number of apoptotic cells in *661W$^{\Delta Etb}$* cells and 661W controls cells with and without serum was analysed (Figure 48) . The number of apoptotic cells was counted and calculated as the relative apoptosis rate of the totality of cells was determined (Figure 49). Serum-treated *661W$^{\Delta Etb}$* cells (2.5 ± 0.1) as well as serum-deprived controls (2 ± 0.06) and serum-deprived *661W$^{\Delta Etb}$* cells showed a higher number of TUNEL-positive cells compared to the serum-treated 661W control cells (1 ± 0.3). Strikingly, serum-deprived *661W$^{\Delta Etb}$* cells (4.1 ± 0.1) showed a significantly increased rate of apoptotic photoreceptor cells compared to all other experimental conditions (serum-treated 661W control cells, serum-deprived 661W cells and serum-treated 661W *661W$^{\Delta Etb}$* cells).

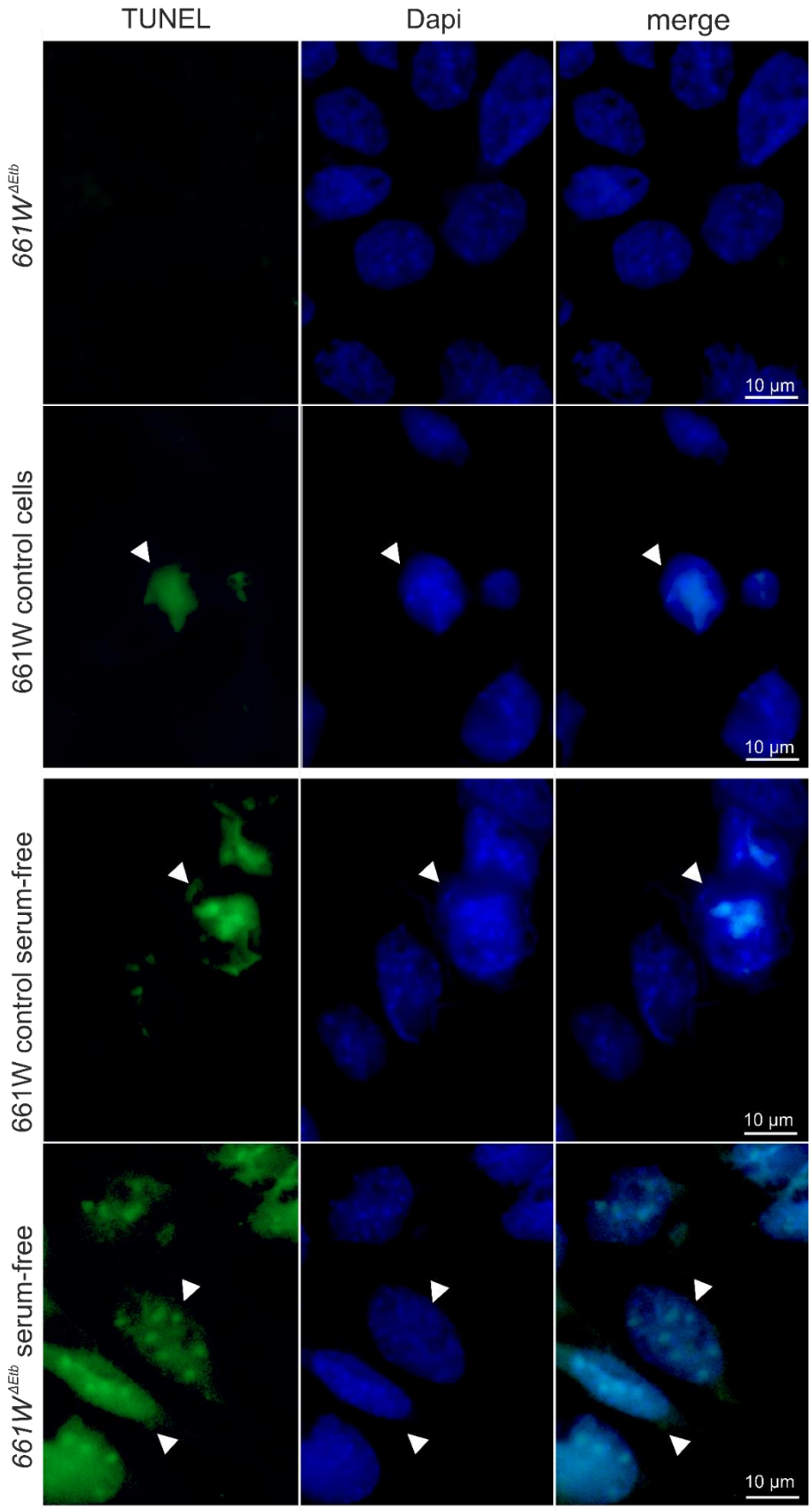

Figure 48 TUNEL staining of 4%PFA fixed *661W$^{\Delta Etb}$* cells and 661W control cells after serum-deprivation for 24 h and after serum-treatment. Numerous TUNEL positive cells were detectable (green) in cells after serum-deprivation for 24 h. The nuclei were stained with Dapi (blue).

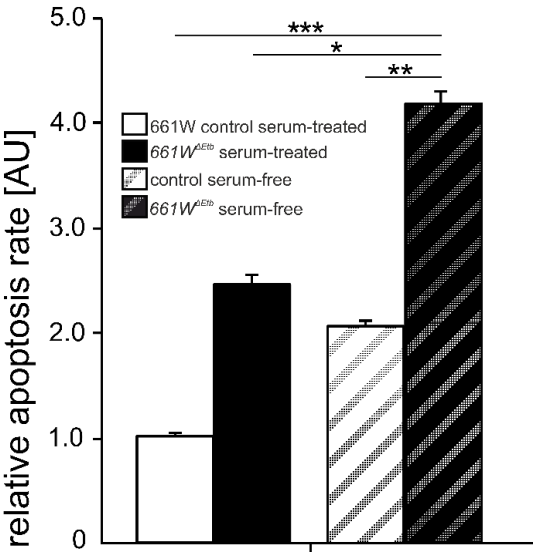

Figure 49 Relative apoptosis rate in *661W$^{\Delta Etb}$* cells and 661W control cells after serum-deprivation for 24 h as wells as in serum-treated *661W$^{\Delta Etb}$* cells and serum-treated 661W control cells. After serum-deprivation, *661W$^{\Delta Etb}$* cells showed a significant increased relative apoptosis rate. Data are means ± SEM, 661W control cells serum-treated n = 6; *Etb$^{\Delta OC}$* serum-treated n = 6; 661W control cells serum-free n = 6; *Etb$^{\Delta OC}$* serum-free n = 6. $p^* = 0.02$; $p^* = 0.005$, $p^{**} = 0.04$, $p^{***} = 0.0001$. one-way ANOVA

3.5.2.2 Relative mRNA expression of Endothelin signalling after serum-deprivation

Next, we analysed the mRNA expression levels of the Endothelin signalling family and therefore compared the relative mRNA expression levels of *Eta*, *Et-1*, *Et-2* and *Et-3* in cell lysates of serum-treated and serum-deprived cells (Figure 50).

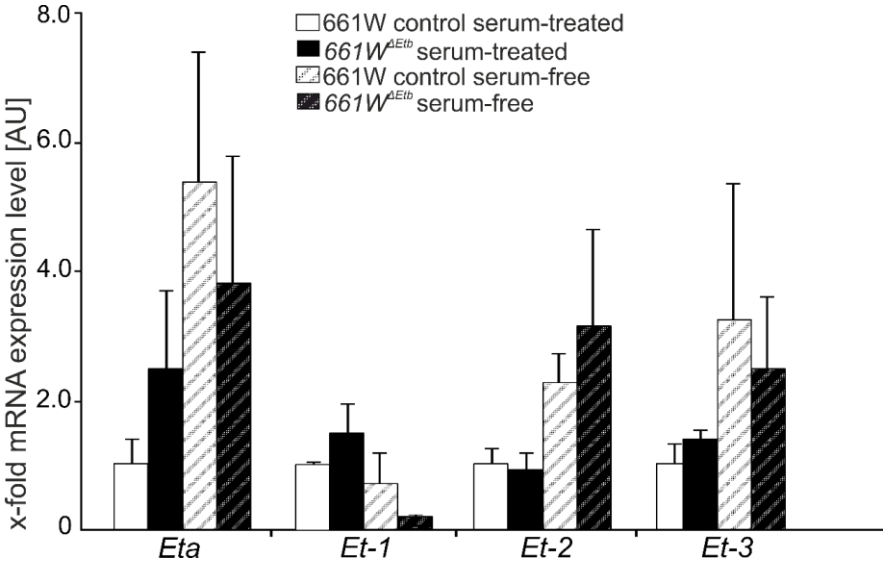

Figure 50 mRNA expression levels of Endothelin signalling in cell lysates of serum-treated *661W$^{\Delta Etb}$* and 661W control cells as well as serum-deprived (24 h) *661W$^{\Delta Etb}$* and 661W control cells. There were no significant alterations detectable. The mean values of *Gapdh* and *Gnb2l* were for normalization. Data are means ± SEM; *Eta*: control serum-treated n =2, 661W$^{\Delta Etb}$ serum-treated n = 2, control serum-free n = 3, *661W$^{\Delta Etb}$* serum-free n = 2; *Et-1*: control serum-treated n =2, *661W$^{\Delta Etb}$* serum-treated n = 3, control serum-free n = 2*; 661W$^{\Delta Etb}$* serum-free n = 3; *Et-2*: control serum-treated n =2*, 661W$^{\Delta Etb}$* serum-treated n = 3, control serum-free n = 3, *661W$^{\Delta Etb}$* serum-free n = 3; *Et-3:* control serum-treated n =2, *661W$^{\Delta Etb}$* serum-treated n = 2, control serum-free n = 2, *661W$^{\Delta Etb}$* serum-free n = 2; p >0.05; one-way ANOVA.

In serum-free *661W$^{\Delta Etb}$* cells, there were no significant alterations of the relative mRNA expression of *Eta* (3.81 ± 1.97), *Et-1* (0.20 ± 0.07) *Et-2* (3.14 ± 1.52) and *Et-3* (2.48 ± 1.13) detectable compared to serum-free 661W control cells (*Eta*: 5.37 ± 2.04; p= 0.64 *Et-1*: 0.70 ± 0.48, p=0.28; *Et-2*: 2.28 ± 0.44, p=0.61; *Et-3*: 3.25 ± 2.11, p=0.78) and to serum-treated cells (661W control cells: *Eta*: 1.00 ± 0.41, p=0.30; *Et-1*: 1.00 ± 0.00, p=0.81 ; *Et-2*: 1.00 ± 0.27, p=0.24; *Et-3*: 1.00 ± 0.33, p=0.34; *661W$^{\Delta Etb}$*: *Eta*: 2.49 ± 1.22, p=0.58; *Et-1*: 1.49 ± 0.47, p=0.07, *Et-2*: 0.92 ± 0.28, p=0.61; *Et-3*: 1.38 ± 0.16, p=0.78).

Taken together, our results show that the lack of Etb in photoreceptor cells does not affect the expression of the remaining endothelin signalling, under physiological as well as pathological conditions.

3.5.2.3 Relative mRNA expression levels of Tgf-β signalling after serum-deprivation

Subsequently, we aimed to analyse whether the deletion of Etb in photoreceptor cells would affect the expression of Tgf-beta signalling. We therefore examined the relative mRNA expression levels of *Tgfbr1*, *Tgfbr2, Tgf-β1, Tgf-β2* and *Tgf-β3* (Figure 51).

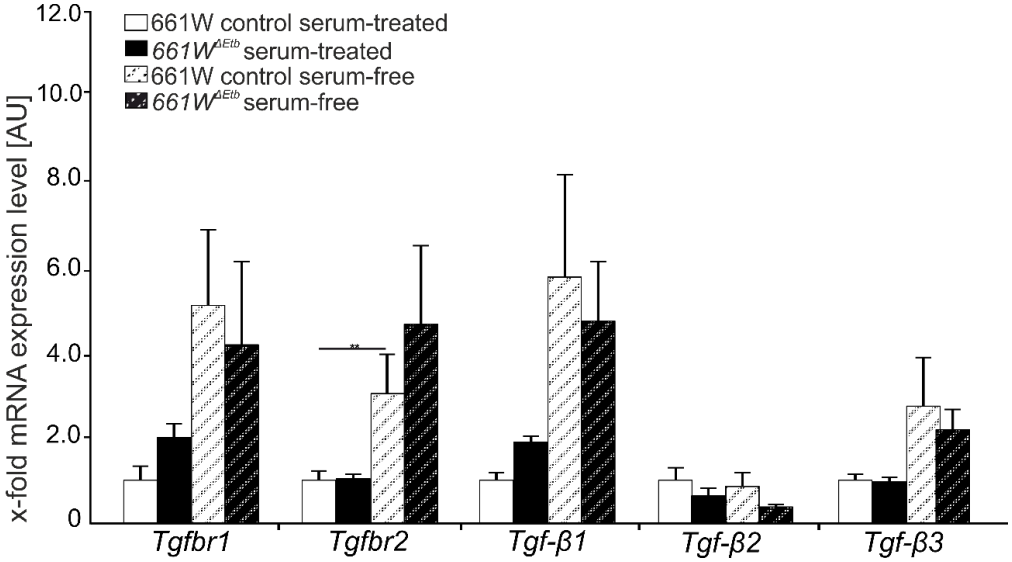

Figure 51 mRNA expression levels of Tgf-β signalling in cell lysates of serum-treated 661W$^{\Delta Etb}$ and 661W control cells as well as serum-deprived (24 h) *661W$^{\Delta Etb}$* and 661W control cells. The relative mRNA expression levels of *Tgfbr2* was significantly in serum-deprived *661W$^{\Delta Etb}$* cells compared to serum-treated controls, whereas the remaining members of Tgf-β signalling were not significantly altered. The mean of values of *Gapdh* and *Gnb2l* were used for normalization. Data are means ± SEM; *Tgfbr1*: control serum-treated n =3, *661W$^{\Delta Etb}$* serum-treated n = 3, control serum-free n = 3, *661W$^{\Delta Etb}$* serum-free n = 3; *Tgfbr2*: control serum-treated n =3, *661W$^{\Delta Etb}$* n = 3, control serum-free n = 3, *661W$^{\Delta Etb}$* serum-free n = 3; *Tgf-β1*: control serum-treated n =3, *661W$^{\Delta Etb}$* serum-treated n = 3, control serum-free n = 3, *661W$^{\Delta Etb}$* serum-free n = 3; *Tgf-β2*: control serum-treated n =3, *661W$^{\Delta Etb}$* serum-treated n = 3, control serum-free n = 3, *661W$^{\Delta Etb}$* serum-free n = 3; *Tgf-β3*: control serum-treated n =3, *661W$^{\Delta Etb}$* serum-treated n = 3, control serum-free n = 3, *661W$^{\Delta Etb}$* serum-free n = 2; $p^* \leq 0.05$; $p > 0.05$, one-way ANOVA.

The relative mRNA expression levels of *Tgfbr1*, *Tgf-β1, Tgf-β2* and *Tgf-β3* were not significantly altered in serum-free *661W$^{\Delta Etb}$* cells (*Tgfbr1*: 4.16 ± 1.98; *Tgf-β1*: 4.72 ± 1.42; *Tgf-β2*: 0.35 ± 0.08; *Tgf-β3*: 2.16 ± 0.52) compared to serum-treated 661W control cells (*Tgfbr1*: 1.00 ± 0.33, *p*=0.69; *Tgf-β1*: 1.00 ± 0.19, *p*=0.07; *Tgf-β2*: 1.00 ± 0.30, *p*=0.10; *Tgf-β3*: 1.00 ± 0.16, *p*=0.11); serum-treated *661W$^{\Delta Etb}$* cells (*Tgfbr1*: 1.99 ± 0.34, *p*=0.34; *Tgf-β1*: 1.88 ± 0.16, *p*=0.12; *Tgf-β2*: 0.62 ± 0.18, *p*=0.24; *Tgf-β3*: 0.96 ± 0.11, *p*=0.10) and serum-free 661W control cells (*Tgfbr1*: 5.06 ± 1.79, *p*=0.75; *Tgf-β1*: 5.74 ± 2.40, *p*=0.74; *Tgf-β2*: 0.84 ± 0.36, *p*=;0.25 *Tgf-β3*: 2.73 ± 1.14, *p*=0.53). After serum-deprivation, the relative mRNA expression levels of *Tgfbr2* was significantly (*p*=0.003) elevated (4.63 ± 1.85) in serum-deprived *661W$^{\Delta Etb}$* cells compared to serum treated controls (1.00 ± 0.23).

Taken together, our results show that serum-deprived photoreceptor cell stress activates Tgf-β signalling (*Tgfbr2*).

3.5.2.4 Relative mRNA expression levels of pro- and anti-apoptotic factors after serum-deprivation

Next, the effect of serum-deprivation on apoptotic pathways was determined by analysing the members of the extrinsic (*Caspase 8*) and intrinsic (*Caspase 9*, *Bim*, *Bax*, *Bad*) pathway of apoptosis as well as the anti-apoptotic factor *Bcl2* (Figure 52).

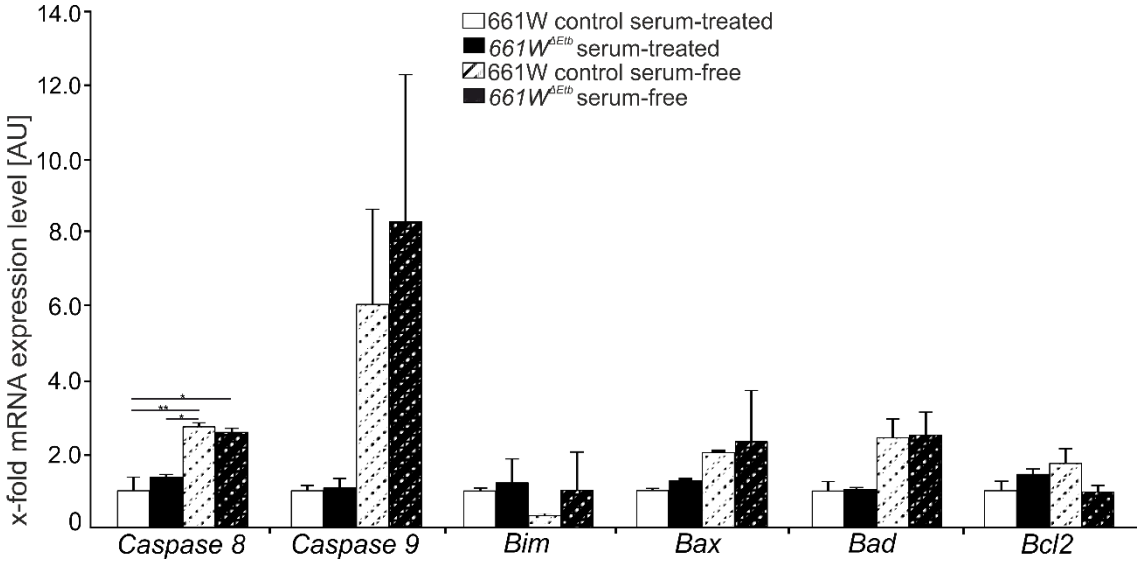

Figure 52 mRNA expression levels of pro- and anti-apoptotic factors in cell lysates of serum-treated *661W$^{\Delta Etb}$* and 661W control cells as well as serum-deprived (24 h) *661W$^{\Delta Etb}$* and 661W control cells. The relative *Caspase 8* mRNA expression was significantly elevated in serum-deprived 661W control cells and *661W$^{\Delta Etb}$* cells. There were no further significant alterations detectable. The mean value of *Gapdh* and *Gnb2l* were used for normalization. Data are means ± SEM; *Caspase8*: control serum-treated n =3, *661W$^{\Delta Etb}$* serum-treated n = 3, control serum-free n = 3, *661W$^{\Delta Etb}$* serum-free n = 3; *Caspase9*: control serum-treated n =3, *661W$^{\Delta Etb}$* serum-treated n = 3, control serum-free n = 3, *661W$^{\Delta Etb}$* serum-free n = 3; *Bim*: control serum-treated n =3, *661W$^{\Delta Etb}$* serum-treated n = 3, control serum-free n = 3, *661W$^{\Delta Etb}$* serum-free n = 3; *Bax*: control serum-treated n =3, *661W$^{\Delta Etb}$* serum-treated n = 3, control serum-free n = 3, *661W$^{\Delta Etb}$* serum-free n = 3; *Bad*: control serum-treated n =3, *661W$^{\Delta Etb}$* serum-treated n = 3, control serum-free n = 3, *661W$^{\Delta Etb}$* serum-free n = 2; *Bcl2*: control serum-treated n =3, *661W$^{\Delta Etb}$* serum-treated n = 3, control serum-free n = 3, 661W$^{\Delta Etb}$ serum-free n = 2; $p^* \leq 0.05$, $p^{**} \leq 0.01$, p >0.05 one-way ANOVA.

After serum-deprivation, the relative mRNA expression levels of the pro-apoptotic factors *Caspase 9*, *Bim, Bax, Bad* and the anti-apoptotic factor *Bcl2* were not significantly altered in *661W$^{\Delta Etb}$* cells (*Caspase 9*: 8.29 ± 3.99; *Bim*: 1.08 ± 1.00; *Bax*: 2.30 ± 1.45; *Bad*: 2.49 ± 0.67; *Bcl2:* 0.94 ± 0.22) compared to serum-treated 661W control cells (*Caspase 9*: 1.00 ± 0.15, *p*=0.14; *Bim*: 1.00 ± 0.13, *p*=0.49; *Bax*: 1.00 ± 0.06, *p*=0.31; *Bad*: 1.00 ± 0.27, *p*=0.1; *Bcl2:* 1.00 ± 0.26, *p*=0.89), serum-treated *661W$^{\Delta Etb}$* (*Caspase 9*: 1.06 ± 0.26, *p*=0.15; *Bim*: 1.22 ± 0.78, *p*=0.80; *Bax*: 1.23 ± 0.02, *p*=0.54; *Bad*: 1.03 ± 0.06, *p*=0.10; *Bcl2:* 1.41 ± 0.17, *p*=0.17) and serum-free 661W control cells (*Caspase 9*: 6.03 ± 2.59, *p*=0.66; *Bim*: 0.31 ± 0.04, *p*=0.52; *Bax*: 2.02 ± 0.03, *p*=0.87; *Bad*: 2.43 ± 0.52, *p*=0.96; *Bcl2:* 1.71 ± 0.46, *p*=0.20). In contrast, the relative *Caspase 8* mRNA expression was significantly elevated in serum-deprived controls (2.73 ± 0.10) compared to serum-

treated 661W control cells (1.00 ± 0.38, *p*=0.005) and serum-treated *661W$^{\Delta etb}$* cells (1.37 ± 0.07, *p*=0.02). Furthermore, the relative *Caspase 8* mRNA expression levels was significantly increased after serum-deprivation in *661W^{Etb}* cells (2.58 ± 0.11) compared to serum-treated 661W control cells (1.00 ± 0.38, *p*=0.02).

In summary, the serum-deprivation of 661W control cells as well as *661W^{Etb}* cells leads to an activation of the extrinsic pathway of apoptosis (*Caspase 8*).

3.5.2.5 Relative mRNA expression levels of neuroprotective factors after serum-deprivation

At last, we examined the effect of serum-deprivation on the relative mRNA expression of the neuroprotective factors *Lif* and *Fgf2*. As *Et-2* (already mentioned in Chapter 3.5.2.2) is also member of the retinal neuroprotective loop, it is again listed in this chapter.

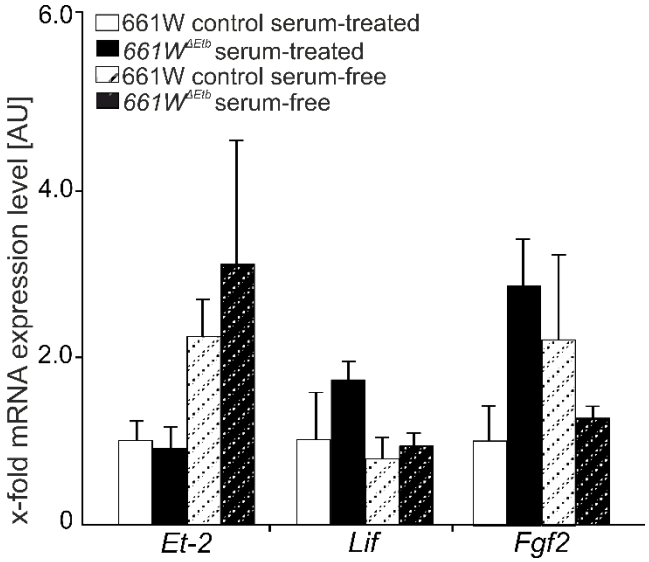

Figure 53 mRNA expression levels of neuroprotective factors in cell lysates of serum-treated *661W$^{\Delta Etb}$* and 661W control cells as well as serum-deprived (24 h) *661W$^{\Delta Etb}$* and controls. There were no significant alterations detectable. The mean value of *Gapdh* and *Gnb2l* were used for normalization. Data are means ± SEM; *Lif*: control serum-treated n =3, *661W$^{\Delta Etb}$* serum-treated n = 3, control serum-free n = 3, *661W$^{\Delta Etb}$* serum-free n = 3; *Fgf2*: control n =3, *661W$^{\Delta Etb}$* serum-treated n = 3; *p* >0.05; one-way ANOVA.

After serum-deprivation, the were no significant alterations of the relative *Et-2*, *Lif* and *Fgf2* mRNA expression levels in *661W$^{\Delta Etb}$* cells (*Lif*: 0.93 ± 0.15; *Fgf2*: 1.25 ± 0.17) compared to serum-treated controls (*Lif*: 1.00 ± 0.54, *p*=0.90; *Fgf2*: 1.00 ± 0.41, *p*=0.68), serum-treated *661W$^{\Delta Etb}$* cells (*Lif*: 1.70 ± 0.85, *p*=0.38; *Fgf2*: 2.78 ± 0.57, *p*=0.14) and serum-untreated controls (*Lif*: 0.76 ± 0.29, *p*=0.65; *Fgf2*: 2.18 ± 1.00, *p*=0.53).

In summary, serum-deprivation does not induce neuroprotection in photoreceptor cells.

3.6 Proteomics analysis: proteasomal dysregulation in photoreceptor cells following Etb-deficiency (*in vivo*)

In cooperation with Dr. Stefanie Hauck (Helmholtz-Zentrum München), we performed proteomics, a large-scale study of the proteome, the totality of proteins, of the *Etb*-deficient *661W$^{\Delta Etb}$* cells and controls (James et al., 1997). The objective of the following proteomics analysis was to identify proteins in photoreceptor cells that were affected by the *Etb* -deficiency and allow to classify the underlying molecular mechanisms that might be affect through the deletion of Etb. With the help of mass spectrometry, the proteome analysis allowed us to identify 5801 proteins among them 144 proteins with a down-regulation and 130 proteins with an up-regulation after correcting the significance for multiple comparison (Figure 54 A). For describing correlation patterns among the analysed proteins, weighted correlation network analysis (WGCNA) was performed in cooperation with Dr. Andreas Neueder (Neurology, University Ulm). The WGCNA network displayed regulated modules (Figure 54 B). Each vertical line represented a specific protein, whereas branches illustrated proteins with highly correlated expression pattern and were summarized to modules. One negatively and one positively module was identified with a significant association to *Etb*-deficiency (Figure 54 C). A positive correlation corresponded to a higher expression or rather a negative correlation to a lower expression in 661WΔEtb cells compared to controls. The highest regulated proteins were defined as hub genes via an intra-module connectivity in the positive module (Pos 1 hub proteins) and negative module (Neg1 hub proteins). Figure 54 (D, E) illustrates the Top 50 hub proteins with the Top 500 strongest connectivities. Mainly, *661W$^{\Delta Etb}$* cells showed significant alterations of protein expression in several sections like catabolic and metabolic processes as well as protein transport. Remarkably, *661W$^{\Delta Etb}$* cells depicted significant alterations in a group of proteins which are associated with proteasomal degradation processes (e.g.PSMA1/3, PSMD13, USP14 Protein) indicating a proteasomal dysregulation following *Etb*-deficiency.

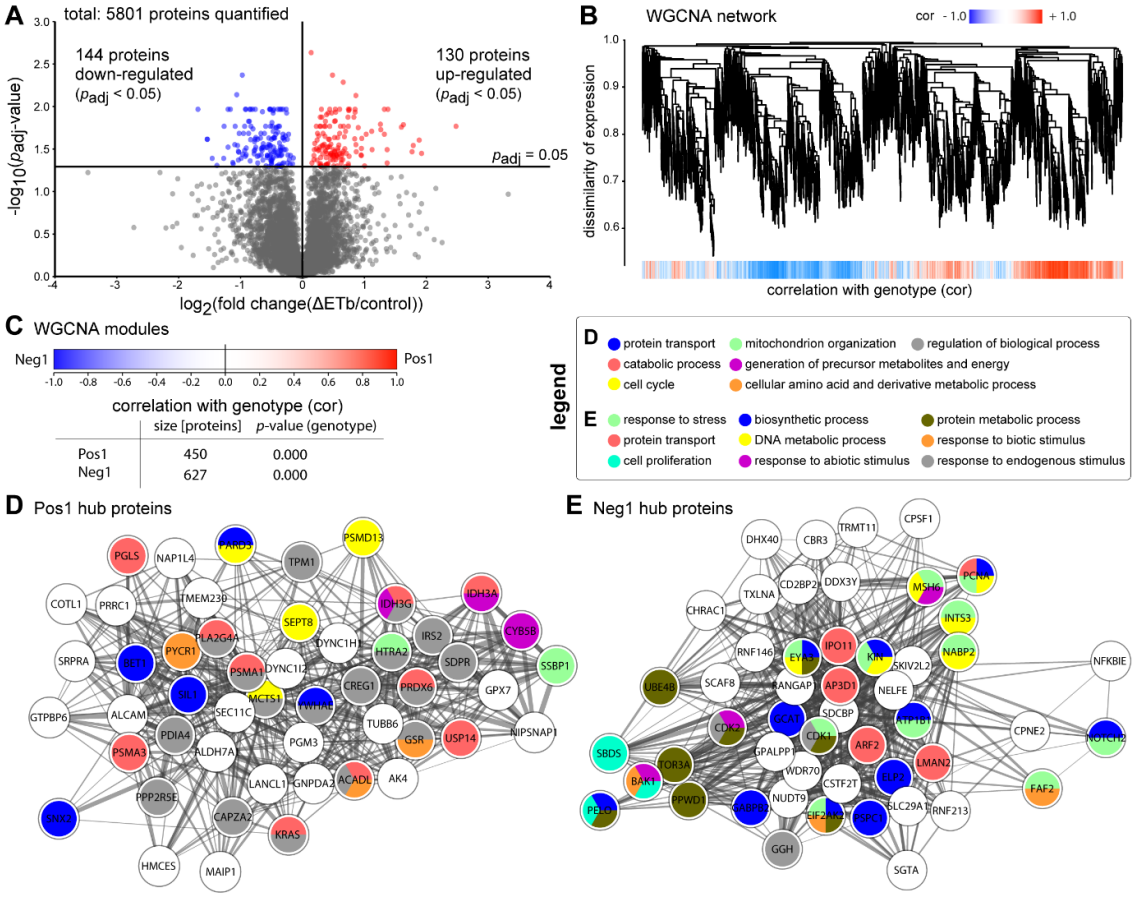

Figure 54 Proteomics and WGCNA analyses of *661W$^{\Delta Etb}$* cells and controls. (A) Volcano Plot showing analysis of dysregulation in *661W$^{\Delta Etb}$* cells and 661W control cells. Padj are Benjamini-Hochberg corrected p-values (two-tailed, homoscedastic student's t-test). (B) WGCNA network displaying regulated modules. Each vertical line represented a specific protein, whereas branches illustrated proteins with highly correlated expression pattern and were summarized to modules. (C) One negatively and one positively correlated module was identified with a significant association to Etb-deficiency. A positive correlation corresponded to a higher expression or rather a negative correlation to a lower expression in *661W$^{\Delta Etb}$* cells compared to controls. (D/E) The highest regulated proteins were defined as hub genes via an intra-module connectivity in the positive module (Pos 1 hub proteins) and negative module (Neg1 hub proteins). The Top 50 hub proteins with the Top 500 strongest connectivities (connecting line) were shown. The strength of each connecting line correlates to the intensity of co-regulation. Hub proteins were coloured according to their ontologies (generic GOslim Ontology for mice). Only significant ontologies are shown (hypergeometric test, Benjamini-Hochberg corrected FDR < 0.05). Remarkably, *661W$^{\Delta Etb}$* cells depicted significant alterations in a group of proteins which are associated with proteasomal degradation processes indicating a proteasomal dysregulation following Etb-deficiency. In cooperation with Dr. Andreas Neueder (Neurology, University Ulm).

4 Discussion

Based on the data of this thesis, we conclude that Etb mediated signalling in the entire eye is (1) essential for the cellular and morphological organization of the lens. (2) Does not obviously affect the retinal morphology but results in an (3) increased expression Eta and of specific pericyte markers indicating that Eta and the pericyte population most likely compensate for the loss of Etb mediated signalling in the retina and the vascular microenvironment, respectively.

We furthermore conclude that the cell type specific deletion of Etb mediated signalling in retinal neurons and Müller cells (4) does not obviously affect the retinal morphology but results in an (5) increased expression of retinal Eta. The data of this thesis furthermore show that after light induced degeneration or serum deprivation, Etb mediated signalling is (6) an essential key regulator of photoreceptor survival that (7) mediates its downstream signalling through activation of Akt signalling, concomitant with (8) the regulation of caspase-mediated apoptosis. Thus, we conclude that Etb-mediated signalling is crucial for photoreceptor survival following traumatic damages.

4.1 Lens phenotype: Endothelin receptor b is essential for cellular homeostasis and Collagen IV synthesis in the lens

Quite intriguingly, we observed morphological alterations of the lens in 30% of the *Etb*$^{\Delta eye}$ mice, whereas the remaining 70% *Etb*$^{\Delta eye}$ mice and controls manifested lenses with normal appearance. One possible explanation for the non-fully penetrant effects could be due to a varying degree of cells that are affected by the deletion of Etb following tamoxifen induced recombination.

The affected lenses showed a collapsed, vacuolated structure. Presumably, a rupture of the lens capsule led to a release of lenticular material in the vitreous and we furthermore observed scar-like formation in the raptured areas.

Similar to our findings, comparable pathologies of the lens were already observed at our department in mice with a Tgf-β1 overexpression in the lens, driven by the very strong chicken βB1-crystallin promotor (Flügel-Koch et al., 2002). This promotor has been shown to drive lens-specific expression and to be active in both primary and secondary lens fibres from embryonic (E) day 12.5 until adulthood (Flügel-Koch et al., 2002; Duncan et al., 1996). In these transgenic lenses, besides the degeneration and deformation of anterior fibres, also epithelial cells underwent apoptotic cell death leading to a missing

lens epithelium following Tgf-β1 overexpression. Probably, this phenotype was due the high activity of the βB1-crystallin promotor and the consequently resulting very high expression of Tgf-β1, as other Tgf-β1 overexpressing mice using the less active, but also lens-specific αA-crystallin promoter (αA–TGF-β1) showed no comparable lens pathologies (Srinivasan et al., 1998; Overbeek et al., 1985; Flügel-Koch et al., 2002). The lens phenotype in Tgf-β1 overexpression mice was already manifested at embryonic stages suggesting developmental lenticular disorganization, which probably based on the βB1-crystallin promotor activation and Tgf-β1 expression starting its activity at E12.5. The tamoxifen inducible chicken β actin promoter in *Etb*$^{\Delta eye}$ mice was induced at adult age and led to a downregulation of endothelin receptor b (Etb). Thus, based on our data, we hypothesized that a deletion of Etb in the lens might lead to a rupture of the lens epithelium and in turn of the lens capsule resulting to the release of lenticular material in the vitreous and the formation of scarring structures. The lens epithelium is a simple cuboidal epithelium (Forrester, 1996) and regulates osmotic concentration and volume of the lens via Na^+/K^+-ATPase pumps in the lens epithelial cells (Candia, 2004). In this regard, there are publication showing that *Et-1* has an inhibitory effect on Na^+/K^+-transport as measurements of ouabain-sensitive potassium (^{86}Rb) *ex vivo* indicated that a dose-dependent treatment with *Et-1* reduced the rate Na^+/K^+-ATPase–mediated potassium transport in porcine lens resulting in a detectable increase of the sodium content of the lens (Okafor and Delamere, 2001). This Et-1 mediated effect was suppressed by a pharmacological inhibition of Eta and Etb suggesting that Et1 slows active Na^+/K^+-transport by a mechanism involving an activation of both endothelin receptors (Okafor and Delamere, 2001). Similar Et-1 mediated inhibitory effects on Na^+/K^+-ATPase were also shown in cultured rat vascular smooth muscle cells (Meyer-Lehnert et al., 1989) and in the rat renal proximal tubule (Garvin and Sanders, 1991). It is therefore reasonable to assume that the lack of Etb in the lens epithelium of *Etb*$^{\Delta eye}$ mice resulted in a disturbed Na^+/K^+-transport and thus the collapse of the cellular homeostasis of the lens.

Furthermore, the lens capsule, a specialized thickened basement membrane, is mainly composed of the extra cellular matrix protein collagen IV, which comprises a family of six polypeptides, subunits alpha1(IV)-alpha6(IV), each of which is encoded by a distinct gene (COL4A1-A6) (Kelley et al., 2002). Mutations in COL4A3,COL4A4, and COL4A5 like in the Alport Syndrome prevent the proper assembly of a specialised collagen network, in basement membranes. Amongst other pathologies, these mutations are associated with an increased risk of lens capsular rupture (Firtina et al., 2009), quite similar to the observed phenotype in *Etb*$^{\Delta eye}$ mice. Our immunohistochemical staining against collagen IV showed a distinct and continuous collagen IV expression on top of

the lens capsule in the control mice, whereas fluorescence intensity was attenuated in *Etb*$^{\Delta eye}$ mice without any lens phenotype. However, *Etb*$^{\Delta eye}$ mice demonstrating the lens phenotype, showed only a weak and punctual collagen IV signal in the lens capsule. Therefore, we hypothesized that Etb-deficiency in the lens is associated with a gradually reduced collagen IV expression in the lens capsule resulting in a collagen improper capsular network formation and finally resulting in the rupture of the lens. Supporting our hypothesis Rao *et al*. found a dose-dependent Et-1 mediated regulation of collagen synthesis in primary cultured human lamina cribrosa cells (Rao et al., 2008). However, this effect was mediated via both receptors as only a dual pharmacological blockage of *Eta* and *Etb* inhibited collagen protein expression (Rao et al., 2008), while the blocking of *Eta* and *Etb* alone had no effects on collagen expression (Rao et al., 2008). Similar effects were reported from studies using human peritoneal mesothelial cells and fibroblasts where a combined *Eta/Etb*-blockage also interrupted *Et-1* mediated collagen synthesis (Morgera et al., 2003, 2003, 2003; Shi-Wen et al., 2001, 2001). However, as our Eta staining showed only very faint Eta signals in the lens, Etb is obviously the most dominant endothelin receptor in the lens. Thus, the lack of Etb in the lens of in *Etb*$^{\Delta eye}$ mice might very well result in an impaired collagen IV synthesis.

4.2 The regulation of the endothelin receptors

Remarkably, we could show a compensatory regulation of *Eta* and *Etb* receptors in retinal samples*.* Retinal lysates of *Etb*-deficient *Etb*$^{\Delta eye}$ mice showed a two-fold increase in *Eta* expression compared to controls. Moreover, retinal lysates of *Etb*$^{\Delta OC}$ mice showed a two-fold and significant increase in *Eta* expression compared to controls. These findings suggest that an upregulation of *Eta* expression might compensate for the lacking expression of *Etb.* Regarding vascular motricity, it has already been shown that *Eta* and *Etb* receptors underly a complex synergistic interaction (Just et al., 2004) to regulate the balance between primarly *Eta*-mediated vasoconstriction in smooth muscle cells and *Etb* promoted vasodilatation in vascular endothelial cells (Kedzierski and Yanagisawa, 2001; Hirata et al., 1993; Davenport et al., 2016). In this context Just and coworkers showed that *Etb* mediated vasodilation, caused by a selective pharmacological agonistic via direct infusion into the renal artery of rats, only after a pharmacological stimulation of *Eta,* which indicates a close interaction of both receptors *(Just et al., 2004)*. Furthermore, such Eta/Etb receptors' synergy has been shown in the vasculature as an *Et-1* induced contraction of vascular smooth muscle cells measured by isometrically recordings of an *ex vivo* isolated rabbit pulmonary artery was only completely inhibited by a combined pharmacological blockage of both receptors, but not by *Eta* or *Etb only* (Fukuroda et al.,

1994b). This indicates that the activation of either only Eta or only Etb may be sufficient to compensate the expression of the lacking receptor and to cause vasoconstriction (Fukuroda et al., 1994b). Remarkably, *Etb*$^{\Delta eye}$ mice showed no vascular phenotype, probably due to the compensatory effect of Eta. It is reasonable to assume that the pericytes might be one of the cell-types reacting with an increased Eta expression. *Eta* is expressed by these cells (McDonald et al., 1995) and we furthermore detected an increased number of pericytes enclosing the vasculature of *Etb*$^{\Delta eye}$ mice by immunohistochemical staining concomitant with an upregulation of the mRNA expression of the pericyte marker *Ng-2* and *Pdgfrb* in retinae of *Etb*$^{\Delta eye}$ mice. In contrast, in our *in vitro* experiments *Eta* levels were not altered between *Etb*-deficient photoreceptor cells (*661W*$^{\Delta OC}$) and 661W control cells.

4.3 Etb deficiency and its effects on the retinal and choroidal vasculature

Endothelin signaling is involved in a variety of physiological functions, above all the regulation of vasomotricity, blood pressure and vascular homeostasis (Rautureau et al., 2015). Regarding the vasculature, Eta is predominantly expressed by vascular smooth muscle cells, whereas Etb is expressed by both vascular smooth muscle and endothelial cells (Guan et al., 2015). Given physiological conditions, the two receptors are considered to possess synergistic but also opposite actions with Eta and Etb promoting vasoconstriction and vasoconstriction, whereas Etb on endothelial cells contributes additionally to vasodilation (Schneider et al., 2007). Just as a short reminder, of the two analysed mouse strains in this thesis (*Etb*$^{\Delta eye}$ and *Etb*$^{\Delta OC}$), only in *Etb*$^{\Delta eye}$ animals the deletion of Etb affected all ocular cells (including (peri)vascular cells), while in *Etb*$^{\Delta OC}$ mice the deletion was restricted to retinal neurons and Müller cells only. Thus remarkably, the *Etb*$^{\Delta eye}$ mice manifested no obvious morphological alterations of the retinal and choroidal vasculature. In this context it is important to note that the CAGGCre-ER recombinase in *Etb*$^{\Delta eye}$ mice was activated at the age of four weeks to induce Etb-deficiency, a time point when retinal vessel development was already completed. Presumably, an induction of the CAGGCre-ER recombinase before or during vascular development might result in quite remarkable vascular pathologies.

Hypoxia-inducible factor 1-alpha (Hif1α), which is a very sensitive marker for hypoxia (Majmundar et al., 2010), was expressed in comparable amounts in retinal lysates of *Etb*$^{\Delta eye}$ mice and controls, indicating, that the retinal perfusion and blood supply was not affected through the deletion of Etb. There are reports of a conditional knockout mouse

strain with an endothelial cell-specific Etb-deficiency (*Etb flox/flox* Tie2-Cre) showing impaired endothelium-dependent vasodilatation in *ex vivo* aortic ring assays, presumably due to an endothelial dysfunction (Bagnall et al., 2006). Though, an *in vivo* long-term telemetric recording of the carotid arterial pressure in *Etb flox/flox* Tie2-Cre mice showed that the ablation of Etb in endothelial cells had no influence on blood pressure, regardless of dietary salt intake (Bagnall et al., 2006). This outcome was quite surprising as the *in vivo* measurement of the plasma Et-1 concentration in *Etb* flox/flox Tie2-Cre mice via radioimmunoassay by a direct cardiac puncture showed elevated plasma Et-1 levels, concomitant with increased vasodilatation (Bagnall et al., 2006). Increased Et-1 levels might be a result of an interference of a very sensitive Et1/Etb-balance in the vasculature or a disturbed clearance of Et1 by the lack of endothelial Etb. The prolonged exposure to increased Et-1 levels might have caused a downregulation or desensitization of Eta activity leading to an inconspicuous blood pressure (Bagnall et al., 2006). In our analyses, the endothelial cell marker cluster of differentiation 31 (Cd31) was comparably expressed between $Etb^{\Delta eye}$ mice and controls.indicating that the number of endothelial cells was not affected by the ablation of Etb. When comparing the *Et-1* and *Et-2* mRNA expression levels between $Etb^{\Delta eye}$ mice and controls, we could not detect significant differences following Etb-deficiency. Consequently, both ligands, *Et-1* and *Et-2* can still mediate signal through the remaining Eta. This might maintain the functionality of endothelial cells in $Etb^{\Delta eye}$ mice and maybe an explanation for the normal vascular appearance. In contrast, the relative *Et-3* mRNA expression levels were significantly increased in $Etb^{\Delta eye}$ mice. *Et-3* has a higher binding affinity for Etb and signals mainly through this receptor (Kedzierski and Yanagisawa, 2001; Barton and Yanagisawa, 2008). It is therefore tempting to speculate that *Et-3* tries to compensate for the lack of Etb by increasing its expression.

Besides the endothelial cells of the inner vessel wall, blood vessels further consist of perivascular cells like smooth muscle cells, expressing a-Sma, and pericytes, expressing e.g. a-Sma, Ng-2 or Pdgfrb (Bergers and Song, 2005)). These cells wrap around endothelial cells and envelop the surface of the vascular tube (Gaengel et al., 2009; Ahmed and El-Badri, 2018) to regulate (micro)vascular blood flow by altering capillary diameter e.g. in response to endogenous signals, presumably mediated by neurons (Ahmed and El-Badri, 2018; Ribatti et al., 2011; Winkler et al., 2017; Thomas et al., 2017). In our analyses, $Etb^{\Delta eye}$ mice had a comparable *α-Sma* expression compared to controls potentially indicating that smooth muscle cell population was not affected through the Etb deletion. Remarkably, we were able to detect a significant elevation of mRNA expression levels of the proteoglycan *glial antigen-2* (*Ng-2*) and *platelet-derived growth factor receptor-β* (*Pdgfrb*), which are both well-known surface marker for

pericytes, in the retinae of *Etb*$^{\Delta eye}$ mice (Ozerdem et al., 2001). This could be confirmed by an immunohistochemical staining against *Ng-2,* which showed a higher number of pericytes enclosing the vessels of *Etb*$^{\Delta eye}$ mice. These finding could indicate that an increased number of pericytes following Etb deletion, might be a compensatory reaction to promote vessel stability and functionality.

In summary, our findings show that the ablation of Etb in the entire eye had no effect on endothelial cells, whereas the expression of pericyte markers was increased, indicating an increased number of pericytes and a possible early onset of vascular remodelling.

Nevertheless, we decided to not further utilize the *Etb*$^{\Delta eye}$ mice for analysis regarding Etb-mediated neuroprotection as the lens phenotype would obviously have a tremendous impact on the light damage experiments and the subsequently planned molecular analyses. Consequently, we exclusively used *Etb*$^{\Delta OC}$ mice with a deletion of Etb in retinal neurons and Müller cells only to study the neuroprotective role of Etb in the retina, which was the main goal of this study.

4.4 Etb is essential for the neuroprotection of photoreceptors after light induced-damage

Light damage experiments were performed in *Etb*$^{\Delta OC}$ mice and control littermates to induce photoreceptor cell death. Following light exposure, the deletion of Etb in retinal neurons and Müller cells led to a significantly increased apoptosis of photoreceptors, concomitant with a thinning of the outer nuclear layer (ONL), which strongly indicates that Etb mediates neuroprotective effects for photoreceptor survival. In accordance with these findings are our *in vitro* data obtained from serum-deprived *661W*$^{\Delta Etb}$ cells that demonstrated a significantly higher number of apoptotic cells compared to serum deprived 661W control cells. Moreover, previous data from our group showed that a pharmacological inhibition of Etb mediated signalling using BQ788 (a specific Etb inhibitor) resulted in a significantly higher number of light-induced photoreceptor apoptosis in a mouse model with constantly elevated Et-2/Etb levels (Braunger et al., 2013a) and others showed a significantly lower survival of photoreceptors following BQ788 treatment in a model of genetically induced photoreceptor degeneration (Joly et al., 2007). Taken together, these findings clearly highlight the importance of Etb mediated signalling in the retina for photoreceptor survival.

Our data furthermore showed that the apoptosis of photoreceptors in *Etb*$^{\Delta OC}$ mice and in serum-deprived *661W*$^{\Delta Etb}$ cells was mediated via an extrinsic pathway indicated by a

significant elevation of *Caspase-8*, which is an important mediator of the extrinsic death-receptor mediated apoptosis (Niquet and Wasterlain, 2004).

As the deletion of Etb in $Etb^{\Delta OC}$ animals affects retinal neurons and Müller cells, we cannot exclusively name the specific cell type that might be responsible for the observed neurodegenerative effect. The *in vitro* data from $661W^{\Delta Etb}$ cells showed, that the deletion of Etb was sufficient to increase their apoptotic cell death, a finding that clearly supports the hypothesis that the Etb deletion might promote an autocrine-mediated cell death. However, unpublished data from our group show that mice with a Müller cell specific deletion of Etb ($Etb^{\Delta MC}$) had a significantly higher number of apoptotic photoreceptor cells following light-induced degeneration. Thus, the pro-apoptotic effect might be additionally mediated in a paracrine manner presumably by Müller cells, which are coupled physically and metabolically to photoreceptors and control photoreceptors' survival (Reichenbach et al., 1993; Rattner and Nathans, 2005).

The undergoing neurodegenerative processes following light exposure also resulted in an activation of the *Tgf-β* signalling pathway, as we detected significant elevated levels of *Tgf-β2* and *Tgf-β3* in light-exposed $Etb^{\Delta OC}$ mice compared to controls. Our workgroup recently published that the *Tgf-β* signalling pathway protects retinal neurons from developmental programmed cell death, as *Tgf-β receptor type 2*-deficient mice showed a significantly increased apoptotic death of retinal neurons during embryonic and postnatal development (Braunger et al., 2013b). As the deletion of Etb in photoreceptors and Müller cells resulted in an increased retinal degeneration the activation of further neuroprotective signalling pathways like *Tgf-β* signalling might be an attempt of the retina to compensate for the ongoing degeneration.

The precise role of endothelin signaling pathway in the retina is still not fully understood. There are reports e.g. that the intravitreal injection of Et-2 resulted in a breakdown of the blood retinal barrier with increased vascular leakage, vascular endothelial growth factor expression, and infiltrating macrophages (Saeds et al, 2018). In contrast, our workgroup published that an upregulation of *Et-2* mediated the protection of photoreceptors from light damage via *Etb* mediated signaling (Braunger et al., 2013a) and others showed that elevated *Et-2* levels promoted photoreceptor survival in a mouse model of inherited photoreceptor degeneration (Bramall et al., 2013). In the current study, we confirmed a significant increase of *Et-2* expression in control and $Etb^{\Delta OC}$ mice following light induced photoreceptor degeneration. Remarkably, following light-induced damage, the *Et-2* expression was significantly higher in $Etb^{\Delta OC}$ mice compared to controls suggesting a higher susceptibility to light of *Etb*-deficient mice, most likely due to the disruption of the *Etb* -signalling. Although *Eta, Et-2 and Et-3* were significantly overexpressed in light-

exposed *Etb*$^{\Delta OC}$ retinae, most likely to compensate for the lacking function of *Etb*, this was obviously not sufficient to compensate for the neurodegenerative effect that we observed in *Etb*$^{\Delta OC}$ animals following light exposure. Taken together, these data strongly indicate that in particular *Etb* mediated signalling is essential for a functioning neuroprotective signalling in the retina and in particular for photoreceptor survival.

Photoreceptor-derived Et-2 has already been shown to act as general stress signal following photoreceptor injury (Rattner and Nathans, 2005). There are reports that albino wildtype mice showed a significant upregulation of Etb in Müller cells following light-induced damage, which suggests that photoreceptor-derived Et-2 can bind to Etb on Müller cells and that Müller cells can increase their sensitivity to Et-2 in response to retinal injury (Rattner and Nathans, 2005). Binding of Et-2 to its Etb receptor on Müller cells might furthermore result in an activation of Müller cells to mediate neuroprotection and repair mechanisms (Bringmann et al., 2006). Furthermore, there are reports that Müller cells react in a paracrine manner to photoreceptor cell stress (e.g. light induced degeneration) by an upregulation of the neuroprotective factors like leukemia inhibitory factor (*Lif*) and fibroblast growth factor 2 (*Fgf2*) (Joly et al. 2008; Gao und Hollyfield 1996; Joly et al. 2007). As expected, following light exposure *Lif* was significantly increased in controls and *Etb*$^{\Delta OC}$ mice. The cytokine Lif mediates its neuroprotective signal through two receptors specific for Lif signalling, the cytokine receptor gp130 and LIFRb, an obligatory co-receptor for LIF, which are both expressed in Müller cells and photoreceptors (Ueki et al., 2009). Quite intriguingly, the amount of *Et-2* overexpression seems to correlate with *Lif* expression which might result from a dependent and reciprocal interaction between *Et-2* and *Lif*. This has been confirmed by Joly *et al*. who showed that *Lif*-deficient mice had constitutively and significantly downregulated retinal *Et-2* expression levels and expressed *Et-2* only after intravitreal injections of recombinant LIF (Joly et al., 2008). Moreover, light-induced or genetic-induced photoreceptor degeneration resulted in an elevated expression of *Lif* in Müller cells, presumably mediated through the increased Et-2 expression levels (Bürgi et al., 2009; Joly et al., 2008). Besides Müller cells, Lif is also expressed in astrocytes as well as in a small number of microglial cells (Banner et al., 1997). This might explain the increased *Lif* expression levels in *Etb*$^{\Delta OC}$ mice, although the Lif-mediating Et-2/Etb signalling was disturbed.

In different models of photoreceptor degeneration, *Fgf2* is significantly upregulated (Gao and Hollyfield, 1996) and is considered as survival-promoting factor for photoreceptor cells (Faktorovich et al., 1990). Fgf2 is expressed by various cells in the retina e.g. photoreceptors, Müller cells and astrocytes (Li et al., 1997, 1997; Amin et al., 1997;

Irmady et al., 2011) and mediates its signalling by fibroblast growth factor receptors (Fgfr) on Müller cells (Kinkl et al., 2002). Fgf2 mediated signalling plays an essential role in development and maintenance of photoreceptors (Cornish et al., 2004). Joly *et al*. showed that intravitreal injections of recombinant LIF induces the expression of *Fgf2* in *Lif*-deficient mice, indicating a dependent and reciprocal interaction between *Fgf2* and *Lif*, too (Joly et al., 2008). Hence, the observed significant upregulation of *Fgf2* in light-exposed $Etb^{\Delta OC}$ mice compared to light exposed controls is most likely a consequence of the concomitant and significant upregulation of *Lif*. Remarkably, light-exposed $Etb^{\Delta OC}$ mice showed a more pronounced photoreceptor damage compared to light-exposed control animals, although the neuroprotective factors *Fgf-2* and *Lif* were significantly upregulated in $Etb^{\Delta OC}$ mice.

The binding of cytokines like Lif to the gp130 receptor activates the PI3K/Akt signalling pathway (Alonzi et al., 2001). Moreover, Fgf2 can also stimulate the activation of PI3K/Akt signalling (Zubilewicz et al., 2001), (Hu et al., 2014). Above all, Akt is essential for cell survival as its activation regulates the expression of anti- and pro-apoptotic factors and multiple proteins, which mediate caspase-independent and caspase dependent apoptosis (Song et al., 2005; Datta et al., 1997; Zhou et al., 2000; Jeong et al., 2008; Suhara et al., 2002). Furthermore, the PI3K/Akt-signalling pathway has often been reported to act neuroprotective for several types of neuronal cells (Nakazawa et al., 2003) and in particular in promoting the survival of cytokine-dependent neurons (Alonzi et al., 2001). The activation of Akt involves its phosphorylation to phospho(p)Akt (Song et al., 2005). We detected comparable protein levels of Akt between light-exposed $Etb^{\Delta OC}$ mice and controls, whereas phospho(p)Akt was strongly decreased in light-exposed $Etb^{\Delta OC}$ mice indicating an impaired activation of Akt. Quite intriguingly, our data strongly suggest that the Akt signaling pathway could not be stimulated through the significantly increased *Lif* or *Fgf2* expression levels in light-exposed $Etb^{\Delta OC}$ animals. This finding clearly highlights the importance of Etb-mediated signalling in retinal neurons and Müller cells for the activation of Akt and its impaired activation might furthermore very well explain the observed enhanced neurodegeneration in $Etb^{\Delta OC}$ animals following light exposure.

We therefore conclude that Etb is an essential key regulator of retinal neuroprotection that mediates its downstream signalling through activation of Akt signalling, concomitant with the regulation of caspase-mediated apoptosis. Moreover, our data identify Et-2 and its signalling through Etb as the essential and even more potent neuroprotective event for photoreceptor survival compared to that of Fgf2 and Lif. In summary, our data identify

Etb mediated signalling as a promising approach for the development of new therapeutic strategies in the context of retinal degenerations.

5 Future directions

One of the future directions of the project will aim to elucidate the intracellular events of Etb mediated signaling. The proteome analysis of *661W*$^{\Delta Etb}$ cells (in cooperation with Dr. S. Hauck and Dr. A. Neueder) allowed us to identify a group of proteins which are associated with proteasomal degradation processes (e.g. PSMA1/3, PSMD13, USP14 Protein) indicating a proteasomal dysregulation following *Etb*-deficiency. The proteasome is essential for the maintenance of cellular homeostasis by controlling the intracellular degradation of defective proteins (Campello et al., 2013; Orlowski, 1999). Moreover, the proteasome regulates proteolytic processes in apoptosis and plays also an important role in the activation of Akt and the proteasomal degradation of its activated form pAkt (Wójcik, 2002; Noguchi et al., 2014), which identifies the Etb-triggered proteasomal dysregulation in *661W*$^{\Delta Etb}$ cells as highly relevant in the context of neuroprotection. There is already data published showing that proteasomal insufficiency correlates with various forms of neurodegenerative disorders including Parkinson's Disease (Lim and Tan, 2007), Huntington's Disease (Ortega and Lucas, 2014) and inherited retinal degenerations like Retinopathia pigmentosa (Illing et al., 2002) and Age-related Macular Degeneration, presumably associated with misfolding or mistargeting of cytosolic and membrane proteins (Lobanova et al., 2013). Thus, a more thorough understanding of the potential Etb-mediated regulation of proteasomal activity has the distinct potential to lead to the development of novel therapeutic strategies in the context of retinal degenerations.

6 Material and methods

6.1 *In vivo* experiments

6.1.1 Housing conditions

Etb$^{\Delta OC}$ mice (*Etb fl/fl;α-Cre)*, *Etb*$^{\Delta eye}$ mice (*Etb fl/fl;CAG-CreER*^{TM}*), Etb fl/fl* littermates and albino (CD1) wildtype mice were used for the *in vivo* experiments in this thesis. Albino (CD1) wildtype mice were bred in the animal facility of the University of Regensburg. Etb fl/fl mice were a generous gift from Prof. Miles L. Epstein (Druckenbrod et al., 2008) (Department of Anatomy, Neuroscience Training Program, School of Medicine and Public Health, University of Wisconsin, Madison, Madison, Wisconsin). *Etb fl/fl* mice were initially in a 129SV background. To be able to perform light-induced photoreceptor degeneration, the mice and needed to be backcrossed with CD1 wildtype mice for at least seven generations to obtain albino *Etb fl/fl* mice. *α-Cre* mice (CD1 background, (Marquardt et al., 2001) and *CAG-CreER*^{TM} (CD1 background, (Hayashi and McMahon, 2002)), purchased from Charles River (Sulzfeld, Germany).

All procedures conformed to tenets of the National Institutes of Health Guidelines on the Care and Use of Animals in Research, the EU Directive 2010/63/E, and the Uniform Requirements for manuscripts submitted to Biomedical journals. All animals used for this thesis were kept under optimizing conditions with a temperate at 23 °C $\pm$ 2°C. The mice had access to food and water *ad libitum*. All mice were kept in a light-dark cycle of 12 hours per day with a light intensity of approximately 400 lux.

6.1.2 Animal models and Cre/loxP-System

The Cre/loxP-System is a frequently used experimental approach for the deletion of target genes in a specific temporal or cell-type specific manner, that allows the circumventing of potential embryonic lethality (Kühn and Torres, 2002). The Cre gene encodes a DNA Cre recombinase originated from bacteriophage P1 (Sternberg and Hamilton, 1981). Cre recombinase is able to recognize and recombine characteristic DNA sequences ,the so called loxP or flox-sites, flanking the sequence of a specific target gene, (Sternberg and Hamilton, 1981; Tian et al., 2006), finally resulting in the deletion of the target gene (Kühn and Torres, 2002). The Cre recombinase is controlled through cell- or tissue-specific promotor elements and can be constitutive or drug-inducible (Tian et al., 2006).

For the generation of *Etb*$^{\Delta eye}$ mice with a deletion of Etb in the entire eye, mice carrying two unrecombined *Etb fl/fl* alleles flanking exon 3 of the Etb gene (Druckenbrod et al., 2008) were crossed with *Etb fl/fl;CAG-CreER*^{TM} mice, that were heterozygous for transgenic *CAG-CreER*^{TM} recombinase. The genetic background of all experimental mice was albino (CD1). Resulting *Etb fl/fl;CAG-CreER*^{TM} mice were used as experimental animals als will be referred to as *Etb*$^{\Delta eye}$. *CAG-CreER*^{TM} -negative littermates with two unrecombined *Etb fl/fl* alleles were used and referred to as control mice. The Cre recombinase in *CAG-CreER*^{TM} mice is tamoxifen-inducible under the control of a chicken-beta-actin hybrid promotor exhibiting a robust, ubiquitous activity following tamoxifen treatment. The Cre recombinase in *CAG-CreER*^{TM} mice was activated through intraperitoneal injections of 50 µl tamoxifen [20mg/ml]. The mice were injected for 5 days and twice each day (9 am and 5 pm) starting at the age of 4 weeks.

For the generation of *Etb*$^{\Delta OC}$ mice with a deletion of Etb in retinal neurons and Müller cells, mice carrying two unrecombined *Etb fl/fl* alleles flanking exon 3 of the Etb gene (Druckenbrod et al., 2008) were crossed with *Etb fl/fl;α-Cre* mice, that were heterozygous for transgenic *α-Cre* recombinase (Marquardt et al., 2001). The genetic background of all experimental mice was albino (CD1). Resulting *Etb fl/fl;α-Cre* mice were used as experimental animals and are referred to as *Etb*$^{\Delta OC}$. *α-Cre*-negative littermates with two unrecombined *Etb fl/fl* alleles were used as control mice. The *α-Cre* recombinase is under the control of a Pax6 promotor, exhibits a robust expression starting at embryonic day (E) 10.5 in cells that derive from the inner layer of the optic cup.

6.1.3 Light damage

Etb$^{\Delta OC}$ mice at the age of 6 to 8 weeks were dark adapted for a period of 5 days before light exposure. For light-induced photoreceptor degeneration, the mice were placed in reflective plastic cages and exposed to diffuse cool, white fluorescent light coming from the top of the cage with an intensity of 5000 lux for 1 h. After light exposure, the mice were hold for 6 h (RNA and protein analysis), 30 h (TUNEL) or 14 days (morphometric analysis) in cyclic, dim light for recovery and then sacrificed. The light damage experiments were always performed in the early morning.

6.1.4 Puncture of the eye and intravitreal injections

Wildtype albino (CD1) mice were anesthetized using isoflurane (Ecuphar GmbH, Greifswald, Germany) punctured through the basal limbus and in case of an injection, the mice received an injection of 3 µl 1xPBS in the vitreous using a 33-gauge needle.

6.1.5 Preparation of ocular tissue

The mice were sacrificed by atlanto-occipital dislocation and the eyes were enucleated. For histological sections, the entire eye was removed carefully und incubated in the respective fixative (Methyl Carnoy, 4 % (w/v) PFA or Cacodylat-Buffer). For molecular analysis, the eye was cut with a razor blade along the ora serrata and the anterior eye segment was removed without bruising the lens. The retina was detached from the RPE and sclera with gentle brushes from the position of the optic nerve head and transferred immediately in a 2 ml Eppendorf tube on ice for containing TriFast™ Trizol or EDTA-Buffer (Chapter 6.3.6) for RNA or protein analyses.

6.1.6 Cardial perfusion

Mice were anesthetized by intraperitoneal injections containing a solution of ketamine (75mg/ml) and Xylazine (5mg/ml). After a complete anaesthesia of the mice, the thoracic and abdominal cavity was opened to gain access to the heart and the abdominal aorta. The injection needle was punctured into the left ventricle and a relief cut was carried out in the abdominal aorta. The mice were perfused with FITC-dextran to visualize retinal vasculature or fixative (Methyl Carnoy or 4 % (w/v) PFA) for immunohistochemistry. After perfusion, the eyes of the mice were enucleated for performing sagittal sections (Chapter 6.5.2 and 6.5.3) or retinal flatmounts (Chapter 6.1.7).

6.1.7 Preparation of retinal flatmounts

If not yet perfused cardially, mice were sacrificed by atlanto-occipital dislocation. The eyes were enucleated and fixed in 4% (w/v) PFA for 1 h at room temperature. The eye was cut with a razor blade along the ora serrata and the anterior eye segment and the lens were removed. The retina was brushed out gently and transferred on an object slide, which had an area circuited with a fat pen (PapPen) and was moisturized with 0.1M phosphate buffer (Php). The retina was incised on four opposite positions, to spread the retina flat on an object slide.

6.2 *In vitro* experiments

6.2.1 Cell line and culture conditions

The murine immortalized photoreceptor cell line (661W) was provided from the laboratory of Prof. Dr. E. Tamm (Institute of Human Anatomy and Embryology, University of Regensburg). Untreated cells were cultured in an incubator (Hera Safe, Heraeus, Hanau, Germany) at 37°C and 5% CO_2 conditions and nourished with 4,5% Glucose DMEM-Medium containing 1% fetal bovine serum (FBS), 10% Penicillin/Streptavidin (P/S). Transfected *661W$^{\Delta Etb}$* cells and controls were nourished with 4,5% Glucose DMEM-Medium containing 1% FBS, 10% P/S and 6 µg/ml Puromycin. All treatments, passaging and other procedures of the cells as well as production of buffers and solutions were performed under a sterile working bench (Hera Safe, Heraeus, Hanau, Germany). Glassware, buffers and solutions were autoclaved prior to use and sterile packed plastic material was used.

6.2.2 Passaging of cells

After reaching a confluence of 70-80%, the cell culture medium was removed and the cells were washed twice with 1xPBS to get rid of remaining culture medium. Afterwards, the cells were superseded from the bottom of the cell culture flask by trypsinization with 1ml 0.25% trypsin and transferred in falcons. By adding serum-containing DMEM medium, trypsin was inactivated and the suspension was centrifuged for 5 min at 1000 rpm. The cell pellet was resuspended in cell culture medium and a defined number of cells (100,000-200,000) were seeded in a new cell culture dish. The cells were harvested during the period of passage (P) 10 to 15. For further treatments, the cells were counted using Neubauer counting chamber and a defined number of cells (100,000-200,000) was seeded in 6 wells.

6.2.3 Serum-deprivation for 24 h

To cause cell stress and apoptosis, *661W$^{\Delta Etb}$* cells and controls (100,000) were seeded in 6-well plates with serum-containing DMEM-Medium (1% P/S, 10% FBS, 6 µg/ml Puromycin). After 2 to 3 hours, when the cells attached to the dish, the dishes were washed 3x times with 1xPBS to completely remove remaining medium. The cells were then incubated with 3 ml DMEM medium (1% P/S, 6 µg/ml Puromycin) containing 0% FBS for 24 h. For further analysis cells were fixed with 4%PFA or scraped from the dish.

6.2.4 CRISPR/Cas9-System

Clustered regularly interspaced short palindromic repeats (CRISPR)/CRISPR-associated (Cas9) protein 9 system is a genome editing tool (Zhang et al., 2014). In this thesis, it was used to delete Etb in the photoreceptor cell line 661W.

6.2.4.1 Cas9-Vector and sgRNA

The main components of the CRISPR/Cas9 system are sgRNA and theCas9 enzyme. Whereas the sgRNA guides the Cas9 enzyme to the target site on the genomic DNA, the Cas9 enzyme cleaves the target site (Harms et al., 2014). The used DNA plasmid vector (pSpCas9(BB)-2A-Puro-(PX459) V2.0) containing Cas9 from *S. pyogenes* with Puromycin resistance (*E.coli*: Ampicillin) and cloning backbone for sgRNA (Ran et al., 2013) was purchased from Addgene (Massachusetts, USA). The targets of sgRNAs were designed (in cooperation with Dr. Andreas Neueder, University Ulm) using the software genome compiler.

6.2.4.2 Transformation of the vector in E.coli

The vector was transformed in the DH5α chemically competent *E.coli* strain purchased from Thermo Fisher (Schwerte, Germany) using the following protocol:

- Unfreeze 50 µl of *E.coli* on ice
- Add 5 ng vector and mix
- Incubate for 30 min on ice
- Temperature shock at 42°C for 45 sec (water bath)
- Incubate on ice for 30 sec
- Add 500 µl LB Medium
- Incubate for 20 min at 37°C
- Centrifugation for 20 min at full speed
- Decant supernatant and resuspend the remaining LB Medium
- Spread suspension on LB_0 Plate and incubate overnight at 37°C

The next day, a single colony was picked and incubated shaking in 5 ml LB Medium containing Ampicillin overnight at 37°C. Afterwards, the suspension was centrifuged at 4000 rpm for 20 min and the supernatant was decanted. The vector was obtained by using the QIAPrep Spin MiniPrep Kit from Qiagen (Hilden, Germany) following the manufacturer's' instructions (Chapter 6.2.4.3).

- Unfreeze 50 µl of *E.coli* on ice
- Add 5 ng vector and mix

- Incubate for 30 min on ice
- Temperature shock at 42°C for 45 sec (water bath)
- Incubate on ice for 30 sec
- Add 500 µl LB Medium
- Incubate for 20 min at 37°C
- Centrifugation for 20 min at full speed
- Decant supernatant and resuspend the remaining LB Medium
- Spread suspension on LB_0 Plate and incubate overnight at 37°C

6.2.4.3 Purification of DNA vector

For purification of the DNA plasmid vector, the QIAPrep Spin MiniPrep Kit from Qiagen (Hilden, Germany) was used according to the manufacturer's protocol:

- Resuspend (by vortexing) pelleted bacterial cells in 250 µl Buffer P1 and transfer to Eppendorf tube
- Add 250 µl Buffer P2 and mix thoroughly by inverting the tube 4-6 times until the solution comes clear. Do not allow the lysis reaction to proceed for more than 5 min
- Add 350 µl Buffer N3 and mix immediately and thoroughly by inverting the tube 4-6 times
- Centrifuge for 10 min at 13000 rpm
- Apply 800 µl supernatant to QIAprep 2.0 spin column by pipetting
- Centrifuge for 30-60 sec and discard the flow-through
- Wash the column by adding 0.5 ml Buffer PB
- Centrifuge for 30-60 sec and discard flow-through
- Wash the column by adding 0.75 ml Buffer PE
- Centrifuge for 30-60 sec and discard the flow-through
- Centrifuge for 1 min to remove residual wash buffer
- Place column in a clean 1.5 ml Eppendorf tube
- To elute DNA, add 30 µl (preheated at 37°C) to the centre of the column
- Centrifugation for 1 min at 13000 rpm

6.2.4.4 Digestion with BbsI

The restriction enzyme BbsI was used to cut the plasmid vector outside the Cas9 and sgRNA sequences to linearize the plasmid. Therefore, 10 µg of the vector were digested

with 2 µl BbsI (New England Biolabs, Frankfurt am Main, Germany) and 2.5 µl of the corresponding buffer and filled up with ddH_2O to a Volume of 25 µl. The suspension was incubated overnight at 37°C.

6.2.4.5 Gel extraction of the linearized vector

The linearized vector was separated by gel electrophoresis with a 2% agarose gel for 20 min at 120 V. Under UV-light, the band of the successful digested vector was cut out from the agarose gel and transferred to a 1.5 ml Eppendorf tube by using the NucleoSpin® Gel and PCR Clean-Up Kit from Macherey-Nagel (Düren, Germany) performing the following protocol:

- Add 500 µl NT-buffer
- Melt gel slice at 60°C and load on column
- Spin column for 30 sec at 10000 rpm
- Discard flow-through
- Add 600 µl washing-buffer and spin for 30 sec at 10000 rpm
- Discard flow-trough
- Add 600 µl washing-buffer and spin for 30 sec at 10000 rpm
- Discard flow-trough
- Spin for 1 min at 13000 rpm
- Transfer column on Eppendorf tube
- add 50 µl 10 mM Tris-Cl pH 8.0 and
- Incubate for 30 sec
- spin for 30 sec at 10000 rpm to eluate of vector

6.2.4.6 Phosphorylation annealing of oligonucleotides

Regarding its short length, sgRNA can be synthesized directly from a double-stranded DNA template obtained by annealing two oligonucleotides (Harms et al., 2014). The suitable pair of DNA oligonucleotides contained the target sequence at Exon 2 of the Etb gene (Etb_2aI_fwd: CACCGGCCGGTGATTAACGGCCAGA; Etb_2aI_rev: AAACTCTGGCCGTTAATCACCGGCC; and purchased from Invitrogen, Germany). Furthermore, the oligonucleotides were phosphorylated to prevent a recirculation of the vector during ligation by using the T4 DNA Ligation Kit from New England Biolabs (Frankfurt am Main, Germany) and performing the following approach:

Reagent	Volume
Etb_2aI_fwd [100 µM]	1 µl
Etb_2aI_rev [100 µM]	1 µl
10x T4 Ligation Buffer	1 µl
dH_2O	6.5 µl
T4 Polynucleotide Kinase	0.5 µl

Table 1 Phosphorylation and annealing of oligonucleotides

The suspension was incubated at 37°C for 30 mins and afterwards heat-shocked at 95 °C for 5 min. After cooling down at room temperature, 190 µl dH_2O was added.

6.2.4.7 Cloning of sgRNA target sequences into a plasmid

The DNA oligonucleotides were cloned in the linearized vector by the following approach:

Reagent	Volume
Linearized plasmid vector	50 ng
Oligonucleotides	1 µl
10x T4 Ligation Buffer	1 µl
T4 Ligase	1 µl
Add dH_2O	10 µl

Table 2 Cloning approach

The suspension was incubated for 20 min at room temperature. Afterwards, 4 µl of the ligation were transformed in *E.coli* by performing the transformation protocol from Chapter 6.2.4.2) Vector-containing *E.coli* were selected by an ampicillin-resistance, therefore it is essential to use LB_{AMP} plates instead of LB_0 plates. After picking a single colony, the vector was obtained by using the QIAPrep Spin MiniPrep Kit from Qiagen (Hilden, Germany) following the manufacturer's' instructions (Chapter 6.2.4.3). The eluated vector was sequenced (Microsynth SeqLab, Göttingen Germany) for its correctness.

6.2.4.8 Transfection of 661W and generation of single colonies

The cloned and circular plasmid vector (Chapter 6.2.4.16.2.4.7) was transfected in 661W cells for generating a cellular deletion of Etb (*661W$^{\Delta Etb}$*). Control 661W cells still expressing Etb were transfected with the unmodified plasmid vector only containing Cas9 (Chapter 6.2.4.1). The day before transfection 200000 cells/per well were counted via Neubauer cell counter and seeded in a 6 wells plate with 2 ml DMEM Medium (1%

P/S, 10% FBS). For transfection JetPRIME *in vitro* DNA transfection reagent from Polyplus (Illkirch, France) was used according to the following protocol:

- Dilute 1µg DNA plasmid vector in 200 µl jetPRIME Buffer
- Mix by vortexing and spin down briefly
- Add 2 µl jetPRIME, vortex for 10 sec and spin down briefly
- Incubate for 20 min at room temperature
- Add 200 µl of transfection mix per well drop wise onto the cells in serum containing DMEM
- Incubate for 48 h at 37°C

To create single colonies, *661W$^{\Delta Etb}$* and controls with a cell number of 50000 cells/well were seeded in a 6-well plate with 3 ml puromycin-containing DMEM Medium (1% P/S, 10% FBS, 6 µg/ml Puromycin) and incubated to a confluency of 90%. Cells were removed from 6-well plate bottom with 1 ml Trypsin. The Trypsin cell suspension was 1:100 diluted with DMEM Medium (1% P/S, 10% FBS, 6 µg/ml Puromycin) by mixing 0.1 ml Trypsin cell suspension and 9.9 ml DMEM Medium. This was repeated twice and subsequently 100 µl of the diluted suspension were applied in a 96-well plate. Single wells of 96-well plate containing only a single cell were determined by using conventional light microscopy. We have chosen four single colonies each for *661W$^{\Delta Etb}$* and 661W control cells for further analysis.

6.2.4.9 Antibiotica kill curve

For creating a stable knockout cell line, *661W$^{\Delta Etb}$* cells and controls containing a Puromycin resistance were selected with Puromycin-containing DMEM Medium (1% P/S, 10% FBS, 6 µg/ml Puromycin). The optimal Puromycin concentration of 6µg/ml was determined by an antibiotic kill curve. The optimal dose was set as lowest antibiotic concentration that kills untreated 661W cells (without Puromycin-resistance) after one week. In this dose-dependent experiment, the untreated 661W cells were incubated with an increasing amount of Puromycin starting with a concentration of 2 µg/ml up to 22 µg/ml. Therefore, cell number were determined by using the Neubauer counting chamber and 80000 cells/per well were seeded in a 24-well plate with DMEM Medium (1% P/S, 10% FBS). The next day, Puromycin containing DMEM was added according to the following protocol:

Increasing Puromycin concentration →

0 µg/ml →	2 µg/ml →	4 µg/ml →
6 µg/ml →	8 µg/ml →	10 µg/ml →
12 µg/ml →	14 µg/ml →	16 µg/ml →
18 µg/ml →	20 µg/ml →	22 µg/ml →

Table 3 Schemata for Puromycin kill curve

The optimal concentration of 6 µg/ml was determined.

6.3 List of material

6.3.1 Reagents

Description	Supplier
0,05 % Trypsin/EDTA	PAA The Cell Culture Company, Pasching, Austria
10 x PCR buffer	Qiagen, Hilden, Germany
2-mercaptoethanol	Serva, Heidelberg, Germany
Acetic acid	Merck, Darmstadt, Germany
Acetone	Merck, Darmstadt, Germany
Agarose	Biozym Scientific, Oldendorf, Germany
Albumin Fraction V (BSA)	Roth, Karlsruhe, Germany
Ammonium peroxodisulfate (APS), 10% (w/v)	Roth, Karlsruhe, Germany
BC Assay Reagent A + B	Interchim, Wörgl, Austria
BC Assay Reagent 1 + 2	Roth, Karlsruhe, Austria
Bromphenolblau	Sigma-Aldrich, Taufkirchen, Germany
CDP-Star	Roche, Penzberg, Germany
Chloroform	Roth, Karlsruhe, Germany
Coomassie® Brilliant Blue R-250	Sigma-Aldrich, Taufkirchen, Germany
Corn oil	Sigma-Aldrich, Taufkirchen, Germany
Desoxynucleosid-triphosphate (dNTPs)	Qiagen, Hilden, Germany
Dimethylsulfoxid (DMSO)	Roth, Karlsruhe, Germany
DL-Dithiothreitol (DTT)	Sigma-Aldrich, Taufkirchen, Germany
Dulbecco's Modified Eagle Medium (DMEM)	PAA The Cell Culture Company, Pasching, Austria
EDTA	Roth, Karlsruhe, Germany
Epon	Serva, Heidelberg, Germany
Ethanol, absolute	Roth, Karlsruhe, Germany
Ethidiumbromide	Serva, Heidelberg, Germany
Fluorescent Mounting Medium	DakoCytomatio, Hamburg, Germany
Formaldehyde	Roth, Karlsruhe, Germany
Epon	Serva, Heidelberg, Germany
Glutaraldehyde, 25% in water	Serva, Heidelberg, Germany
Glycerin	Merck, Darmstadt, Germany
Glycin	Merck, Darmstadt, Germany
Guanidin HCL	Roth, Karlsruhe, Germany
HEPES	Sigma-Aldrich, Taufkirchen, Germany
Hydrochloric acid (37%)	Merck, Darmstadt, Germany
IsoFlo® Isoflurane	Ecuphar GmbH, Greifswald, Germany
Isopropanol	Sigma-Aldrich, Taufkirchen, Germany
Ketamine	Wirtschaftsgenossenschaft Deutscher Tierärzte (WDT), Garbsen, Germany

Luminata™ Forte	Millipore Corporation, Billerica, USA
Magnesium chloride (50 mM)	Bioloine, Luckenwalde, Germany
Methanol	Merck, Darmstadt, Germany
Mowiol 4-88	Roth, Karlsruhe, Germany
N,N,N',N',-Tetramethylethylenediamine (TEMED)	Roth, Karlsruhe, Germany
Non-fat milk powder (MM)	Roth, Karlsruhe, Germany
Paraformaldehyde (PFA)	Non-fat milk powder
PBS	PAA The Cell Culture Company, Pasching, Austria
Penicillin-Streptomycin	Pasching, Austria
peqGold TriFast™	PeqLab, Erlangen, Germany
Phalloidin	Sigma-Aldrich, Taufkirchen, Germany
Phosphatase-Inhibitor Mix	Sigma-Aldrich, Taufkirchen, Germany
Potassium chloride	Roth, Karlsruhe, Germany
Protease-Inhibitor Mix	Sigma-Aldrich, Taufkirchen, Germany
Puromycin	InvivoGen, California, USA
Rotiphorese® Gel 30 (30% Acrylamide)	Roth, Karlsruhe, Germany
Saccharose	Roth, Karlsruhe, Germany
SDS (Sodium dodecylsulfat)	Roth, Karlsruhe, Germany
Sodium chloride	Roth, Karlsruhe, Germany
Tergitol® solution	Sigma-Aldrich, Taufkirchen, Germany
Tissue-k®	Sakuram Zoeterwoude, Niederlande
Tris HCl	Roth, Karlsruhe, Germany
Triton-X-100	Roth, Karlsruhe, Germany
Tween® 20	Roth, Karlsruhe, Germany
Urea	Merck, Darmstadt, Germany
Vectashield Mounting Medium for Fluorescence with DAPI	Vector Laboratories, Burlingame, USA
Water ROTISOLV® HPLC Gradient Grade	Roth, Karlsruhe, Germany
Xylazine	Serumwerk Bernburg, Bernburg, Germany

Table 4 Reagents

6.3.2 Commercial kits and enzymes

Enzyme/Kit	Supplier
BbsI	New England Biolabs, Frankfurt am Main, Germany
MWO I	New England Biolabs, Frankfurt am Main, Germany
QIAprep Spin Miniprep Kit	Qiagen, Hilden, Germany
Takyon™ kits for SYBR® Assays	Eurogentec, Lüttich, Belgien
Mango Taq	Bioline, Luckenwalde, Germany
Proteinase K	Roth, Karlsruhe, Germany

qScript™ cDNA Synthesis Kit	Quanta Bioscience, Gaithersburg, USA
BaseScope® Detection Reagent Kit Red	Advanced Cell Diagnostics, Newark USA
JetPRIME *in vitro* DNA transfection reagent	Polyplus, Illkirch, France
NucleoSpin® Gel and PCR Clean-Up Kit	Macherey-Nagel, Düren, Germany
T4 DNA Ligation Kit	New England Biolabs, Frankfurt am Main, Germany

Table 5 Commercial kits and enzymes

6.3.3 Oligonucleotides for genotyping

Primer	Species	Orientation	Sequence 5' to 3'
Cre	*Mus musculus*	forward	ATGCTTCTGTCCGTTTGCCG
Cre	*Mus musculus*	reverse	CCTGTTTTGCACGTTCACCG
Etb	*Mus musculus*	forward	CTGAGGAGAGCCTGATTGTGCCAC
Etb	*Mus musculus*	reverse	CGACTCCAAGAAGCAACAGCTCG
Etb Neo	*Mus musculus*	forward	CGACTCCAAGAAGCAACAGCTCG
Rd1 common	*Mus musculus*	forward	CTACAGCCCCTCTCCAAGGTTTATAG
Rd1 WT	*Mus musculus*	reverse	ACCTGCATGTGAACCCAGTATTCTATC
Rd1 TG	*Mus musculus*	reverse	AAGCTAGCTGCAGTAACGCCATTT

Table 6 Oligonucleotide primer for genotyping

6.3.4 Oligonucleotides for quantitative RT-PCR

Primer	**Species**	**Orientation**	**Sequence 5' to 3'**
α-Sma	*Mus musculus*	forward	CAACCGGGAGAAAATGACC
α-Sma	*Mus musculus*	reverse	CAGTTGTACGTCCAGAGGCATA
Bad	*Mus musculus*	forward	GGGAGCAACATTCATCAGCAGG
Bad	*Mus musculus*	reverse	CATCCCTTCATCCTCCTCGGTC
Bax	*Mus musculus*	forward	GTGAGCGGCTGCTTGTCT
Bax	*Mus musculus*	reverse	GGTCCCGAAGTAGGAGAGGA

BCl2	*Mus musculus*	forward	GTACCTGAACCGGCATCTG
BCl2	*Mus musculus*	reverse	GGGGCCATATAGTTCCACAA
Bim	*Mus musculus*	forward	GACAGAACCGCAAGGTAATCCCGACG
Bim	*Mus musculus*	reverse	TAGGATCCCCTCAATGCCTTCTCCATACCAG
Caspase 8	*Mus musculus*	forward	TTGAACAATGAGATCCCCAAAA
Caspase 8	*Mus musculus*	reverse	CCATTTCTACAAAATTTCAAGCAG
Caspase 9	*Mus musculus*	forward	GCCAGAGGTTCTCAGACCAG
Caspase 9	*Mus musculus*	reverse	TCCCTGGAACACAGACATCA
Cd31	*Mus musculus*	forward	CGGTGTCTAGCCAATTCC
Cd31	*Mus musculus*	reverse	CGACAGGATGGAAATCACAA
Et1	*Mus musculus*	forward	TCCTTGATGGACAAGGAGTGT
Et1	*Mus musculus*	reverse	CCCAGTCCATACGGTACGA
Et2	*Mus musculus*	forward	ACCTCCTCCGAAAGCTGAG
Et2	*Mus musculus*	reverse	TTTCTTGTCACCTCTGGCTGTA
Et3	*Mus musculus*	forward	TCCTTCTCGGGCTCACAG
Et3	*Mus musculus*	reverse	GGGACCCTGGGACACACT
Eta	*Mus musculus*	forward	AGGAACGGCAGCTTGCGGAT
Eta	*Mus musculus*	reverse	AGCAACAGAGGCAGGACTGA
Etb_Exon2	*Mus musculus*	forward	AATGGTCCCAATATCTTGATCG
Etb_Exon3	*Mus musculus*	reverse	TCCAAATGGCCAGTCCTCT
Fgf2	*Mus musculus*	forward	CCAACCGGTACCTTGCTATG
Fgf2	*Mus musculus*	reverse	CCAGTCGTTCAAAGAAGAAACAC
Gapdh	*Mus musculus*	forward	TGTCCGTCGTGGATCTGAC
Gapdh	*Mus musculus*	reverse	CCTGCTTCACCACCTTCTTG
Gnb2l	*Mus musculus*	forward	TCTGCAAGTACACGGTCCAG
Gnb2l	*Mus musculus*	reverse	ACGATGATAGGGTTGCTGCT
Iba-1	*Mus musculus*	forward	GGATTTGCAGGGAGGAAAAG
Iba-1	*Mus musculus*	reverse	TGGGATCATCGAGGAATTG

Lif	*Mus musculus*	forward	AAACGGCCTGCATCTAAGG
Lif	*Mus musculus*	reverse	AGCAGCAGTAAGGGCACAAT
Ng-2	*Mus musculus*	forward	CTTGGCCTTGTTGGTCAGAT
Ng-2	*Mus musculus*	reverse	CACCTCCAGGTGGTTCTCC
Pdgfrb	*Mus musculus*	forward	ACCTCAAAAGGTGTCCACGA
Pdgfrb	*Mus musculus*	reverse	GTGTGCTCACCACCTCGTAT
Rpl32	*Mus musculus*	forward	GCTGCCATCTGTTTTACGG
Rpl32	*Mus musculus*	reverse	TGACTGGTGCCTGATGAACT
Tgf-β1	*Mus musculus*	forward	TGGAGCAGCATGTGGCACC
Tgf-β1	*Mus musculus*	reverse	GTCAGCAGCCGGGTTACCA
Tgf-β2	*Mus musculus*	forward	TCTTCCGCTTGCAAAACC
Tgf-β2	*Mus musculus*	reverse	GTGGGAGATGTTAAGTCTTTGGA
Tgf-β3	*Mus musculus*	forward	CCCTGGACACCAATTACTGC
Tg-fβ3	*Mus musculus*	reverse	TCAATATAAAGGGGGTACA
Tgf-βr1	*Mus musculus*	forward	AATGTTACGCCATGAAAATATCC
Tgf-βr1	*Mus musculus*	reverse	CGTCCATGTCCCATTGTCTT
Tgf-βr2	*Mus musculus*	forward	TGCTACCTCCAAGTGTGGCTG
Tgf-βr2	*Mus musculus*	reverse	TATAGGGTCCCCAGCAGAGGC
Ubiquitin C	*Mus musculus*	forward	GTCGCTGTGTGAGGACTGC
Ubiquitin C	*Mus musculus*	reverse	CCTCCAGGTGATGGTCTTA

Table 7 Oligonucleotide primer for real-time RT-PCR

6.3.5 Antibodies

6.3.5.1 Primary antibodies

Protein	Blocking	Source	Supplier
Akt 1:1000	5 % non-fat dry milk	rabbit	Cell Signaling Technology, Danvers, USA
Collagen IV 1:50	2%BSA/0.1 M Php	rabbit	Rockland Immunochemicals Inc., Limerick, USA
Eta 1:100 (histology)	5 % non-fat dry milk	rabbit	Alomone Labs, Jerusalem, Israel
Etb 1:1000	5 % non-fat dry milk	rabbit	Alomone Labs, Jerusalem, Israel
Gapdh 1:5000	5 % non-fat dry milk	rabbit H, M,	Cell Signaling Technology, Danvers, USA
Gfap 1:100	2 % BSA/0.2 % CWFG/0.1%Triton/0.1 M Php	chicken	LifeSpan Biosciences, Seattle, USA
Gs 1:100 (histology)	2 % BSA/0.2 % CWFG/0.1%Triton/0.1 M Php	goat	Santa Cruz Biotechnology, Inc., Dallas, USA
Hif1α 1:200	5 % non-fat dry milk	rabbit	Cayman Chemical, Michigan, USA
Iba-1 1:1000 (histology)	2 % BSA/0.2 % CWFG/0.1%Triton/0.1 M Php	rabbit	Wako (Osaka, Japan)
Ng-2 1:100 (histology)	5%BSA/0.3%Triton/ 0.1 M Php	rabbit	Milipore, Massachusetts, USA
phospho-Akt1:1000	3 % BSA	rabbit	Cell Signaling Technology, Danvers, USA
Pv-1 1:25 (histology)	2 % BSA/0.2 % CWFG/0.1%Triton/0.1 M Php	Rat	Santa Cruz Biotechnology, Inc., Dallas, USA

Table 8 Primary antibody

6.3.5.2 Secondary antibodies

Secondary antibody	**Supplier**
Alexa Fluor® 488 donkey anti-goat IgG (H+L) (histology)	Invitrogen, Carlsbad, USA
Alexa Fluor® 488 goat anti-chicken IgG (H+L) (histology)	Invitrogen, Carlsbad, USA
Alexa Fluor® 546 goat anti-chicken IgG (H+L) (histology)	Invitrogen, Carlsbad, USA
Cy™3-conjugated AffiniPure anti-rabbit IgG (histology)	Jackson ImmunoResearch Europe Ltd., Ely, UK
Goat anti-rabbit IgG, HRP-linked	Cell Signaling Technology, Danvers, USA
goat anti-rabbit igG, AP-linked	Cell Signaling Technology, Danvers, MA, USA

Streptavidin, Alexa Fluor® 555 conjugate (histology)	Life Technologies, Eugene, USA

Table 9 Secondary antibodies

6.3.6 Solutions and buffers

Description	Supplier
EZ-Run Pre-Stained Rec Protein Ladder	Thermo Fisher Scientific, Schwerte, Germany
Gene Ruler 100 bp Plus DNA Ladder	Thermo Fisher Scientific, Schwerte, Germany

Table 10 Molecular weight standard and DNA standard

Solution/buffer	Composition
0,1 M Cacodylat-Buffer	10,7g Cacodylacid in 500ml dH_2O
0.1 M Phosphate buffer pH 7.4	100 ml 0.2 M Na_2HPO_4 x $2H_2O$ with 0.2 M NaH_2PO_4 x H_2O to pH 7.4 dilute to 0.1 M with dH_2O
10x electrode buffer	250mM Tris/HCl 400mM Glycine 1% (w/v) SDS in dH_2O, ad 1 l
10x TBS, pH 7.4	30 g Tris 80 g sodium chloride 2 g potassium chloride dH_2O ad 1 l, autoclave
Coomassie-Detaining Solution	500 ml Methanol 10 ml Acetic acid 0.2 g Coomassie-Brilliant Blue R-250 Add dH_2O 1 l
Coomassie-Staining Solution	40 ml Methanol 2ml Acetic acid 0.2 g Coomassie-Brilliant Blue R-250 Add dH_2O 100 ml
Detection Buffer, pH 9	15,76 g 0,1 M Tris(HCl (pH 6,8) 5,84 g 0,1 M NaCl Add dH_2O 1 l
EDTA lysis buffer	0,5ml 1mM EDTA 0,01753g NaCl 50µl HEPES (1M) 0,7µl 70% Tergitol (NP-40) 6µl Protease-Inhibitor-Mix M 6µl Phosphatase-Inhibitor-Mix 637,3µl H_2O
EM Fixative	2,5% Paraformaldehyd 2,5% Glutaraldehyd in 0,1M Cacodylatbuffer
Epon stem A	62 ml Glyidether 100 with 100 ml DDSA
Epon stem B	100 ml Glyidether 100 with 89 ml NMA

In situ hybridization BaseScope® Fixative	25 ml Formalin 225 ml dH_2O 1g/l NaH_2PO_4 1.625g/l Na_2HPO_4
Lämmli-Buffer (6x)	350 mM Tris-HCl, pH 6,8 10 % SDS 30 % Glycerol 5 % ß-Mercapoethanol 0,2 % Bromphenolblue
LB_0-Medium	950 ml dH_2O 10 gTryptone 10 g NaCl 5 g Yeast extract
Methyl-Carnoy	60 % Methanol 30 % Chloroform 10 % acetic acid
Mouse tail lysis buffer	100mM Tris-HCl, pH 8,0 5mM EDTA 0,2% SDS 200mM NaCl add 400ml dH_2O
Mowiol with DAPI	6.0 g Glycerine + 2.4 g Mowiol 4-88 (1h,RT) add 6.0 ml dH_2O (sterile) (1h, RT) add 12 ml 0.2 M Tris HCl, pH 8.5 (2h,50°C) add 25 mg/ml DABCO DAPI (1:10)
PBS, 10x, pH 7,4	80g NaCl 2g KCl 4,4g Na_2HPO_4 2,4g KH_2PO_4 Add dH_2O 1l
SDS-Solution, 19% (w/v)	10 g SDS Add dH_2O 100 ml
SDS-PAGE-Running-Buffer, 10x	250mM Tris/HCl, pH 6,8 30% Glycerin 8% (w/v) SDS Add dH_2O 1l
TBE, 10x	108g Tris-base 55g boric acid 40ml 0,5M EDTA pH 8,0 Add dH_2O 1l pH 7,0
TBS, 10x, pH 7,4	30 g Tris 80 g NaCl 2 g KCl Add dH_2O 1l
TBST, 1x	100 ml 10 x TBS 0.05 % (v/v) Tween 20 ad 1 l dH_2O
Transfer buffer, 10x	5,8 g Tris 2.9 g Glycine 200 ml Methanol 3.7 ml 10% (w/v) SDS Ad 1 l H_2O

Tris/HCl, 1,0 M, pH 6.8	121.14 g Tris/HCl ad 1 l dH_2O
Tris/HCl, 1,0 M, pH 8.8	181.71 g Tris/HCl ad 1 l dH_2O
Urea buffer	25 ml 10% SDS 10 ml 1 M Tris pH 6.8 100 µl 0.5 M EDTA pH 8 750 µl β-mercaptoethanol 24 g Urea
Washing buffer for protein isolation	0,3 M Guanidin HCl dissolve in 95% Ethanol

Table 11 Solutions and buffers

6.3.7 Technical equipment

Device designation	Supplier
Axiovert 40 CFL	Zeiss, Göttingen, Germany
CFX Connect Realt-Time System	BioRad, München, Germany
Consort E835 Electrophoresis Power Supply	Sigma-Aldrich, Taufkirchen, Germany
Embedder	EM TP Leica, Wetzlar, Germany
GenoPunch	Fine Science Tools, Heidelberg, Germany
HeatSealer RS 232	4titude, Berlin, Germany
Hera Cell 150 incubator	Heraeus, Hanau, Germany
Hera Safe steril working bench	Heraeus, Hanau, Germany
Embedding station	EM TP Leica, Wetzlar, Germany
Inolab pH-Meter	WTW GmbH, Weilheim, Germany
Julabo SW20 waterbath	JulaboLabortechnik GmbH, Seelbach, Germany
Kern PJL 2100-2M Analysenwaage	Kern & Sohn GmbH, Balingen-Fommern, Germany
LAS 3000 intelligent Dark Box	Fujifilm, Duesseldorf, Germany
Memmert water bath	Memmert GmbH, Schwabach, Germany
Mettler AE 163 special accurancy scales	Mettler Toledo, Gießen, Germany
Microm HM 500 OM Kryostat	Microm International, Walldorf, Germany
Microscop Axio Imager Z1	Zeiss, Goettingen, Germany
MilliQ Plus PF Ultrapure water system	Millipore Corporation, Billerice, USA
Model 45-101-I Class II Electrophoresis System	PeqLab Biotechnology GmbH, Erlangen, Gemrany
NanoDrop-1000 Spectrophotometer	PeqLab Biotechnology GmbH, Erlangen, Gemrany
Pipetman Pipettes	Gilson, Middleton, USA
Research pipettes	Eppendorf, Hamburg, Germany
Semi-Dry electrophoretic transfer cell	PeqLab Biotechnology GmbH, Erlangen, Gemrany
Sonorex RK 102	BANDELIN electronic GmbH& Co. KG, Berlin, Germany

Sunrise-Basic ELISA Reader	Tecam Austria GmbH, Karlsruhe, Germany
SuperCut 2050	Cambridge Instruments, Nußloch, Germany
Systec V75 Autoclave	Systec GmbH, Wettenburg, Germany
T100™Thermal Cycler	Biorad, Munich, Germany
Thermomixer comfort	Eppendorf, Hamburg, Germany
TonoLab Tonometer	Icare Finnland, Helsinki, Finnland
UV light screen	Bachhofer Laboratoriumsgeräte, Reutlingen, Germany
Ultracut E-Ultramicrotom	Reichert-Jung, Kirchseeon, Germany
Ultra Thurax	Biolabproducts, Bebensee, Germany
Vortex Genie 2	Scientific Industries Inc., New York, USA
Centrifuges 5415D, 5415R, 5804R, 5810R	Eppendorf, Hamburg, Germany

Table 12 Technical equipment

6.3.8 Consumable supplies

Description	Supplier
3 MM Blotting (“Whatman”)-Paper	Neolab, Heidelberg, Germany
Biosphere Filter Tips	Sarstedt, Nürnbrecht, Germany
CellScraper	Sarstedt, Nürnbrecht, Germany
Centrifuge 5415D, 5415R, 5804R, 5810R	Eppendorf, Hamburg, Germany
Culture Slides	BD Falcon, Bedford, USA
Cover slips, 24 x 60 mm	Menzel-Gläser, Braunschweig, Germany
Dispomed Syringe, single use	Dispomed Witt oHG, Gelnhausen, Germany
Easy Flasks Nunclon ™Δ T25, T75	Nunc, Rosklide, Denmark
Ecoflo Dissecting instruments	Dispomed Witt oHG, Gelnhausen, Germany
Falcon reaction tubes, 15 ml, 50 ml	Sarstedt, Nürnbrecht, Germany
Glasware	Schott, Roth, VWR, Germany
Green Nitrile Gloves	Kimtech, Koblenz, Germany
Hard-Shell®PCR plates 96-well, thin-wall	BioRad, München, Germany
Liquid Blocker PAP-Pen	SCI Science Services, München, Germany
Multidishes Nunclon ™Δ 6-well	Nunc, Rosklide, Denmark
Multi-Reaction tubes, 0,5 ml; 1.5 ml; 2 ml	Roth, Karlsruhe, Germany
Omnifix syringe, sterile	B. Braun, Wertheim, Germany
Optically Clear Heat Seal	BioRad, München, Germany
Parafilm	Pechiney Plastic Packaging, Chicago, USA
Pasteur pipettes	Brand, Wertheim, Germany

PCRSoft Tubes, 0,2 ml	Biozym, Hessisch Oldendorf, Germany
Personna Razorblades	American Safety Razor Company, Verona, USA
Pipet tips	Sarstedt, Nürnbrecht, Germany
PCR Plates, 96 well	4titude, Berlin, Germany
Petri dishes 94x16 mm PS	Greiner bio-one, Kremsmünter, Austria
Ro free blue gloves	Ulma, Neu-Ulm, Germany
Protein LoBind Tubes	Eppendorf, Hamburg, Germany
PVDF-Western Blot Membrane	Roche, Mannheim, Germany
Serological pipettes	Sarstedt, Nürnbrecht, Germany
Sterican injection cannula	B. Braun, Wertheim, Germany
SuperFrost®Plus object slides	Menzel-Gläser, Braunschweig, Germany

Table 13 Consumable supplies

6.4 Molecular biology

6.4.1 DNA analysis

6.4.1.1 Purification/Extraction of genomic DNA

For genotyping, genomic DNA from an ear biopsy was isolated. Therefore, a 2 mm piece of the ear was punched by using the genopuncher (Fine Science Tools) under isoflurane (Ecuphar GmbH, Greifswald, Germany) anesthesia. The tissue samples were transferred in a 1.5 ml Eppendorf tube for digestion. 200 µl mouse tail lysis buffer (Chapter 6.3.6) and 2 µl Proteinkinase K were added for DNA isolation. Afterwards, the samples were incubated shaking overnight in 50°C and 750 rpm. The next day, 200 µl isopropanol were added in the tubes and mixed. For precipitation of the DNA the samples were incubated at 4°C for 5 min. After centrifugation for 5-10 min at 13000 rpm, the supernatant was discarded and 200 µl 70% Ethanol was added. The tubes were mixed and incubated at room temperature (RT) for 5 minutes to wash the pellet and dissolve any remaining salt in the tube. After centrifugation for 5-10 min at 13000 rpm, the ethanol was poured off and the tube again was centrifuged for 1 min 13000 rpm. The remaining ethanol was pipetted off and the pellet dried for 5 minutes. Finally, the DNA was dissolved in 50 µl of 5 mM Tris pH 8.0. After incubation for 5 min at RT the samples were centrifuged for 30 seconds to pellet the debris. The concentration was measured at the Nanodrop (Chapter 2.1.5) and to a concentration of 100ng/µl.

6.4.1.2 Polymerase chain reaction (PCR)

The PCR is a molecular method to amplify specific sequences of the DNA. Therefore, a sample of DNA with a target sequence, the template, and two primers, which are complementary to the target sequence and set the start point for DNA polymerase, are needed. The DNA polymerase is a heat stable enzyme which is able to synthesize new DNA strands by using deoxyribonucleotide triphosphates (dNTPs) as single units for the newly synthesized DNA and needs $MgCl_2$ for its functionality. In general, PCR reactions consist of 20-50 cycles with 3 temperature steps. The first two steps are denaturation steps causing single strand DNA through melting and the annealing for the primer binding to the template. The last step is the elongation where the DNA polymerase synthesizes a new DNA strand by complementary base pairing of the dNTPs to the template. The duration and temperature of the single steps are dependent and variant on several parameters like length of primers or DNA polymerase. In addition to the samples that needed to be tested, every PCR analysis was carried out using a negative (containing H2O instead of DNA) and a positive (DNA from an animal that had already been screened positive before in the specific PCR) control.

6.4.1.2.1 Genotyping of leucin variant in RPE65 gene

A point mutation at position 450 of the RPE 65 gene resulting in a base exchange from methionine to leucine defines the susceptibility of animals to light-induced photoreceptor degeneration (Wenzel et al., 2001). As mice carrying the leucin mutation are more sensitive to light damage, it is important to genotype the experimental mice for the leucine variant of PRE 65. The following protocol and program were used:

Reagent	Volume in µl
5x PCR buffer	10
dNTPs	1
MgCl2 (50 mM)	2,5
Primer MWOI rev/fwd (1:10)	1
Taq Polymerase	1
H2O	32,5
DNA	2

Table 14 PCR reaction mix for RPE 65 PCR

Gene	Species	Alignment	Sequence 5' to 3'
MWO I	mus musculus	forward	CACTGTGGTCTCTGCTATCTTC
MWO I	mus musculus	reverse	GGTGCAGTTCCACTTCAGTT

Table 15 Primer for RPE65 PCR

Temperature	Duration	Cycles
94°C	2 min	
94°C	30 s	
55°C	45 s	34 x
72°C	1 min	
72°C	5 min	
10°C	hold	

Table 16 Program for RPE 65 PCR

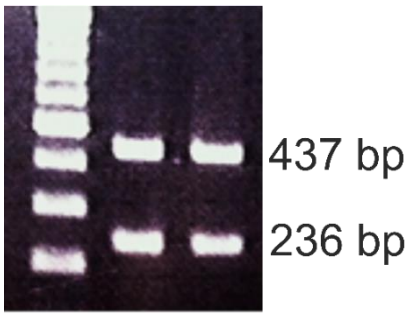

Figure 55 PCR Product after digestion

12 µl of the 673 bp PCR product were digested with 8 µl H_2O and 0.3 µl of the restriction enzyme MWO I at 37°C for 3 h. The leucine codon generates a restriction site for MWOI, which results after enzymatic digestion in two DNA products of 437 bp and 236 bp.

6.4.1.2.2 Genotyping of Endothelin receptor type b

The PCR strategy was designed to results in two products: one for the wildtype Etb situation (500 bp (WT)) and one for the floxed situation (199 bp (TG)). Due to of different annealing-temperatures of the specific primers that needed to be used, two different PCR protocols were used. Only mice carrying two floxed alleles (= 199bp positive PCR signal) for Endothelin receptor b (Etb) were used for experiments.

ETB WT		ETB TG	
5x buffer	3.0 µl	5x buffer	3.0 µl
dNTPs (10mM)	0.4 µl	dNTPs (10mM)	0.4 µl
$MgCl_2$ (50mM)	0.5 µl	$MgCl_2$ (50mM)	0.5 µl
WT forward primer	0.3 µl	WT forward primer	0.3 µl
WT reverse primer	0.3 µl	Neo reverse primer	0.3 µl
Taq polymerase	0.5 µl	Taq polymerase	0.5 µl
H_2O	8.0 µl	H_2O	8.0 µl
DNA	2.0 µl		2.0 µl

Table 17 PCR reaction mix for Etb PCR

Temperature	Duration	Cycles
95°C	3 min	
94°C	45 s	
56°C (WT) 62°C (TG)	45 s	36 x
72°C	1 min 10 sec	
72°C	5 min	
10°C	hold	

Table 18 Program for Etb PCR

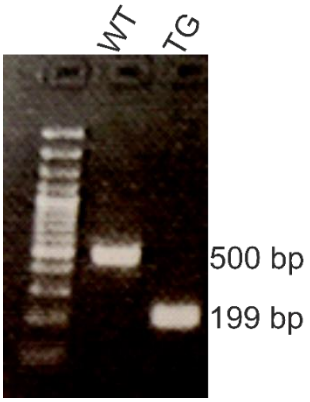

Figure 56 PCR Product of Etb-PCR. *WT=Etb, TG=floxed Etb*

6.4.1.2.3 Genotyping of Cre recombinase

Only mice carrying the Cre recombinase (PCR-Product with 270 bp) will exhibit an Etb deletion after Cre mediated recombination. Therefore, all experimental mice were genotyped for Cre recombinase. Floxed Etb mice without Cre recombinase were used as controls.

Cre	
5x buffer	3.0 µl
dNTPs (10mM)	0.3 µl
$MgCl_2$ (50mM)	0.5 µl
WT forward primer	0.3 µl
WT reverse primer	0.3 µl
Taq Polymerase	0.4 µl
H_2O	8.2 µl
DNA	2.0 µl

Temperature	Duration	Cycles
95°C	3 min	
94°C	30 s	
61°C	30 s	35 x
72°C	35 sec	
72°C	5 min	
10°C	hold	

Table 19 PCR reaction mix for Cre PCR (left) and program for PCR (right).

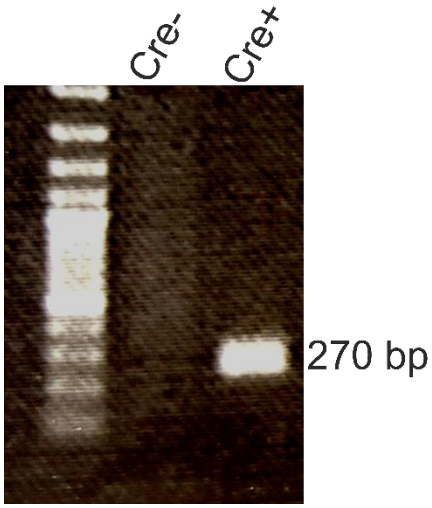

Figure 57 PCR-product for Cre-PCR

6.4.1.2.4 Genotyping of Rd1 (retinal degeneration 1) recombinase

The mutation Retinal degeneration 1 (Rd1) leads to a degeneration of photoreceptors. As we focus on photoreceptors in the current thesis, it was of high interest to genotype all experimental mice for Rd1 mutation. The Rd1 PCR product results in two products of 240 bp (WT) and 560 bp (TG). Mice only positive for 240bp (WT) were used for experiments.

Rd1 WT		**Rd1 TG**	
5x buffer	5 µl	5x buffer	5.0 µl
dNTPs (10mM)	0.5 µl	dNTPs (10mM)	0.5 µl
$MgCl_2$ (50mM)	0.5 µl	$MgCl_2$ (50mM)	0.75 µl
Rd1 common fwd	0.5 µl	Rd1 common fwd	0.65 µl
WT reverse	0.5 µl	TG reverse	0.65 µl
Mango Taq polymerase	1.0 µl	Mango Taq polymerase	0.65 µl
H_2O	16.0 µl	H_2O	15.8 µl
DNA	1.0 µl	DNA	1.0 µl

Table 20 PCR reaction mix for Rd1 PCR

Temperature	**Duration**	**Cycles**
94°C	2 min	
94°C	30 s	
58°C	40 s	34 x
72°C	45 sec	
72°C	5 min	
10°C	hold	

Table 21: Program for Rd1 PCR

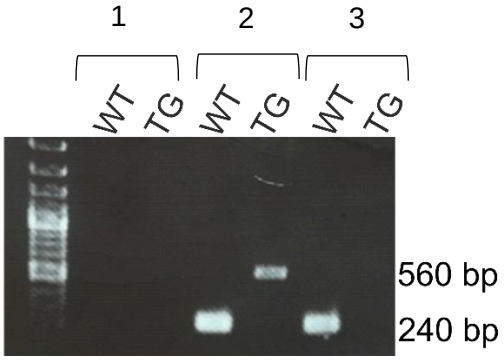

Figure 58 PCR-Product for Rd1-PCR. *(1) negative control (2) +/- for Rd1 (3) -/- for Rd1*

6.4.1.2.5 Agarose gel electrophoresis

The amplified PCR products were visualized and analysed by gel electrophoresis using 2% agarose gels. For their preparation, 2g agarose in 100 ml TBE buffer was boiled and after short cooling mixed with 3 µl ethidium bromide. Ethidium bromide intercalates with the double stranded DNA and can be visualized by its fluorescence under UV light. during electrophoresis, the DNA fragments are separated according to their molecular size in the agarose gel. Therefore, 10 µl of the PCR products were loaded to the gel. To allow for a precise determination of the PCR product size, 2.5 µl of a DNA standard (Gene Ruler 100 bp Plus DNA Ladder) with defined molecular size was loaded on the very left position of each gel. Electrophoresis was performed at 130 V for 30 minutes and the PCR products were then visualized by using UV light with a wave length of 302 nm.

6.4.2 RNA analysis

6.4.2.1 RNA Isolation

The prepared tissues or scraped cells were transferred in 2.0 ml tubes on ice and treated with 500 µl TriFast™, a monophasic solution including phenol and guanidinium thiocyanate which inactivates RNAses and stabilizes the RNA. The samples were homogenized and RNA was isolated performing the following protocol:

- Add 200 µl chloroform per ml TriFast, vortex
- Incubate 10 min at RT
- Centrifuge 20 min 14000 rpm, 4 °C
- Transfer upper transparent aqueous phase to new 1.5 ml tube
  (store other phases for protein isolation at -20 °C, Chapter 6.4.3.1)
- Add 500 µl isopropanol per ml TriFast, vortex
- Freeze overnight at -20 °C
- Centrifuge at 14000 rpm, 4 °C, remove supernatant
- Wash pellet in 1 ml 70% ethanol per ml TriFast, vortex
- Incubate 10 min on ice
- Centrifuge at 14000 rpm, 4 °C, remove supernatant

  } repeat

- Solve pellet in 14 µl RNase-free water
- Store at -80 °C

6.4.2.2 Quantification of RNA

The concentration of the RNA was determined by using the NanoDrop spectrophotometer (Chapter 6.3.7). Thereby, the optical density at λ = 260 nm (OD_{260}), the absorption maximum of nucleic acids (DNA, RNA), and at λ = 280 nm (OD_{280}), the absorption maximum of proteins, was used in comparison to the solvent (H_2O). The concentration was calculated with following formula:

Concentration [µg/ml] = OD_{260} × 40 µg/ml

The ratio of OD_{260} and OD_{280} gives information about the purity of the RNA. The optimum of peqGOLD TriFast™ isolated RNA should be > 1.7 $A_{260/280}$-ratio.

6.4.2.3 Synthesis of complementary DNA (cDNA)

cDNA can be synthesized from messenger RNA (mRNA) templates by reverse transcriptase, an RNA-dependent DNA polymerase, which operates on the single strand of mRNA and generates its complementary DNA. First-strand cDNA synthesis was performed by using the qScript™ cDNA Synthesis Kit (Quanta Bioscience, Gaithersburg, USA) according to manufacturer's instructions. RNA that was not reversely transcribed served as negative control (-RT). The following protocol was used for cDNA synthesis:

	Volume in µl	
Reagent	**+ RT**	**- RT**
iScript reverse transcriptase	1	-
5x script	4	4
1 µg RNA in H_2O	15	16

Table 22 PCR reaction mix for cDNA synthesis

Temperature	**Duration**
22°C	5 min
42°C	30 min
85°C	5 min
4°C	hold

Table 23 PCR protocol for cDNA synthesis

The synthesized cDNA samples were used for RT-PCR and stored at -20°C.

6.4.2.4 Quantitative real-time RT-PCR

Quantitative real-time RT-PCR analyses were performed with the reversed transcribed samples (+RT), each analysed as triplets, using the Bio-Rad CFX Connect™ Real-Time PCR Detection System. A H_2O control and RNA that was not reverse transcribed (–RT) served as negative controls for real-time RT-PCR. The PCR products can be detected using SYBR-Green I, which intercalates within the double stranded cDNA. For relative quantification the geometric mean values of the housekeeping genes *ribosomal protein L32* (*RPL32*), *glyceraldehyde 3-phosphate dehydrogenase* (*Gapdh*) and *guanine nucleotide-binding protein subunit beta-2-like* (*Gnb2l*) or *ubiqutitin c* (*Ubc*) were used. Quantitative real-time RT-PCR was performed with the following protocol:

Reagent	Housekeeper	Neuroprotective factors
10x Puffer ROX	7,50 µl	7.50 µl
Primer fw stock	0,06 µl	0.06 µl
Primer rv stock	0,06 µl	0.06 µl
H2O	4,38 µl	1.38 µl
cDNA	3 µl	6 µl
Σ	15 µl	15 µl

Table 24 Solution mix for real-time RT-PCR

Step	Temperature	Duration	Cycle
Denaturation	94°C	20 sec	
Annealing	60°C	10 sec	50x
Extension	60°C	20 sec	

Table 25 Real-time RT-PCR program

Afterwards, the 96-well plate was heat sealed and the samples were centrifuged. Then, the plate was placed in the Real-time RT-Detection System and the program was run as described in Table 25. Using CFX Manager™ Software and Excel software the relative expression of mRNA levels could be calculated according to the $\Delta\Delta C_T$-method (Livak, Schmittgen, 2001).

6.4.3 Protein analysis

6.4.3.1 Protein isolation with peqGold TriFast™

The harvested retinae or scraped cells were prepared for RNA analysis and protein were isolated from the lower phase that emerges during the TriFast isolation process (after adding chloroform). The following steps were performed for protein isolation:

- Add 300 µl 100 % ethanol per ml TriFast, vortex
- Incubate 3 min at RT
- Centrifuge 5 min at 2000 rpm, 4 °C
- Remove pellet
- Add 1500 µl isopropanol per ml TriFast, vortex
- Incubate 10 min at RT
- Centrifuge 10 min at 12000 rpm, 4 °C
- Remove supernatant
- Wash pellet 20 min with 2000 µl TriFast washbuffer at RT
- Centrifuge 5 min at 7600 rpm, 4°C
- Remove supernatant

repeat 3x

- Add 2000 µl 90 % ethanol per ml TriFast, vortex
- Incubate 20 min at RT
- Centrifuge 5 min at 7600 rpm, 4°C
- Dry pellet
- Solve pellet in 200 µl urea buffer with 0.1 % protease inhibitor and 0.1 % phosphatase inhibitor
- Incubate 5 min in thermomixer at 1000 rpm, 95 °C
- Centrifuge 5 min at 12000 rpm, 4 °C
- Remove pellet
- Store at – 20 °C (short term)/ – 80 °C (long term)

6.4.3.2 Protein isolation with EDTA-Buffer

EDTA Buffer is particularly used for the isolation of membrane bound proteins, like Endothelin receptor b (Etb). As it contains the non-ionic detergent Tergitol, it is able to detach Etb out of the cell membrane without its denaturation. For protein isolation, 200 µl EDTA-buffer were used for each retina or each 6-well containing confluent cells. The retinae were homogenized, the cells were superseded with the use of cell scrapers and

transferred to a new reaction tube. The samples were incubated on a shaker at 4°C for 1 h, then centrifuged at 13.000 rpm for 15 min. The supernatant contains the proteins.

6.4.3.3 SDS polyacrylamide gel electrophoresis (SDS-PAGE)

The fractionation of proteins from retinal and cellular lysates for western blot analysis was performed on SDS-polyacrylamide gels using electrophoresis system of PeqLab Biotechnology GmbH. The concentration of the gels depends on the molecular weight of the analysed protein. In this work the resolving gel was prepared with a concentration of 10 % (Table 26) and casted between two glass plates with two plastic spacers fixed in the casting frame. The liquid resolving gel was covered with isopropanol to sustain a clearly defined border to the stacking gel. After polymerization, the isopropanol was removed completely and the stacking gel (Table 26) placed on top. A comb was placed within the stacking gel to gain 10 chambers for loading the samples. The stacking gel is needed to concentrate the protein samples. In contrast, in the resolving gel the proteins are separated according to their molecular weight.

Reagent	Stacking gel	Resolving gel (10%)
dH_2O	0.68 ml	1.9 ml
Rotiphorese® Gel 30	0.17 ml	1.7 ml
Tris-HCl, 1M, pH 6.8	0.13 ml	-
Tris-HCl, 1.5M, pH 8.8	-	1.3 ml
10% SDS	0.01 ml	0.05 ml
10% APS	0.01 ml	0.05 ml
TEMED	0.001 ml	0.004 ml

Table 26 Protocol for stacking and resolving gel

After polymerization the gels were placed in an electrophoresis chamber according to the manufacturer's instructions and filled with 1x electrode buffer (Chapter 6.3.6). The combs were removed, and the protein samples were pipetted in the pockets of the stacking gel. Additionally, 5 µl of the pre-stained protein ladder with defined molecular size was applied in the pocket on the left side. The separation of the proteins was performed at 20 mA per gel for about 60-80 minutes.

6.4.3.4 Semi-dry blotting

The separated proteins were transferred from the gel to a PVDF-membrane (0.45 um pore size) using a semidry electroblot system. 6 Whatman paper and a PVDF membrane were cut to a size of 7 x 9 cm. The membrane was activated in methanol for about 30 seconds and equilibrated in 1x transfer buffer. The Whatman paper were also incubated in 1x transfer buffer. The blotting was performed for 45 min at 14 V and 180 mA (per gel) and assembled as seen in Table 27. Thereby it is important to remove the sacking gel and to avoid bubbles between PVDF membrane and resolving gel.

Cathode (-)
3 whatman paper
Resolving gel
PVDF membrane
3 whatman paper
Anode (+)

Table 27 Assembly scheme of semi-dry blot

2.2.3.4 Immunodetection of specific protein bands

After semidry-blotting, the PVDF membrane was incubated at room temperature in blocking solution under permanent shaking for 1 h to block unspecific protein-binding sites. The blocking solution is listed in (Table 28). After blocking, the PVDF membrane was washed 3x 5 min in TBS-T and incubated with the primary antibody overnight at 4 °C (unless otherwise stated in Table 28). The next day, the membrane was again washed three times with TBS-T for 5 min and then incubated at room temperature with the secondary antibody for 1 h.. All antibodies and corresponding blocking solution used in this thesis are shown in Table 28. After adding HRP substrate for HRP-coupled secondary antibodies or CDP-Star for AP-coupled secondary antibodies, the resulting chemiluminescence was detectable using the LAS 3000 Intelligent Dark Box (Fujifilm). The final evaluation of the target proteins relative to the housekeeper protein Gapdh was performed with Aida Image Data Analyzer v.4.06 software (Raytest) and Excel software.

Protein	Blocking solution	Primary antibody	Secondary antibody
Etb	5 % non-fat dry milk	Rabbit-anti ETB 1:750 in 0,5% Blotto/TBST, 4°C, 2 nights (Alomone Labs)	anti-rabbit HRP conjugated 1:5000 in 0.5 % MM/TBST, 4°C, overnight (Cell Signaling Technology)
Akt	5 % non-fat dry milk	rabbit-anti AKT 1:1000 in 0,5%Blotto/TBST, 4°C, overnight (Cell Signaling Technology)	anti-rabbit AP conjugated 1:5000 in 0.5 % BSA/TBST, RT, 1h (Cell Signaling Technology)
Hif1α	5 % non-fat dry milk	Rabbit-anti HIF1α 1:200 in 0,5%MM/TBST, 4°C, 2 nights (Cayman Chemical)	anti-rabbit HRP conjugated 1:5000 in 0.5 % BSA/TBST, RT, 1h (Cell Signaling Technology)
pAkt	2%BSA	rabbit-anti pAKT, 1:2000 in 0,2%BSA/TBST,4°C, overnight (Cell Signaling Technology)	anti-rabbit HRP conjugated 1:5000 in 0.5 % BSA/TBST, RT, 1h (Cell Signaling Technology)
Gapdh 1:1000, HRP-linked	Corresponding blocking buffer	rabbit-anti GAPDH 1:5000 in blocking buffer, 1h RT or overnight 4°C (Cell Signaling Technology)	

Table 28 Antibodies used for western blot analyses with blocking solution and secondary antibody

6.4.4 Proteomic analysis (Proteomics)

In cooperation with Dr. Stefanie Hauck (Helmholtz Zentrum, Munich, Germany), we performed proteomics of *61W$^{\Delta Etb}$* cells and 661W control cells (James et al., 1997). The statistical analyses and WGCNA network analyses were performed in cooperation with Dr. Andreas Neueder (University Ulm, Germany).

First, 100.000 cells were seeded in 6-well plates until reaching confluency. For cell lysis, medium was withdrawn by suction and the cells were washed three times with 1xPBS. 500 µl EDTA-Buffer was added on each 6-well and incubated for 10 min on ice. Then the cells were scraped from the bottom of the plate and transferred to Eppendorf Protein LoBind Tubes and homogenized. Protein-lysates with a concentration of 10 µg were used for further proteasome analysis. Therefore, the data-independent acquisition (DIA) method, high resolution mass spectroscopy (Lepper et al., 2018) was performed by Dr. Stefanie Hauck (Helmholtz Zentrum, Munich, Germany). For describing correlation patterns among the analysed proteins, weighted correlation network analysis (WGCNA) was performed in cooperation with Dr. Andreas Neueder (Neurology, University Ulm).

6.5 Histology

6.5.1 Morphometric analysis of semi-thin sections

For the analysis of the retinal morphology, semi-thin sections were performed and analysed via light microscopy. For a morphometric quantification spider diagrams were performed.

6.5.1.1 Embedding and preparing of semi-thin sections

For morphological and morphometric analysis, the dissected eyes were incubated in EM-fixative (Chapter 6.3.6) for 24 h at 4 °C. The next day, the eyes were washed three times for 20 min with 0,1 M cacodylat-buffer (Chapter 6.3.6) and afterwards dehydrated through an ascending alcohol series (70 %, 80 %, 90 %, 100 %). Finally, the eyes were embedded in epon (Ethanol/Aceton 1:1, Aceton 100 %, Epon/Aceton 1:2, Epon/Aceton 2:1, Epon 100 %) and hardened for 24 h at 60 °C and for 48 h at 90 °C. Semithin sections of 1.0 µm thickness were cut along the mid-horizontal (nasal-temporal) plane and stained by Richardson's stain (RICHARDSON et al., 1960) and analysed via light microscopy.

6.5.1.2 Spider diagrams

For morphometric analysis, the thickness of the inner and outer nuclear layer was measured. Therefore, the length of both hemispheres of the sections was measured via Image J then the total length of each hemisphere divided through 10 to define the

distance between the individual measure points. Finally, the thickness of the outer nuclear layer was measured at the defined measure points. The means of the measure points were blotted in a spider diagram beginning at the OS of the temporal side across the ONH to the OS at the nasal side and statistical analysis was performed to compare single measure points between control and conditional knockout mice.

6.5.2 Embedding and preparing of frozen sections

Dissected eyes were fixed for 4 h in Methyl Carnoy (10 % glacial acetic acid, 60 % methanol, 30 % chloroform). Therefore, the eyes were transferred to 50 % and 25 % methanol for 20 min each and washed 2 times in 0.1 M Php. Afterwards the eyes were incubated in 10 %, 20 %, 30 % sucrose/PBS each at least 4 h at 4 °C. The eyes were shock frozen in Tissue TEK mounting medium and 12 µm sagittal sections were cut using a cryostat.

Dissected eyes were fixed in 4%PFA for 4 h. Afterwards, the eyes were washed twice in 0.1 M Php and then incubated in 10 %, 20 %, 30 % sucrose/PBS each at least 4 h at 4 °C. The eyes were shock frozen in Tissue TEK and 12 µm sagittal sections were cut by using a cryostat. The sections were placed on glass slides and either immediately used for further staining or stored at -20 °C.

6.5.3 Embedding and preparing of paraffin sections

Eyes were fixed in 4 % PFA for 4 h and washed twice in 0.1 M Php. Afterwards, the eyes were transferred to 50 % and 70 % isopropanol each for 1 h and finally embedded in paraffin. Using a Supercut-microtome, 6 µm thin paraffin slices were cut and transferred onto glass slides. For further staining the paraffin sections were deparaffinized in the following steps:

- 2 x 10 min xylol
- 2x 10 min 100 % isopropanol
- 2x 10 min 96 % isopropanol
- 2x 10 min 80 % isopropanol
- 10 min 70 % isopropanol
- Aqua dest.

6.5.4 Immunohistochemistry

6.5.5 Antibodies for immunochemistry

Primary antiboy	Fixation	Pretreatment	Blocking	Secondary antibody
Collagen IV 1:50, overnight 4°C	Methyl Carnoy (Kryo)	none	2%BSA/0.1 M Php, 1 h RT	goat anti-rabbit Cy™3 IgG 1:2000 in 0.5%BSA/0.03%Triton / 0.1 M Php, 48 h 4°C
Eta 1:100, overnight 4°C	4%PFA (Kryo)	none	5 % non-fat dry milk/0.1 M Php overnight 4°C	Goat anti-chicken IgG Alexa 546 highly cross adsorbed, 1h RT
Gfap 1:2000, overnight 4°C	4%PFA (Kryo)	none	2 % BSA/0.2 % CWFG/0.1%Triton/0. 1 M Php, 1 h RT	Goat anti-chicken IgG Alexa 488 highly cross adsorbed, 1h RT
Gs 1:100, (overnigh t 4°C	4%PFA (Paraffin)	0.5% Triton, 30 min RT	2 % BSA/0.2 % CWFG/0.1%Triton/0. 1 M Php, 1 h RT	Donkey anti-goat IgG Alexa 488 1:1000 highly cross adsorbed 1h RT
Iba-1 1:1000, overnight 4°C	Flatmounts, 4%PFA (Paraffin)	1 h 0.05 M NH_4Cl 1 h 0.5%Triton/0. 1M Php	2 % BSA/0.2 % CWFG/0.1%Triton/0. 1 M Php, 1 h RT	goat anti-rabbit Cy™3 IgG 1:2000 in 0.2% BSA, 0.02% CWFG, 0.01% Triton, 0.1M Php
Ng-2 1:100, 48 h 4°C	FITC-perfused flatmounts	none	5%BSA/0.3%Triton/ 0.1 M Php, 1 h RT	goat anti-rabbit Cy™3 IgG 1:2000 in 0.5%BSA/0.03%Triton / 0.1 M Php, 48 h 4°C
Pv-1 1:25, overnight 4°C	Methyl Carnoy (Kryo)	none	2 % BSA/0.2 % CWFG/0.1%Triton/0. 1 M Php, 1 h RT	Biotinylated anti-rat IgG 1:500 1h RT, Streptavidin, Alexa Fluor® 555 conjugate

Table 29 Antibodies used for immunohistochemistry blocking solution and secondary antibody

6.5.6 Terminal deoxynucleotidyl transferase dUTP nick end labeling (TUNEL)

TUNEL is a method for detecting DNA fragmentation which is characteristic for apoptosis. The assay is based on the presence of nicks in the DNA that can be identified by terminal deoxynucleotidyl transferase. The terminal deoxynucleotidyl transferase detects dUTPs which are secondarily labeled with a fluorescence marker. Therefore, the Apoptosis Detection System (DeadEnd Fluometric TUNEL, Promega) was used to detect apoptotic cell death in retinae of animals 30 h after light damage. The TUNEL assay was performed on paraffin sections (4% PFA) with the following protocol and the sections were afterwards mounted with Mowiol containing Dapi.

Reagent	Duration in minutes
50% Isopropanol	5
Aqua dest.	5
0,89% NaCl	5
1x PBS	5 (2x)
4% PFA	15
1xPBS	5 (2x)
Proteinase K (1:500 in 0,1 M Php)	8
1xPBS	5 (2x)
4% PFA	5
1xPBS	5 (2x)
Equilibration Buffer (37°)	60
2xSSC	15
1xPBS	5

Table 30 Protocol for TUNEL-assay

6.5.7 In situ hybridization Base Scope®

In situ hybridization (ISH) Base Scope® was performed to detect mRNA signals of Etb in sagittal sections of CD1 wildtype mice, *Etb*$^{\Delta eye}$ and *Etb*$^{\Delta OC}$ mice and corresponding controls and *661W*$^{\Delta Etb}$ cells and 661W control cells. In situ hybridization (ISH) Base Scope® reagents and probes were provided by courtesy of Prof. Dr. Charlotte Wagner (University Regensburg, Germany).

6.5.7.1 Fixation

Mice were perfused (Chapter 6.1.6) with In situ hybridization Base Scope® Fixative (Chapter 6.3.6) and incubated with this buffer for 24 h at room temperature. The day before performing ISH Base Scope® cells were seeded (10000 cells/well) on glass platelets in a 6-well plate until reaching confluency of 70-80%. Afterwards the cells were fixed on the glass platelets in 4%PFA for 30 min at room temperature and washed three times with 1xPBS.

6.5.7.2 Paraffin embedding of murine ocular tissue

After fixation, the eyes were enucleated and embedded in paraffin according to the following protocol. All analytical reagents were used with the quality grade *pro analysis* (p.a.).

- 2 x 70% EtOH
- 2 x 80% EtOH
- 2 x 90% EtOH
- 1 x 100% EtOH
- 1x 100 % isopropanol

} 30 min, shaking at room temperature

- 1x 100 % isopropanol (45°C), 45 min
- 1x 1:1 isopropanol/paraffin suspension (60°C), 45 min
- 2x 24h paraffin (60°C)

By using a Supercut-microtome, 6 µm thin paraffin slices were cut and transferred onto glass slides.

6.5.7.3 Deparaffinization and preparation for In situ hybridization Base Scope®

Before performing in situ hybridization Base Scope® by using the Base Scope® Detection Reagent Kit Red the slices were deparaffinized according to the manufacturers' protocol:

- Dry slices for 1 h at 60°C in the dry oven
- 2x10 min Xylol, RT
- 2x 2 min 100% EtOH, RT
- Dry slices on air for 5 min, RT
- Drop Base Scope® H_2O_2 on slides and incubate for 10 min, RT
- 2x 15 sec RNAase free H_20
- 15 min Base Scope® Target Retrieval Reagent
- 2x 15 sec RNAase free H_20
- 2x 100 % EtOH, RT
- Dry slides overnight, RT
- Draw barrier with hydrophobic barrier pen around each sagittal section

Base Scope® Detection Reagent Kit Red

- 30 min BaseScope® Protease III, 40°C in oven
- 3-5x short washing steps with RNAase free H_20
- 2h BaseScope® Target probe (mM-ETB), 40°C
- 2x 2 min washing step with BaseScope® washing buffer
- Hybridize signal amplification molecule (AMP0) for 30 min, 40°C
- 2x 2 min washing step with BaseScope® washing buffer
- Hybridize signal amplification molecule (AMP1) for 15 min, 40°C

- 2x 2 min washing step with BaseScope® washing buffer
- Hybridize signal amplification molecule (AMP2) for 30 min, 40°C
- 2x 2 min washing step with BaseScope® washing buffer
- Hybridize signal amplification molecule (AMP3) for 30 min, 40°C
- 2x 2 min washing step with BaseScope® washing buffer
- Hybridize signal amplification molecule (AMP4) for 15 min, 40°C
- 2x 2 min washing step with BaseScope® washing buffer
- Hybridize signal amplification molecule (AMP5) for 30 min, RT
- 2x 2 min washing step with BaseScope® washing buffer
- Hybridize signal amplification molecule (AMP6) for 15 min, RT
- 2x 2 min washing step with BaseScope® washing buffer
- Incubte with Reagent A and Reagent B solution (1:60) for 10 min to detect signal
- 2x1 min Haematoxylin solution to stain nuclei
- 3x short washing steps with RNAase free H_20 until slides are clear
- 1x 10 sec 0.02 % ammonium hydroxide-solution
- 3-5x short washing steps with RNAase free H_20
- Dry slides for 15 min in the dry oven, 60°C
- Mount slides

We performed additional co-staining against Gs, Gfap and Collagen IV in the Cd1 wildtype mice. Subsequently to the last washing step the regular staining protocols (Chapter 6.5.5) were performed.

6.5.8 Microscopy

The immunohistochemical stainings were analysed using the Axio Imager Z1-mircoscope (Carl Zeiss, Goettingen, Germany) or the Laser Scanning microscope LSM 510 Meta (Carl Zeiss, Goettingen, Germany).

6.5.9 Statistical analysis

Comparisons between the mean variables of two groups were made by a two-tailed Student's t-test (heteroscedastic, two-tailed) using Excel software and comparisons between the mean variables of more than two groups were made by One-way ANOVA followed by Bonferroni post-hoc test using SPSS software. P values ≤ 0.05 were considered to be statistically significant. All results are expressed as mean ± SEM.

References

Ahmed TA, El-Badri N (2018) Pericytes: The Role of Multipotent Stem Cells in Vascular Maintenance and Regenerative Medicine. In: Cell biology and translational medicine. Advances and challenges (Turksen K, ed), pp 69–86. Cham, Switzerland: Springer.

Alonzi T, Middleton G, Wyatt S, Buchman V, Betz UA, Müller W, Musiani P, Poli V, Davies AM (2001) Role of STAT3 and PI 3-kinase/Akt in mediating the survival actions of cytokines on sensory neurons. Molecular and cellular neurosciences 18:270–282.

Alrashdi SF, Deliyanti D, Talia DM, Wilkinson-Berka JL (2018) Endothelin-2 Injures the Blood-Retinal Barrier and Macroglial Müller Cells: Interactions with Angiotensin II, Aldosterone, and NADPH Oxidase. The American journal of pathology 188:805–817.

Amin RH, Frank RN, Kennedy A, Eliott D, Puklin JE, Abrams GW (1997) Vascular endothelial growth factor is present in glial cells of the retina and optic nerve of human subjects with nonproliferative diabetic retinopathy. Investigative ophthalmology & visual science 38:36–47.

Anand-Apte B, Hollyfield JG (2010) Developmental Anatomy of the Retinal and Choroidal Vasculature. In: Encyclopedia of the eye (Dartt DA, Besharse JC, Dana R, eds), pp 9–15. Amsterdam [Netherlands]: Elsevier/Academic Press.

Anderson DH, Fisher SK (1976) The photoreceptors of diurnal squirrels: Outer segment structure, disc shedding, and protein renewal. Journal of Ultrastructure Research 55:119–141.

Arai H, Hori S, Aramori I, Ohkubo H, Nakanishi S (1990) Cloning and expression of a cDNA encoding an endothelin receptor. Nature 348:730–732.

Bagnall AJ, Kelland NF, Gulliver-Sloan F, Davenport AP, Gray GA, Yanagisawa M, Webb DJ, Kotelevtsev YV (2006) Deletion of endothelial cell endothelin B receptors does not affect blood pressure or sensitivity to salt. Hypertension (Dallas, Tex. : 1979) 48:286–293.

Banner LR, Moayeri NN, Patterson PH (1997) Leukemia inhibitory factor is expressed in astrocytes following cortical brain injury. Experimental neurology 147:1–9.

Barton M, Yanagisawa M (2008) Endothelin: 20 years from discovery to therapy. Canadian journal of physiology and pharmacology 86:485–498.

Bergers G, Song S (2005) The role of pericytes in blood-vessel formation and maintenance1. Neuro-Oncology 7:452–464.

Bramall AN, Szego MJ, Pacione LR, Chang I, Diez E, D'Orleans-Juste P, Stewart DJ, Hauswirth WW, Yanagisawa M, McInnes RR (2013) Endothelin-2-mediated protection of mutant photoreceptors in inherited photoreceptor degeneration. PloS one 8:e58023.

Braunger BM, Ohlmann A, Koch M, Tanimoto N, Volz C, Yang Y, Bösl MR, Cvekl A, Jägle H, Seeliger MW, Tamm ER (2013a) Constitutive overexpression of Norrin activates Wnt/β-catenin and endothelin-2 signaling to protect photoreceptors from light damage. Neurobiology of disease 50:1–12.

Braunger BM, Pielmeier S, Demmer C, Landstorfer V, Kawall D, Abramov N, Leibinger M, Kleiter I, Fischer D, Jägle H, Tamm ER (2013b) TGF-β signaling protects retinal neurons from programmed cell death during the development of the mammalian

eye. The Journal of neuroscience : the official journal of the Society for Neuroscience 33:14246–14258.

Bringmann A, Pannicke T, Grosche J, Francke M, Wiedemann P, Skatchkov SN, Osborne NN, Reichenbach A (2006) Müller cells in the healthy and diseased retina. Progress in retinal and eye research 25:397–424.

Bürgi S, Samardzija M, Grimm C (2009) Endogenous leukemia inhibitory factor protects photoreceptor cells against light-induced degeneration. Molecular Vision 15:1631–1637.

Büssow H (1980) The astrocytes in the retina and optic nerve head of mammals: a special glia for the ganglion cell axons. Cell and tissue research 206:367–378.

Campello L, Esteve-Rudd J, Cuenca N, Martín-Nieto J (2013) The ubiquitin-proteasome system in retinal health and disease. Molecular neurobiology 47:790–810.

Candia OA (2004) Electrolyte and fluid transport across corneal, conjunctival and lens epithelia. Experimental eye research 78:527–535.

Castañares C, Redondo-Horcajo M, Magan-Marchal N, Lamas S, Rodriguez-Pascual F (2006) Transforming growth factor-beta receptor requirements for the induction of the endothelin-1 gene. Experimental biology and medicine (Maywood, N.J.) 231:700–703.

Chakravarthy U, Douglas AJ, Bailie JR, McKibben B, Archer DB (1994) Immunoreactive endothelin distribution in ocular tissues. Investigative ophthalmology & visual science 35:2448–2454.

Choritz L, Rosenthal R, Fromm M, Foerster MH, Thieme H (2005) Pharmacological and functional characterization of endothelin receptors in bovine trabecular meshwork and ciliary muscle. Ophthalmic research 37:179–187.

Clozel M, Gray GA, Breu V, Löffler BM, Osterwalder R (1992) The endothelin ETB receptor mediates both vasodilation and vasoconstriction in vivo. Biochemical and biophysical research communications 186:867–873.

Cornish EE, Natoli RC, Hendrickson A, Provis JM (2004) Differential distribution of fibroblast growth factor receptors (FGFRs) on foveal cones: FGFR-4 is an early marker of cone photoreceptors. Molecular Vision 10:1–14.

Datta SR, Dudek H, Tao X, Masters S, Fu H, Gotoh Y, Greenberg ME (1997) Akt phosphorylation of BAD couples survival signals to the cell-intrinsic death machinery. Cell 91:231–241.

Davenport AP, Hyndman KA, Dhaun N, Southan C, Kohan DE, Pollock JS, Pollock DM, Webb DJ, Maguire JJ (2016) Endothelin. Pharmacological reviews 68:357–418.

Druckenbrod NR, Powers PA, Bartley CR, Walker JW, Epstein ML (2008) Targeting of endothelin receptor-B to the neural crest. Genesis (New York, N.Y. : 2000) 46:396–400.

Dryja TP, Li T (1995) Molecular genetics of retinitis pigmentosa. Human Molecular Genetics 4:1739–1743.

Duncan MK, Li X, Ogino H, Yasuda K, Piatigorsky J (1996) Developmental regulation of the chicken βB1-crystallin promoter in transgenic mice. Mechanisms of Development 57:79–89.

Elmore S (2007) Apoptosis: a review of programmed cell death. Toxicologic pathology 35:495–516.

Faktorovich EG, Steinberg RH, Yasumura D, Matthes MT, LaVail MM (1990) Photoreceptor degeneration in inherited retinal dystrophy delayed by basic fibroblast growth factor. Nature 347:83–86.

Ferrari S, Di Iorio E, Barbaro V, Ponzin D, Sorrentino FS, Parmeggiani F (2011) Retinitis Pigmentosa: Genes and Disease Mechanisms. Current Genomics 12:238–249.

Filep JG, Battistini B, Côté YP, Beaudoin AR, Sirois P (1991) Endothelin-1 induces prostacyclin release from bovine aortic endothelial cells. Biochemical and biophysical research communications 177:171–176.

Firtina Z, Danysh BP, Bai X, Gould DB, Kobayashi T, Duncan MK (2009) Abnormal Expression of Collagen IV in Lens Activates Unfolded Protein Response Resulting in Cataract*. The Journal of biological chemistry 284:35872–35884.

Flügel-Koch C, Ohlmann A, Piatigorsky J, Tamm ER (2002) Disruption of anterior segment development by TGF-beta1 overexpression in the eyes of transgenic mice. Developmental dynamics : an official publication of the American Association of Anatomists 225:111–125.

Forrester J v. (1996) The eye. Basic sciences in practice. London: Saunders.

Fukuroda T, Fujikawa T, Ozaki S, Ishikawa K, Yano M, Nishikibe M (1994a) Clearance of circulating endothelin-1 by ETB receptors in rats. Biochemical and biophysical research communications 199:1461–1465.

Fukuroda T, Ozaki S, Ihara M, Ishikawa K, Yano M, Nishikibe M (1994b) Synergistic inhibition by BQ-123 and BQ-788 of endothelin-1-induced contractions of the rabbit pulmonary artery. British Journal of Pharmacology 113:336–338.

Gaengel K, Genové G, Armulik A, Betsholtz C (2009) Endothelial-mural cell signaling in vascular development and angiogenesis. Arteriosclerosis, thrombosis, and vascular biology 29:630–638.

Gao H, Hollyfield JG (1996) Basic fibroblast growth factor: increased gene expression in inherited and light-induced photoreceptor degeneration. Experimental eye research 62:181–189.

García M, Vecino E (2003) Role of Müller glia in neuroprotection and regeneration in the retina. Histology and histopathology 18:1205–1218.

Garvin J, Sanders K (1991) Endothelin inhibits fluid and bicarbonate transport in part by reducing Na+/K+ ATPase activity in the rat proximal straight tubule. Journal of the American Society of Nephrology : JASN 2:976–982.

Good TJ, Kahook MY (2010) The role of endothelin in the pathophysiology of glaucoma. Expert opinion on therapeutic targets 14:647–654.

Grimm C, Remé CE (2013) Light damage as a model of retinal degeneration. Methods in molecular biology (Clifton, N.J.) 935:87–97.

Guan Z, VanBeusecum JP, Inscho EW (2015) Endothelin and the renal microcirculation. Seminars in nephrology 35:145–155.

Gyllensten Lars J., Hellström BEO (1954) Experimental Approach to the Pathogenesis of Retrolental Fibroplasia: I. Changes of the Eye Induced by Exposure of Newborn Mice to Concentrated Oxygen. Acta Paediatrica 43:131–148.

Hamel C (2006) Retinitis pigmentosa. Orphanet journal of rare diseases 1:40.

Harms DW, Quadros RM, Seruggia D, Ohtsuka M, Takahashi G, Montoliu L, Gurumurthy CB (2014) Mouse Genome Editing using CRISPR/Cas System. Current protocols in human genetics / editorial board, Jonathan L. Haines … [et al.] 83:15.7.1-15.7.27.

Hayashi S, McMahon AP (2002) Efficient recombination in diverse tissues by a tamoxifen-inducible form of Cre: a tool for temporally regulated gene activation/inactivation in the mouse. Developmental biology 244:305–318.

Hickey KA, Rubanyi G, Paul RJ, Highsmith RF (1985) Characterization of a coronary vasoconstrictor produced by cultured endothelial cells. The American journal of physiology 248:C550-6.

Hirata Y, Emori T, Eguchi S, Kanno K, Imai T, Ohta K, Marumo F (1993) Endothelin receptor subtype B mediates synthesis of nitric oxide by cultured bovine endothelial cells. The Journal of clinical investigation 91:1367–1373.

Hol EM, Pekny M (2015) Glial fibrillary acidic protein (GFAP) and the astrocyte intermediate filament system in diseases of the central nervous system. Current opinion in cell biology 32:121–130.

Hu Y, Lu H, Zhang J, Chen J, Chai Z, Zhang J (2014) Essential role of AKT in tumor cells addicted to FGFR. Anti-cancer drugs 25:183–188.

Hughes S, Yang H, Chan-Ling T (2000) Vascularization of the human fetal retina: roles of vasculogenesis and angiogenesis. Investigative ophthalmology & visual science 41:1217–1228.

Illing ME, Rajan RS, Bence NF, Kopito RR (2002) A rhodopsin mutant linked to autosomal dominant retinitis pigmentosa is prone to aggregate and interacts with the ubiquitin proteasome system. The Journal of biological chemistry 277:34150–34160.

Irmady K, Zechel S, Unsicker K (2011) Fibroblast growth factor 2 regulates astrocyte differentiation in a region-specific manner in the hindbrain. Glia 59:708–719.

Jeong S-J, Dasgupta A, Jung K-J, Um J-H, Burke A, Park HU, Brady JN (2008) PI3K/AKT inhibition induces caspase-dependent apoptosis in HTLV-1-transformed cells. Virology 370:264–272.

Joly S, Lange C, Thiersch M, Samardzija M, Grimm C (2008) Leukemia inhibitory factor extends the lifespan of injured photoreceptors in vivo. The Journal of neuroscience : the official journal of the Society for Neuroscience 28:13765–13774.

Joly S, Pernet V, Chemtob S, Di Polo A, Lachapelle P (2007) Neuroprotection in the juvenile rat model of light-induced retinopathy: evidence suggesting a role for FGF-2 and CNTF. Investigative ophthalmology & visual science 48:2311–2320.

Just A, Olson AJM, Arendshorst WJ (2004) Dual constrictor and dilator actions of ET(B) receptors in the rat renal microcirculation: interactions with ET(A) receptors. American journal of physiology. Renal physiology 286:F660-8.

Kaufman PL, Alm A, Adler FH (2003) Adler's physiology of the eye. Clinical application. St. Louis: Mosby.

Kawamura H, Oku H, Li Q, Sakagami K, Puro DG (2002) Endothelin-induced changes in the physiology of retinal pericytes. Investigative ophthalmology & visual science 43:882–888.

Kedzierski RM, Yanagisawa M (2001) Endothelin system: the double-edged sword in health and disease. Annual review of pharmacology and toxicology 41:851–876.

Kefalov VJ (2012) Rod and cone visual pigments and phototransduction through pharmacological, genetic, and physiological approaches. The Journal of biological chemistry 287:1635–1641.

Kelley PB, Sado Y, Duncan MK (2002) Collagen IV in the developing lens capsule. Matrix Biology 21:415–423.

Kinkl N, Hageman GS, Sahel JA, Hicks D (2002) Fibroblast growth factor receptor (FGFR) and candidate signaling molecule distribution within rat and human retina. Molecular Vision 8:149–160.

Klaassen I, van Noorden CJF, Schlingemann RO (2013) Molecular basis of the inner blood-retinal barrier and its breakdown in diabetic macular edema and other pathological conditions. Progress in retinal and eye research 34:19–48.

Kolb H, Fernandez E, Nelson R (1995) Webvision: The Organization of the Retina and Visual System. Salt Lake City (UT).

Kominami K, Nakabayashi J, Nagai T, Tsujimura Y, Chiba K, Kimura H, Miyawaki A, Sawasaki T, Yokota H, Manabe N, Sakamaki K (2012) The molecular mechanism of apoptosis upon caspase-8 activation: quantitative experimental validation of a mathematical model. Biochimica et biophysica acta 1823:1825–1840.

Krishnamoorthy RR, Rao VR, Dauphin R, Prasanna G, Johnson C, Yorio T (2008) Role of the ETB receptor in retinal ganglion cell death in glaucoma. Canadian journal of physiology and pharmacology 86:380–393.

Kühn R, Torres RM (2002) Cre/loxP recombination system and gene targeting. Methods in molecular biology (Clifton, N.J.) 180:175–204.

Langmann T (2007) Microglia activation in retinal degeneration. Journal of leukocyte biology 81:1345–1351.

Lau J, Dang M, Hockmann K, Ball AK (2006) Effects of acute delivery of endothelin-1 on retinal ganglion cell loss in the rat. Experimental eye research 82:132–145.

Lepper MF, Ohmayer U, Toerne C von, Maison N, Ziegler A-G, Hauck SM (2018) Proteomic Landscape of Patient-Derived CD4+ T Cells in Recent-Onset Type 1 Diabetes. Journal of proteome research 17:618–634.

Li S, Zhang A, Cao W, Sun X (2016) Elevated Plasma Endothelin-1 Levels in Normal Tension Glaucoma and Primary Open-Angle Glaucoma: A Meta-Analysis. Journal of ophthalmology 2016:2678017.

Li ZY, Chang JH, Milam AH (1997) A gradient of basic fibroblast growth factor in rod photoreceptors in the normal human retina. Visual neuroscience 14:671–679.

Li ZY, Possin DE, Milam AH (1995) Histopathology of bone spicule pigmentation in retinitis pigmentosa. Ophthalmology 102:805–816.

Lim K-L, Tan JMM (2007) Role of the ubiquitin proteasome system in Parkinson's disease. BMC Biochemistry 8:S13.

Liu C-H, Wang Z, Sun Y, Chen J (2017) Animal models of ocular angiogenesis: from development to pathologies. FASEB journal : official publication of the Federation of American Societies for Experimental Biology 31:4665–4681.

Lobanova ES, Finkelstein S, Skiba NP, Arshavsky VY (2013) Proteasome overload is a common stress factor in multiple forms of inherited retinal degeneration. Proceedings of the National Academy of Sciences of the United States of America 110:9986–9991.

Luo X, Shen Y-m, Jiang M-n, Lou X-f, Shen Y (2015) Ocular Blood Flow Autoregulation Mechanisms and Methods. Journal of ophthalmology 2015.

Lupien C, Brenner M, Guérin SL, Salesse C (2004) Expression of glial fibrillary acidic protein in primary cultures of human Müller cells. Experimental eye research 79:423–429.

Lutty GA, McLeod DS (2018) Development of the hyaloid, choroidal and retinal vasculatures in the fetal human eye. Progress in retinal and eye research 62:58–76.

MacCumber MW, D'Anna SA (1994) Endothelin receptor-binding subtypes in the human retina and choroid. Archives of ophthalmology (Chicago, Ill. : 1960) 112:1231–1235.

Majmundar AJ, Wong WJ, Simon MC (2010) Hypoxia inducible factors and the response to hypoxic stress. Molecular cell 40:294–309.

Mannu GS (2014) Retinal phototransduction. Neurosciences 19:275–280.

Marc RE, Jones BW, Watt CB, Strettoi E (2003) Neural remodeling in retinal degeneration. Progress in retinal and eye research 22:607–655.

Marquardt T, Ashery-Padan R, Andrejewski N, Scardigli R, Guillemot F, Gruss P (2001) Pax6 is required for the multipotent state of retinal progenitor cells. Cell 105:43–55.

Masland RH (2012) The neuronal organization of the retina. Neuron 76:266–280.

McDonald DM, Bailie JR, Archer DB, Chakravarthy U (1995) Characterization of endothelin A (ETA) and endothelin B (ETB) receptors in cultured bovine retinal pericytes. Investigative ophthalmology & visual science 36:1088–1094.

Meyer-Lehnert H, Wanning C, Predel HG, Bäcker A, Stelkens H, Kramer HJ (1989) Effects of endothelin on sodium transport mechanisms: potential role in cellular Ca2+ mobilization. Biochemical and biophysical research communications 163:458–465.

Morgera S, Schlenstedt J, Hambach P, Giessing M, Deger S, Hocher B, Neumayer H-H (2003) Combined ETA/ETB receptor blockade of human peritoneal mesothelial cells inhibits collagen I RNA synthesis. Kidney international 64:2033–2040.

Mustafi D, Engel AH, Palczewski K (2009) Structure of cone photoreceptors. Progress in retinal and eye research 28:289–302.

Nakazawa T, Shimura M, Tomita H, Akiyama H, Yoshioka Y, Kudou H, Tamai M (2003) Intrinsic activation of PI3K/Akt signaling pathway and its neuroprotective effect against retinal injury. Current Eye Research 26:55–63.

Nickla DL, Wallman J (2009) THE MULTIFUNCTIONAL CHOROID. Progress in retinal and eye research 29:144–168.

Niquet J, Wasterlain CG (2004) Bim, Bad, and Bax: a deadly combination in epileptic seizures. The Journal of clinical investigation 113:960–962.

Noguchi M, Hirata N, Suizu F (2014) The links between AKT and two intracellular proteolytic cascades: ubiquitination and autophagy. Biochimica et biophysica acta 1846:342–352.

Noske W, Hensen J, Wiederholt M (1997) Endothelin-like immunoreactivity in aqueous humor of patients with primary open-angle glaucoma and cataract. Graefe's Arch Clin Exp Ophthalmol 235:551–552.

Okafor MC, Delamere NA (2001) The inhibitory influence of endothelin on active sodium-potassium transport in porcine lens. Investigative ophthalmology & visual science 42:1018–1023.

Organisciak DT, Vaughan DK (2010) Retinal light damage: mechanisms and protection. Progress in retinal and eye research 29:113–134.

Orlowski RZ (1999) The role of the ubiquitin-proteasome pathway in apoptosis. Cell death and differentiation 6:303–313.

Ortega Z, Lucas JJ (2014) Ubiquitin-proteasome system involvement in Huntington's disease. Frontiers in molecular neuroscience 7:77.

O'Sullivan ML, Puñal VM, Kerstein PC, Brzezinski JA, Glaser T, Wright KM, Kay JN (2017) Astrocytes follow ganglion cell axons to establish an angiogenic template during retinal development. Glia 65:1697–1716.

Overbeek PA, Chepelinsky AB, Khillan JS, Piatigorsky J, Westphal H (1985) Lens-specific expression and developmental regulation of the bacterial chloramphenicol acetyltransferase gene driven by the murine alpha A-crystallin promoter in transgenic mice. Proceedings of the National Academy of Sciences of the United States of America 82:7815–7819.

Ozerdem U, Grako KA, Dahlin-Huppe K, Monosov E, Stallcup WB (2001) NG2 proteoglycan is expressed exclusively by mural cells during vascular morphogenesis. Developmental dynamics : an official publication of the American Association of Anatomists 222:218–227.

Pagon RA (1988) Retinitis pigmentosa. Survey of Ophthalmology 33:137–177.

Parmeggiani F (2011) Clinics, epidemiology and genetics of retinitis pigmentosa. Current Genomics 12:236–237.

Patan S (2004) Vasculogenesis and angiogenesis. Cancer treatment and research 117:3–32.

Penn JS (2008) Retinal and Choroidal Angiogenesis. s.l.: Springer Netherlands.

Pierce EA, Avery RL, Foley ED, Aiello LP, Smith LE (1995) Vascular endothelial growth factor/vascular permeability factor expression in a mouse model of retinal neovascularization. Proceedings of the National Academy of Sciences of the United States of America 92:905–909.

Purves D, Williams SM (2001) Neuroscience. Sunderland, Mass: Sinauer Associates.

Ran FA, Hsu PD, Wright J, Agarwala V, Scott DA, Zhang F (2013) Genome engineering using the CRISPR-Cas9 system. Nature protocols 8:2281–2308.

Rao VR, Krishnamoorthy RR, Yorio T (2008) Endothelin-1 Mediated Regulation of Extracellular Matrix Collagens in Cells of Human Lamina Cribrosa. Experimental eye research 86:886–894.

Rattner A, Nathans J (2005) The genomic response to retinal disease and injury: evidence for endothelin signaling from photoreceptors to glia. The Journal of neuroscience : the official journal of the Society for Neuroscience 25:4540–4549.

Rautureau Y, Coelho SC, Fraulob-Aquino JC, Huo K-G, Rehman A, Offermanns S, Paradis P, Schiffrin EL (2015) Inducible human endothelin-1 overexpression in endothelium raises blood pressure via endothelin type A receptors. Hypertension (Dallas, Tex. : 1979) 66:347–355.

Reichenbach A, Bringmann A (2013) New functions of Müller cells. Glia 61:651–678.

Reichenbach A, Stolzenburg J-U, Eberhardt W, Chao TI, d. Dettmer, Hertz L (1993) What do retinal Müller (glial) cells do for their neuronal ‘small siblings’? Journal of Chemical Neuroanatomy 6:201–213.

Ribatti D, Nico B, Crivellato E (2011) The role of pericytes in angiogenesis. The International journal of developmental biology 55:261–268.

RICHARDSON KC, JARETT L, FINKE EH (1960) Embedding in epoxy resins for ultrathin sectioning in electron microscopy. Stain technology 35:313–323.

Risau W (1997) Mechanisms of angiogenesis. Nature 386:671–674.

Sachsenweger M, Klauss V (2014) Augenheilkunde. Stuttgart: Thieme.

Sakurai T, Yanagisawa M, Takuwa Y, Miyazaki H, Kimura S, Goto K, Masaki T (1990) Cloning of a cDNA encoding a non-isopeptide-selective subtype of the endothelin receptor. Nature 348:732–735.

Schmitt SI, Bielmeier CB, Braunger BM (in press) New insights into endothelin signaling and its diverse roles in the retina. Retinal Degenerative Diseases.

Schneider MP, Boesen EI, Pollock DM (2007) Contrasting actions of endothelin ET(A) and ET(B) receptors in cardiovascular disease. Annual review of pharmacology and toxicology 47:731–759.

Shintani K, Shechtman DL, Gurwood AS (2009) Review and update: current treatment trends for patients with retinitis pigmentosa. Optometry (St. Louis, Mo.) 80:384–401.

Shi-Wen X, Denton CP, Dashwood MR, Holmes AM, Bou-Gharios G, Pearson JD, Black CM, Abraham DJ (2001) Fibroblast matrix gene expression and connective tissue remodeling: role of endothelin-1. The Journal of investigative dermatology 116:417–425.

Song G, Ouyang G, Bao S (2005) The activation of Akt/PKB signaling pathway and cell survival. Journal of cellular and molecular medicine 9:59–71.

Sorrentino FS, Matteini S, Bonifazzi C, Sebastiani A, Parmeggiani F (2018) Diabetic retinopathy and endothelin system: microangiopathy versus endothelial dysfunction. Eye (London, England) 32:1157–1163.

Srinivasan Y, Lovicu FJ, Overbeek PA (1998) Lens-specific expression of transforming growth factor beta1 in transgenic mice causes anterior subcapsular cataracts. The Journal of clinical investigation 101:625–634.

Stahl A, Connor KM, Sapieha P, Chen J, Dennison RJ, Krah NM, Seaward MR, Willett KL, Aderman CM, Guerin KI, Hua J, Löfqvist C, Hellström A, Smith LEH (2010) The mouse retina as an angiogenesis model. Investigative ophthalmology & visual science 51:2813–2826.

Sternberg N, Hamilton D (1981) Bacteriophage P1 site-specific recombination. Journal of Molecular Biology 150:467–486.

Stone J, Itin A, Alon T, Pe'er J, Gnessin H, Chan-Ling T, Keshet E (1995) Development of retinal vasculature is mediated by hypoxia-induced vascular endothelial growth factor (VEGF) expression by neuroglia. The Journal of neuroscience : the official journal of the Society for Neuroscience 15:4738–4747.

Strauss O (2005) The retinal pigment epithelium in visual function. Physiological reviews 85:845–881.

Suhara T, Kim H-S, Kirshenbaum LA, Walsh K (2002) Suppression of Akt Signaling Induces Fas Ligand Expression: Involvement of Caspase and Jun Kinase Activation in Akt-Mediated Fas Ligand Regulation. Molecular and Cellular Biology 22:680–691.

Taniguchi T, Okada K, Haque MSR, Sugiyama K, Kitazawa Y (1994) Effects of endothelin-1 on intraocular pressure and aqueous humor dynamics in the rabbit eye. Current Eye Research 13:461–464.

Tezel G, Kass MA, Kolker AE, Becker B, Wax MB (1997) Plasma and aqueous humor endothelin levels in primary open-angle glaucoma. Journal of glaucoma 6:83–89.

Thomas HM, Cowin AJ, Mills SJ (2017) The Importance of Pericytes in Healing: Wounds and other Pathologies. International Journal of Molecular Sciences 18.

Tian Y, James S, Zuo J, Fritzsch B, Beisel KW (2006) Conditional and inducible gene recombineering in the mouse inner ear. Brain Research 1091:243–254.

Torbidoni V, Iribarne M, Ogawa L, Prasanna G, Suburo AM (2005) Endothelin-1 and endothelin receptors in light-induced retinal degeneration. Experimental eye research 81:265–275.

Ueki Y, Le Y-Z, Chollangi S, Muller W, Ash JD (2009) Preconditioning-induced protection of photoreceptors requires activation of the signal-transducing receptor gp130 in photoreceptors. Proceedings of the National Academy of Sciences of the United States of America 106:21389–21394.

van der Wijk A-E, Vogels IMC, van Veen HA, van Noorden CJF, Schlingemann RO, Klaassen I (2018) Spatial and temporal recruitment of the neurovascular unit during development of the mouse blood-retinal barrier. Tissue & cell 52:42–50.

Vecino E, Rodriguez FD, Ruzafa N, Pereiro X, Sharma SC (2016) Glia-neuron interactions in the mammalian retina. Progress in retinal and eye research 51:1–40.

Vingolo EM, Lupo S, Grenga PL, Salvatore S, Zinnamosca L, Cotesta D, Petramala L, Letizia C (2010) Endothelin-1 plasma concentrations in patients with retinitis pigmentosa. Regulatory peptides 160:64–67.

Wang M, Wong WT (2014) Microglia-Müller cell interactions in the retina. Advances in experimental medicine and biology 801:333–338.

Wenzel A, Grimm C, Samardzija M, Remé CE (2005) Molecular mechanisms of light-induced photoreceptor apoptosis and neuroprotection for retinal degeneration. Progress in retinal and eye research 24:275–306.

Wenzel A, Remé CE, Williams TP, Hafezi F, Grimm C (2001) The Rpe65 Leu450Met Variation Increases Retinal Resistance Against Light-Induced Degeneration by Slowing Rhodopsin Regeneration. J. Neurosci. 21:53–58.

West H, Richardson WD, Fruttiger M (2005) Stabilization of the retinal vascular network by reciprocal feedback between blood vessels and astrocytes. Development (Cambridge, England) 132:1855–1862.

Williams DS, Arikawa K, Paallysaho T (1990) Cytoskeletal components of the adherens junctions between the photoreceptors and the supportive Müller cells. The Journal of comparative neurology 295:155–164.

Winkler EA, Rutledge WC, Kalani MYS, Rolston JD (2017) Pericytes Regulate Cerebral Blood Flow and Neuronal Health at a Capillary Level. Neurosurgery 81:N37-N38.

Wójcik C (2002) Regulation of apoptosis by the ubiquitin and proteasome pathway. Journal of cellular and molecular medicine 6:25–48.

Wollensak G, Löffler B, Beyermann B, Ihling C (2002) An immunohistochemical study of endothelin-1 converting enzyme in the human eye. Current Eye Research 24:6–11.

Wright AF, Chakarova CF, Abd El-Aziz MM, Bhattacharya SS (2010) Photoreceptor degeneration: genetic and mechanistic dissection of a complex trait. Nature reviews. Genetics 11:273–284.

Xu D, Emoto N, Giaid A, Slaughter C, Kaw S, deWit D, Yanagisawa M (1994) ECE-1: a membrane-bound metalloprotease that catalyzes the proteolytic activation of big endothelin-1. Cell 78:473–485.

Yanagisawa M, Kurihara H, Kimura S, Tomobe Y, Kobayashi M, Mitsui Y, Yazaki Y, Goto K, Masaki T (1988) A novel potent vasoconstrictor peptide produced by vascular endothelial cells. Nature 332:411–415.

Zhang F, Wen Y, Guo X (2014) CRISPR/Cas9 for genome editing: progress, implications and challenges. Human Molecular Genetics 23:R40-6.

Zhou H, Li X-M, Meinkoth J, Pittman RN (2000) Akt Regulates Cell Survival and Apoptosis at a Postmitochondrial Level. The Journal of Cell Biology 151:483–494.

Zubilewicz A, Hecquet C, Jeanny JC, Soubrane G, Courtois Y, Mascarelli F (2001) Two distinct signalling pathways are involved in FGF2-stimulated proliferation of choriocapillary endothelial cells: a comparative study with VEGF. Oncogene 20:1403–1413.

Abbreviations

%	percent
°C	degree Celsius
µ	micro (10^{-6})
α	alpha
APS	ammonium persulfate
β	beta
Bad	Bcl2 associated death promotor
Bax	Bcl2 associated X
BCl2	B-Cell Lymphoma 2
Bim	BH3-only BCL-2-interacting mediator of cell death
bp	base pair
BSA	bovine serum albumin
cDNA	complementary deoxyribonucleic acid
Ct	cycle threshold
CWFG	cold water fish gelatine
Da	dalton
DAPI	4’,6-diamidino-2-phenylindole
dH_2O	distilled water
DNA	deoxyribonucleic acid
dNTP	2’-deoxyribonucleotide-5’-triphosphate
DTT	DL-Dithiothreitol

E	embryonic day
EDTA	ethylenediaminetetraacetic acid
EM	electron microscopy
ER	estrogen receptor
et al.	and others
Et/ET	Endothelin
Eta/ETA	Endothelin receptor type a
*Etb/*ETB	Endothelin receptor type b
EtOH	ethanol
FGF2	Fibroblast growth factor 2
FITC	Fluorescein Isothiocyanate
fl	flox
g	gram
GAPDH	Glycerinaldehyd-3-phosphat-Dehydrogenas
GCL	Ganglion cell layer
GFAP	glial fibrillary acidic protein
GNB2L	Guanine Nucleotide Binding Protein 2L
GS	Glutamine synthetase
h	hour
H_2O	water
HCl	hydrochloric acid
HEPES	2-(4-(2-Hydroxyethyl)-1-piperazinyl)-ethansulfonacid

HRP	horseradish peroxidase
IBA-1	ionized calcium-binding adapter protein 1
IgG	immunoglobin G
INL	Inner nuclear layer
IPL	Inner plexiform layer
ISH	In situ hybridization
kb	kilobase
kDa	kilodalton
l	litre
LB	lysogeny broth
Lif/LIF	leukemia inhibitory factor
m	milli (10^{-3})
M	molar (mol/l)
mA	milliampere
mg	miligram
min	minute/s
ml	millilitre
mRNA	messenger ribonucleic acid
µ	micro
n	nano (10^{-9})
NFL	nerve fibre layer
NH_4Cl	ammoniumchloride
ONL	Outer nuclear layer

OPL	Outer plexiform layer
ONH	optic nerve head
OS	ora serrata
NO	nitric oxide
P	postnatal day
PAGE	polyacrylamide gel electrophoresis
PBS	phosphate buffered saline
PCR	polymerase chain reaction
PFA	paraformaldehyde
PVDF	polyvinylidene fluoride
PV-1	plasmalemma vesicle associated protein
RGC	retinal ganglion cell
RNA	ribonucleic acid
RPE	Retinal pigment epithelium
rpm	rounds per minute
RT	reverse transcriptase; room temperature
SDS	sodium dodecylsulfate
sec	seconds
SEM	standard error of the means
TBS	tris buffered saline
TBST	tris buffered saline with tween
TEMED	tetramethylethylenediamine
TG	transgen

Tgf-β/ TGF-β	transforming growth factor beta
Tris	Tris(hydroxymethyl)aminomethan
TRITON	tert-Octylphenylpolyoxyethylen
UV	ultra violet
V	voltage
v/v	by volume
w/v	weight per volume
WT	wildtype
Σ	summa

Figure legend

Table legend

Danksagung

An erster Stelle möchte ich mich bei Herrn Prof. Dr. Tamm bedanken, der es mir ermöglich hat diese Arbeit an seinem Lehrstuhl durchzuführen.

Des Weiteren möchte ich mich bei Pro Retina Deutschland e. V. bedanken, die mich und mein Projekt im Rahmen eines Promotionsstipendiums drei Jahre lang finanziell unterstützt haben.

Mein ganz besonderer Dank gilt Frau Prof. Dr. Dr. Barbara Braunger für die hevorragende fachliche Betreuung dieser Doktorarbeit, für deine Geduld und dafür, dass du mir auch aus der Ferne immer zur Seite standest. Ich werde mich stets gerne an unsere zahlreichen wissenschaftlichen und .persönlichen Gespräche zurückerinnern. Ohne deine motivierenden Worte, dein offenes Ohr und deine unermüdlichen Bemühungen wäre die Arbeit in diesem Umfang nicht möglich gewesen!

Des Weiteren möchte ich ganz herzlich bei Frau Prof. Dr. Charlotte Wagner für die Übernahme des Zweitgutachtens bedanken und dafür, dass sie mir die Durchführung der Methodik der In situ Hybridisierung (BaseScope) ermöglich hat. Diese Methode war eine Bereicherung für diese Arbeit.

Mein herzlicher Dank geht zudem an Herrn Dr. Andreas Neueder, der durch seine statistischen Auswertungen ausschlaggebend für die Proteomics Analysen war. Außerdem vielen Dank für deinen unermüdlichen Einsatz und Hilfestellungen in der „CRISPR-Selbsthilfegruppe“. In diesem Zuge möchte ich mich auch herzlich bei Frau Dr. Stefanie Hauck für die Durchführung der Proteomics Analysen bedanken.

Mein besonderer Dank gilt Elke Stauber, Margit Schimmel, Angelika Pach und Silvia Babl, die mir bei Fragen und Problemen in der Molekularbiologie und Histologie immer weiter geholfen haben. Außerdem möchte ich euch für die vielen heiteren Stunden neben der Laborarbeit danken!

Desweiteren möchte ich Anna Huber danken, die mich im Rahmen ihrer Bachelorarbeit in dieser Arbeit tatkräftig untersützt hat.

Als nächstes möchte ich mich bei der „Sammlung“ bedanken. Danke für die tolle Arbeitsatmosphäre und dafür, dass es dank euch sogar in den stressigsten Zeiten Spaß macht in die Arbeit zu gehen.

Vielen Dank Frau Dr. Anja Schlecht, die mich zu Beginn herzlich in die Arbeitsgruppe aufgenommen hat und mir in allen Lebens- und Laborlagen immer eine große Hilfe war. Tausend Dank an Kristina Elsner und Christina Bielmeiner für die wahnsinnig große Untersützung und dass ihr mir vor allem in der Endphase meiner Doktorarbeit den Rücken freigehalten habt. Ihr seid die Besten! Christina, danke dass du in jeder noch so stressigen Zeit mein Ruhepol warst! Franziska Scherl möchte ich danken, dass du mir immer ein Lächeln auf die Lippen zauberst. Bei Dr Andrea Dillinger möchte ich mich ganz besonders bedanken. Danke, dass du immer weißt was zu tun ist und ich mit jeglichen Problemen zu dir kommen kann. Du warst mir eine große Stütze die letzen Jahre!

Besonders danken möchte ich zudem meinem Lebensgefährten Raphael, der mich in jeder noch so stressigen Phase immer wieder aufgeheitert und untersützt hat. Danke, dass du so viel Geduld und Rücksicht genommen hast.

Von tiefstem Herzen möchte ich meinen Eltern und meiner Familie danken, die mir das Studium in Regensburg ermöglicht haben. Ihr habt immer an mich geglaubt und all meine Entscheidungen unterstützt!

Ehrenwörtliche Erklärung

Hiermit versichere ich, Sabrina Ines Schmitt, ehrenwörtlich, dass ich die vorliegende Dissertation mit dem Titel: „Endothelin signalling in the retina“ selbstständig und ohne fremde Hilfe verfasst und keine anderen als die angegebenen Hilfsmittel benutzt habe. Die Stellen der Arbeit, die dem Wortlaut oder dem Sinn nach anderen Werken entnommen wurden, sind in jedem Fall unter Angabe der Quelle kenntlich gemacht. Die Arbeit ist noch nicht veröffentlicht oder in anderer Form als Prüfungsleistung vorgelegt worden.

Regensburg, den_____

_____

Unterschrift